# A Genome-wide RNAi Screen Identifies Combinatorial Efficacy of CX-5461 with Homologous Recombination Deficiency and Topoisomerase I inhibition in Ovarian Cancer

**Shunfei Yan**

Submitted in total fulfilment of the requirements of the degree of
Doctor of Philosophy

September 2019

Faculty of Medicine, Dentistry, and Health Science
The Sir Peter MacCallum Department of Oncology
The University of Melbourne

Produced on archival quality paper

# Abstract

High-grade serous ovarian cancer (HGSC) is common, with poor prognosis. Limited therapeutic options are available, and the development of new therapies is of high priority. The RNA Polymerase I (Pol I) transcription inhibitor CX-5461 has shown efficacy in both chemotherapy-sensitive and -resistant ovarian cancer through its ability to activate the DNA damage checkpoint. Here, we combine a genome-wide RNAi screening approach with a focussed drug screen to identify potential targets whose inhibition can enhance the efficacy of CX-5461. We demonstrate that CX-5461 combined with knockdown of homologous recombination DNA repair genes shows cooperative cell proliferation inhibition in several HGSC cell lines. We also demonstrate combinatorial efficacy between CX-5461 and topoisomerase 1 (TOP1) depletion or the TOP1 poison Topotecan. The combination induces cell death, cell cycle arrest and senescence even after drug withdrawal. The mechanism of their cooperativity relies on a cell cycle-independent, nucleolar DNA damage response (DDR) associated with topological stress at the ribosomal DNA and is independent of the ability to inhibit PoI I transcription or induce global replication stress. Despite dose-limiting toxicities hampering the broad use of Topotecan in the clinic, combined treatment with CX-5461 and low-dose Topotecan exhibits striking therapeutic efficacy *in vivo*, thus providing evidence for a novel strategy to treat HGSC.

# Declaration

- This is to certify that:

- The thesis comprises only my original work except where indicated in the Preface

- Due acknowledgement has been made in the text to all other materials used;

- The thesis is fewer than 100,000 words in length, exclusive of table, maps, bibliographies and appendices

Shunfei Yan

September 2019

# Preface

Except where indicated below, all experiments *in vitro* and *in vivo* were designed, performed and analysed by me under supervision of Prof Richard Pearson and Dr Keefe Chan. The RNAi screen as well as the mini compound screen were conducted with the assistance of Assoc Prof Kaylene Simpson and her team (Victorian Centre of Functional Genomics, PMCC). All the animal experiments were conducted with the assistance of Assoc Prof Carleen Cullinane and her team (Translational Research Laboratory, TRL, PMCC). The OVCAR3 cell line adopted for xenograft studies was generated by Dr George Au-Yeung (Cancer Genetics and Genomics Program, PMCC). Some of the western blotting experiments were conducted with the assistance of Dr Keefe Chan.

I estimate my contribution to each results chapter to be:

Chapter 3: 90 percent
Chapter 4: 100 percent
Chapter 5: 95 percent

No work presented in this thesis has been submitted for any other qualification or performed prior to candidature enrolment

# Acknowledgement

Four years after I started my PhD study, my post-graduate research finally comes to the end, together with my identity as a student. It is time for me to express my sincere gratitude to a number of people who have supported me during the whole journey.

First and foremost, I need to say thank you to my most supportive and thoughtful supervisor Prof Rick Pearson. Rick has always had my back whenever I have any problems with my research, career and my personal life. It would be impossible for me to come to Australia and conduct the world-class research in the oncology field without the financial and emotional support from Rick (particularly the jokes!). Thank you, Rick!

I also need to say thank you to Dr Keefe Chan. As my co-supervisor, Keefe spent tons of time in modifying my reports and presentations, reviewing my research progress, making suggestions on my research plan and even helping me to conduct the actual experiments in spite of the enormous pressure he has received from his own research project and duty as a father. I cannot imagine how my research would be without the help of Keefe. Thank you, Keefe!

Additionally, I need to thank for all the members of the Pearson lab, the oncogenic signalling and growth control program, cluster 7 and PMCC who have generously offered their reagents and help to facilitate my study and research. I also need to send special regards to Assoc Prof Owen Caroline, who provided lots of advice for my career and studentship affairs. Thank you, all!

Last but not least, I need to thank the world-class coffee in Melbourne, which prevented me from falling asleep during work and meetings, and kept me up with high-working efficiency all day long! : )

Shunfei Yan
September 2019

# Table of Contents

# List of Tables and Figures

# Chapter 1. Introduction

## 1.1. Poor prognosis of ovarian cancer

Ovarian cancer (OC) ranks as the seventh most common cancer in females worldwide (8th overall), with 240,000 new cases diagnosed every year. It is one of the deadliest gynaecological cancers, causing more than 152,000 deaths worldwide, and over 1,000 in Australia [1]. OC is often (~85%) diagnosed at advanced stage (stage III or above) due to the location of the lesion and the lack of symptoms in early stages [2]. The overall five-year survival rate of OC is 43% (90% for stage I and only 19% for stage IV) and has not significantly improved over the past thirty years when compared with other cancers such as breast cancer, which has raised from 60% to 89% [3]. There is also no effective method to prevent OC. Clearly, the identification of new therapeutic strategies and biomarkers of early detection is essential for achieving better patient outcome.

## 1.2. Characteristics of high grade serous ovarian cancer (HGSC)

OC is classified into three main types: (i) epithelial (EOC), (ii) germ cell and (iii) stromal. EOC origins from the epithelium, the outer cells that cover the ovary, fallopian tubes and uterus. This type is common and accounts for >90% of all OC cases. Germ cell tumours are derived from the reproductive cells of the ovary, while stromal ovarian cancer originates from hormone-producing cells. Both of these types are rare (1~2%) [4].

There are five major histological subtypes of EOC, namely, high-grade serous carcinoma (HGSC), low-grade serous carcinoma (LGSC), endometrioid carcinoma (ENOC), clear cell carcinoma (CCC) and mucinous carcinoma (MUC), with the prevalence of ~60%, ~9%, ~15%, ~12% and ~4% respectively [5, 6] (Table 1.1). HGSC has a similar morphology under microscopy to LGSC except

for marked nuclear atypia and increasing number of mitoses. However, they have major differences in terms of origins and genomic profile. There is strong evidence suggesting that most HGSCs start from fallopian tube epithelium, while LGSCs likely originate from ovarian surface epithelium [5, 7, 8]. Whole genome sequencing studies have shown that *TP53* mutations are nearly universal in HGSC samples (>95%), while such mutations are rare in LGSC [6, 9, 10]. Furthermore, it has been reported that about 15-20% of HGSC patients have germline mutations of the breast-related cancer antigen (*BRCA)* gene [11]. *BRCA1/2* play a crucial role in the homologous recombination (HR) DNA repair process. When taking the mutations of other HR components into account, i.e. *RAD51* and *Fanconi anaemia (FA)* genes, then up to 50% of HGSCs are deficient in HR [12, 13]. This may explain why most HGSC have a favourable initial response rate to current standard chemotherapy, while later relapse and development of acquired drug resistance are frequent. Recent comparative genomic hybridization (CGH) studies also showed that HGSC have a higher level of DNA amplifications and deletions compared to other EOC subtypes. These are associated with genomic instability in HGSC, which might be a consequence of *TP53* and HR deficiency [11, 14]. Some other oncogenic mutations, such as *EGFR, PI3K, AKT2, c-MYC, ERBB2* have also been reported, but the variation is high between different studies [14, 15].

In addition to histological subtypes, EOC has also been classified by other criteria. For example, the Bowtell group sorted serous and endometrioid ovarian cancer into six molecular subtypes (C1-C6) based on gene-expression patterns including stromal, mesenchymal, immune, cell motility, cell surface/secreted markers, *β-catenin/TCF/LEF* transcription targets and *MAPK* pathway activation signatures [16]. Moreover, the Thiery and Mori groups identified five distinct molecular subtypes of EOC (Epi-A, Epi-B, Mes, Stem-A and Stem-B) which show different pathway enrichment in fibrinolysis, metastasis, extracellular matrix, *TGFβ* and

chromatin modification [17]. Another classification system includes the concept of Type I and Type II ovarian cancer, which distinguishes ovarian carcinogenesis by its origin. Those histological subtypes with clearly stated precursor lesions, such as endometroid, clear cell, mucinous and low grade serous carcinoma, are designated as Type I ovarian cancer, while Type II is assigned to those with unclear origins or developed *de novo* from the fallopian tube and/or ovarian surface epithelium, such as HGSC [18, 19]. However, clinically, histological subtypes are still currently being used as the standard classification system for diagnosis and treatment.

### 1.3. Current and emerging therapeutic options for HGSC and outcomes

The current standard therapeutic approach for treating HGSC is optimal debulking surgery (removing as much of the tumour tissue as possible) followed by adjuvant chemotherapies with a combination of platinum-based (e.g., carboplatin or cisplatin) and taxane-based (e.g., paclitaxel) drugs [2]. Platinum-based compounds cause DNA adducts that induce DNA damage and trigger cell death [20]. Meanwhile, taxane-based compounds block mitosis by stabilising microtubule polymers [21]. Most HGSCs (80%) are initially sensitive to platinum/taxane therapy but acquired drug resistance emerges during subsequent treatment cycles. Primary chemotherapy resistance is observed in 15–20% of cases [2, 22]. Generally, patients with BRCA1/2 mutations have better prognosis after platinum-based chemotherapy than their non-BRCA1/2 mutated counterparts. This is due to the impaired HR functions of BRCA1/2 mutated cells to repair DNA double-strand breaks (DSB) caused by DNA-damaging agents, resulting in massive genomic instability and cell death [23, 24]. Despite this, cases of relapse are frequently observed in over 80% of patients [25].

Recurrent ovarian cancer can be divided into two groups. For those that are still 'platinum-sensitive', re-challenge with platinum-based therapies is normally the first option until the tumour becomes platinum-resistant or the patients can no longer tolerate the side-effects [2]. The platinum compounds are often used in combination with other drugs (e.g., paclitaxel or liposomal doxorubicin) to increase the response rate (RR) and extend the progression-free survival (PFS) [25]. The recent introduction of poly (ADP-ribose) polymerase (PARP) inhibitors, including Olaparib and Niraparib, has led significant change in clinical practice [26-28]. PARP enzymes play indispensable roles in base excision repair (BER) and single-strand DNA break (SSB) repair pathways. When encountering an SSB, PARP1 binds to the break and uses NAD+ to add poly (ADP-ribose) (PAR) polymers onto itself (auto-PARylation), histones and chromatin-associated proteins. This modification leads to the relaxation of chromatin and serves as a scaffold to recruit DNA damage repair proteins [29]. When PARP is inhibited, SSB will remain unrepaired, either leading to DSB directly or causing replication-associated DSB, both of which require HR to repair [30, 31]. This results in synthetic lethality when treating HR-deficient tumours that are unable to repair DSB [27, 32, 33]. In addition to the inhibition of SSB repair, PARP inhibitors can also trap PARP on DNA, causing replication stress [29, 34, 35]. In a recent phase 3 trial (the SOLO1 trial) evaluating the efficacy of Olaparib as maintenance therapy in patients with newly diagnosed, BRCA1/2 mutated, advance ovarian cancer (including high-grade serous and endometrioid ovarian cancer), the treatment of Olaparib reduced the risk of disease progression or death by 70% compared to placebo, which brought substantial PFS patient benefit [36]. Additionally, as cancer cells are more dependent on the complementary pathways, such as BER and single-strand repair pathways, to repair DNA damage and survival, the therapeutic effect of PARP inhibitors could be further exploited by combining with platinum-based drugs [37, 38]. A Phase 2, randomized trial in recurrent platinum-sensitive ovarian cancer showed that the combination of

Olaparib with carboplatin and paclitaxel followed by Olaparib monotherapy improved PFS from 9.6 to 12.2 months compared with the paclitaxel/carboplatin-treated arm [39]. Besides PARP inhibitors, angiogenesis inhibitors including vascular endothelial growth factor (VEGF) inhibitors (Bevacizumab) and VEGF receptor inhibitors (Pazopanib, Cediranib, etc) present another option for 'platinum-sensitive' patients [2, 25, 40]. Multiple trials have demonstrated that adding anti-angiogenic agents to chemotherapy can significantly improve PFS but fail to improve the overall survival (OS), while the underlying mechanisms are still unclear [25]. Further investigation is also required to determine which patients would benefit most from these anti-angiogenesis therapies.

Nevertheless, OC inevitably develops acquired resistance to platinum-therapies, which are classified as 'platinum-resistant' [41]. The whole-genome sequencing (WGS) analysis performed by the Bowtell group in acquired platinum-resistant and platinum-sensitive HGSC patients revealed four main molecular changes associated with acquired chemo-resistance, two of which are related to the restoration of HR function, including reversions of germline BRCA1 or BRCA2 mutations and loss of BRCA1 promoter methylation. The overexpression of the drug efflux pump MDR1, as well as the alteration in molecular subtypes that have been associated with poor drug uptake and primary chemo-resistance, are the other two major causes. The Bowtell group also identified a high correlation between Cyclin E (CCNE1) amplification and primary chemo-resistance [11, 42, 43].

Even the latest approved PARP inhibitors cannot avoid the development of resistant disease. PARP inhibitor resistance occurs through multiple mechanisms, including the restoration/reactivation of HR pathways, the overexpression of the drug efflux pump MDR1 and the loss/mutation of PARP [44-46]. As the therapeutic efficacy of PARP inhibitors is largely dependent on compromised HR,

it is not surprising that the restoration/reactivation of HR results in resistance to PARP inhibitors. Multiple mechanisms can cause the restoration/reactivation of HR, including but not restricted to direct reversion mutations of BRCA1/2 genes [44, 47, 48], the mutation of p53-binding protein 1 (53BP1), alterations in microRNAs that shift the balance of DNA repair from NHEJ to HR [49, 50], or the increased stability of the replication forks [51]. A closer examination of these mechanisms reveals that there is a significant overlap between the drug resistance mechanisms of PARP inhibitors and platinum-based therapies. In fact, cross-resistance between PARP inhibitors and platinum compounds has already been identified in some studies [47]. Thus, although the improved selectivity and tolerability of PARP inhibitors has remarkably influenced the clinical treatment of HR-deficient OC, it still cannot solve the problem of drug resistance in OC treatment [52]. Thus, new therapies that can overcome drug resistance, including the restoration/reactivation of HR function, are still of high demand to improve the prognostic outlook of OC patients.

For these ‘platinum-resistant’ patients, and those with primary chemotherapy resistance (‘platinum-refractory’), several salvage regimens are available including PARPi, which still work in some cases as its therapeutic mechanism is not totally reliant on HR status [53]. A recent report has demonstrated that PARP-1 can promote ribosome biogenesis and cell proliferation through PARylation of DDX21, an RNA helicase that localizes at nucleoli and promotes rDNA transcription when ADP-ribosylated, and this process can be blocked by PARPi irrespective of BRCA status [54]. Other options include Topoisomerase I inhibitors (e.g., Topotecan), Topoisomerase II inhibitors (Etoposide or Doxorubicin), microtubule inhibitors (Paclitaxel), alkylating reagents (Altretamine, Ifosfamide), anti-metabolites (Gemcitabine), estrogen receptor (ER) inhibitors (Tamoxifen, in ER-positive tumours) and epidermal growth factor receptor 2 (ERBB2, or HER2) inhibitors (Herceptin, in HER2-positive tumours)

[55, 56]. These drugs can either be used as monotherapies or in combinations [25, 41, 57]. However, the response rate (RR) is merely 10% and the OS is miserably short, indicating a high possibility of developing resistance to these drugs [25].

Due to the rapid progress in molecular pathology-based diagnosis and drug development in the last decade, a number of emerging therapies are underway (Table 1.2). One practical and direct way is to target the phosphatidylinositol-3-kinase (PI3K)/ Protein kinase B (PKB, also known as AKT)/mammalian target of rapamycin (mTOR)-signalling pathway, which is hyperactivated in some HGSC tumours (Table 1) [14, 15]. A recent phase 2 trial combining the mTORC1 inhibitor Everolimus and the aromatase inhibitor Letrozole (which inhibits estrogen production) showed a promising extension of PFS regardless of platinum sensitivity [58]. However, no significant improvement was seen when using Temsirolimus, another mTORC1 inhibitor, alone [15, 59, 60]. Some trials have also attempted to target PI3K/AKT/mTOR by inhibiting upstream tyrosine kinase receptors (EGFR, HER2, IGF-1R, etc) either with antibodies or small molecular inhibitors, but with moderate and variable outcomes [56]. The disappointing results may be explained by the complexity and redundancy of these pathways, which might be resolved by using drug combinations. Moreover, it is also difficult to define which patients would benefit from these therapies [15].

The recent breakthrough in immune checkpoint inhibitors has opened a new door for ovarian cancer therapy development. Immune checkpoints are a group of negative regulators attenuating normal T-cell activation to prevent pathologic over-activation, which may result in the development of autoimmune or inflammatory disorders. These include programmed cell death ligand 1 (PD-L1)/programmed cell death 1 (PD-1), cytotoxic T lymphocyte-associated protein 4 (CTLA-4), and many other molecules [61]. However, tumour cells may also take advantage of this system to escape from immune surveillance that normally

eliminate malignant cells from the body, i.e. by overexpressing PD-L1 on the tumour cell surface, which will inhibit the activity of $T_{eff}$ cells [62-64]. As a result, by inhibiting immune checkpoints with antibodies, e.g. anti-PD-1 (Opdivo, Keytruda), anti-PD-L1 (Tecentriq), or anti-CTLA-4 (Yervoy), it is possible that the tumour immune-suppressive microenvironment could be reversed and the immune surveillance system could be reactivated to execute its function [62, 65-67]. A number of trials have been conducted and marked effects have been seen in some solid tumours, especially in melanoma, renal cancer and lung cancer [68-70]. The results in ovarian cancer are also promising. PD-1/PD-L1 blockade in advanced and platinum-resistant EOC showed consistent, durable and significant RR at 10-17% and disease control rate (DCR) at 40-50% [71-74], while CTLA-4 antibody achieved durable response lasting for more than 4 years in a patient previously immunised with an ovarian tumour cell vaccine GVAX [74]. GVAX is irradiated, patient-derived pancreatic cancer cells genetically modified to secrete the cytokine granulocyte-macrophage colony stimulating factor (GM-CSF), which is expected to stimulate the immune system [75]. Since most patients experience stabilisation of disease rather than regression, drug combinations are currently being investigated to boost the therapeutic potential for immune checkpoint blockade, especially with other kinds of immunotherapies or conventional cytotoxic chemotherapies, which have been reported to be able to enhance the immunogenicity of cancer [76-78]. These trials are still ongoing and the results are promising. With the rapid growth of the cancer immunology field, it is anticipated that immunotherapy will be a game-changer in future ovarian cancer treatment.

Another drug currently under development, APR-246 (also known as PRIMA-1MET), adopts a unique and interesting approach to treat OC by targeting mutant p53, a target previously regarded as ‘undruggable’ [79, 80]. APR-246 reactivates p53 by binding covalently to cysteines in mutant p53, leading to structural

refolding and restoration of wild-type p53 function, thus inducing cell apoptosis [81]. As p53 is almost universally mutated in HGSC, and has a crucial role in tumour initiation [11], there is a strong rationale for reactivation of mutant p53 to allow dramatically improved therapy of a wide range of chemo-resistant and chemo-refractory HGSC. In fact, research has shown that APR-246 overcomes resistance to chemotherapies in both ovarian cancer cell lines and primary cancer cells from patients [79, 80]. Phase Ib/II trials of APR-246 in combination with platinum-based therapy in both platinum-sensitive and resistance patients are currently underway [81].

A few other candidates, e.g. new angiogenesis inhibitors, new PI3K/AKT/mTOR-signalling pathway inhibitors, new chemo-drugs, and anti-α-folate receptor (FR) therapies, are also under investigation [2, 25, 40]. However, there is a lack of convincing clinical trial results to support their efficacy.

## 1.4. Dysregulated RNA Polymerase I (Pol I) transcription in cancer and its implication in HGSC

### 1.4.1. Upregulated Pol I transcription in malignant cells

Distinct from bacterial transcription being conducted by a single RNA polymerase, Pol I is the only RNA Polymerase in mammalian that transcribes the 45S pre-ribosomal RNA (rRNA), which is rapidly processed into the 28S, 5.8S and 18S rRNAs. Together with the 5S rRNA (transcribed by RNA Polymerase III) and a variety of ribosomal proteins (RP) derived from the translation of RNA Polymerase II transcribed mRNAs, they form functional ribosomes [82]. As actively growing and proliferating cells are highly reliant on ribosomes to produce

proteins for replication, Pol I transcription can contribute up to 60% of the global cellular transcription levels [83]. rDNA transcription predominantly occurs in the nucleoli (rRNA synthesis can also happen in mitochondria [84]), where approximately 400 copies of rDNA genes are present as tandem repeats. Enlarged nucleoli, an indication of accumulated macromolecules at the sites of rRNA synthesis, can be detected in cancer cells by microscopy and are often regarded as a marker of malignancy [85, 86]. As the total number of mRNA molecules is greater than the number of ribosomes in most cell types, while the synthesis of rRNA limits the production of ribosomes, the transcription of rDNA is the rate-limiting step of protein synthesis and hence cell growth especially in highly proliferating cells [87]. Inhibition of RNA Polymerase I Transcription Factor (TIF-IA, also known as RRN3) function by a dominant-negative mutant can retard the growth of HEK293T cells, while the overexpression of a constitutively active version of TIF-IA can further accelerate proliferation, even in rapidly growing HEK293T cells [88]. Alterations in nucleolar morphology and increased synthesis of 45S pre-rRNA together with the activation of an alternative pre-RNA synthetic pathway, have also been related to the aggressiveness of human breast cancer cells [89]. Similar up-regulation of Pol I transcription has also been observed in hepatitis B (HBV) and hepatitis C (HCV) virus-infected hepatocellular carcinomas (HCCs) [90, 91]. However, even though the role of dysregulated Pol I transcription in facilitating tumourigenesis and cancer progression has long been observed, the molecular basis of how this process is regulated was largely overlooked until recent years [92].

### 1.4.2. Brief overview of Pol I transcription machinery

There are three major stages in Pol I transcription (as well as transcription by other RNA polymerases), namely initiation, elongation and termination. Figure 1.1A

shows a simplified diagram describing Pol I transcription initiation. In human cells, the first event in Pol I pre-initiation complex formation (PIC) is the binding of the upstream binding factor (UBF) to the upstream control element (UCE) in the rDNA promoter region. UBF is a key transcription factor for rDNA genes and is specifically localised at the nucleolus. This colocalization is cooperatively regulated by the first high-mobility group (HMG) box (HMG box 1), the C-terminal acidic region (AR) and the linker region (LR) between the HMG and AR region of the UBF protein. The truncation of the AR domain attenuates its localisation at the nucleolus and redistribute it throughout the nucleus, while the interruption of the HMG box 1 can entirely abolish its localisation at the nucleolus [93]. UBF binds to the minor groove of DNA as a dimer and wraps the DNA into a right-handed loop at 140bp length with its HMG box, a motif known to bind DNA. This manoeuvre brings the core promoter and the UCE into close proximity, thus creating the correct scaffold for the promoter selectivity factor (SL1 complex) to bind to the core promoter and C-terminal of UBF [94-96]. Pol I is then recruited to PIC via TIF-IA (RRN3), a regulatory factor that is associated with the initiation-competent subpopulation of Pol I (Pol Iβ) [94, 95]. The SL1 complex contains one TATA-binding protein (TBP) and at least four Pol I-specific TBP-associated factors (TAFs), which facilitate the specific recognition of the rDNA promoter and recruitment of Pol I. It has also been reported that SL1 can stabilise the dynamic binding of UBF dimers to the rDNA promoter region, as well as maintain the hypomethylation status in the rDNA promoter region [82, 83, 97]. After the formation of PIC, the Pol I enzyme needs to be released from the complex to conduct efficient transcription, namely ‘promoter escape’, which is mediated by the phosphorylation of RRN3 and the binding of UBF to PAF53, a Pol I-specific heterodimer [82, 98]. As described previously, this is a rate-limiting step in rDNA synthesis and the phosphorylation status of RRN3 has a significant impact on cell growth [88]. The phosphorylation of RRN3 is regulated by multiple pathways in response to intracellular or extracellular changes, e.g. cell cycle,

nutrient, and drug treatment, which will be reviewed later [99].

Although Pol I can independently generate a basal level of rDNA transcription, the efficient elongation of rDNA genes requires several other proteins, including Topoisomerase I/IIα which relieve the positive and negative supercoiling ahead of and behind the Pol I transcription complex [82, 100-103]. A number of DDR and repair components are also incorporated into the 'Pol I holoenzyme', including TFIIH, Cockayne syndrome B protein (CSB), Werner's syndrome helicase (WRN), Ku70/80 and several components of the NER machinery [104-106]. They are proposed to conduct transcription-coupled DNA repair occurring at rDNA genes to promote rDNA transcription, however the exact mechanism is still not fully understood [107]. Notably, UBF also plays an important role during this stage by phosphorylation-dependent remodelling of the rDNA chromatin, and its distribution is not restricted to the rDNA promoter region or the rDNA gene [108-110]. Our laboratory has previously demonstrated that the depletion of UBF1 directly silences the rDNA genes via increased binding of linker histone H1, an assembly of transcriptionally inactive chromatin structures that impedes the accessibility of the chromatin [111-113]. Besides, a few other chromatin remodellers are also involved in this process with various functions, e.g. the histone chaperones nucleolin, nucleophosmin, nucleosome remodelling and deacetylation (NuRD) complex and Williams syndrome transcription Factor (WSTF) [114, 115]. Transcription termination also involves a number of DNA binding elements and enzymes, including transcription termination elements binding factor TTF-I which pauses Pol I [116], the Polymerase I and transcript release factor PTRF [117], the 5' end to 3' end exonuclease XRN2 which cleaves the nascent rRNA [118] and the RNA helicase SEN1 which releases the rRNA from the rDNA [82, 119]. TTF-I has also been associated with re-initiation of Pol I by facilitating the juxtaposition of the terminator and promoter elements, which results in the formation of DNA loops [82, 117].

### 1.4.3. Regulation of Pol I transcription

Figure 1.1B summarises the positive and negative regulators of Pol I transcription. Pol I transcription is generally regulated by two mechanisms, namely the number of active rDNA genes and the rate of transcription [82]. These two mechanisms are dynamically regulated; for example, the decrease in active rDNA copy number can be compensated by an increased rate of Pol I transcription, resulting only in a minor change in overall rRNA synthesis [113, 120].

The number of actively transcribed rDNA genes can be affected by multiple factors, including but not restricted to the copy number of rDNA genes [121, 122], the methylation status in rDNA promoter region [123-127], the competitive binding of UBF and nucleosome components (histones) in rDNA coding regions [96, 111, 128, 129], the distribution of histone modifications at the rDNA promoter and intergenic spacers (IGS) [127, 128, 130], the binding of the insulator binding protein CTCF at the spacer promoter of rDNA [128, 130], and the binding of nucleolar remodelling complex (NoRC) associated RNA (also known as pRNA) to the rDNA promoter region [131]. NAD-dependent deacetylase sirtuin-1 (SIRT1) has been reported to be involved in NoRC by deacetylating TIF-IB, which will silence the rDNA and form heterochromatin in response to nutrient deprivation [132-134].

c-MYC, a transcription factor frequently amplified in cancer, plays a key and broad role in regulating Pol I transcription [135]. c-MYC activates rDNA transcription by both direct binding to rDNA promoter region and promoting the expression of Pol I transcription cofactors, including UBF, SL1 and RRN3 [136]. The binding of c-MYC to the rDNA chromatin is correlated to the increase in the acetylation of histone H3 and H4, which is an indicator of an open chromatin structure [137, 138]. c-MYC has also been reported to interact with TBP and TAF

components of the SL1 complex, which may facilitate recruitment of Pol I to the rDNA promoter [137]. It can also enhance the expression of RPs, which further promotes the manufacturing of ribosomes [85, 139].

Some other pathways also contribute to Pol I transcription regulation, especially the ERK pathway and PI3K/AKT/mTOR pathway [140]. The extracellular signal-regulated kinase (ERK, also known as MAPK) pathway is a signalling cascade that transfers the mitotic signal from cell-surface receptors, mainly receptor tyrosine kinases (RTK, e.g. HER2) or G-protein-coupled receptors (GPCRs), to the nucleus via a chain of protein kinases (Ras-Raf-MEK-ERK, Ras is not a kinase but a GTPase) [141]. It is one of the most frequently mutated and activated pathways in human cancer (~30%), which plays a predominant role in cell growth and proliferation [142]. c-MYC, TIF-IA and UBF are among the numerous targets of ERK [85]. Upon phosphorylation, the MYC protein is stabilised, thus facilitating its role in transcriptional regulation [143]. The previously described constitutively activated version of TIF-IA that accelerates the proliferation of HEK293T cells was generated by replacing a specific serine (serine 633) phosphorylated by ERK to aspartate (S→D), which mimics constitutive phosphorylation [88, 139]. ERK phosphorylates UBF at its HMG boxes and regulates Pol I elongation by inducing rDNA chromatin remodelling [108, 144, 145]. In addition, ERK has been reported to stimulate the expression of TBP, which is a key component of the SL-1 complex, as well as cyclin D, whose downstream kinases CDK4/6 phosphorylate and activate UBF [139, 146].

Similar to the ERK pathway, the PI3K/AKT/mTOR pathway is another important kinase cascade that transmits and amplifies the proliferative signals from membrane-bound receptors (e.g. HER2, HER2 activates both ERK and AKT pathways), which is frequently mutated and activated in human cancer [147, 148]. For example, phosphatase and tensin homolog (PTEN), a negative regulator of

downstream AKT pathway by dephosphorylating phosphatidylinositol-3,4,5-trisphosphate ($PIP_3$), is found mutated in more than 70% of prostate cancer cases [149-151]. Although the PI3K/AKT/mTOR pathway promotes cell proliferation and growth mainly by stimulating protein translation via mTOR complex 1 (mTORC1) activation [152], our laboratory as well as others have shown that the AKT pathway has a more direct role in regulating Pol I transcription [153]. We previously showed that the ribosomal protein S6 kinase 1 (S6K1), a major downstream target of mTORC1, phosphorylates UBF at its C-terminal activation domain, and a rapamycin-insensitive mutant of S6K1 stimulates rDNA transcription in the absence of serum [154, 155]. We have also shown that AKT can cooperate with c-MYC to promote rDNA transcription independent of mTORC1 [156], probably through casein kinase II (CK2), a protein kinase which can be phosphorylated and activated by AKT, which in turn phosphorylates and activates TIF-IA [157, 158].

A number of negative regulators are also involved in Pol I transcription regulation, including some well-known tumour suppressors, like PTEN, p53 and RB [139]. It is not surprising to detect enhanced rDNA transcription in PTEN mutant tumour cells when the inhibitor of AKT activation has been removed [159]. However, reports have also shown that PTEN may regulate the Pol I machinery in a more direct way as it can be co-immunoprecipitated with SL-1 and be crosslinked to rDNA repeats [160]. p53 is mutated in half of human tumours, and has been reported to repress rDNA transcription at multiple levels by both direct and indirect mechanisms [161]. Research has shown that recombinant p53 inhibits rDNA transcription in a cell-free transcription system by blocking the interaction between UBF and SL-1, and this blockade can be abolished by some point mutations that are commonly found in human cancer [162]. p53 can also activate the retinoblastoma tumour suppressor protein (RB) via p21, which binds to UBF and inhibits its interactions with SL-1 [161, 163-165]. Additionally, p53 can

suppress the expression of c-MYC by direct binding to its promoter [166], promote PTEN gene expression by direct binding to its upstream element [167], and deactivate mTOR via the tuberous sclerosis (TSC) 1/2 complex [168]. Furthermore, p53 can slow down rDNA transcription by inducing expression of the downstream CDK4/6 inhibitor p21 and thus blocking cell cycle progression [169]. As described previously, CDK4/6 can phosphorylate and activate UBF [146]. A p53 regulator, the nucleolar ARF protein ($p14^{ARF}$) has been shown to regulate Pol I transcription through both p53-dependent and -independent pathways [170]. Hyperproliferative signals provoked by oncogenic stimuli (e.g. RAS mutant) can activate $p14^{ARF}$, which can either bind and inhibit mouse double minute 2 homolog (MDM2) to ubiquitinate and inactivate p53 or bind to the rDNA gene promoter and interfere with UBF phosphorylation [161, 170]. Taken together, the ARF-p53-RB axis regulates both cell cycle and Pol I transcription, posing an important barrier against tumorigenesis.

However, from what has been reviewed above, it is clear that the regulatory pathways of Pol I transcription are complex and have significant crosstalk between each other. One potential mechanism of tumours becoming resistant to the inhibitors against these pathways is by the activation of redundant pathways that override the inhibition [148, 171, 172]. Therefore, it is important to target pathways as far downstream as possible to reduce the likelihood of redundancy or to use combination treatments to achieve complete blockade of the pathways [173-175].

### 1.4.4. Altered Pol I regulation pathways in HGSC

The expression of components of the Pol I transcription machinery has recently been found to be increased after chemotherapy, including UBF, POLR1B (the

second largest catalytic subunit of Pol I) and RRN3 [176]. Moreover, the Pol I regulation pathway has been found consistently altered in HGSCs [177]. As has been reviewed in previous sections, p53 mutation is predominant in HGSC and can be found in almost every HGSC case. The mutation of p53 is believed to be an early and crucial event in the initiation of HGSC and has been associated with the high chromosomal instability observed in HGSC [9, 11]. Next generation sequencing studies of p53 mutated HGSCs revealed that the majority of mutations occurs in exon 5-8, all of which encode the DNA-binding domain of p53 protein [178-180]. Of the mutations, 60-70% were missense and commonly associated with high p53 accumulation in cells. Low p53 accumulation was seen in 60% of HGSC associated with non-missense mutations, which accounts for 10-15% of the total mutations [181]. This is an interesting finding because the aggregated mutant p53, compared to p53 null, not only abrogates the tumour suppressor function of wild-type p53, but also promotes tumour progression and drug resistance in ovarian cancer, and is therefore considered a gain-of-function mutation [182-184]. It also highlights the involvement of nonsense-mediated mRNA decay (NMD) in carcinogenesis. NMD is a conserved surveillance mechanism used by the cells to eliminate transcripts with premature termination codons [185]. The NMD has been associated with the downregulation of tumour suppressor genes, like BRCA2, with NMD-elicit mutations which contribute to the genesis of particular cancers, though in the case of p53 it might be beneficial as the premature p53 transcripts could carry deleterious gain-of-function mutations [186-189]. The acquired function of mutant p53 is related to its altered binding to some chromatin regulatory genes, including methyltransferases MLL1 and MLL2 as well as acetyltransferase MOZ, which promotes genome-wide increases of histone methylation and acetylation [184, 190, 191]. This is also the reason why the restoration of wild type p53 function by targeting mutant p53 is increasingly gaining attention. Loss of RB, another negative regulator of Pol I transcription, is also found in 11% of HGSCs [192, 193]. This might be an

indication of drug resistance, which will be discussed in the following paragraph.

Alteration in the PI3K/AKT/mTORC1 pathway is found in 40% of HGSCs and is often associated with poor prognosis [15, 192]. The most common alterations are the amplification or upregulation of PIK3K and AKT1/2/3, which account for 20% and 15% of HGSCs respectively, with few overlaps between each other. Mutations are rare for both genes [15, 192]. On the other hand, the loss or mutation of PTEN accounts for 5-7% of HGSCs [192, 194]. Amplification or mutations in other genes such as HER2, mTOR, TSC1/2 have also been reported, but the incidence is low [194]. Although there is a strong rationale to treat HGSCs with PI3K/AKT/mTOR inhibitors due to its high frequency, clinical trial results have generally been disappointing [195]. A recent study indicated that this may be caused by 1) the activation of the ERK pathway, 2) loss of RB, and 3) altered expression of AKT isoforms [192]. As a result, the dual inhibition of AKT and ERK pathways or the use of pan-AKT inhibitors may be required for future therapy development. Detailed molecular analysis of tumour samples will also be necessary to identify the patients who will benefit most from the treatment.

Alterations in the ERK pathway occur in one-third of HGSCs, including the amplification of RAS isoforms (13%), the amplification of BRAF (7%) and loss or mutation of neurofibromatosis type 1 (NF1) (12%), a negative regulator of RAS [192, 196]. The high level of phosphorylated and activated MAPK has been related to the poor prognosis of HGSC, with median OS at 39 months compared to low pMAPK at 52 months [197]. However, it can also be used as a predictive marker for MEK inhibitor treatments as demonstrated in pre-clinical models [198]. Notably, upregulation in the ERK pathway frequently overlaps with upregulation in the AKT pathway (~40%) [192], which further confirms the crosstalk between these two pathways, and suggests the necessity of dual inhibition of both pathways. In fact, Dr Karen Sheppard from our program has already shown that the

combination of selective PI3K/mTOR and RAS/ERK pathway inhibitors can induce synergistic inhibition of ovarian cancer cell growth [173].

A key regulator of Pol I transcription, c-MYC, together with CCNE1 and MDS1 and EVI1 complex locus protein EVI1 (MECOM), are also found highly amplified in more than 20% of tumours by somatic copy number alterations (SCNAs) analysis [177, 199]. c-MYC overexpression is sufficient to independently transform the immortalised human fallopian tube secretory epithelial cell (FTSEC), and form high-grade Müllerian carcinomas that show morphologic, histologic, immunophenotypical, and genomic similarity to human HGSC, revealing the crucial and fundamental role of c-MYC in HGSC development [200].

## 1.5. Rationale to use CX-5461, an RNA Polymerase I transcription inhibitor, to treat ovarian cancer

As Pol I transcription has a significant impact on cell proliferation and its regulatory pathways are frequently altered in HGSC, it is rational to investigate the potential of targeting Pol I transcription for cancer therapy development [201]. Moreover, Pol I is the downstream of many OC oncogenes and therefore its targeting may overcome many of the resistance mechanisms to pathway inhibitors [99, 103, 156, 202-207]. Several compounds are currently available, including Actinomycin D, BMH-21 and CX-5461 [208]. Until 2009, Actinomycin D, a classic chemotherapy drug, has been the only compound that has shown selective inhibition of Pol I transcription. Actinomycin D blocks the elongation of Pol I by intercalating the GC-rich regions of DNA within the transcription complex, and shows specific Pol I inhibition at a concentration lower than 5nM [209]. However, Actinomycin D also inhibits Pol II transcription and DNA replication at higher

doses, causing strong DNA damage and toxicity that limits its use in the clinic [210]. In 2010, BMH-21 was identified in a cell-based high-throughput screen of synthetic chemical libraries using p53 transcriptional activation as the readout, and later was characterised as a Pol I transcription inhibitor [211]. It acts by binding to GC-rich DNA within the rDNA, inhibits Pol I transcription and activates degradation of the Pol I catalytic subunit RPA194 (POLR1A) and the Pol I complex [212, 213]. However, it does not activate DNA damage signalling, and instead induces cell cycle arrest and apoptosis via p53-dependent nucleolar stress, and has shown therapeutic effects in vivo [211, 214, 215].

On the other hand, CX-5461, a novel Pol I transcription inhibitor developed by our program in collaboration with Cylene Pharmaceuticals (now Senhwa Biosciences), not only reduced rDNA transcription [216, 217], but showed therapeutic efficacy in a variety of blood and solid tumours, either as a single agent or in combination [205, 217, 218] (Table 1.3). CX-5461 is the first Pol I transcription-specific inhibitor introduced to the clinic. In a phase I dose-escalation study in patients with advanced haematological malignancies (Peter MacCallum Cancer Centre, Melbourne, Australia), therapeutic efficacy (partial response + stable disease) was observed in 6 out of 16 patients with heavily pre-treated advanced hematologic malignancies [219]. The encouraging results have provided support for further clinical trials with larger number of patients. Meanwhile, another phase I/II trial in triple-negative breast cancer (TNBC) with BRCA1/2 mutations or homologous recombination deficiency (HRD) is currently being conducted in Vancouver, BC, Canada. Different from Actinomycin D, CX-5461 inhibits Pol I transcription by disrupting the recruitment of the SL1 complex to rDNA promoter region, thus impeding the initiation stage of Pol I transcription [218, 220]. CX-5461 executes its anti-proliferative effect via multiple mechanisms (Figure 1.2). In a B-cell lymphoma mouse model, CX-5461 induces nucleolar disruption and activation of p53-dependent apoptotic signalling while

sparing the normal B cell population, thereby working similarly to BMH-21 [221]. More specifically, CX-5461 treatment causes nucleolar disruption, releasing ribosomal proteins (RP), particularly RPL5 and RPL11, from the nucleolus, and their binding to MDM2, a p53 E3 ubiquitin ligase, leads to the accumulation of p53. This process can be blocked by overexpressing mutant p53 or the apoptosis inhibitor BCL-2 [221, 222]. However, in acute lymphoblastic leukaemia (ALL) cells, CX-5461 induces caspase-dependent apoptosis independent of p53 status. Instead CX-5461 activates the DNA damage checkpoint ataxia telangiectasia-mutated (ATM)/ ATM- Rad3-related (ATR) pathways, and its therapeutic effect can be further enhanced in combination with ATR inhibitors [223] or checkpoint kinases 1 and 2 (CHK1/2) inhibitors [224], which we have further confirmed in p53-null B-cell lymphoma [220]. Moreover, our data showed that the activation of ATM/ATR pathways is caused by an unusual open chromatin structure by an unknown mechanism that does not induce conventional DNA damage, and is specific to CX-5461 but not Actinomycin D [220]. The p53-independent anti-tumoural effect of CX-5461 has also been observed in a number of other mouse models of blood and solid tumours, including colorectal carcinoma [225], epithelial ovarian cancer [176, 225], melanoma [218], prostate cancer [226], multiple myeloma (MM) [227] and acute myeloid leukaemia (AML) [228]. In aggressive AMLs, CX-5461 outperforms standard chemotherapies and reduces leukaemia-initiating cell (LIC) populations via both p53-dependent apoptosis and p53-independent cell cycle arrest [228]. In multiple myeloma, CX-5461 induces p53-independent apoptosis by suppressing c-MYC expression, which is associated with MYC mRNA silencing mediated by RPL5 and the RNA-induced silencing complex (RISC) [227]. In osteosarcoma, CX-5461 induces p53-dependent autophagy-mediated cell death via the mTOR pathway [229]. A similar autophagy phenotype has also been reported in melanoma cells but it seems to be p53-independent [218].

CX-5461 has shown therapeutic potential in epithelial ovarian cancer as well. Selective lethality of CX-5461 against BRCA1/2 deficient cancer cells has been identified in various malignancies, including ovarian cancer cells. In these cases, CX-5461 acts as a DNA G-quadruplex stabiliser and induces DNA damage that is repaired by homologous recombination (HR) and non-homologous end joining (NHEJ) pathways [225]. However, CX-5461 only shows a variable response in EOC patient-derived xenograft (PDX) models with mixed background [176]. As HR deficiency occurs only in half of the HGSC patients, and restoration of HR function is a major cause of drug resistance, targeting HR-proficient HGSCs is still a critical challenge in the ovarian cancer therapy field.

One feasible alternative approach is to use drugs in combination. CX-5641 has shown enhanced therapeutic effects when combined with other drugs. In prostate cancer, using CX-5461 together with a PIM kinase inhibitor dramatically reduced large invasive lesions in both high-MYC and low-MYC expression mouse models and PDXs [226]. In lymphoma, combining CX-5461 with the mTORC1 inhibitor Everolimus doubled survival of Eμ-Myc lymphoma-bearing mice via independent pathways of each drug [230]. As a result, there is a rationale to investigate whether CX-5461 can cooperate with other drugs to treat HR-proficient HGSCs.

## 1.6. The DNA damage response (DDR) as a response to CX-5461 treatment

Cells are constantly dealing with DNA damage caused by various exogenous and endogenous DNA-targeting exposures, such as replication stress, telomere shorting, UV light, chemical toxins, and reactive oxygen species (ROS) that are generated during general metabolism and inflammation. Tens of thousands of DNA lesions are generated in the human body per day [231]. These lesions can stall genome replication and transcription, and if not repaired or improperly repaired, they could lead to mutations or large-scale genomic aberrations that may

lead to neurodegeneration, infertility, immunodeficiencies, and tumorigenesis, posing a significant threat to the survival of lives [232]. In order to cope with these threats, the body utilises intricate signalling pathways and repair mechanisms to regulate a variety of DNA lesions to protect genomic stability. In addition, a dysregulated DDR is frequently associated with cancer development, which may result in hypersensitivity or resistance to cancer therapy and can be exploited for the improvement of cancer treatment [233]. Cells can activate a number of distinct pathways responding to different types of DNA damage with common and distinct mechanisms, which will be covered in details in the following section (Table 1.4 and Figure 1.3).

### 1.6.1. DNA damage sensors and DNA damage repair

#### DNA double-strand break repair

Double-strand DNA breaks (DSBs) are the most dangerous DNA lesions as they can lead to massive loss of genetic information, chromatin translocation and cell death [234]. On the other hand, a number of cancer treatments utilise DSBs to kill cancer cells. DSBs can be induced by ionizing radiation (IR) and TOP2 inhibitors (e.g. doxorubicin) directly, both of which are widely used for cancer treatment [235, 236]. DSBs can also be indirectly generated from other DNA lesions, for example, a replication fork colliding with a single-strand break (SSB) or collapsed replication forks [237]. This mechanism plays an even more important role in cancer therapy because it can be used to target replicating cells but spare the non-replicating cells. A handful of chemotherapeutic agents depend on this ‘DNA lesions to DSBs’ conversion including cisplatin and Topoisomerase I (TOP1) inhibitors [238]. Non-homologous end joining (NHEJ) and homologous recombination (HR) are the two major pathways involved in repairing DSBs.

NHEJ is a repair pathway that can happen in all cell cycle phases (some reports claim that NHEJ only happens in G0/G1), while HR is another pathway which only occurs in the late S and G2 phases as it requires the homologous sequences on the sister chromatid [239]. In mammalian cells, the direct DSBs are predominantly repaired by NHEJ, while HR is specifically required for the repair of indirect DSBs induced by the collapsed replication forks (caused by the replication stress). Furthermore, HR is involved in repair of inter-strand cross-links (ICLs), which can cause replication stress as well, where it collaborates with NER [240, 241].

The canonical NHEJ (C-NHEJ) repair process can be divided into three stages. 1) When DSBs occur, the Ku70/Ku80 complex binds to the exposed DNA ends, followed by the recruitment and activation of the catalytic subunit DNA-PKcs. 2) Activated DNA-PKcs is then recruited and phosphorylates a variety of nucleases (e.g. Artemis), polymerases and polynucleotide kinases to process the ends. 3) The processed DNA ends are re-ligated by the XRCC4-LIG4 complex [242]. However, in the absence of functional C-NHEJ genes, like Ku70/80, a redundant alternative end-joining (alt-NHEJ or A-EJ) also exists [243]. When engaged by the alt-NHEJ, the DSBs ends are resected by MRE11 and CtIP nucleases, leaving short single-strand DNAs ready to be annealed [244, 245]. Microhomologic annealing with 2 to 4 complementary nucleotides then occurs between the ssDNA overhangs and the gap is filled by XRCC1 and Ligase III [246].The alt-NHEJ is highly mutagenic, particularly deleterious mutagenic, and is thus regarded as a significant contributor to the poor repair accuracy of NHEJ [247].

The HR repair process can be divided into four steps, namely 1) initiation, 2) homologous pairing and DNA strand exchange, 3) DNA heteroduplex extension, and 4) resolution [248]. Upon the detection of DSBs, the exposed DNA breaks are processed by nucleases and helicases (MRN nuclease complex, MRE11-

RAD50-NBS1) to form ssDNA at 3' tails of both ends via BRCA1, which competes with 53BP1, a promoter of NHEJ, to promote HR repair [249-252]. The MRN complex also activates ataxia-telangiectasia mutated (ATM), which phosphorylates a number of substrates including CHK2, MRE11, NBS1, H2AX and RAD51 to induce S and G2 arrest and stimulate HR repair [253]. Replication protein A (RPA) is then recruited to the ssDNA to protect it from forming secondary DNA structures [254]. The recruitment of RPA can activate ataxia-telangiectasia and Rad3-related (ATR), which can also phosphorylate a number of substrates (just like ATM) including CHK1 and RAD51 to induce S and G2 arrest and stimulate HR repair [255]. Next, RAD51 proteins are assembled onto the ssDNA with help of BRCA2 and RAD51 paralogs (RAD51B, RAD51C, etc.), and form a nucleoprotein filament called the presynaptic filament [256, 257]. The presynaptic filament is stabilised by RAD54, and invades into the homologous dsDNA region of sister chromatids to form a joint molecule. The RAD51 proteins are then removed by RAD54, followed by the recruitment of DNA polymerase to synthesise DNA using sister chromatids as templates [258, 259]. After the repair of the DNA breaks, the DNA heteroduplex is resolved or dissolved by Holliday junction resolvase and DNA ligase or RecQ helicase and topoisomerase III respectively, both of which produce two intact repaired dsDNA molecules [260].

NHEJ most frequently occurs during V(D)J recombination in the early stages of T and B cell maturation when a large number of DSBs generate highly diversified immunoglobins and T cell receptors [261]. This process is physiological and is not considered as a threat to genomic stability. However, during normal cellular homeostasis, the formation of DSBs is often pathologic and requires high-confidence repair to maintain the integrity of the genome. Even though NHEJ is able to repair the majority of the DSBs without an error, under circumstances when multiple DSBs exist, there is a high possibility that the NHEJ pathway would re-join the wrong DNA ends and create chromatin deletions or

translocations, which pose a significant threat to genome integrity. Furthermore, DSBs are not always blunt and single-strand DNA overhangs are sensitive to DNA modification enzymes such as endonucleases or polymerases (including the alt-NHEJ), which can cause frame shift mutations in the genome even if NHEJ re-ligates the right ends [262]. The unreliable DNA repair caused by NHEJ has been exploited by the latest gene editing technique CRISPR-Cas9, which induces multiple DSBs in the coding region of target genes. Deletions, insertions or frame-shift mutations are likely to occur if these DSBs are repaired by NHEJ, thus delivering efficient gene knockout [263].

Compared to NHEJ, homologous recombination (HR) uses a more reliable procedure to repair DSBs. Different from NHEJ, which can be activated throughout the cell cycle, HR repair is normally active for the repair of DSBs and ICLs during S and G2 phases when the sister chromatids are available [264]. HR also occurs during meiosis when DSBs are created intentionally to facilitate the recombination between sister chromatids which, in turn, promotes genetic diversity in the offspring [265]. In comparison with NHEJ, the HR provides an error-free, but less-efficient DSB repair pathway to maintain genomic stability. HR is the preferred way cells use to repair pathologic DSBs, as homologous recombination-deficient (HRD) cells demonstrate slower proliferation rate and hypersensitivity to genotoxic drugs compared to HR-proficient cells [266, 267]. However, when faced with excessive DSBs or defects in HR repair pathways, cells can only use error-prone NHEJ as a salvage DNA repair pathway, which leads to a more mutagenic genome and later tumourigenesis [268]. Due to the lack of homologous sequence pairing, NHEJ may join the wrong ends when multiple DSBs are happening at the same time, thus causing chromatin loss or chromatin translocation. The unfaithful repair by NHEJ has been considered to be the cause of the BCR-ABL fusion which is commonly found in chronic myelogenous leukaemia (CML), acute lymphoblastic leukaemia (ALL) or acute myelogenous

leukaemia (AML) [269]. This HR deficiency-chromosomal instability model is also currently being used to explain the initiation and progression of HGSC [11].

**Base Excision Repair**

Base excision repair (BER) removes abnormal bases which are oxidized, deaminated or alkylated. These abnormal bases are recognised and removed by corresponding glycosylases, causing apurinic/apyrimidinic (AP) sites [270]. The AP sites are then hydrolysed by an AP endonuclease, such as APE1, creating a DNA 'nick' [271]. The 'nick' can be repaired either by short-patch BER which fills a single nucleotide or by long-patch BER which fills up to 13 nucleotides. The single nucleotide in the short patch repair is replaced by DNA polymerase-β (Pol β) and the gap is re-ligated by ligase 3 (LIG3), and up to 13 nucleotides in long patch repair are replaced by Pol δ or Pol ε and re-ligated by LIG1 [272-274]. Both types of BER are promoted by XRCC1 and PARP1, which serve as molecular scaffold for the components of BER [240, 275-277].

**Mismatch repair**

Mismatch repair (MMR) is similar to BER, which corrects the altered bases (mispaired or fraudulent nucleotide) in the genome. The difference between MMR and BER is that MMR does not rely on the lesion-specific N-glycosylases of BER to recognise DNA lesions, which allows MMR to repair a wider range of base alterations [278]. MMR recognises abnormal bases by MSH2-MSH3 heterodimers, followed by the recruitment of MutLα complex (MLH1 and PMS2) to the lesion [279]. The endonuclease 1 (EXO1) is then recruited to cleave out the damaged oligonucleotide [280]. The resynthesis step is same as the long-patch BER [240, 275, 281].

## DNA single-strand break repair

The single-strand breaks (SSBs) repair is similar to BER (part of BER ). SSBs are the most common lesions that occur in cells, which are predominantly generated as BER intermediates (the DNA 'nick'). The stalling of TOP1 enzymes on chromatin is another source of SSBs [276]. Different from BER, trapped TOP1 needs to be removed by tyrosyl-DNA phosphodiesterase 1 (TDP1) [282-284]. The exposed DNA ends may need to be modified by polynucleotide kinase phosphatase (PNKP; a 3′ DNA phosphatase and 5′ DNA kinase) to restore the correct chemical configuration for base replacement and re-ligation [285]. The following steps are the same as BER [275, 276]. Examining the role of TOP1 in the response to targeting rDNA transcription with CX-5461 is a major focus of the studies described in the later part of this thesis and a detailed introduction of the functions of TOP1 can be found in Chapter 5.

## Nucleotide excision repair

Nucleotide excision repair (NER) acts to repair bulky DNA adducts such as UV-light-induced lesions (mostly intra-strand crosslinks, but can be inter-strand crosslinks as well) [286]. It is also partially involved in ICL repair [287]. NER is classified into transcription-coupled repair (TC-NER) which removes DNA lesions blocking RNA polymerase progression and global genomic repair (GG-NER), which remove DNA lesions independent of transcription [288]. The initial steps are different for these two pathways: the TC-NER requires Cockayne syndrome WD repeat protein A (CSA) and CSB [289], while the GG-NER is dependent on Xeroderma pigmentosum group C-complementing protein (XPC)–RAD23B and DNA damage-binding protein (DDB) to recognise the lesions [290]. XPA, replication protein A (RPA) and TFIIH are involved in both pathways [291-

293]. The damaged oligonucleotides are removed by XPG and ERCC1–XPF [294, 295], and the following resynthesis step is exactly the same as the long-patch BER [232, 240, 275]. It is worth noting that the trans-lesion synthesis (TLS), mediated by Pol ν, REV1 and Pol ζ, may be used to bypass the inter-strand crosslinks, which leave NER an error-prone repair pathway [296].

**Inter-strand crosslinks repair**

ICLs are DNA lesions that the nucleotides of complementary DNA strands are covalently linked, thus preventing the separation of the DNA double helix and inhibiting transcription and replication. It is one of the main exogenous causes of replication stress [297]. While the transcriptional coupled ICLs are mainly repaired by the NER pathways, the repair of replication coupled ICLs requires the cooperation of NER, HR and Fanconi anaemia (FA) pathways [298]. The FA pathway is extremely complex, with over 15 components. Some components are components of other DNA repair pathways. For example, FANCD1 is BRCA2 while FANCO is RAD51C, both of which are crucial components of HR [299]. The FANC and HR pathways indeed work closely with each other to repair the ICLs. When the replication fork is stalled by an ICL, the FANCM–FAAP24–MHF1/2 complex recognises the stalled replication fork structure and recruits the FA core complex to the ICL region [300]. FANCM also activates the ATR-CHK1 cell cycle checkpoint response, which in turn phosphorylates multiple FA proteins, including FANCA/E/D2/I [301-303]. Monoubiquitinated FANCD2 (the monoubiquitylation is crucial for FANCD2's function) and FANCI are then recruited to the DNA lesion and act as a platform to recruit multiple nucleases, possibly FANCP/SLX4 or ERCC1–XPF, to execute nucleolytic incisions flanking the ICL [304-306]. The incision creates DSBs as well as leaves the cross-linked nucleotides isolated and tethered to the complementary strand, which is bypassed by TLS [307]. NER removes remaining adducts and fills the gap. The

DSB created by the incision is repaired by HR using the newly synthesized DNA strands, rather than the sister chromatid, as the template [308]. Lastly, the USP1–UAF1 complex removes monoubiquitin from FANCD2-I [309, 310]. Due to the existence of TLS, ICL repair is error prone and is a source of point mutations [311, 312].

**The repair of replication stress**

Replication stress is a phenomenon when the DNA replication machinery is obstructed by intracellular or extracellular factors, such as stalled TOP1 enzymes or ICLs, which results in stalled replication forks. These forks, if not restored, would lead to replication fork collapse, which may result in DSBs and seriously undermine genomic stability and cell survival. Replication stress can arise from various sources, including but not restricted to ssDNA caused by missing nucleotides (e.g. nicks and gaps) , DNA lesions (e.g. adducts and dimers), R-loops, DNA secondary structure, or enzymes trapped on the DNA [313].

Nicks and gaps are common by-products of several DNA repair pathways (e.g. nucleotide excision repair (NER) and base excision repair (BER)) and the release of topological stress by TOP1, which cleaves one strand of the DNA helix to relieve the topological stress (See details of TOP1 in section 5.1.1). A DSB forms passively when the DNA replication machinery encounters a DNA nick or gap. The repair of this type of DSB is very similar to conventional HR, which also involves i) initiation, (ii) homologous pairing and DNA strand exchange, (iii) DNA heteroduplex extension, and (iv) resolution, except that the intact DNA branch, rather than the sister chromatid, is used as the template of the repair [313].

The DNA replication machinery can also be stalled by DNA adducts, proteins trapped on chromatin or DNA secondary structures, like G4-DNA or RNA-DNA

hybrids (R-loops, see details about R-loops in section 5.2.8). Upon the blockade of DNA replication machinery, RPA protein binds to the ssDNA in the stalled replication forks to prevent the formation of secondary DNA structures [314]. It also activates DDR components, particularly ATR, to inhibit cell cycle progression and suppression of late origin firing, which provides additional time to allow the source of stress to be removed [315, 316]. However, it is possible that the stress cannot be removed, and the forks fail to restart and collapse, leading to DSB formation. Under this scenario, conventional HR would restore replication using sister chromatids as templates [313, 317].

Replication stress can also happen when the replication machinery encounters DNA dimers, which are commonly caused by UV-B or other chemicals. DNA dimers block the progression of DNA polymerases but not DNA helicases, thus uncoupling the replication machinery and creating long ssDNA between the lesion and helicases [318]. Similar to other scenarios, RPA proteins binds to the ssDNA and activates downstream response factors including ATR and ATM, which stall the helicase in order to repair to the lesion [319-322]. The DNA dimer-induced replication stress can be overcome by two different mechanisms: i) The DNA dimers, together with the adjacent nucleotides, can be cleaved by nucleases (e.g. Mus81) and creates DSBs [323]. The DSBs are then repaired by HR using the intact DNA strand as the template; ii) The replication fork can reverse, rewind the parental DNA and extrude the newly replicated strands. The stalled DNA strands then employ the HR pathway and bypass the DNA lesion using the extruded strands as templates. This lesion bypass pathway is also termed “DNA damage tolerance” (DDT) [324].

CX-5461 has been reported to induce replication stress by both Xu, et al. and our group [225, 325]. Also, Xu, et al. proposed that the CX-5461 induces replication stress as a G4-DNA stabiliser [225]. Due to the strong association of CX-

5461/TOP1 and replication stress, we investigated its contribution to the combination of CX-5461 and TOP1 inhibition, and the details can be found in section 5.2.7.

### 1.6.2. Cellular responses to DNA damage

The DDR is not only a DNA damage sensing-repair mechanism, but also orchestrates the cell cycle via checkpoint signalling cascades to provide sufficient time for repair and prevent replication and mitosis with DNA damage, which, if not repaired, will lead to mitotic catastrophe and genomic instability (Figure 1. 3). Three PI3K-related protein kinase (PIKK) family of enzymes, ATM, ATR and DNA-PKcs, play the central role in this cascade [326]. ATM is recruited by the MRN complex to the lesion upon DSB generation and is activated via autophosphorylation at S1981 [327], while ATR binds to the RPA-coated ssDNA via its partner protein ATR interacting protein (ATRIP) in response to multiple types of DNA damage (BER, MMR, NER, ICL, HR, etc), and is activated by autophosphorylation at T1989 [328], which is recognised by topoisomerase binding partner 1 (TOPBP1) in complex with the RAD17-RFC2-5 clamp loader, the 9-1-1 complex (RAD9–RAD1–HUS1), Claspin, and RHINO [328]. DNA-PKcs is traditionally regarded as a key component of non-homologous end-joining (NHEJ) (See Chapter 1.1.5 for details), but has recently been reported to regulate ATM [329]. This regulation can be both positive and negative; while the presence of DNA-PKcs promotes the stability of ATM protein [330], it negatively regulates ATM activity through phosphorylation of ATM at multiple sites [331].

ATM/ATR/DNA-PKcs phosphorylate several shared or unique substrates, with the most studied ones being RPA32 (by all three PIKKs), checkpoint kinases 1 and 2 (CHK1 by ATR and CHK2 by ATM/DNA-PKcs [332]), KRAB-associated protein 1(KAP1 by ATM and ATR), 53BP1 (by ATM) [333, 334], p53 (by ATM

and ATR), and H2AX (by ATM/ATR, or by DNA-PKcs in the absence of ATM) [335].

RPA32 (also called RPA2) is one of the three subunits of RPA that binds and acts as the first sensor of ssDNA [336]. ssDNA is commonly caused by DNA damage or replication/transcriptional stress. The binding of RPA not only prevents the ssDNA from forming secondary DNA structures, but also activates the DDR, particularly ATR, to inhibit cell cycle progression and suppress late origin firing, which provides additional time to allow the source of stress to be removed [337, 338]. Multiple PIKK-mediated phosphorylation sties have been identified at the N-terminus of RPA32, including S4, S8, T21, S12 and S33, however, there is no consensus about how these three PIKKs target specific sites [339]. A popular model is that upon the formation of the RPA-ssDNA complex, it is recognised and phosphorylated by the ATRIP-ATR complex at S33. In turn, S33 phosphorylation promotes the ATM/DNA-PKcs-mediated phosphorylation at S4, S8 and S12 [340, 341]. The full activation of ATR is dependent on the phosphorylation of S4 and S8, and mutations at these sites can largely impair the capability of ATR to phosphorylate the downstream targets like CHK1 [329]. TOPBP1 is also required for this process [321].

53BP1 is a large protein with molecular weight over 200kDa. It does not carry any enzymatic activity but instead serves as a recruitment platform for other DDR components, including RAP1 interacting factor 1 (RIF1) and Pax transactivation domain-interacting protein (PTIP), both of which are the key components of C-NHEJ [342]. 53BP1 is a highly regulated protein with numerous phosphorylation sites including 32 PIKKs and 41 CDKs phosphorylation sites. It has been reported that ATM phosphorylates 53BP1 at multiple sites, including T302, S831, S176, S178 and S452 [343], while the binding of 53BP1 to ATM also promotes the self-phosphorylation of ATM at S1981, as well as the phosphorylation of CHK2 at

Y68 by ATM [344]. 53BP1 can also be phosphorylated by ATR in the case of UV-induced DNA damage [343]. After phosphorylated by ATM, 53BP1 recruits RIF1 and PTIP to the DSB sites, blocks the DNA ends resections and activates the downstream NHEJ DNA repair process, with the exact mechanisms remaining unclear [345]. One of the profound roles played by the 53BP1 during this process is its competitive binding to the DSB sites against BRCA1, a key initiator of the HR process, thus acts as an antagonist of the HR (See details of HR and BRCA1 in section 1.6.1). The loss of BRCA1 blocks the resections of DNA breaks and shifts the balance of DNA repair towards the 53BP1 mediated C-NHEJ [346], while the double knockout of BRCA1 and 53BP1 rescues the BRCA1 deficiency and shifts the balance back to HR [347]. The competition between BRCA1 and 53BP1 thus orchestrates a key decision-making process in determining the pathways used for DSBs repair [348]. However, the question still remains regarding how cells shift from the 53BP1 promoted NHEJ in G1 to the BRCA1 promoted HR in S/G2 under normal circumstances without 53BP1 or BRCA1 deficiencies. Reports have shown that 53BP1(or BRCA1) is still functional in S/G2(or G1) phases in the absence of BRCA1 (or 53BP1), suggesting the existence of a third-party regulatory mechanism [349]. CtIP nucleases have been proposed to be the key regulator in this process as it is resection activity is controlled by the phosphorylation by CDKs in S phase [350], and mutations at its CDK phosphorylation sites lead to the failure of the removal of RIF1 from the DSB sites [349].

CHK1 is activated by ATR-mediated phosphorylation at residues S317 and S345 [351]. Activated CHK1 can further phosphorylate CDC25A and CDC25C, which dissociate their binding from cyclin-dependent kinases 2 and 1 (CDK2 and CDK1), respectively, and maintain CDK2 and CDK1 in an inactive status, thus causing cell cycle arrest at G1/S, S and G2 phases [352, 353]. CHK1 also phosphorylates and activates WEE1, a nuclear kinase that inhibits CDK1 by

phosphorylating it at Y15 [354, 355]. Similarly, CHK2 is activated by ATM/DNA-PKcs-mediated phosphorylation at residue T68 upon DSB generation [356, 357], and the activation of CHK2 can also phosphorylate CDC25A and CDC25C and induce cell cycle arrest and senescence [358, 359].

p53 is one of the main substrates of ATM (some reports claim that p53 can be activated by ATR as well [320]). p53 plays a central role in tumour suppression by either blocking the cell cycle by promoting the expression of p21 or/and p27, a cyclin-dependent kinase inhibitor that is able to bind and deactivate CDK1/2/4/6 [360], or by inducing apoptosis by promoting the expression of apoptosis activators BID, BAX, NOXA and PUMA [361]. ATM stabilises and activates p53 either by directly phosphorylating p53 protein at S15, by phosphorylating p53 protein at S20 via CHK2, or by indirectly phosphorylating and deactivating HDM2, the well-known p53 suppressor [362, 363]. Apart from p53, a recent finding has identified KAP1 as a phosphorylation target of ATM as well. KAP1 has been reported as a suppressor of p21 gene transcription under basal conditions. However, the ATM and CHK2 can phosphorylate KAP1 at S824 and S473 respectively upon DNA damage, and the KAP1 phosphorylation deactivates KAP1-suppressive function and p21 expression is increased [364, 365].

Moreover, ATR (in response to ssDNA or replication stress), ATM or DNA-PKcs in the absence of ATM can phosphorylate the histone H2A variant (H2AX) at serine 139 on chromatin flanking DSB sites [366-368]. This phosphorylation creates a binding platform for Mediator of DNA damage checkpoint protein 1 (MDC1) [369], which subsequently recruits E3 ubiquitin ligase RNF8 and RNF168 to the DSB foci [370, 371]. RNF8 and RNF168 ubiquitylate linker histone H1 at Lys-63 and H2A at Lys-13/15 respectively [372, 373], leading to the recruitment and retention of BRCA1 and 53BP1 to the DSB sites [374]. In general, upon the formation of DSBs, the MRN, ATM, MDC1 and

RNF8/RNF168 are among earlier responders found at the DSB foci, followed by the 53BP1 and BRCA1 and the downstream cascades [370].

Recently, a new pathway has emerged to connect DNA damage to inflammation, senescence, and cancer. The cGAS–cGAMP–STING pathway is a conserved mechanism that is used to detect the existence of microbial DNA in the cytosol to alert the host immune system to respond to microbial infections [375]. However, recent research has revealed that this pathway can respond to innate accumulation of cytoplasmic DNA caused by DNA damage by cytotoxic drugs or irradiation as well [376, 377]. Briefly, the cGAS–cGAMP–STING pathway consists of cyclic guanosine monophosphate (GMP)–adenosine monophosphate (AMP) synthase (cGAS), which is a DNA sensor that triggers innate immune responses through producing the second messenger cyclic GMP-AMP (cGAMP), which in turn binds and activates the adaptor protein Stimulator of Interferon Genes (STING).

The cytosolic DNA is typically in the form of micronuclei, which is the result of intense DNA damage and genomic instability. Genomic instability includes DNA alterations ranging from nucleotide instability (NIN) to microsatellite instability (MIN) and chromosomal instability (CIN) [378]. Micronuclei indicate CNI which is the most common form of genomic instability and can cause changes in both chromosome number and structure. A number of methods are available to assess each type of genomic instability, including karyotyping (CIN), flow cytometry (CIN), single nucleotide polymorphism (SNP) arrays (CIN, NIN), genome sequencing (CIN, NIN), and polymerase chain reaction (PCR) (MIN) [379]. Upon binding cytosolic DNA, cGAS catalyses the reaction of GTP and ATP to form cyclic cGAMP [380]. cGAMP then binds to stimulator of interferon genes (STING), which phosphorylates IRF3 via TBK1 [381]. IRF3, in turn, translocates to the nucleus to activate transcription of inflammatory genes including ligands of natural killer (NK) cells such as NKG2D ligands, type I IFNs and other

cytokines [382]. These inflammatory proteins attract NK cells and CD8+ T lymphocytes to remove the damaged cells [383].

In addition to the inflammatory responses, it has been reported that the cGAS–cGAMP–STING pathway can regulate cellular senescence as well. It is believed that cGAS–cGAMP–STING-induced senescence occurs mainly via the senescence-associated secretory phenotype (SASP) [384, 385]. SASP is a phenomenon by which senescent cells produce and release a group of cytokines, chemokines and proteases, such as IFN-β, IL-1β, IL-6, and IL-8, to the extracellular environment to modulate senescent cells themselves and the microenvironment [383]. Multiple reports have shown that these cytokines, as well as interferons can enhance senescence either via p53 pathways or via ATM/ATR pathways by enhancing the levels of reactive oxygen species (ROS) [386-388].

Taken together, the DDR is a highly complex network, which has evolved to maintain genomic stability and prevent disease, and generally plays a suppressive role in tumorigenesis, although sometimes it can be taken advantage of by tumour cells to act against the cytotoxic drug by increasing DNA repair capacity or facilitating the invasion and metastasis [389]. The genesis of a high proportion of HGSC is associated with alterations in the DDR pathways that are the target for first line therapy with platinum-based cytotoxics and now PARP inhibitors. Furthermore, targeting the DDR is also a key therapeutic mechanism of CX-5461 based therapies (See section 1.5 and 1.6.1). Therefore, a better understanding of the DDR network is required for the development of new therapies, including CX-5461 based therapies, to combat OVCA.

## 1.7. Hypothesis, aims and approach

Currently there is a lack of therapeutic options for chemo-refractory and chemo-resistant HGSC patients, and the prognosis is dismal. New therapies are required to improve the prognosis of ovarian cancer patients. The association between low rDNA CpG methylation level (high transcription level of rDNA) and shorter PFS in ovarian cancer [390, 391] as well as the frequent alteration in the complex RAS/PI3K/MYC network regulating Pol I activity in HGSCs [208] has made ribosome biogenesis a logical target for OVCA treatment. CX-5461, a Pol I transcription inhibitor, has shown therapeutic efficacy in a number of blood and solid tumours, and is currently undergoing clinical trials in advanced haematological malignancies and breast cancer. However, as of yet it has only shown moderate effects in EOC, especially those with proficient HR pathways. In fact, our preliminary data utilising a panel of 36 ovarian cancer (OVCA) cell lines suggest that acute CX-5461 treatment results in cell cycle arrest but not cell death. As a result, we hypothesise that some genes can be targeted to enhance the therapeutic outcome of CX-5461 in HGSC with proficient HR pathways. By adopting a genome-wide RNAi screen approach, we aim to identify potential targets, preferably drug targets, whose inhibition can cooperate with CX-5461 to enhance its anti-tumoural effect against ovarian cancer.

## Table 1.1 Histotypes and genetic alterations of OC

| | Epithelial type | | | | | Germ type | Stromal type |
|---|---|---|---|---|---|---|---|
| **Subtypes** | High-grade serous carcinoma (HGSC) | Low-grade serous carcinoma (LGSC) | Clear cell carcinoma (CCC) | Endometrioid carcinoma (ENOC) | Mucinous carcinoma (MUC) | - | - |
| **Origin** | Fallopian tube epithelium | Ovarian surface epithelium | Endometrium | Endometrium | Unclear | Primitive germ cells | Sex-cord stromal cells |
| **Prevalence (of all OC cases)[1]** | ~54% | ~8% | ~11% | ~13% | 3~4% | 1~2% | 1~2% |
| **Genomic instability** | High | Low | Low | Low | Low | Low | Low |
| **Genetic alteration** | TP53 mut (>90%) | TP53 wt | TP53 wt | TP53 wt[2] | TP53 wt | TP53 wt | TP53 wt |
| | BRCA1/2(~15%) HR deficiency (up to 50%) | HR deficiency rare (<8%) | HR proficient | HR proficient | HR proficient | HR proficient | HR proficient |
| | EGFR, PI3K, AKT2, c-MYC, ERBB2 | KRAS, BRAF, ERBB2 (>68%) | ARID1A PIK3CA | CTNNB1(~44%) ARID1A PIK3CA | KRAS (up to 80%) ERBB2 | c-KIT Cyclin D2 | FOXL2 DICER1 |
| **5-years survival rate** | ~40% | ~70% | >70% | >90% | ~78% | >82% | >90% |

[1]The sum is not 100% as some rare OC subtypes are not included in the table.
[2]Some reviews have claimed that *TP53*mut in late ENOC could be up to 50%, while some other reviews have indicated that those samples should better be classified as HGSC [5, 16].

## Table 1.2 Novel drugs recently approved or under development for OC

| Category | | Agent (manufacturer) | Mechanism of action | Clinical status |
|---|---|---|---|---|
| Targeted agents | VEGF-dependent angiogenesis inhibition | Cediranib (AZD2171) (AstraZeneca) | Oral VEGFR-1,-2,-3 tyrosine kinase inhibitor | Failed as single drug; Phase II as drug combination |
| | | Nintedanib (BIBF1120) (Boehringer Ingelheim) | Oral VEGFR, PDGFR, FGFR tyrosine kinase inhibitor | Failed as single drug; Phase III as drug combination |
| | PARP inhibitors | Olaparib (AZD2281) (AstraZeneca) | Oral Poly (ADP-ribose) polymerase-1,-2 inhibitor | FDA Approved |
| | | Rucaparib (CO-338) (Clovis Oncology) | Oral Poly (ADP-ribose) polymerase-1,-2 inhibitor | FDA Approved |
| | | Niraparib (MK-4827) (Merck) | Oral Poly (ADP-ribose) polymerase-1,-2 inhibitor | FDA Approved |
| | MEK inhibitors | Selumetinib (AZD6244) (AstraZeneca) | Oral inhibitor of MEK-1,-2 | Phase II as single drug; Phase I as drug combination |
| | | Binimetinib (MEK162) (Novartis) | Oral inhibitor of MEK-1,-2 | Failed as single drug; Phase I as drug combination |
| Cytotoxic agents | | Etirinotecan pegol (NKTR-102) (Nektar) | Inhibits Topoisomerase I (IV) | Phase II as single drug |
| | | Paclitaxel poliglumex (CT2103) (CTI BioPharma) | Mitotic inhibitor (IV) | FDA approved |
| | | Lurbinectedin (PM1183) (PharmaMar) | Marine-derived DNA minor groove binder (IV) | FDA approved |
| Therapeutic vaccines | | Catumaxomab (Trion Pharma) | Trifunctional antibody binds EpCAM, CD3, and Fc receptor | FDA approved, but commercially failed |

## Table 1.3 Current application of CX-5461

| Tumour types | Treatments | Models | Mechanisms |
|---|---|---|---|
| B-cell lymphoma | CX-5461 only [179] | Cell lines, xenografts and mouse models | p53-dependent apoptosis via nucleolar stress |
| | CX-5461+Everoulimus [188] | Cell lines and xenografts | Independent pathways of each drug |
| B-cell lymphoma (p53-null) [189] | CX-5461 only | Cell lines and xenografts | p53-independent cell cycle arrest via DNA damage checkpoint |
| | CX-5461+CHK1/2i | Cell lines and xenografts | p53-independent cell death |
| Acute lymphoblastic leukemia | CX-5461 only [182] | Cell lines | p53-independent cell cycle arrest via DNA damage checkpoint |
| | CX-5461+ATM/ATRi [181] | Cell lines | p53-independent apoptosis |
| | CX-5461+CHK1/2i [181] | Cell lines | p53-independent apoptosis |
| Acute myeloid leukemia [186] | CX-5461 only | Cell lines, xenografts and PDX | p53-dependent apoptosis and -independent cell cycle arrest |
| Multiple myeloma [185] | CX-5461 only | Cell lines | p53-independent apoptosis via c-MYC suppression |
| Osteosarcoma[187] | CX-5461 only or CX-5461+doxorubicin | Cell lines and xenografts | p53-dependent autophagy-mediated cell death |
| Pancreatic cancer [176] | CX-5461 only | Cell lines, xenografts | p53-independent autophagy |
| Melanoma [176] | CX-5461 only | Cell lines, xenografts | p53-independent autophagy |
| Prostate cancer[184] | CX-5461+ PIM kinase inhibitor | Cell lines, mouse model and PDXs | p53-independent cell cycle arrest |
| Multiple types with BRCA1/2 deficiency [183] | CX-5461 only | Cell lines, xenografts and PDXs | p53-independent cell death |
| Epithelial ovarian cancer [190] | CX-5461 only | Cell lines and PDXs | p53-independent cell cycle arrest |
| Advanced haematological malignancies | CX-5461 only | Ongoing clinical trial | N/A |
| Breast cancer | CX-5461 only | Ongoing clinical trial | N/A |

## Table 1.4 Predominant DNA damage repair pathways

| DDR mechanism | Type of damage | Source of damage | Damage sensors | Signal transducers | Damage repair effectors | Cell cycle dependency |
|---|---|---|---|---|---|---|
| **Mismatch repair (MMR)** | DNA mismatches and insertion/deletion loops | DNA replication | MSH2, MSH3, MSH6, MLH1, PMS2 | | EXO1, POLD, LIG1 | G1/S |
| **Base excision repair (BER)** | Abnormal DNA bases | Alkylating agents, etc | DNA glycosylase, APE1 | | As for SSBR | G1/S |
| **Single-strand break repair (SSBR)** | Single-strand DNA breaks | IR, ROS, TOP I inhibitors, H2O2, alkylating agents, etc | PARP | | XRCC1, PNKP, POLβ, FEN1, TDP1, Aprataxin, LIG1, LIG3A | G1/S |
| **Nucleotide excision repair (NER)** | Lesions that disrupt the DNA double-helix | Alkylating agents, X-linkers, bulky base adducts and UV photo-products | RNA polymerase, XPC, DDB2, CSA | XPA, XPF, RPA | XPG ERCC1 POLE POLD1 LIG1, LIG3 | G1/S |
| **Interstrand cross-link (ICL) repair** | ICLs | X-linking agents | FA core complex (FANCA, B, C, E, F, G, L and M) | BRCA2, FAND2, BRIP1, PALB2], RAD51C, SLX4 | Shared with HR, TLS, and NER | S |
| **Translesion synthesis (TLS)** | Base damage blocking replication-fork progression | UV, alkylating Agents, ICL, etc | PCNA | RAD6, RAD18 | REV1, POLH POLI, POLK | S |
| **Non-homologous end-joining (NHEJ)** | Double-strand DNA breaks ( DSBs) | IR, TOP2 Inhibitors, V(D)J | Ku70/Ku80 | DNA-PK | XRCC4, XLF, LIG4, APLF, Artemis PAXX, WRN | G1/S/G2 |
| **Homologous recombination (HR)** | DSBs | Stalled replication forks, ICLs, sites of meiotic recombination, TOP I inhibitors | MRN | ATM, ATR, MK2, CtIP, BRCA1/BARD1, BRCA2, PALB2, RPA | RAD51, MUS81/EME, SLX1/SLX4, RTEL1, BLM, TOP3, POLQ, PARI, RECQL5, FANCJ, BLM | S/G2 |
| **ATM-mediated DDR signalling** | DSBs | | MRN | ATM, CHK2, MDC1, 53BP1, MCPH1/BRIT1, RNF8, RNF168/RIDDLIN and BRCA1 | | S/G2 |
| **ATR-mediated DDR signalling** | ssDNA, resected DSBs | | ATRIP, RPA, RAD9-RAD1-HUS1 | ATR, CHK1, Claspin, MCPH1/BRIT1 and BRCA1, CtIP | | S/G2 |

**Figure 1.1 The initiation and regulation of Pol I transcription**

**A**. A brief diagram of the mechanism for Pol I transcription initiation. **B**. A summary of the key positive and negative regulators of Pol I transcription and their regulatory targets.

**A**

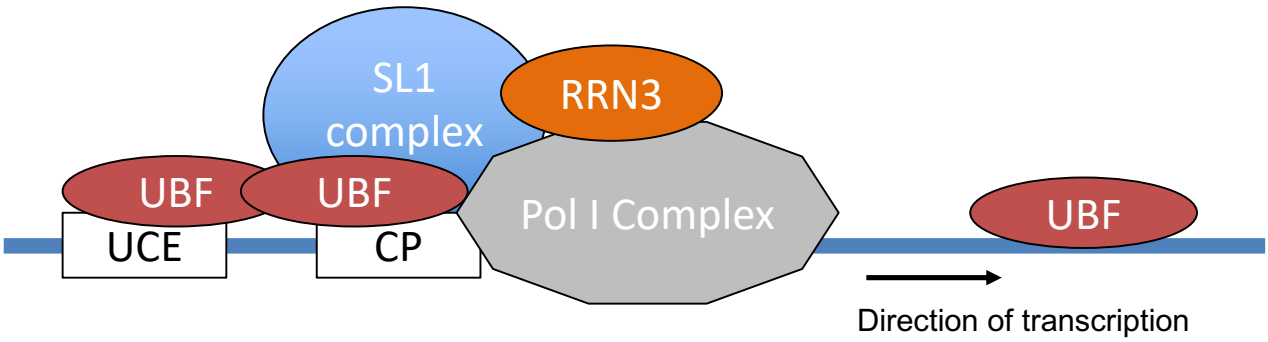


**B**

Key Pol I transcription regulators

| Positive regulators | Negative regulators | Target of the regulators |
|---|---|---|
| PAF53, c-MYC, ERK, S6K1, CDK4/6, AKT | p53, p21, $p14^{ARF}$ | UBF |
| c-MYC, ERK, CK2, AKT | | RRN3 |
| c-MYC, ERK | PTEN, p53, p21, RB | SL1 |
| TFIIH, CSB, WRN, Ku70/80, NER components, TOP1/2 | | Transcriptional associated DNA damages |
| UBF, demethylation, CTCF, c-MYC, mutant p53 | Methylation, histones, NoRC, SIRT1, p53, $p14^{ARF}$ | rDNA chromatin |

**Figure 1.2 p53-dependent and -independent mechanisms of CX-5461**

A schematic diagram of the p53-dependent and -independent anti-tumoural mechanisms of CX-5461. The p53-dependent mechanism involves the release of ribosomal proteins (RP), particularly RPL5 and RPL11, from the nucleolus, and their binding to MDM2, a p53 E3 ubiquitin ligase, leads to the accumulation of p53, thus causing apoptosis and cell cycle arrest. On the other hand, the p53-independent mechanism induces cell cycle arrest via ATM/ATR pathways, with the exact triggers remaining unknown.

*Figure 1.2 is a direct re-use of Figure 3 with no modification from *Yan, S.; Frank, D.; Son, J.; Hannan, K.M.; Hannan, R.D.; Chan, K.T.; Pearson, R.B.; Sanij, E. The Potential of Targeting Ribosome Biogenesis in High-Grade Serous Ovarian Cancer. Int. J. Mol. Sci.* ***2017****, 18, 210.* (https://www.mdpi.com/1422-0067/18/1/210)

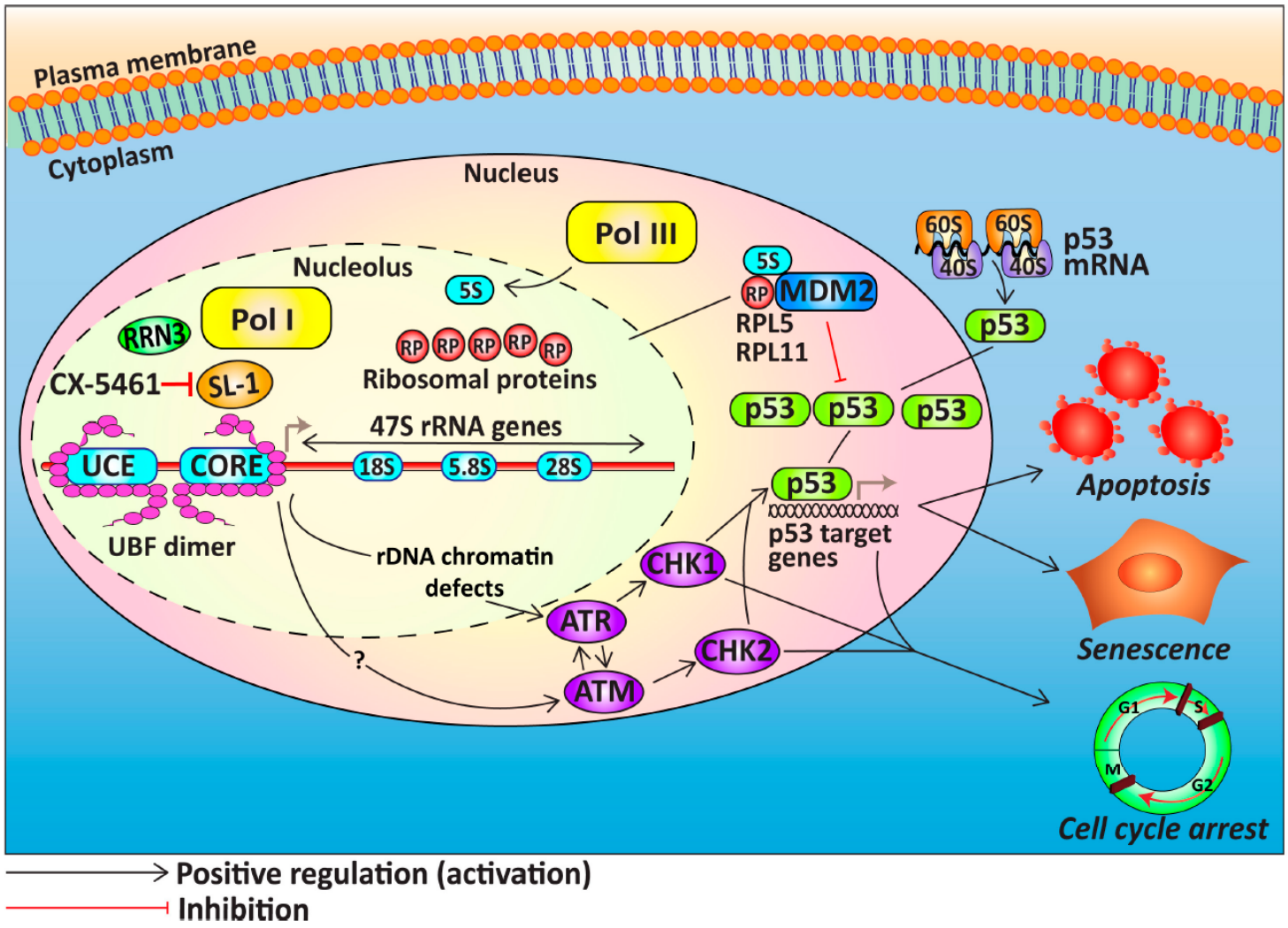
Plasma membrane
Cytoplasm
Nucleus
Nucleolus
Pol III
Pol I
RRN3
CX-5461
SL-1
5S
RP
Ribosomal proteins
47S rRNA genes
UCE
CORE
18S
5.8S
28S
UBF dimer
rDNA chromatin defects
?
ATR
ATM
CHK1
CHK2
MDM2
RPL5
RPL11
60S
40S
p53 mRNA
p53
p53 target genes
Apoptosis
Senescence
G1
S
M
G2
Cell cycle arrest
Positive regulation (activation)
Inhibition

**Figure 1.3 Summary of the DNA damage repair mechanisms**

A schematic summary of the currently known DNA damage repair mechanisms including the base excision repair (BER), mismatch repair (MMR), nucleotide excision repair (NER), non-homologous end joining (NHEJ), homologous recombination (HR) and inter-strand crosslink (ICL) repair. Although the sensors of different types of DNA damage are normally different from each other, there is significant overlap during the repair process, especially in ICL repair.

*Figure 1.3 is a direct re-use of Figure 2, 3, 4b and 5 with no modification from *Curtin NJ, DNA repair dysregulation from cancer driver to therapeutic target. Nature Reviews Cancer. **2012**, 12:801.* (https://www.nature.com/articles/nrc3399#article-info).

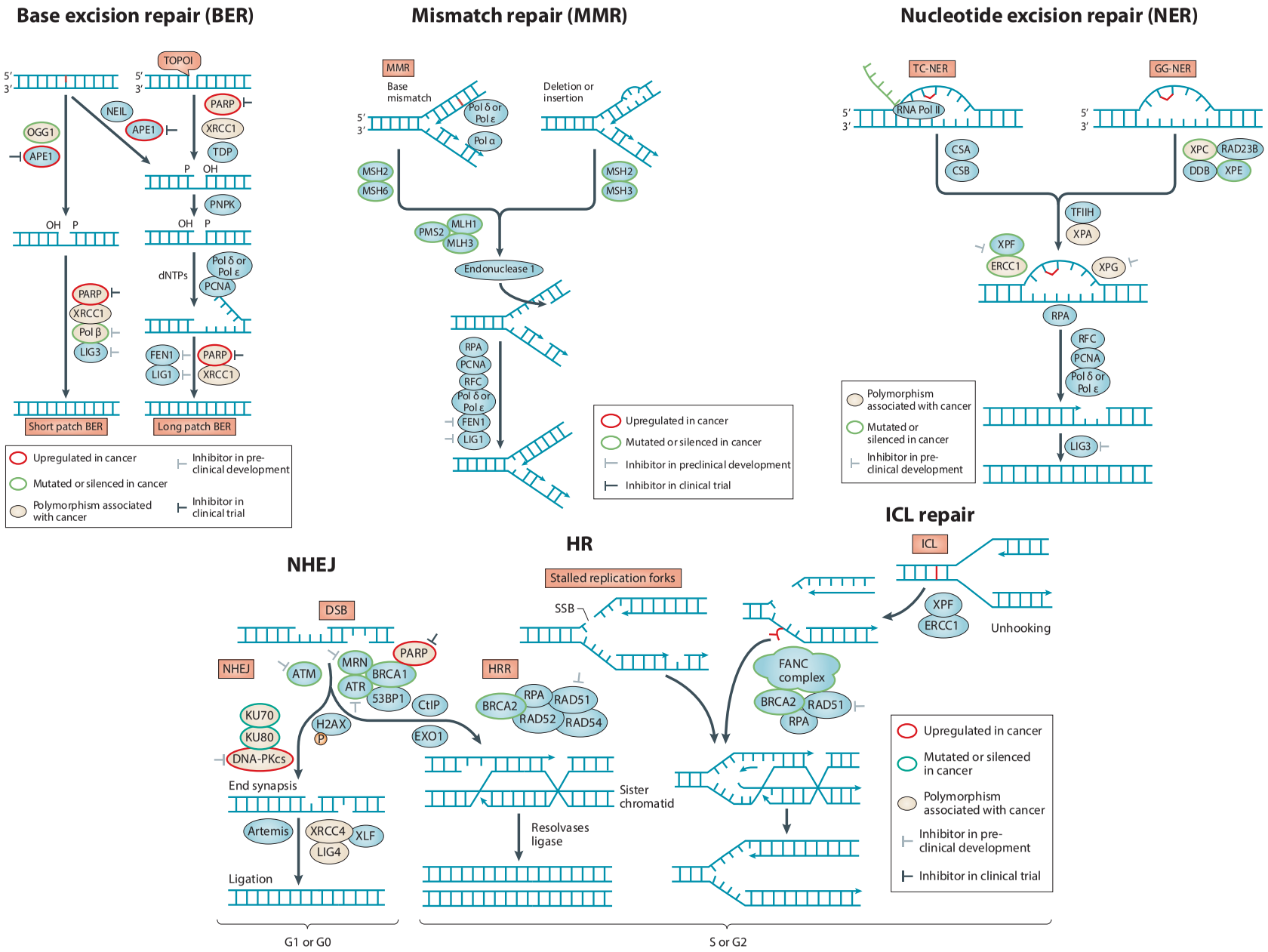
Base excision repair (BER)
TOPOI
5′
3′
NEIL
APE1
OGG1
APE1
PARP
XRCC1
TDP
P
OH
PNPK
OH
P
dNTPs
Pol δ or Pol ε
PCNA
PARP
XRCC1
Pol β
LIG3
FEN1
LIG1
PARP
XRCC1
Short patch BER
Long patch BER
Upregulated in cancer
Mutated or silenced in cancer
Polymorphism associated with cancer
Inhibitor in pre-clinical development
Inhibitor in clinical trial
Mismatch repair (MMR)
MMR
Base mismatch
Deletion or insertion
Pol δ or Pol ε
Pol α
MSH2
MSH6
MSH2
MSH3
PMS2
MLH1
MLH3
Endonuclease 1
RPA
PCNA
RFC
Pol δ or Pol ε
FEN1
LIG1
Upregulated in cancer
Mutated or silenced in cancer
Inhibitor in preclinical development
Inhibitor in clinical trial
Nucleotide excision repair (NER)
TC-NER
GG-NER
RNA Pol II
CSA
CSB
XPC
RAD23B
DDB
XPE
TFIIH
XPA
XPF
ERCC1
XPG
RPA
RFC
PCNA
Pol δ or Pol ε
LIG3
Polymorphism associated with cancer
Mutated or silenced in cancer
Inhibitor in pre-clinical development
ICL repair
ICL
XPF
ERCC1
Unhooking
NHEJ
DSB
NHEJ
ATM
PARP
MRN
BRCA1
ATR
53BP1
CtIP
KU70
KU80
DNA-PKcs
H2AX
P
EXO1
End synapsis
Artemis
XRCC4
XLF
LIG4
Ligation
HR
Stalled replication forks
SSB
HRR
BRCA2
RPA
RAD51
RAD52
RAD54
Sister chromatid
Resolvases ligase
FANC complex
BRCA2
RAD51
RPA
Upregulated in cancer
Mutated or silenced in cancer
Polymorphism associated with cancer
Inhibitor in pre-clinical development
Inhibitor in clinical trial
G1 or G0
S or G2

**Figure 1.4 ATM- and ATR-mediated DDR and cell cycle checkpoint**

A schematic diagram of the ATM/ATR-mediated DDR signalling cascade to the cell cycle checkpoint (adopted from *Nicola C. 2012*). ATM mainly responds to DSBs while ATR reacts to a variety of DNA damage lesions whenever the RPA-ssDNA complex is formed. There is significant crosstalk among the ATM-CHK2 and ATR-CHK1 cascades, which facilitate the amplification of DDR signalling but also pose a challenge to dissect the pathways in mechanistic studies.

*Figure 1.4 is adapted from Figure 6 with modifications from *Curtin NJ, DNA repair dysregulation from cancer driver to therapeutic target. Nature Reviews Cancer. **2012**, 12:801.* (https://www.nature.com/articles/nrc3399#article-info).

Specifically, additional pathway components (p21 and KAP1), cross-talks between CHK1/CHK2 and CDC25A/C, and DNA lesions (the negative supercoiling) were added to the figure to better represent the updated understanding of the pathways since Curtin's review was published 7 years ago in 2012.

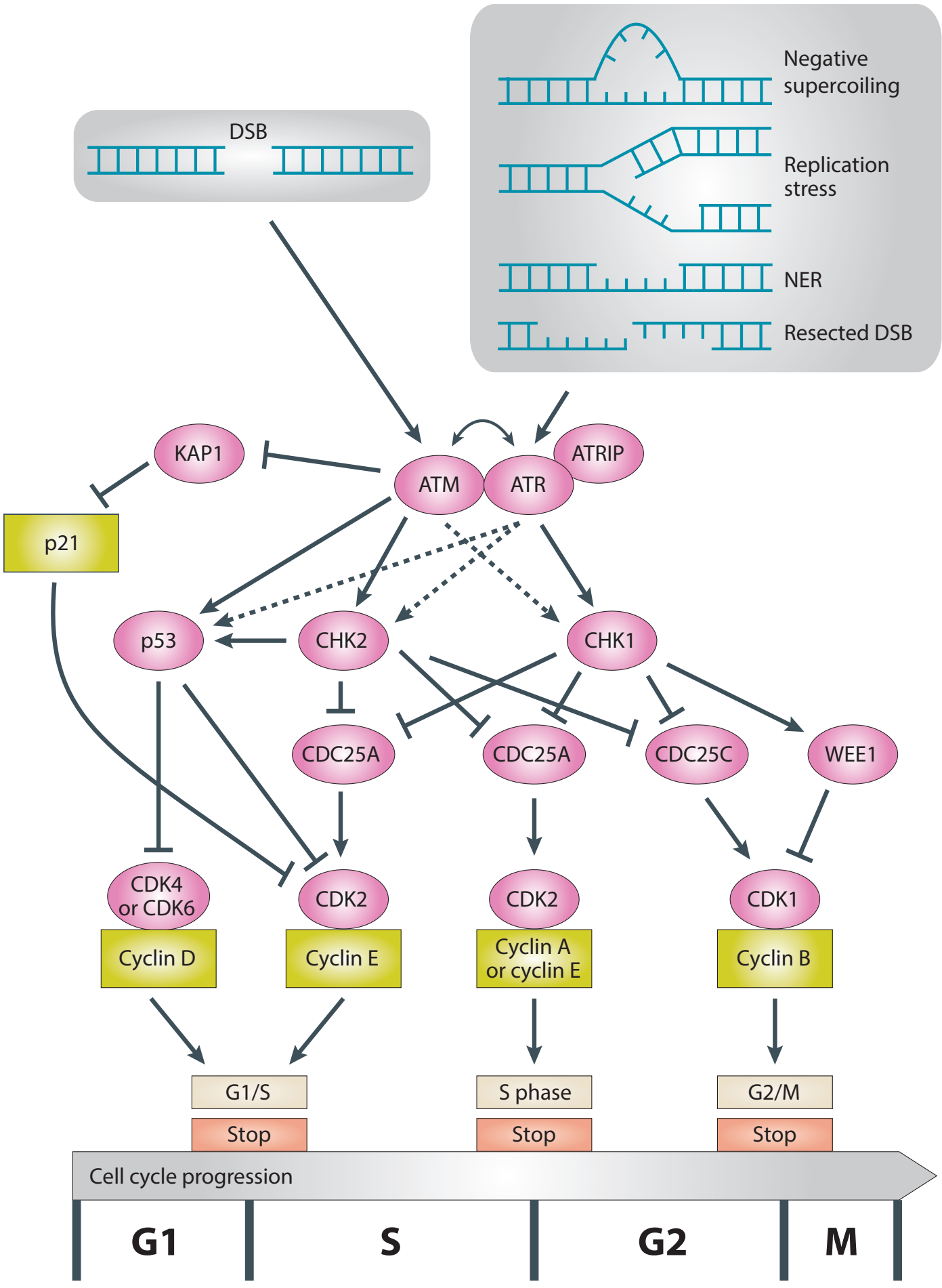
Negative supercoiling
Replication stress
NER
Resected DSB
DSB
KAP1
ATRIP
ATM
ATR
p21
p53
CHK2
CHK1
CDC25A
CDC25A
CDC25C
WEE1
CDK4 or CDK6
CDK2
CDK2
CDK1
Cyclin D
Cyclin E
Cyclin A or cyclin E
Cyclin B
G1/S
S phase
G2/M
Stop
Stop
Stop
Cell cycle progression
G1
S
G2
M

# Chapter 2. Materials and Methods

## 2.1. Cell lines and cell culture

OVCAR3, OVCAR4, CAOV3 and SKOV-3 cell lines were obtained from the National Cancer Institute. All cell lines were short tandem repeat (STR) characterised against ATCC or ExPASy database to ensure the authenticity of the origin. Mycoplasma tests were performed routinely by PCR to prevent contamination. All cells were cultured in RPMI-1640 media (Gibco) supplemented with 10% Fetal Bovine Serum (FBS, Sigma) and 2mM GlutaMax (Gibco) at 37°C and 5% CO2.

## 2.2. Cell line authentication and mycoplasma testing

The cell line authentication was performed using the short tandem repeat (STR) profiling analysis service provided by the Victorian Centre of Functional Genomics (VCFG) or Australia Genome Research Facility (AGRF). The mycoplasma test was performed using the polymerase chain reaction (PCR) method. Briefly, the cell line genomic DNA was purified using the NucleoSpin Tissue DNA purification kit (Macherey-Nagel). The PCR was performed using the following conditions:

**Primer sequences:**

Myco = 520 bp

*Forward – YGCCTGVGTAGTAYRYWCGC*

*Reverse – GCGGTGTGTACAARMCCCGA*

* *YR* are redundant base pairs, ie 'wild cards' for all myco species

Cytochrome b + control band = 375 bp

*Forward – CCATCCAACATCTCAGCATGATGAAA*

*Reverse – GCCCCTCAGAATGATATTTGTCCTCA*

**PCR reaction**

| **Stock buffers** | **Final concentrations** | **1 x 25 µL** |
|---|---|---|
| 5x buffer (-)$MgCl_2$ | 1x | 5 µL |
| 25 mM $MgCl_2$ | 2.5 mM | 2.5 µL |
| 10 mM dNTPs | 0.4 mM each | 1 µL |
| 5u/µL Promega Go Taq DNA polymerase | 1.25 u | 0.25 µL |
| 10 µM myco For * | 1.25 µM | 3 µL |
| 10 µM myco Rev * | 0.3 µM | 0.75 µL |
| 10 µM cytB For * | 0.6 µM | 1.5 µL |
| 10 µM cytB Rev * | 0.6 µM | 1.5 µL |
| Sample in K buffer | | 2 µL |
| MQ $H_2O$ | | 7.5 µL |

PCR Thermocycling Protocol:

| | | | |
|---|---|---|---|
| 1) | 94 °C | 3’ 00”} | x1 |
| 2) | 94 °C | 1’ 00”} | |
| | 50 °C | 1’ 00”} | x35 |
| | 72 °C | 1’ 00”} | |
| 3) | 72 °C | 10’00”} | x1 |
| 4) | 10 °C | ∞ | |

Electrophoresis of the PCR product was run using a 2% agarose gel. All cells should have a 375bp cytochrome b band, but mycoplasma-contaminated cells would have an extra 520bp band.

## 2.3. Pharmacological inhibitors

CX-5461 was provided by Cylene Pharmaceuticals and Senhwa Biosciences (San Diego, CA, USA) and was dissolved in 50 mM $NaH_2PO_4$. Topotecan (trade name Hycamtin) was purchased from Novartis and was dissolved in 0.9% saline. Q-VD-OPh (pan-caspase inhibitor) was purchased from APExBIO and was dissolved in DMSO. Streptonigrin, B02 and Spironolactone were purchased from Sigma-Aldrich and was dissolved in DMSO. Pentoxifylline was purchased from Sigma-Aldrich and was dissolved in water. AT13387 (Onalespib), 17-AAG (Tanespimycin), KU-55933 (ATM inhibitor), VE-821 (ATR inhibitor) and ActinomycinD were purchased from Selleckchem and was dissolved in DMSO. Doxorubicin and cisplatin solution were purchased from Hospira and diluted in 1xPBS. TMPyP4 (G4-DNA stabiliser) was purchased from Santa Cruz Biotechnology and was dissolved in water.

## 2.4. High-throughput RNAi screen and analysis

The RNAi screen and analysis protocol were established and performed with the help of the Victorian Centre of Functional Genomics (VCFG). Briefly, on a typical day of primary screen, 160µl Dharmafect (DF) 4 (Horizon Discovery) was mixed with 50ml Opti-MEM (Gibco), and 44µl lipid:Opti-MEM mixture was then aliquoted to 384-well plates containing 6µl 1µM SMARTpool siRNA duplexes (Horizon Discovery) using BioTek EL406 washer dispenser. The transfection mixture was mixed and complexed for 20 minutes, and 12.5µl mixture was then

aliquoted into other three plates (4 replicates in total) using Caliper ALH3000 liquid handling platform. During this period, OVCAR4 cells were trypsinised and diluted to $5.6x10^4$ cells/ml. 25µl OVCAR4 cells (1400 cells) were then dispensed into 384-well plates using the EL406, with the final concentration of the SMARTpool siRNA at 40nM. Plates were pulse-spun and were then incubated at 37°C and 5% CO2. 24 hours later, the transfection media was replaced with 50ul RPMI-1640 media (10% FBS + 2mM GlutaMAX) containing either 80nM CX-5461 or 400nM $NaH_2PO_4$. Cells were further incubated for 48hrs and were then fixed with 2% PFA in 1xPBS for 10min, followed by permeabilization in 0.3% TritonX-100 in 1xPBS (PBST) for 10min. Cells were washed with 1xPBS once and were next stained with 100ng/ml DAPI (Gibco) for 20min. Cells were washed with 1xPBS twice and then sent for imaging analysis using ArrayScan VTI high-content system (Thermo Fisher Scientific). For the secondary screen, the 1µM SMARTpool siRNAs were replaced by 0.45µM individual siRNA duplexes, with all the other conditions remaining the same.

## 2.5. BRCA2 and TOP1 knockdown using siRNA

Knockdown of BRCA2 and TOP1 was performed using similar conditions to the screen. Briefly, 6.36µl Dharmafect 4 was mixed with 1993.64µl Opti-MEM. 660µl lipid: Opti-MEM MEM mixture was then mixed with 90µl 1µM OTP-NT, siTOP1 or siBRCA2 SMARTpool siRNAs to reach a final concentration of 40nM. The transfection mixture was mixed and complexed for 20 minutes, and 125µl mixture was then aliquoted into 8-well chamber slides (Nunc Lab-Tek II). 14,000 OVCAR4 cells in 250µl RPMI-1640 media were then added on top of the mixture and was incubated for 24hrs before a media change to standard RPMI-1640 media. Cells were cultured for another 48 hours before drug treatment and immunofluorescent staining.

## 2.6. Generation of inducible BRCA2 knockdown OVCAR4 cell lines

**24h before transfection**

Plate T75 flask (Greiner) with $5x10^6$ HEK293T cells in 10mL HEK293T media (DMEM+10%FBS+2mM GlutaMax).

**Transfection**

Change media with 10 mL fresh HEK293T media.

Mix the following in serum-free DMEM:

| | |
|---|---|
| VSVG | 2.25 μg (1 μg/μl stock) |
| RSV-REV | 2.25 μg (1 μg/μl stock) |
| pMDLg/pRRE | 2.25 μg (1 μg/μl stock) |
| pLKO-TetON-shBRCA2 | 6.75 μg |
| Polyethylenimine (PEI) | 67.5 μl (1 μg/μl stock) |
| DMEM | up to 500 μl |

Vortex, incubate for 30-45 min at RT. Add to HEK293T cells, swirl well to distribute.

pLKO-TetON-shBRCA2 plasmid was kindly provided by Prof. Madalena Tarsounas [392]; the lentivirus packaging plasmids VSVG, RSV-REVand pMDLg/pRRE were purchased from Addgene; PEI was from Sigma Aldrich and DMEM media is from Gibco.

**24 hours post-transfection**

Change media with 8mL fresh HEK293T media

Plate $5x10^5$ OVCAR4 cells in T75 flask for transduction.

**Transduction**

AM (8:00-9:00): Harvest 1st batch virus. Filter viral supernatant through sterile 0.45-μm filter (Millipore) into tube. Add 8 μg/ml polybrene (Sigma Aldrich). Replace 8mL media on HEK293T cells. Aspirate media from OVCAR4 cells. Add virus + polybrene to the cells. Incubate for 8 hours.

PM (4:00-5:00): Harvest 2nd batch virus. Filter viral supernatant through sterile 0.45-μm filter into tube. Add 8μg/ml polybrene. Add virus + polybrene to the cells.

**24 hours post-transduction**

Change to the routine cell culture media. Culture the cells from another 72 hours in the presence of 1μg/ml puromycin (Sigma Aldrich) to select the successfully transfected cells. Add 0.2μg/ml doxycycline (Sigma Aldrich) to induce the BRCA2 knockdown.

## 2.7. RT-qPCR for BRCA2 knockdown efficiency, SASP and Pol I transcription inhibition

### 2.7.1 RNA extraction

RNeasy Mini Kit (QIAGEN) was used for RNA extraction and purification. All steps were conducted according to the manufacture's protocol. Briefly, cells were washed with cold 1xPBS and was then lysed with 350μl Buffer RLT. 500ul 70% ethanol was then added to the lysate, and the mixture was transferred to RNeasy Mini spin columns. The flow-through was discarded after centrifugation, and the

columns were further washed with Buffer RW1 and Buffer RPE. The purified RNA was then eluted in RNase-free water and was quantified using a Nanodrop spectrophotometer (Thermo Fisher Scientific).

### 2.7.2 Reverse transcription and complementary DNA (cDNA) synthesis

100ng RNA sample in 14.7µl RNase-free water was mixed with 4µl 5x First-strand buffer (Invitrogen), 0.2µl RNase Inhibitor (Invitrogen), 0.1µl 0.1M Dithiothreitol (DTT) and 1µl DNase (Promega). The mixture was incubated at 37°C for 15 minutes and then at 65°C for another 15 minutes for DNase heat inactivation. The DNase treated sample was then mixed with 1.3µl Random hexamers (Invitrogen), 3µl 10mM dNTP and 8.7µl RNase-free water. The mixture was incubated at 65°C for 5 minutes and on ice for 1 minute. 4µl 5x First-strand buffer, 1µl 0.1M DTT, 1µl RNase Inhibitor and 1µl SuperScript III Reverse Transcriptase (Invitrogen) were then added into the mixture. The cocktail was incubated at 25°C for 5 minutes, followed by 50°C for 60 minutes and 70°C for 15 minutes.

### 2.7.3 Quantitative Real-time Polymerase Chain Reaction (qPCR)

The synthesised cDNA from 2.7.2. was diluted 50 times in RNase-free water, and 4µl diluted cDNA sample was mixed with 5µl 2x Fast SYBRGreen Master Mix (Thermofisher) and 1µM specific primers (forward and reverse). The qPCR mixture was plated in triplicate in MicroAmp Optical 96-well reaction plates (Applied Biosystem). The plates were sealed and spun at 2000rpm for 5min at 4°C. the RT-qPCR reaction was performed by the StepOne Plus Real-Time PCR

system (Applied Biosystems) using relative quantification and a 0.7°C melt-curve increment. Primers used are listed in Table 2.2. RNase-free water was used as negative control, while NONO was used as internal control.

## 2.8. Protein extraction and quantification for western blots

Protein was extracted from exponentially growing cells following indicated treatments. Cells were washed with 1xPBS twice and were then lysed with western solubilization buffer (see Table 2.3 for formulas). The lysate was heated at 95°C for 5 minutes, sheared 3 times with a 26-gauge needle and centrifuged at 13000rpm for 1 minutes to remove insoluble precipitate. The detergent-compatible protein assay (500-0112, Bio-Rad) was used to determine the protein concentration using a Benchmark Microplate reader (170-6850, Bio-Rad) and bovine serum albumin (BSA) (B9000S, New England Biolabs) as the standard.

## 2.9. Western blots for DDR components

Equal amounts (~20μg) of protein were prepared in 6x sample loading buffer and separated by SDS-polyacrylamide gel electrophoresis (SDS-PAGE) in western running buffer (Table 2.3) using the mini-Protean Tetra Cell system (Bio-Rad) with either 12% or 5% SDS-PAGE resolving gel (Table 2.3) depending on the molecular weight (mw) of target proteins (5% for protein with mw>100kD, and 12% for mw<100kD). PageRuler Plus MW ladder (26629 Thermo Fisher) and Hi-Mark MW ladder (LC5699 Thermo Fisher) were used to indicate the protein molecular size. Protein was wet transferred to Immobilon-P polyvinylidene fluoride (PVDF) membranes (IPVH00010 Millipore) in wet transfer buffer at 4°C (5% gels: 180min at 70V in 5% MeOH transfer buffer; 12% gels: 60min at 250mA in 15% MeOH transfer buffer). PVDF membranes were blocked 5% skim milk

(w/v) (Diploma) + TBST (prepared fresh) for 45 minutes and were washed 3x 5 min in TBST to remove milk. Membranes were then incubated with primary antibodies diluted in 5% BSA + TBST + 0.02% sodium azide at 4°C overnight on the roller (except anti-tubulin antibody, which was diluted in 5% skim milk (w/v) +TBST). Membranes were washed 3x10 min in TBST and incubated with horse-radish-peroxidase (HRP)-conjugated secondary antibodies in 5% skim milk (w/v) + TBST for 2 hours at room temperature on a roller. Membranes were further washed in 3x10 min in TBST to remove residual antibodies and developed with Amersham ECL Western Blotting Detection Reagent (GE Lifescience). Membranes were exposed to X-ray films (Fujifilm SuperRX). Tubulin served as a loading control.

## 2.10. IF staining for RAD51 foci, G4-DNA stabilisation, TOP1 expression and R-loop formation

5,000 OVCAR4 cells were seeded into 8-well Nunc™ Lab-Tek™ II Chamber Slides™ (Catalog# 154534) per well. Cells were cultured for 72 hours, followed by drug treatments for 3 hours at indicated doses together with 10μM 5-ethynyl-2'-deoxyuridine (EdU). Cells were then processed for immunofluorescence staining as follows.

**For R-loop (DNA:RNA hybrids, S9.6), pRPA32 S4/S8, pRPA2 S33 and pATR T1989:**

1) Wash slides 2x in ice cold PBS
2) Fix in 4 % PFA for 10min at RT
3) Wash 2x in cold PBS
4) Permeabilisation: ice-cold methanol for 10 min and ice-cold acetone for 1 min on ice

5) Wash 3x 5min with PBS on rocker

6) Block in 1x PBS + 5% Goat (or chicken) serum + 0.3% Triton X-100 for 30mins at RT in humid chamber

7) Incubate slides with primary antibodies diluted in 1x PBS + 1% BSA + 0.3% Triton X-100 for 1hr at 37$^{0}$C in humid chamber (add 100µl of antibody mix & cover with a coverslip)

8) Wash 3x 5min in PBS on rocker

9) Incubate slides with DAPI and fluorochrome-conjugated secondary antibodies diluted at 1:600 in 1x PBS + 1% BSA + 0.3% Triton X-100 for 1hr at 37$^{0}$C in humidified chamber protected from light (add 100µl of antibody mix & cover with a coverslip)

10) Wash 3x 5min in PBS on rocker (Protect from light)

11) Incubate with EdU staining buffer for 30min

12) Wash 3x 5min in PBS on rocker

13) Mount with Vectashield Mounting Media (VectorLabs) and seal slides with a coverslip and nail polish

**For all other antibodies:**

1) Wash slides 2x in ice cold PBS

2) Fix in 4 % PFA for 10min at RT

3) Wash 2x in cold PBS

4) Permeabilise with 0.3% Triton X-100 in PBS for 10mins at RT

5) Block in 1x PBS + 5% Goat (or chicken) serum + 0.3% Triton X-100 for 30mins at RT

6) Incubate slides with primary antibodies diluted in 1x PBS + 1% BSA + 0.3% Triton X-100 for 1hr at 37$^{0}$C in humid chamber (1:100 RAD51 and 1:100 gammaH2AX antibodies)

7) Wash 3x 5min in PBS on rocker

8) Incubate slides with DAPI and fluorochrome-conjugated secondary antibodies (Mouse-488/Rabbit-594) diluted 1:500 in 1x PBS + 1% BSA + 0.3% Triton X-100 for 1hr at 37$^{0}$C in humid chamber (Protect from light)

9) Wash 3x 5min in PBS on rocker

10) Incubate with EdU staining buffer for 30min

11) Wash 3x 5min in PBS on rocker

12) Mount with Vectashield Mounting Media (Vectorlabs) and seal slides with a coverslip and nail polish

## 2.11. Image acquisition and analysis

The screen images were captured using an Arrayscan VTI high content system (Thermofisher) and analysed with Cellomics software (Thermofisher). High-resolution images were captured by a Zeiss ELYRA PS.1 confocal microscope and were analysed with ImageJ (FIJI) [393] and CellProfiler [394].

## 2.12. Cell death and cell cycle analysis (FACS)

For flow cytometry analysis of cell death and cell cycle, cells were labelled with 10μM BrdU for 30min, and the supernatants were collected into a 50ml tube. Cells were rinsed with 1xPBS once (the wash was collected as well), and trypsinised with 0.25% Trypsin-EDTA. The trypsin was neutralised by 1ml cell growth media, and all the liquid and cells were collected into the 50ml tubes. Cells were rinsed with cold 1xPBS once, and were then suspended in 1ml cold 1xPBS. 5mL ice-cold 80% ethanol was drop-wisely added into the tubes while maintaining a gentle vortex, and the mixture was incubated on ice overnight. The fixed cells were spun down, and were resuspended in 1ml of 2N HCl/0.5% Triton X-100 (v/v) for 30min. The fixed cells were spun down again, and were

resuspended in 1ml 0.1M $Na_2B_4O_7.10H_2O$ (pH 8.5) to neutralise the acid. The cells were then collected and resuspended in 100µl anti-BrdU (Becton Dickinson Cat. #347580) (0.5µg/ml) in dilution buffer (PBS + 2% fetal bovine serum) + 0.5% Tween-20 for 30min at room temperature, washed with dilution buffer, collected and resuspended in 100µl in Alexa Fluor 488 donkey anti-mouse IgG (Invitrogen Cat. #A21202) (5µg/ml) in dilution buffer + 0.5% Tween-20 for 30min on ice, then washed with dilution buffer. Cells were resuspended in 10 µg/ml propidium iodide (PI) in dilution buffer at approximately $2x10^6$ cells/ml, transferred into 5ml polystyrene tubes through a cell-strainer cap, then analysed by flow cytometry on a BD FACS Canto II. Quantitation of cell cycle population was performed using FlowJo analysis software (Figure 2.1 and 2.2).

## 2.13. Drug dose response curves, cell proliferation assay and checkerboard assay

Drug dose response curves, cell proliferation and checkerboard assays were conducted in a similar way as the screen. Briefly, cells were seeded into 96-well plates with cell number adjusted to the treatment time to reach ~90% confluence at the endpoint. 24 hours later, cells were drugged according to the schedule and incubated in a humidified chamber until the endpoints. For ovarian cancer cells, cells were fixed, permeabilised and stained as in the screen, and were counted using an ArrayScan VTI high-content system. For B-lineage acute lymphoblastic leukaemia cells, the cell viability was quantified using CellTiter-Glo (Promega). The drug dose response curves were generated in Prism7 (GraphPad) using ordinary nonlinear regression fit. The 50% inhibition of cell growth ($GI_{50}$) and total growth inhibition (TGI) dosages were obtained by curve interpolation.

## 2.14. Clonogenic assay

The clonogenic assay is a cell biology technique for studying the effectiveness of specific treatments on the survival and proliferation of cells. Briefly, on day 0, 10,000 OVCAR4 cells per well were seeded into 6-well plates (BD Falcon). Cells were cultured for 24 hours, then drugged as indicated. 48 hours after drug treatment, the drugs were removed by washing twice with 1xPBS. Cells were then cultured in normal media for another 5 days until the vehicle cells reached confluency. Cell were then fixed with 100% methanol for 10mins, stained with 0.1% crystal violet solution for at least 20 mins and washed with 1xPBS thoroughly. The stained plates were thoroughly dried and analysed.

## 2.15. DNA comet assay

DNA comet assays were performed using the CometAssay Reagent Kit (4250-050-K Trevigen). All steps were conducted according to the manufacturer's protocol. Briefly, cells treated with indicated pharmacological inhibitors were trypsinised and washed once with ice cold PBS, and then resuspended in ice cold PBS at $1x10^5$ cells per ml. Cells were mixed with molten LMAgarose at 37°C at a ratio of 1:10 and 50µl of the mixture was immediately pipetted onto a CometSlide. The slides were left in the dark at 4°C for 30 minutes to solidify the agarose and was then immersed in 4°C Lysis Solution overnight. On the next day, the slides were immersed in freshly prepared Alkaline Unwinding Solution for 1 hours at 4°C in the dark, and electrophorized in 4°C Alkaline Electrophoresis Solution at 21V, 300mA for 40 minutes. The slides were washed with $ddH_2O$ twice, followed by 70% ethanol for 5 minutes. Slides were dried at 37°C for 15 minutes, and then stained with 2.5µg PI in PBS for 30 minutes at room temperature. Slides were rinsed in $ddH_2O$ twice and completely dried at 37°C.

The comet images were captured using VS120 Virtual Slide Microscope (Olympus) and analysed with OpenComet (a plugin of ImageJ) [395].

## 2.16. Establishment and drug treatment of in vivo xenograft model

All animal studies were conducted according to the protocols approved by the Animal Ethics Committee at the Peter MacCallum Cancer Centre (Ethics number E557). Animals were housed in the animal facilities at the Peter MacCallum Cancer Centre.

### 2.16.1 Subcutaneous engraftment of mice with OVCAR3 cells

OVCAR3 cells for subcutaneous engraftment were obtained from Dr George Au-Yeung and expanded to $5x10^8$ cells (~75 T175 flasks). One the day of transplantation, all cells were harvested from the flasks and $3.8x10^8$ cells were reconstituted in 3.125ml of PBS and mixed with 3.438ml of Matrigel (Corning) on ice. Meanwhile, 50 female NOD scid gamma (NSG) immunodeficient mice at 6-8-weeks old (purchased from the Garvan institute) were anaesthetised by isoflurane and 100µl ice cold PBS:Matrigel mixture with $6x10^6$ OVCAR3 cells was subcutaneous injected into the right flank using a pre-cooled 0.3 ml insulin syringe. Mice were observed until their recovery from the anaesthetic.

### 2.16.2 Assessment of OVCAR3 cell engraftment

Tumour bearing mice were weighed and measured twice weekly (spread evenly throughout the week) when all tumours appeared to be measurable (approximately > 4mm x 4mm). All measurements were recorded using electronic calipers. Once tumours reached an average volume of 100 $mm^3$, mice were

randomised into 4 groups of 10 mice, and that day was defined as day 1. CX-5461 (3 mg/ml) and its vehicle, 25mM $NaH_2PO_4$, were dosed at 0.1ml /10g mouse weight via oral gavage twice weekly (Mon/Thurs or Tues/Fri) while Topotecan (0.5 mg/ml for the first experiment and 0.25 mg/ml for the second one) and its vehicle (Saline) were dosed at 0.1ml/10g mouse weight via intraperitoneal (i.p.) injection twice weekly (Mon/Thurs or Tues/Fri). Mice were dosed for four consecutive weeks for a total of 8 doses. The mice body weight and tumour volumes were closely monitored during and after the treatment period.

### 2.16.3 Sacrifice of the engrafted mice

Mice were sacrificed using cervical dislocation when they demonstrated disease burden compatible with the ethical end-point of the experiment (tumour volume > 1200 $mm^3$ weight loss ≥ 20%, or other signs of illness or distress.

## 2.17. Statistical analysis and the quantification of synergistic effects

Prism 7 (GraphPad) was used for all the statistical analyses as indicated, including dose response curves, student's t-tests, Wilcoxon rank-sum tests (nonparametric test), ordinary one-way ANOVA, Kruskal-Wallis tests (nonparametric one-way ANOVA) and Mantel-Cox tests (survival curve). The synergistic effects were quantified using either Combenefit (software based on the Bliss independence) or CalcuSyn (Biosoft, a software based on the combination index theorem of Chou-Talalay) [396, 397].

## Table 2.1 Antibodies and staining reagents

| Antibody | Company | Catalogue No. | Application (dilution) |
|---|---|---|---|
| **pCHK1 (S345) (133D3)** | Cell Signalling | 2348 | WB (1:1000) |
| **pCHK2 (T68) (C13C1)** | Cell Signalling | 2197 | WB (1:1000) |
| **pATM (S1981) [EP1890Y]** | Abcam | ab81292 | WB (1:2000) |
| **pATR (T1989)** | GeneTex | GTX128145 | WB (1:2000), IF (1:100) |
| **pKAP1 (S824)** | Abcam | Ab133440 | WB (1:1000), IF (1:100) |
| **γH2AX (S139)** | Merck Millipore | 05-636-I | WB (1:1000), IF (1:100) |
| **γH2AX (S139)** | Abcam | ab81299 | WB (1:2000) |
| **H2AX** | Abcam | ab20669 | WB (1:1000) |
| **pRPA32 (S4/S8)** | Bethyl | A300-245A | WB (1:1000), IF (1:100) |
| **pRPA2 (S33)** | Novus | NB100-544 | WB (1:2000), IF (1:200) |
| **RAD51** | Abcam | ab63801 | IF (1:100) |
| **DNA G-quadruplex (G4) (1H6)** | Merck Millipore | MABE1126 | IF (1:100) |
| **DNA-RNA Hybrid (S9.6)** | Kerafast | ENH001 | IF (1:100) |
| **TOP1** | Abcam | ab3825 | IF (1:100) |
| **UBF (F-9)** | Santa Cruz | sc-13125 | IF (1:100) |
| **UBF (WT1F)** | In-house | | IF (1:400) |

| | | | |
|---|---|---|---|
| **Goat-anti-Mouse HRP** | Bio-Rad | 172-1011 | WB (1:10000) |
| **Goat-anti-Rabbit HRP** | Bio-Rad | 170-6515 | WB (1:5000) |
| **Goat-anti-Mouse Alexa Fluor 488** | Thermo Fisher | A-11001 | IF (1:500) |
| **Goat-anti-Rabbit Alexa Fluor 594** | Thermo Fisher | A-11012 | IF (1:500) |
| **DAPI** | Thermo Fisher | D1306 | IF (1:2000) |
| **Click-iT™ EdU Alexa Fluor™ 647 Imaging Kit** | Thermo Fisher | C10340 | IF (1:1000) |
| **BrdU (B44)** | BD Biosciences | 347580 | FACS |
| **Sheep-anti-Mouse IgG FITC** | MP Biomedicals | 0855520 | FACS |
| **Propidium Iodide (PI)** | Sigma Aldrich | P4170 | FACS |

## Table 2.2 Oligo-primers for RT-qPCR

| Gene | Species | Direction | Sequence |
|---|---|---|---|
| **47S pre-rRNA 5' External Transcribed Sequence (5'ETS)** | Human | Forward | GGC GGT TTG AGT GAG ACG AGA |
| | | Reverse | ACG TGC GCT CAC CGA GAG CAG |
| **47S pre-rRNA 5' External Transcribed Sequence (ITS1-2)** | Human | Forward | GAAACCTTCCGACCCCTCT |
| | | Reverse | GCCAGACGAGACAGCAAAC |
| **47S pre-rRNA 5' External Transcribed Sequence (ITS2-1)** | Human | Forward | GAG AGA GAC GGG GAG GGC GG |
| | | Reverse | CCG AGG GAG GAA CCC GGA CC |
| **5S pre-rRNA (5S-1)** | Human | Forward | GTC TAC GGC CAT ACC ACC CT |
| | | Reverse | AGC CTA CAG CAC CCG GTA TT |
| **NONO** | Human | Forward | CAT CAA GGA GGC TCG TGA GAA G |

| | | | |
|---|---|---|---|
| | | Reverse | TGG TTG TGC AGC TCT TCC ATC C |
| **MYC** | Human | Forward | CAG CTG CTT AGA CGC TGG ATT |
| | | Reverse | GTA GAA ATA CGG CTG CAC CGA |
| **BRCA2** | Human | Forward | GCG CGG TTT TTG TCA GCT TA |
| | | Reverse | TGG TCC TAA ATC TGC TTT GTT GC |
| **IL1α** | Human | Forward | ACT GCC CAA GAT GAA GAC CA |
| | | Reverse | CCG TGA GTT TCC CAG AAG AA |
| **IL6** | Human | Forward | AGT GAG GAA CAA GCC AGA GC |
| | | Reverse | CAT TTG TGG TTG GGT CAG G |
| **IL8** | Human | Forward | GTC TGC TAG CCA GGA TCC AC |
| | | Reverse | GCT TCC ACA TGT CCT CAC AA |

| | | | |
|---|---|---|---|
| **CXCL1** | Human | Forward | AGT CAT AGC CAC ACT CAA GAA TGG |
| | | Reverse | GAT GCA GGA TTG AGG CAA G |
| **p16** | Human | Forward | GGG GGC ACC AGA GGC AGT |
| | | Reverse | GGT TGT GGC GGG GGC AGT T |
| **p21** | Human | Forward | GGC AGA CCA GCA TGA CAG ATT |
| | | Reverse | GCG GAT TAG GGC TTC CTC TT |

## Table 2.3 Buffers and reagents

| Reagents | Formulas |
|---|---|
| **Phosphate Buffered Saline (1xPBS)** | 137mM NaCl; 2.7mM KCl; 4.3mM $Na_2HPO_4$; 1.47mM $KH_2PO_4$; $ddH_2O$; Adjust to a final pH of 7.4. |
| **Western sol buffer** | 0.5mM EDTA; 20nM HEPES; 2% (w/v) SDS; Adjust to a final pH of 7.9 |
| **Tris Buffered Saline with Tween20 (TBST)** | 50mM Tris, 150mM NaCl; 0.1% (v/v) Tween20 |
| **6x Protein Sample Loading Buffer** | 2% (w/v SDS), 0.4M Tris-HCL pH 6.8; 48% (v/v) Glycerol; 58mM β-ME; 0.25% (w/v) Bromophenol Blue |
| **Tris-Glycine-SDS Running Buffer (western running buffer)** | 25mM Tris; 192mM Glycine; 0.1% (w/v) SDS pH 8.7 |
| **Tris-Glycine-Methanol Transfer Buffer (wet transfer buffer)** | 25mM Tris; 192mM Glycine; 5% or 15% Methanol |
| **12% SDS-PAGE resolving gel** | 12% (v/v) Acryl/Bis (19:1) polyacrylamide, 375mM Tris-HCL pH 8.7, 0.1% (w/v) SDS, 0.015% (w/v) ammonium persulfate (APS), 0.015% (v/v) tetramethylethylenediamine (TEMED), $ddH_2O$ |
| **5% SDS-PAGE resolving gel** | 5% (v/v) Acryl/Bis (19:1) polyacrylamide, 375mM Tris-HCL pH 8.7, 0.1% (w/v) SDS, 0.015% (w/v) APS, 0.015% (v/v) TEMED, $ddH_2O$ |
| **4% SDS-PAGE stacking gel** | 4% (v/v) Acryl/Bis (19:1) polyacrylamide, 125mM Tris-HCL pH 6.8, 0.1% (w/v) SDS, 0.112% (w/v) APS, 0.112% (v/v) TEMED, $ddH_2O$ |
| **EdU Staining Buffer** | 100mM Tris, pH 8.5; 1mM $CuSO_4$, 100mM ascorbic acid, 10µM Alexa Fluor 647-azide in DMSO |

**Figure 2.1 Analysis of subG1 fraction (cell death)**

HGSC cells (OVCAR3, OVCAR4, CAOV3) treated with pharmacological inhibitors were trypsinised, fixed with 90% ethanol, stained with PI and analysed by flow cytometry (Canto II). **A-C**, 100,000 single cells of the correct morphology containing 2N to 4N DNA content were assessed. **D**, SubG1cells were counted from the DNA content (PI) histogram.

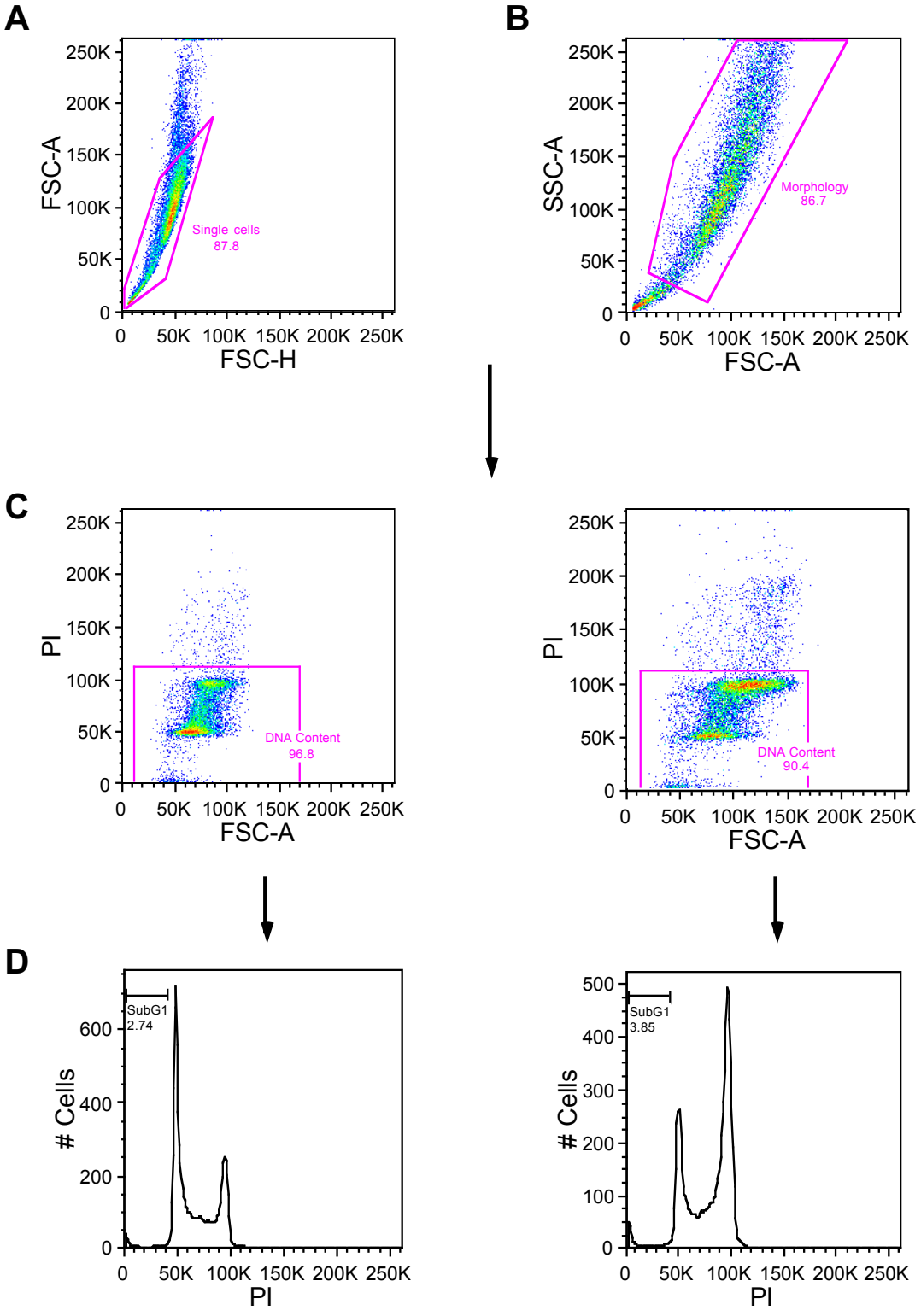
A
FSC-A
FSC-H
Single cells
87.8
B
SSC-A
FSC-A
Morphology
86.7
C
PI
FSC-A
DNA Content
96.8
DNA Content
90.4
D
# Cells
PI
SubG1
2.74
SubG1
3.85

**Figure 2.2 Cell cycle Analysis**

HGSC cells (OVCAR3, OVCAR4, CAOV3) treated with pharmacological inhibitors were labelled with 10μM BrdU for 30min, trypsinised, fixed with 80% ethanol, stained with PI and analysed by flow cytometry (Canto II). **A-C**, 100,000 single cells of the correct morphology containing 2N to 4N DNA content were assessed. **D**, G1 (2N), S (replicating) and G2/M (4N) phase cells were separated and counted using PI-BrdU plots.

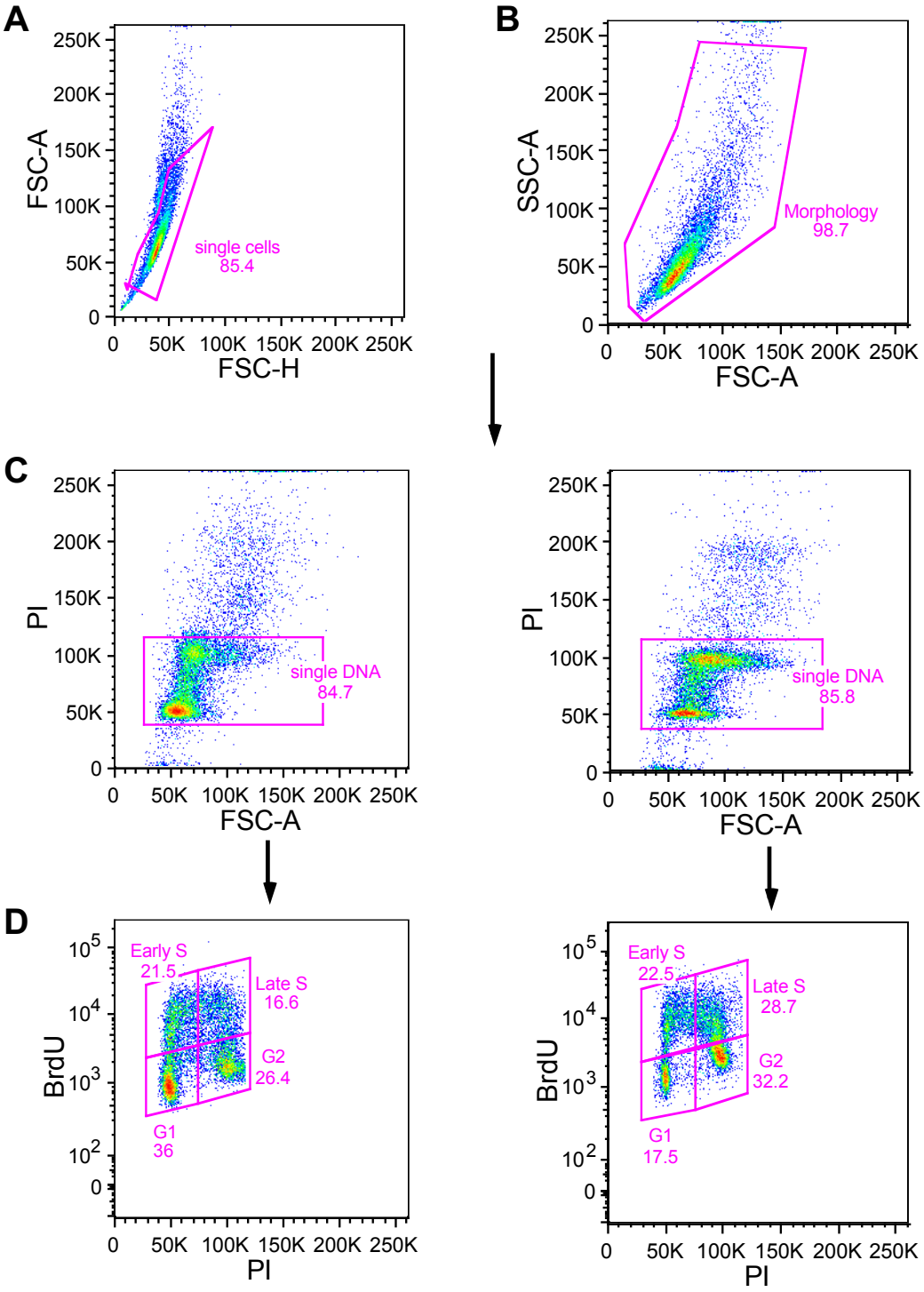
A
FSC-A
FSC-H
single cells
85.4
B
SSC-A
FSC-A
Morphology
98.7
C
PI
FSC-A
single DNA
84.7
PI
FSC-A
single DNA
85.8
D
BrdU
PI
Early S
21.5
Late S
16.6
G2
26.4
G1
36
BrdU
PI
Early S
22.5
Late S
28.7
G2
32.2
G1
17.5

# Chapter 3. Combining a genome-wide RNAi screen and chemical compound screen to identify targets that can cooperate with CX-5461

## 3.1. Introduction

High-throughput screening (HTS) allows researchers, with the help of automation platforms, to conduct large-scale chemical, genetic, or pharmacological tests to identify candidates that can induce certain desired biological effects. Since its introduction in the 1980s, it has gained increasing popularity in the biomedical research field, and is becoming routine in the drug discovery industry [398]. According to a recent survey, one-third of the recently approved drugs (or leads) was first identified using HTS [399].

HTS was initially less frequently used in academic research compared to industry, mainly due to its high cost. However, the completion of the Human Genome Project in 2003, as well as the discovery of RNA interference (RNAi) in 1998, fundamentally changed the approach of biomedical research. The combination of genomics, RNAi/cDNA libraries and HTS (the so-called functional genomics) allows researchers to study the interaction or role of a particular biochemical process even without knowing the exact function of certain genes or drugs. In fact, HTS is currently an important approach to study the function of particular genes by identifying all the interacting components [399].

HTS can be conducted in many different ways, but generally consists of three important steps, namely target library selection, screen method development and hit identification [400]. A target library is the range of candidates from where the potential hits will be selected, which can be antibodies, protein fragments, chemical compounds, RNAi (siRNA, shRNA, miRNA), cDNA or the latest CRISPR-Cas9 guide RNA (sgRNA) [401, 402]. It can differ in scale as well, which can be genome-wide or pathway-specific when using a genomic approach; or range from an FDA-approved drug library with just over 3,000 small molecules to a comprehensive lead library with millions of chemicals in a compound screen.

The screening method is another crucial factor in HTS, which can be performed in a cell-free system, immortalised/primary cells, organoids, worms or animals. In addition, apart from the conventional arrayed screen formats, some genomics-based screens (shRNA, cDNA or sgRNA) can also be performed in pooled formats if cell survival/hyperproliferation is expected, and the enriched hits can be identified by next-generation sequencing (NGS). Hit identification is the last but also the most important step in HTS. Eliminating false-positive/negative results is necessary to ensure the quality/reliability of the screen. As a result, a robust readout/reporter that can represent the desired biological effects is required [400]. Overall, all HTS methods have their own advantages and disadvantages. The most important consideration is to choose the method that can best fit the researcher's requirements. Sometimes more reliable results can be drawn by performing multiple HTSs targeting the same biological effect via different approaches.

## 3.2. Overview of HTS methods and the rationale of using siRNA and chemical compound screens

RNAi, CRISPR-Cas9 and chemical compounds are popular choice of HTS methods. RNAi was first discovered in 1998 by Fire and Mello [403]. The combination of RNAi and the Human Genome Project has allowed researchers to target any gene of interest as long as the DNA sequence of the target is known. RNAi can be delivered in both RNA (siRNA) and DNA (shRNA) forms [404]. siRNAs (small interfering RNAs) are double strand RNA fragments with a typical size of 21-23nt. Upon being transfected into the cells by lipid or polyethyleneimine (PEI), the guide strands that are complementary to the target mRNA incorporate into the RNA-induced silencing complex (RISC), and activate Argonaute, the enzyme that cleaves the complementary mRNA. The passenger

strands are reported to be degraded upon binding of the guide strand to RISC [405]. However, research has shown that the passenger strands can induce RNAi and cause unwanted knockdown effects [406]. As a result, most commercially available siRNAs have chemical modifications on the passenger strands that reduce non-specific binding, thus alleviating off-target effects [407]. Nevertheless, the design of the guide strand sequence is still the key to efficient and reliable RNAi knockdown [408]. shRNA (short hairpin RNA) is siRNA in a DNA form. Different from siRNA, shRNA needs to be encoded into vectors, such as plasmid or virus, before being transfected or transduced into cells. Once in the cells, shRNA is transcribed into a single-strand stem-loop forming a Pri-shRNA. The Pri-shRNA is then sequentially processed (cleaved) by Drosha enzymes to form Pre-shRNA and later Dicer enzymes to form 21-25nt dsRNA duplexes that are similar to siRNA [409]. One advantage of shRNA is that, when encoded into lentivirus or retrovirus, it can incorporate into the genome, thus inducing stable knockdown and allowing researchers to study the long-term effects of inhibiting specific genes.

The introduction of the CRISPR-Cas9 (Clustered Regularly Interspaced Short Palindromic Repeats and CRISPR-associated protein 9) system in 2014 provided a new option for functional genomic studies in the mammalian system [410]. Different from siRNA and shRNA that target mRNAs, CRISPR-Cas9 utilises sgRNA (single guide RNA) and a long RNA scaffold consisting of multiple pieces of pre-designed RNA sequence to target specific DNA sequences. The Cas9 endonuclease can then cleave the genome at specific sites and induce double-strand breaks (DSBs) [411]. DSBs can be repaired by either error-prone non-homologous end joining (NHEJ) or error-free homology-directed repair (HDR). If the Cas9 cut sites are repaired via NHEJ, insertions and/or deletions will be introduced and disrupt the targeted locus [412]. These alterations are permanent

and normally can induce a thorough disruption of desired genes if both copies are edited.

All HTS techniques, including compounds, siRNA, shRNA and CRISPR-Cas9 have their unique pros and cons (Table 3.1). Compound screening using FDA-approved drugs has a great potential for clinical impact. Dose titration can also be applied to avoid losing candidates due to large "single agent" effects of the knockdown/knockout of important factors. However, the number of compounds included in this list is just above 1,000, which makes it less likely to identify novel targets as the compounds are well studied. Meanwhile, a comprehensive compound library may contain millions of drug leads which makes a screen without a specific drug target challenging. siRNA provides a convenient way to manipulate the expression of certain genes. However, its short half-life time limits its use in long-term experiments. In addition, the delivery of siRNA normally requires transfection, which restricts its use in some primary cells that are difficult to transfect [413]. shRNA encoded by lentivirus can partially solve this problem. Lentivirus can achieve high transduction efficiency in most cell lines, even in primary cells. The incorporation of a virus gene into the genome also allows stable knockdown of the desired gene, which provides the opportunity for studying the long-term effect of gene inhibition. However, due to the involvement of infectious virus, safety issues are still a major concern for the large-scale application of this technique. Additionally, both siRNA and shRNA techniques may exhibit off-target effects and the knockdown efficiency is variable between different experiments and cell lines [413]. CRISPR-Cas9, on the other hand, provides a thorough and complete removal of target genes, which is desired in many studies, especially when redundant proteins can still play a major role in a particular biological process. Nevertheless, the variability of gene editing efficiency in individual cells (some are repaired by HDR thus no gene mutation is induced) limits its use in arrayed screens. Recent studies revealing the strong off-target

effects related to CRISPR-Cas9 have also raised concerns about the reliability of CRISPR-Cas9 screening [414-416]. Each screening technique has its advantages and limitations, however, the key is to choose the method that best addresses the biological question.

A genome-wide siRNA screen followed by a focused chemical compound screen was selected for our approach. We made this choice based on a number of reasons:

a. A lentiviral pooled shRNA or sgRNA screen is more suitable for screening for gene inhibition that can promote cell survival/proliferation, while our screen was aimed at identifying gene inhibition that could cause synthetic lethality.
b. Most drugs used in the clinic are inhibitors rather than agonists. As a result, a knockdown screen is more suitable than a cDNA library-based gene overexpression screen.
c. The mechanism of CX-5461 is not fully understood. It is better to screen all available genes rather than particular pathways.
d. siRNA better mimics the effects of drugs than gene editing. The primary goal of our screen is to identify potential drug targets that can synergise with CX-5461 to treat HR proficient HGSC. Similar to chemical compounds, siRNA causes temporary inhibition on the targets, which better mimics the effects of drugs than gene editing which causes permanent effects. Further, compared to CRISPR-Cas9 which thoroughly abolished the expression of the targets, siRNA can only partially inhibit the target expression, which is also similar to chemical inhibitors [417].
e. CRISPR-Cas9 is more suitable for genetic biomarkers screens rather than drug targets screens [418].CRISPR-Cas9 would bring unnecessary noise into the screen. Both Cas9 and CX-5461 cause DDR [225, 419, 420]. The use of CRISPR-Cas9 may interfere with the interaction between CX-5461 and targeted genes and lead to unreliable results. For example, if enhanced

DDR was observed with CRISPR-Cas9 mediated gene knockout, there would be difficulties to distinguish whether the effect is caused by the CRISPR-Cas9 itself or the loss of the gene.

### 3.3. The design of the genome-wide siRNA screen

The screen comprised six different steps (Figure 3.1A):
1) Selection of the most suitable cell line for the screen;
2) siRNA transfection optimisation;
3) The primary screen. The primary screen was performed in a 384-well format in the presence of vehicle or CX-5461 using cell number (DAPI counting) as a readout. The whole-genome SMARTpool siRNA library (Dharmacon) targeting more than 18,000 genes was used in the primary screen. Each pool consists of four siRNA duplexes all designed to target distinct sites within protein-coding genes to ensure efficient gene knockdown effect. Targets that met certain criteria synergistic action with CX-5461 were selected for the secondary deconvolution screen;
4) The secondary deconvolution screen. Individual siRNA duplexes, rather than the pooled siRNA mix, were used for the secondary screen. Targets with two or more of the four siRNA duplexes that met predefined synergistic criteria were regarded as high-confidence candidates and were marked for further investigation;
5) Verification of the identified candidates in other HGSC cell lines;
6) Further in vitro and in vivo investigation of the identified targets.

The workflow of the primary and secondary screen was similar (Figure 3.1B). 1400 OVCAR4 cells were seeded and reversed transfected with siRNA duplexes in 384-well plates (4 replicate plates). 24hrs later, the transfection media was replaced with either vehicle or CX-5461 containing media (2 replicate plates

respectively). Cells were then incubated for another 48hrs before being fixed with paraformaldehyde (PFA). After that, cells were stained with DAPI and counted with Cytation 3 (BioTek).

### 3.4. Cell line selection and screen optimisation

The OVCAR4 cell line was selected for the screen based on following reasons: 1) high genomic similarity to high grade serous ovarian cancer (HGSC) with respect to copy-number alterations [6]; 2) Appropriate doubling time at approximately 43 hours which allowed at least one cell cycle during the drug treatment [421]; 3) Intermediate $GI_{50}$ dosage sensitivity to CX-5461 amongst our 31 human ovarian cancer cell line panel to allow a significant window in which to measure increased sensitivity. Two other HGSC cell lines, CAOV-3 and OVCAR-3, were also selected for validation experiments based on similar criteria (Figure 3.1C). We included the ovarian clear cell cancer (OCCC) line SKOV3 in our panel as well because it was known to be resistant to current platinum-based chemotherapy and the newly introduced PARP inhibitors [422, 423]. The inclusion of the SKOV3 cell line also provides an opportunity to test whether the identified synergistic combination can be applied to other ovarian cancer cell types, which may help to expand the indications of our findings. Additionally, all four cell lines possess functional BRCA1/2 genes and have mutant p53 (OVCAR3, OVCAR4 and CAOV3) or is p53-null (SKOV3) [6].

One key factor in an siRNA screen is cell seeding density. Ideally, the final cell confluence of negative control should be approximately 90%, which creates sufficient dynamic range for synthetic lethality identification. Over-confluency will lead to low transfection efficiency and should be avoided. We identified the

optimum seeding density to be 1400 cells per well by performing a preliminary cell proliferation assay with multiple conditions in 384-well plates (Figure 3.2A).

Another key factor affecting the reliability of siRNA-based screen is the transfection efficiency of siRNA and transfection-related toxicity. Effective gene knockdown will never be achieved if the siRNA duplexes cannot be delivered into the cells. On the other hand, transfection-related toxicity may also cause false-positive results due to unexpected low cell counts. In order to achieve the maximum transfection efficiency with lowest possible toxicity, we carried out a preliminary transfection optimisation experiment to determine the optimal transfection conditions. Briefly, we tested a number of transfection conditions with different transfection reagents (Dharmafect 1,2,3,4) and reagent concentrations, with either OTP-NT or siPLK1/siTOX as negative or positive control respectively. OTP-NT (ON-TARGET*plus*$^{TM}$ Non-targeting) is a non-targeting control siRNA that is used to determine the baseline cellular response in RNAi experiments. Theoretically, it should not cause any cytotoxic effect and the cell survival percentage should always be greater than 90% compared to non-transfected cells. siPLK1, in contrast, targets polo-like kinase 1 (PLK-1), a key component involved in mitotic spindle formation and cell-cycle progression [424, 425]. Depletion of PLK1, especially in cancer cells, dramatically inhibits cell proliferation and induces apoptosis, and is routinely used in the VCFG as a positive control, which should reduce cell viability by 90% [426]. siTOX is another positive control provided by Dharmacon, which should reduce cell viability by 99%. siRRN3 was used as a positive control of synergy effect with CX-5461. RRN3 is a component of the Pol I transcription complex and showed a weak synergistic effect with CX-5461 in our preliminary experiments. After comparing the cytotoxicity and transfection efficiency of multiple transfection conditions, we selected Dharmafect 4 at 0.035µl per well for the following screen (Figure 3.2B and C).

The optimal concentration of CX-5461 also needs to be defined for the screen. Ideally, the dosage should be sufficient to cause a desired effect on the cells while allowing sufficient dynamic range for identifying synthetic lethal effects. We set this threshold at a 20% reduction in relative cell number compared to vehicle-treated cells, which corresponds to a dosage of 80nM CX-5461, as obtained from a dose-response curve performed in a 384-well plate using cells transfected with OTP-NT (Figure 3.2D). We used 10nM linear interval for the CX-5461 dosage points which is not a routine practice for a normal dose response curve (which normally use log ratios to cover large dosage ranges). Although this practice failed to show the cell response at higher dosages of CX-5461, it offers the resolution we need to determine the optimum CX-5461 dosage for the screen.

The final siRNA transfection mixture composes of 1.5µl siRNA duplexes (1µM), 11µl lipid:Opti-MEM (0.035µl Dharmafect 4+10.965µl Opti-MEM), and 25µl OVCAR4 cells (1400 cells). During the screen, the siRNA and lipid:Opti-MEM were mixed and complexed for 20min in plate wells. Cells were then added on top of the mixture into each well by using a liquid handling robot. Plates were short spun and incubated for 24hrs before a media change.

Figure 3.3A demonstrates the typical layout of the screen plates. Columns 1 and 24 were left blank to avoid edge effects (liquid in the edge wells evaporates faster than other wells). Column 2 and 23 are filled with positive/negative controls, while all the remaining wells were filled with SMARTpool siRNAs.

## 3.5. Quality control of the screen

Multiple quality control measures were adopted to ensure the reliability and reproducibility of the screen results, including Z' factor, health report (standard deviation and %CV), plate metric QC (heat map), correlation plots, scatterplots, and data normalisation.

### 3.5.1 Z' factor

Z' factor is a parameter used to evaluate the sufficiency of the dynamic range between positive and negative controls. The formula for Z' factor is:

$$Z' = 1 - \frac{3(SD_{h.v\ control} + SD_{l.v\ control})}{|h.v\ control\ mean - l.v\ control\ mean|}$$

The concept of Z' factor is similar to that of student t-test. It measures the difference between the sum of the SDs of the positive/negative controls and the absolute difference between the means of positive/negative controls. The high SDs or/and the low difference of means would reduce the Z' factor value, indicating the poor differentiation between positive/negative controls. In contrast, a Z' factor close to 1 indicates a significant difference between positive/negative controls. A Z' factor at 0 suggests that the absolute difference between the means is 3 times larger than the sum of the SDs of positive/negative controls, which is the minimum acceptable dynamic range (difference) between positive/negative controls in our study. The Z' factor should always be greater than 0 in our study, especially between siPLK1 (the positive control) and OTP-NT (the negative control). If the factor is negative in certain plates, they are reassessed and repeated if necessary. Poor Z' factors might be caused by a reduced dynamic range (e.g. by low transfection efficiency) or/and high variability.

Figure 3.3B is an example of Z' factors report extracted from the screen. According to the table, the positive/negative control pair (mock/PLK1, OTP/PLK)

in all plates, treatments and replicates have Z' factors greater than zero. While the mock/RRN3 and OTP/RRN3 pairs have low Z' factors under vehicle treatment conditions, the values increased significantly in the drug-treated plates, which indicates the presence of synergistic effects.

### 3.5.2 Health reports

The health reports include the standard deviation and %CV (Coefficient of Variation) of the positive and negative controls in each plate. %CV= standard deviation/mean x 100%. This parameter indicates the variability of controls within every plate, which could be the cause of unexpectedly low Z' factors. Based on our experience with genome-scale screens, we define acceptable %CV between 10-24%, which is a window that still allows consistent statistical determination.

Figure 3.3C is an example of the health reports extracted from the screen. As can be seen from the table, the %CV of mock, OTP, and RRN3 controls are all within %CV=10%. The %CV is quite high for PLK1 which is caused by the low cell number. It is acceptable in this case due to the high cytotoxicity caused by the PLK1 knockdown and the significant dynamic range between PLK1 and OTP groups.

### 3.5.3 Plate metric QC

The plate metric QC compares the numerical differences of the controls on the left (column 2) and right (column 23) sides and presents the results in either table or heat map form. This parameter is used to evaluate if there are any technical issues caused by unequal dispensing by the BioTek. The maximum tolerated difference is 30%.

Figure 3.3D is an example of the LHS vs RHS (left to right column) report extracted from the screen. We can see that the LHS vs RHS ratio in all plates and replicates are within the range (0.7 to 1.3). Figure 3.4A is an example of heat map report extracted from the screen. The distribution of low/medium/high cell count wells is even across the whole plate, indicating no systematic technical issues with the screen.

### 3.5.4 Correlation plots

Correlation plots are used to compare the variability and reproducibility of replicates. The ratio should be as high as possible. A Pearson correlation coefficient (parametric) and Spearman correlation coefficient (non-parametric) over 0.8 indicates a good correlation between replicates. The results are demonstrated as correlation plots.

Figure 3.4B is an example of correlation plots extracted from the screen. The Pearson and Spearman correlation coefficients are 0.89 and 0.87 respectively, both of which indicate good reproducibility between replicate plates. All the replicates with Pearson and Spearman correlation coefficient lower than 0.75 are re-assayed.

### 3.5.5 Scatterplots and normalisation

The raw data of each library plate are accumulated and visualised by accumulated scatterplots, with controls being highlighted by different colours. This is one of the most straightforward and intuitive ways to identify any systematic problem with particular screen runs.

As the whole genome screen was performed in a time span of four months, it was almost inevitable to observe some variability of raw plate readouts between weekly screen runs. Normalisation is the most common strategy adopted to alleviate this problem. In our screen, we normalised data of each library plate to the median of the negative control OTP-NT.

Figure 3.4C and D are the scatterplots of the primary screen before and after normalisation. The primary screen was conducted in batches over a 4-month time period (16 384-well plates per week), so some variations in the cell count readout will be present between different batches. For example, in the vehicle panel of Figure 3.4C, the cell counts of plate 12032-12014 (the box with red dash) is generally lower than that of plate 12015-12018 (the box with blue dash), which makes it difficult to directly compare the results between plates. However, after the normalisation (the vehicle panel of Figure 3.4D), the distribution of the dots (blue, green, cyan and grey ones, which stand for the PLK1, OTP, RRN3 controls and samples respectively) of plate 12032-12018 (the box with red/blue dash) becomes more uniform, which enables comparison between plates. Any plates retaining high variability after normalisation were re-assayed.

## 3.6. Screen cut-off criteria

We set a number of cut-off criteria to identify strong synergistic candidates. We first excluded genes with a very low level of expression based on microarray data (Affymetrix 1.0ST expression array) obtained from Dr Karen Sheppard [173]. The threshold was arbitrarily set at 20 (normalised expression level), and 1,395 out of 18,120 genes were filtered out during this step (Figure 3.5A). Bliss independence was then calculated to quantify the synergistic effect. Bliss

independence is calculated as $\frac{1-Effect(Drug\ A+Drug\ B)}{(1-Effect(Drug\ A))*(1-Effect(Drug\ B))}$, which compares the observed combination effects with the predicted combination effects, and is widely used to analyse drug combination data to screen for candidate drug combinations [427, 428]. In our study, the Drug A is the siRNAs and the Drug B is CX-5461 (Figure 3.5B). Bliss independence lower than 0.9 is considered as synergy, while a value higher than 1.1 is considered as antagonism. Values between 0.9 and 1.1 are regarded as additive effects. However, during the preliminary experiments, we observed some false positive synergy readouts caused by the low relative cell number. For example, assuming the relative cell number of siRNA+CX-5461 (compared to OTP-NT transfected cell w/o CX-5461 treatment) is 0.05, while the relative cell number of siRNA is 0.1, and relative cell number of CX-5461 is 0.8, the Bliss independence is 0.625, which indicates strong synergistic effects. However, the actual change between siRNA+CX-5461 and siRNA is only 0.05, which is too small to be considered as synergistic effects. In order to solve this problem, we adopted another parameter that monitors the reduction of relative cell number between siRNA+CX-5461 and siRNA, whereas the cut-off was set to be higher than 0.25 in the primary screen. The application of these criteria ruled out the majority of the candidates, and the remaining 372 genes were selected for the secondary deconvolution screen (Figure 3.5A and Appendix I).

The secondary screen was conducted in a similar way as the primary screen with the exception that the SMARTpool siRNA mix was replaced by four individual siRNA duplexes targeting the same target. The Bliss independence was set to be lower than or equal to 0.8. Individual siRNA duplexes that can fulfil this criteria were identified as high confidence hits. Genes with more than 2 (out of 4) high confidence hits are classified as potential strong synergistic candidates. 17

potential strong synergistic candidates survived the secondary screen (Figure 3.5A, Table 3.2 and Appendix I).

## 3.7. Summary of the results

372 genes were identified from the primary screen. Gene pathway analysis by MetaCore™ (Thomson Reuters) was performed to identify if these hits were enriched in certain pathways. The results showed gene enrichment in DNA damage, inflammation/immune response, cell adhesion and potassium transport pathways, with DNA damage being at the top of the list (Figure 3.5C).

Among the 372 selected candidates, 17 were validated through the secondary screen (Table 3.2). Pathway enrichment analysis showed predominant enrichment in the DNA damage pathway (Figure 3.5D). Specifically, 3 out of 17 candidates, including RAD54L, BRCA2, and RAD51AP1, belong to this pathway. RAD51AP1 (RAD51 associated protein 1) is a RAD51 accessory protein that specifically stimulates joint molecule (the four-stranded branched intermediates formed by the conversion of the paired broken DNA and homologous duplex DNA during HR) formation through the combination of structure-specific DNA binding and physical contact with RAD51 [429]. RAD54L (DNA repair and recombination protein RAD54-like) is a multifunction protein. RAD54L binds RAD51 via its N-terminus and moves along chromatin to stimulate the DNA strand exchange activity of RAD51 [430]. It is also involved in the removal of RAD51 proteins after DNA joint formation and recombination initiation have occurred [258, 431, 432]. BRCA2, on the other hand, directly binds the single strand DNA during the initial step of the homologous recombination repair and facilitates the binding of RAD51 recombinase to the ssDNA and stimulate strand invasion [249, 433, 434]. These three genes play crucial roles in the homologous

recombination (HR) DNA repair pathway, consistent with the interactions between CX-5461 and HR pathway noted in sections 1.6.1 [429].

Gene network analysis (GNA) was also performed to identify the most critical genes in a range of candidates. GNA is largely based on protein-protein interaction (PPI) network, which records all the experimentally proven (or predicted) protein-protein interactions (connections) [435]. GNA normally identifies a small quantity of highly connected protein nodes, known as hubs, and many poorly connected nodes. It is widely believed that these 'hotspots' (hubs) are more important in organizing the network, which, in turn, convey the biological significance of network architectures, a key concept in systems biology [436]. Under the synthetic lethality genetic screen background, this means that deletion of a hub protein is more likely to be lethal than deletion of a non-hub protein, a phenomenon known as the centrality-lethality rule [437]. This method is commonly used to identify the most potent biomarkers or drug targets from a number of candidates [438]. NetworkAnalyst, with the STRING Interactome protein-protein interaction (PPI) database, was used to analyse and visualise the results in our screen [439]. According to Figure 3.5E and Table 3.3, BRCA2 and TOP1 were identified as the top two hubs measured by degree or betweenness. In a graph network, every gene is treated as a node. The degree of a node is the number of connections (interaction, activation, inhibition, phosphorylation, etc) it has to other nodes. According to the theory of the networking analysis, the more connections the gene has (i.e. the greater the degree value is), the more important role it plays in the gene regulation networks [439]. Thus, the genes with the most connections (the "hubs") are considered the most important genes in the gene network. The betweenness centrality measures the number of shortest paths going through the node, which is also used to measure the importance of nodes.

Based on these analyses, RAD54L, BRCA2, RAD51AP1 and TOP1 were chosen for further in vitro investigation.

### 3.8. A mini chemical compound screen identifies small molecules that can cooperate with CX-5641

siRNAs are powerful tools in genetic studies. However, their application in the clinic is still limited by the delivery efficiency and stability issues [440, 441], although a number of chemically modified or nanoparticle-coated siRNAs are currently under development aiming to solve these problems [442, 443]. In contrast, a more practical way is to use commercially available molecules, preferably approved drugs, to mimic the effects of the siRNA knockdown to confirm the results from the RNAi screen as well as improve the clinical impact of the findings. This approach has been adopted by a number of previous studies and has been proven to be both efficient and effective. For example, Veronica Veschi, et al. combined epigenetic siRNA and chemical screens to identify SETD8 inhibition as a therapeutic strategy for p53 activation in high-risk neuroblastoma [444] while Yen-Ling L. et al utilised a synergistic combination of small molecule inhibitors and RNA interference to target the antiapoptotic BCL-2 protein in head and neck cancer cells [445].

We also adopted a similar approach to identify the potential drug combinations that could improve the drug efficacy of CX-5461 in treating HGSC based on the candidates we identified from the RNAi screen. 9 small molecules targeting the RAD54L, BRCA2, RAD51AP1 and TOP1 were tested in a mini chemical compound screen to identify potential drug combinations with CX-5461, including Topotecan, streptonigrin, B02, AT13387, 17-AAG, spironolactone, pentoxifylline, KU-55933 and VE-82. Among them, Topotecan is a TOP1-

specific inhibitor, which blocks the re-ligation function of the TOP1 enzyme and has been approved as a second-line treatment option for ovarian cancer since 1996 [446, 447]; Streptonigrin has been reported to inhibit RAD54 by both direct binding and generating reactive oxygen species (RAD54 is a ATPase-dependent DNA translocases) [432, 448, 449]; B02 efficiently and specifically inhibits DNA strand exchange activity of RAD51 (RAD51 is a DNA homologous recombinase), and is able to disrupt RAD51 foci formation in response to DNA damage and inhibit DSB repair and DSB-dependent HR [450]; AT13387 (Onalespib) is a heat shock protein 90 (HSP90, a chaperone protein) inhibitor that can disrupt the expression of a variety of proteins including BRCA2, and is currently under phase 1/2 clinical trials either as a single agent or in combination to treat various types of cancer [451-454]; 17-AAG (Tanespimycin) is another HSP90 inhibitor that is also under phase 2 clinical trials [455-457]; spironolactone is an approved drug for antihypertension and has also been found to impair RAD51 foci formation, sensitise cancer cells to DNA damaging agents like PARP inhibitors and cross-linking agents and inhibit tumour growth in xenografts [458]; pentoxifylline is an approved drug for the treatment of cerebral ischemia and a variety of other vascular disorders such as intermittent claudication, which has also shown synergistic effects with radiotherapy in cancer patients through the inhibition of homologous recombination repair [459]; KU-55933 and VE-821 are inhibitors of ATM and ATR, respectively, both of which are under clinical trials and are able to inhibit HR indirectly [460-462]. In addition to these 9 drugs, we also included 4 additional drugs, namely Everolimus (mTORC1 inhibitor), BMN-673 (Talazoparib, PARP inhibitor), Cisplatin and ABT-199 (Venetoclax, BCL-2 inhibitor) since they have demonstrated synergy with CX-5461 in our previous studies [230], have been approved for ovarian cancer treatment or their target is present in the candidate list.

The focussed chemical compound screen was performed in a similar format as the RNAi screen. Briefly, 450 OVCAR4 cells in 40ul media were seeded into 384-well plates on Day 0 using the EL406 microplate dispenser (BioTek). Fewer cells were seeded as the drug treatment period was 5 days in the chemical compound screen compared to 2 days in the siRNA screen. 24 hours later (Day 1), media was replaced by the media containing pharmacological inhibitors of interest either with or without 50nM CX-5461. 5 days after the drug treatment (Day 6), cells were fixed and counted (Figure 3.6A). The cell counts were normalised to the median cells counts of the vehicle (DMSO)-treated cells either with or without CX-5461 treatment, e.g. the Topotecan/CX-5461 co-treated cells were normalised to 50nM CX-5461-treated cells, while the Topotecan-treated cells were normalised to vehicle-treated cells. 8 different doses were used to test the effects of drug combination with a fixed dose of CX-5461 (50nM) (Figure 3.6B). 50nM is approximately the $GI_{40}$ dosage of CX-5461 at 5 days of treatment, which leaves a sufficient window for the identification of synergistic effects.

The screen results were presented in a heatmap format by Prism 7 software using the mean relative cell number generated from N=5 experiments (Figure 3.6C). The red and blue colours represent low and high mean relative cell number respectively. Cells with dual treatment of chemical inhibitors and CX-5461 were compared in parallel with cells treated with chemical inhibitors only. If the co-treatment of both drugs could alter the drug response pattern and sensitise the cells to the tested chemical compounds, then the chemical compound potentially synergises with CX-5461. Strong synergy with dual treatment occurs when dual treatment is ‘red’ and chemical inhibitors only treatment is ‘blue’ at the same dosage. Drug combinations with increased sensitivity at two or greater continuous dosage points are defined as potential synergistic combinations and highlighted with green boxes in Figure 3.6C, which indicates that CX-5461 can synergise with

the chemical compound within a reasonable dosage window (at least 1 log) with a continuous trend.

The results revealed that 11 out of the 14 combinations have synergistic effects at different degrees. Specifically, 17-AAG, KU-55593，BMN-673 and cisplatin have the strongest synergistic effects with CX-5461 with respect to dosage windows (6-8 dosages), followed by spironolactone, AT13387, B02, Topotecan, VE-821, KU-55593+VE821 at 3-5 dosages. Topotecan and streptonigrin synergised with CX-5461 with a relatively narrow dosage window at 2 dosages. In contrast, pentoxifylline, Everolimus and ABT-199 did not show any synergistic effect with CX-5641. With regard to the degree of synergistic effects, 17-AAG at dosage point 2, Topotecan at dosage point 4, KU-55593+VE821 at dosage point 5 and BMN-673 at dosage point 4 had the strongest synergistic pattern. On the other hand, although streptonigrin showed synergistic effects with CX-5461, it only presented at low dosage points which was insufficient to inhibit cell growth. In summary, a number of HR, DDR and TOP1 inhibitors showed synergy with CX-5461, which further confirmed the results of our RNAi screen as well as provided new potential therapeutic opportunities for ovarian cancer.

## 3.9. Discussion

The studies presented in this chapter utilised both high-throughput genetic and pharmacological tools to screen for potential new targets whose inhibition could synergise with RNA Polymerase I inhibitor, CX-5461, to treat HGSC in a cell line model. After the primary and secondary siRNA-based screens, 17 genes were identified from the library as high confidence hits for synergistic effects with CX-5461. These hits were enriched in the HR repair pathways including RAD54L, RAD51AP1, and BRCA2, while gene network analysis revealed that the BRCA2 and TOP1 were the most important genes in the list.

One concern about the RNAi screen is that only a small number of candidates (17 genes) were identified from our screen which equates to less than 1% of the library. We attributed this circumstance to two potential causes. First, we defined strict criteria for selecting the strongest synergistic candidates. There may still be accessory/other important interactors to be identified from the screen data if we use less strict inclusion criteria. Second, the 48hrs drug treatment time used in the screen was empirically determined by our experience in haematological malignancies in which rapid apoptosis can be induced by CX-5461 within six hours [221]. However, we observed distinct responses of ovarian cancer cells to CX-5461 treatment compared to blood cancer cells. Cell cycle arrest, rather than apoptosis, was observed after CX-5461 treatment, and the $GI_{50}$ dosage (the concentration of drug that causes a 50% reduction in proliferation) was significantly lower after prolonged treatment, which indicates a delayed response to CX-5461 in ovarian cancer cells. This means that we were likely to have seen stronger synergistic effects and identified more candidates if we treated cells for longer time periods.

Another concern regarding the 17 genes is that the results of the pathway enrichment analysis might be biased due to the limited number of inputs. We thus further verified these findings using a mini chemical compound screen in addition to the siRNA screen to identify potential synergistic drug combinations. A number of pharmacological inhibitors were included in the screen including potential HR, DDR and TOP1 inhibitors as well as approved drugs for ovarian cancer. A fixed dose of CX-5461 was combined with pharmacological inhibitors at different doses, which allowed us to identify the trend and strength of the synergistic effects as well as the therapeutic window for each synergistic combination. We did not see any synergy with the CX-5461/Everolimus combination, which has demonstrated strong synergistic effects in treating MYC-driven lymphoma [230]. This highlights the distinct responses between different types of cancer. Encouragingly, a number of HR, DDR as well and TOP1 inhibitors showed good synergy with CX-5461. Specifically, HSP90 inhibitors, 17-AAG and AT13387; the RAD51 inhibitor B02 and potential HR inhibitor spironolactone showed remarkable synergistic effects in inhibiting cell proliferation with CX-5461 at various dosages, supporting a correlation between HR deficiency and high CX-5461 sensitivity. As HR status can be determined by the gene sequencing of mutations in the HR pathways, personalised medicine could be provided to HGSC patient with different genetic background. For those HR-deficient patients, CX-5461, which does not induce strong DNA damage and is well tolerated in patients, may provide an alternative treatment option for this patient cohort in addition to conventional chemotherapies, which damage DNA and is associated with strong side effects. This prospect is strongly supported by studies conducted by other groups. Xu, et al. showed that CX-5461 can induce selective lethality in BRCA1/2 deficient colorectal and triple negative breast cancer (TNBC) xenografts [225]. For those patients possessing proficient HR pathways and are likely to be insensitive to the conventional chemotherapies, drug combinations with CX-5461 and the HR inhibitors described above might be an option. However, risks are

associated with this option as the systematic inhibition of HR pathway might lead to the hypersensitivity of normal tissues to CX-5461, which could result in severe side effects. This concern could be mitigated as ovarian cancer patients with germline BRCA mutations are currently receiving standard chemotherapies [463]. Furthermore, both ATM and ATR inhibitors, KU-55593 and VE821, have shown strong synergistic effects with CX-5461, indicating that not only DNA damage repair pathways, but also DNA damage sensing and signalling pathways are involved in the cellular response to the CX-5461 treatment. This result further supports our previous finding that CX-5461 activates non-canonical ATM/ATR signalling [420]. Additionally, CX-5461 synergises with the classic and emerging drugs used for first and second-line ovarian cancer treatment, including cisplatin, Topotecan and PARP inhibitor BMN-673 (Talazoparib). One important outcome from our findings is that although CX-5461 alone is not efficient in killing ovarian cancer cells, it can enhance the effects of standard therapies. This concept is further strengthened when taking the potential adverse effects into account. Unlike conventional chemotherapeutic drugs, CX-5461 does not induce severe side effects such as haematological suppression or neurotoxicity. However, CX-5461 does result in phototoxicity, causing mucositis, nausea, dry eyes and hand-foot syndrome [464, 465]. All these side effects are minor and easy to control. This may allow CX-5461 to be a safe drug combination partner with established drugs to treat ovarian cancer.

The synergistic candidates identified from the siRNA screen and mini drug screen will allow us to potentially improve the therapeutic efficacy of CX-5461 in treating ovarian cancer. We selected BRCA2 and TOP1 for further investigation based on their highest ranking in the gene analysis network and that they are current drug targets in ovarian cancer treatment. BRCA2 plays a predominant role in the HR pathway and is the second most frequently mutated gene in HGSC (15~20%) [11]. BRCA2-deficient ovarian cancer is normally sensitive to

chemotherapy and has a better prognosis than its proficient counterparts. This selectivity has also been observed with CX-5461, which has been reported to be a DNA G-quadruplex (G4-DNA) stabiliser [225]. G4-DNA is a naturally formed four-stranded DNA secondary structure that has been shown to regulate various cellular pathways including DNA replication, gene expression and telomere maintenance [466-468]. G4-DNA can be unwound and resolved by DNA helicases such as such as Pif1, FANCJ, Bloom syndrome (BLM) [466, 469]. The persistence of G4-DNA caused by a stabiliser or the absence of these helicases induces replication fork stalling and collapse. The HR pathway has been reported to play a role in the repair of this damage [470]. The potential of targeting BRCA2 compromised tumours using G4-DNA stabilisers, such as PDS or CX-5461, has been investigated in multiple studies, and the results are promising [225, 471]. The presence of BRCA2 in the candidate list is a good demonstration of the efficacy and reliability of the screen.

TOP1 encodes DNA topoisomerase I, a highly conserved housekeeping enzyme that relieves the supercoiling and torsional tension of DNA caused by DNA replication and transcription by transiently nicking and re-joining one of the two strands of DNA [472]. TOP1 can be inhibited by Camptothecin and its chemical derivatives, Topotecan and Irinotecan [473]. Intriguingly, Topotecan is currently being used in the clinic as a second-line treatment option for chemo-resistant HGSC, which suggests that TOP1 plays a critical role in HGSC development and will be discussed in greater detail in the following chapter [447, 474]. In short, BRCA2 and TOP1 showed a strong presence in both clinical and laboratory indications and were thus selected for in-depth investigation. Some of the other candidates from the mini drug screen including the ATM/ATR inhibitors, cisplatin and PARP inhibitors, are currently being investigated by Dr Elaine Sanij from our laboratory in combination with CX-5461 to treat ovarian cancer.

**Table 3.1 Summary of the HTS methods available in Victorian Centre of Functional Genomics (VCFG) in Peter MacCallum Cancer Centre**

| Category | Compounds | siRNA | shRNA | sgRNA (CRISPR-Cas9) |
|---|---|---|---|---|
| **Scale** | Library from WEHI including FDA approved drugs (~4100) | Genome-wide (>18000 genes) or customised | Genome-wide (>18000 genes) or customised | Genome-wide (>19000 genes) |
| **Formats** | Arrayed | Arrayed | Pooled | Pooled |
| **Delivery** | Direct treatment | Transfection | Lentivirus infection | Lentivirus infection |
| **Effect** | Depending on individual drugs | Transient (2-7 days) knockdown | Stable knockdown | Stable knockout |
| **Advantages** | Clinical impact; Controllable dosage | Can target almost every gene | Can target almost every gene; Long-term effect | Can target almost every gene; Permanent effect |
| **Disadvantages** | Limited coverage; Mechanism of some drugs are not clear | Off-target effects; Some cell lines are difficult to transfect; Knockdown efficiency is not guaranteed; Short effective time | Off-target effects; Knockdown efficiency is not guaranteed | Off-target effects; Some genes' knockout is lethal |

## Table 3.2 High confidence synergistic candidates list

| # of siRNA duplexes | Candidates | | | |
|---|---|---|---|---|
| **4/4** | RAD54L | BRCA2 | | |
| **3/4** | LHFPL2 | | | |
| **2/4** | SACS | SELE | ATP9B | BCL2L13 |
| | RAD51AP1 | FUCA1 | MYO18B | ZNF77 |
| | ANKRD36 | BPIFB4 | C18orf19 | IGFBP1 |
| | USH1G | TOP1 | | |

## Table 3.3 List of top hubs

| Label | Degree | Betweenness |
|---|---|---|
| TOP1 | 23 | 827.97 |
| BRCA2 | 21 | 731.17 |
| RAD54L | 7 | 200.87 |
| RAD51 | 3 | 156.63 |
| RAD51AP1 | 3 | 97 |
| TP53 | 2 | 432.13 |
| RAD52 | 2 | 73.67 |
| RECQL | 2 | 73.67 |
| UBC | 2 | 49 |
| DMC1 | 2 | 15.63 |
| RAD51C | 2 | 15.63 |
| RAD51B | 2 | 15.63 |

**Figure 3.1 Design of the screen**

**A**. The screen consisted of six different procedures: 1) cell line selection, 2) transfection optimisation, 3) primary screen, 4) secondary screen, 5) testing in other cell lines and 6) further studies in vitro and in vivo. **B**. The workflow of the primary and secondary screen. During a typical round of the primary or secondary screen, the OVCAR4 cells were seeded and reverse transfected on Day 1. On Day 2, the transfection media was removed and replaced by the fresh growth media with either vehicle or 80nM CX-5461. Cells were cultured for another 2 days, and were fixed, stained and counted on Day 4. **C.** $GI_{50}$ dosages (concentration of drug to cause 50% inhibition of cell growth) of our panel of 36 ovarian cancer cell line after 48 hours treatment of CX-5461. The raw data were provided by Dr Karen Sheppard. Cell lines with mutant p53 are in red, while ones with wild type p53 are in blue. This is no correlation between p53 status and CX-5461 sensitivity. The OVCAR3, OVCAR4, CAOV3 and SKOV3 cell lines that were used in our study are indicated by the red arrows.

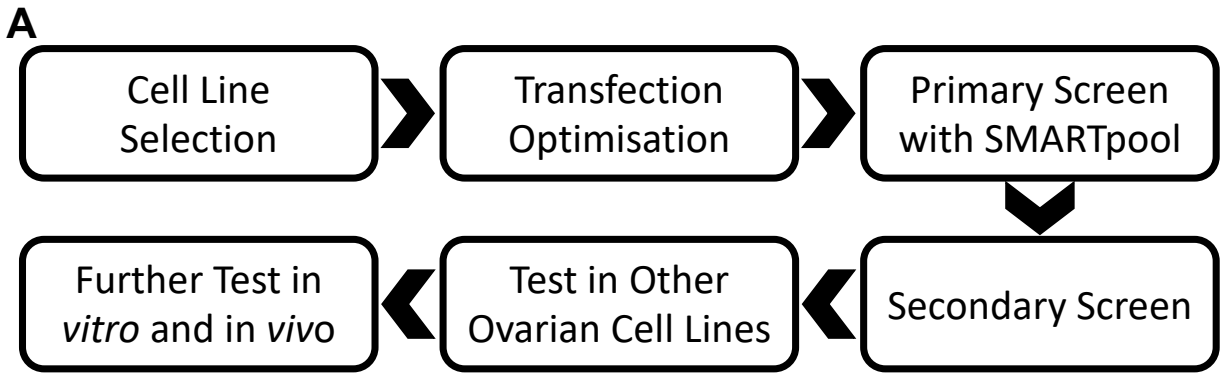
A
Cell Line Selection
Transfection Optimisation
Primary Screen with SMARTpool
Secondary Screen
Test in Other Ovarian Cell Lines
Further Test in *vitro* and in *vivo*

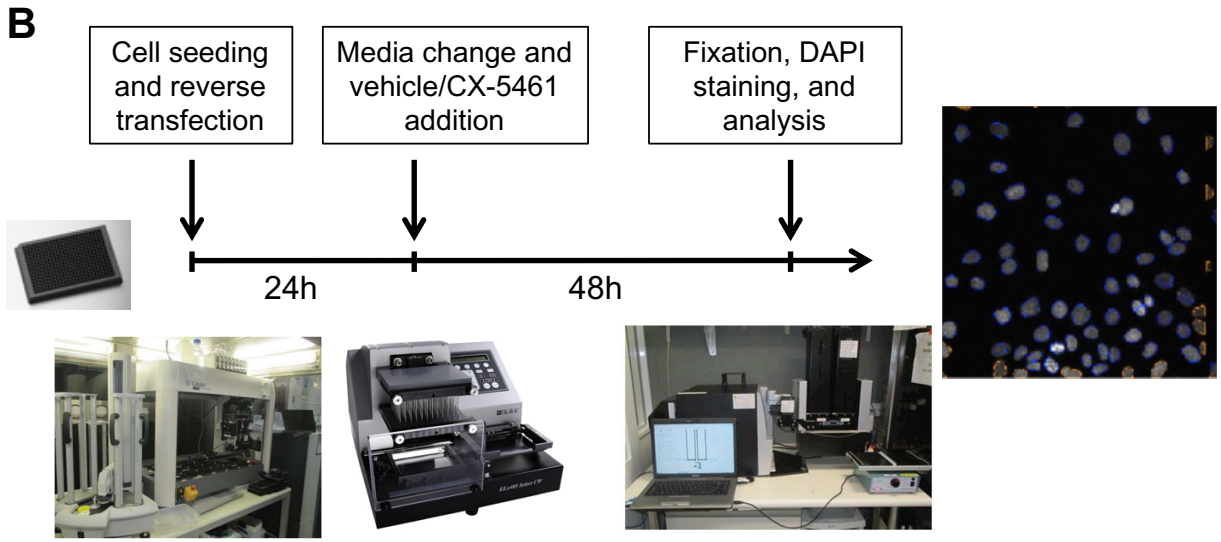
B
Cell seeding and reverse transfection
Media change and vehicle/CX-5461 addition
Fixation, DAPI staining, and analysis
24h
48h

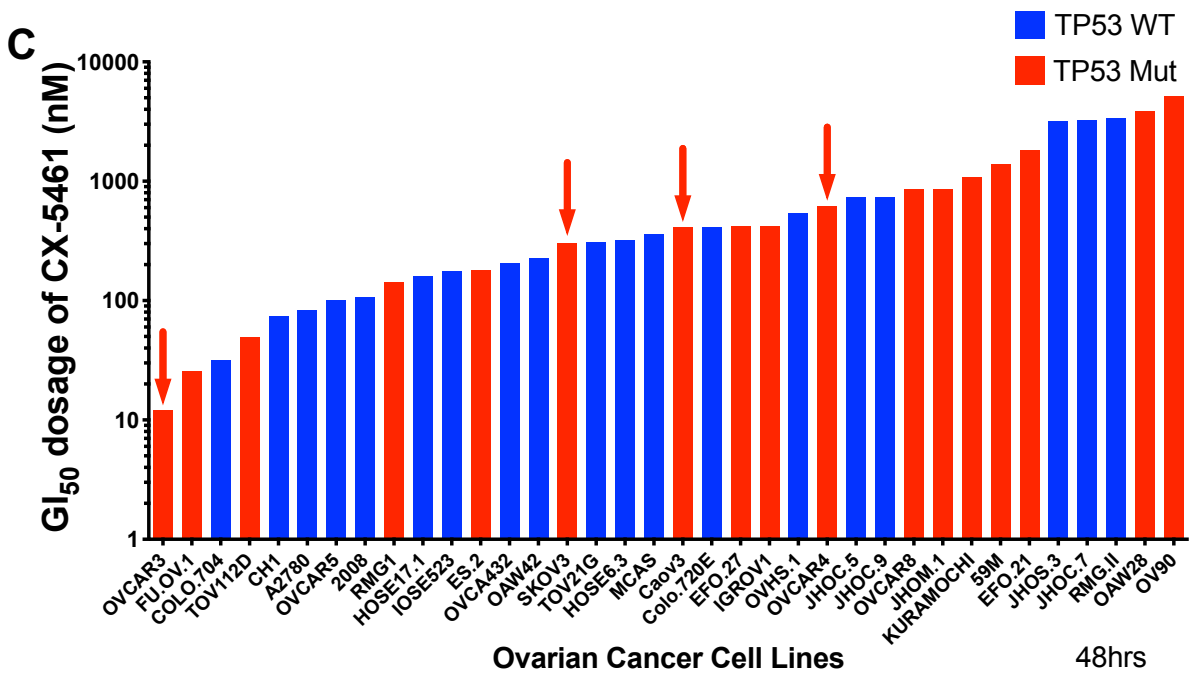
C
TP53 WT
TP53 Mut
GI50 dosage of CX-5461 (nM)
10000
1000
100
10
1
OVCAR3
FU.OV.1
COLO.704
TOV112D
CH1
A2780
OVCAR5
2008
RMG1
HOSE17.1
IOSE523
ES.2
OVCA432
OAW42
SKOV3
TOV21G
HOSE6.3
MCAS
Caov3
Colo.720E
EFO.27
IGROV1
OVHS.1
OVCAR4
JHOC.5
JHOC.9
OVCAR8
JHOM.1
KURAMOCHI
59M
EFO.21
JHOS.3
JHOC.7
RMG.II
OAW28
OV90
Ovarian Cancer Cell Lines
48hrs

**Figure 3.2 Screen optimization**

**A.** A series of experiments using cells with different transfection conditions (with OTP-NT) were tested to determine the optimal cell seeding density. A cell confluence of 90% 48 hours after OTP-NT transfection was necessary. 1400 cells per well met this requirement and was thus selected for the actual screen. **B**. OTP-NT transfected cells were compared to non-transfected cells to determine the cytotoxicity of the transfection conditions. DF3 and DF4 demonstrated lower toxicity than DF1 and DF2 as the relative cell number was always above 0.9 when compared to non-transfected control. **C**. siPLK1 and siTOX were used as the positive controls to determine the efficiency of different transfection conditions. Relative cell number lower than 0.15 with siPLK1 and Relative cell number lower than 0.05 with siTOX indicated high transfection efficiency. DF4 at 0.03µl and 0.04µl per well met these criteria. N=1 experiment. **D.** The $IC_{20}$ dosage (concentration of drug to cause 20% reduction of cell number compared to vehicle) of CX-5461 (80nM) after 48 hours treatment was selected for the screen as it could cause a reduction in cell number that still allowed sufficient dynamic range for identifying synthetic lethal effects. Combined data of N=3 experiments presented as mean±SD.

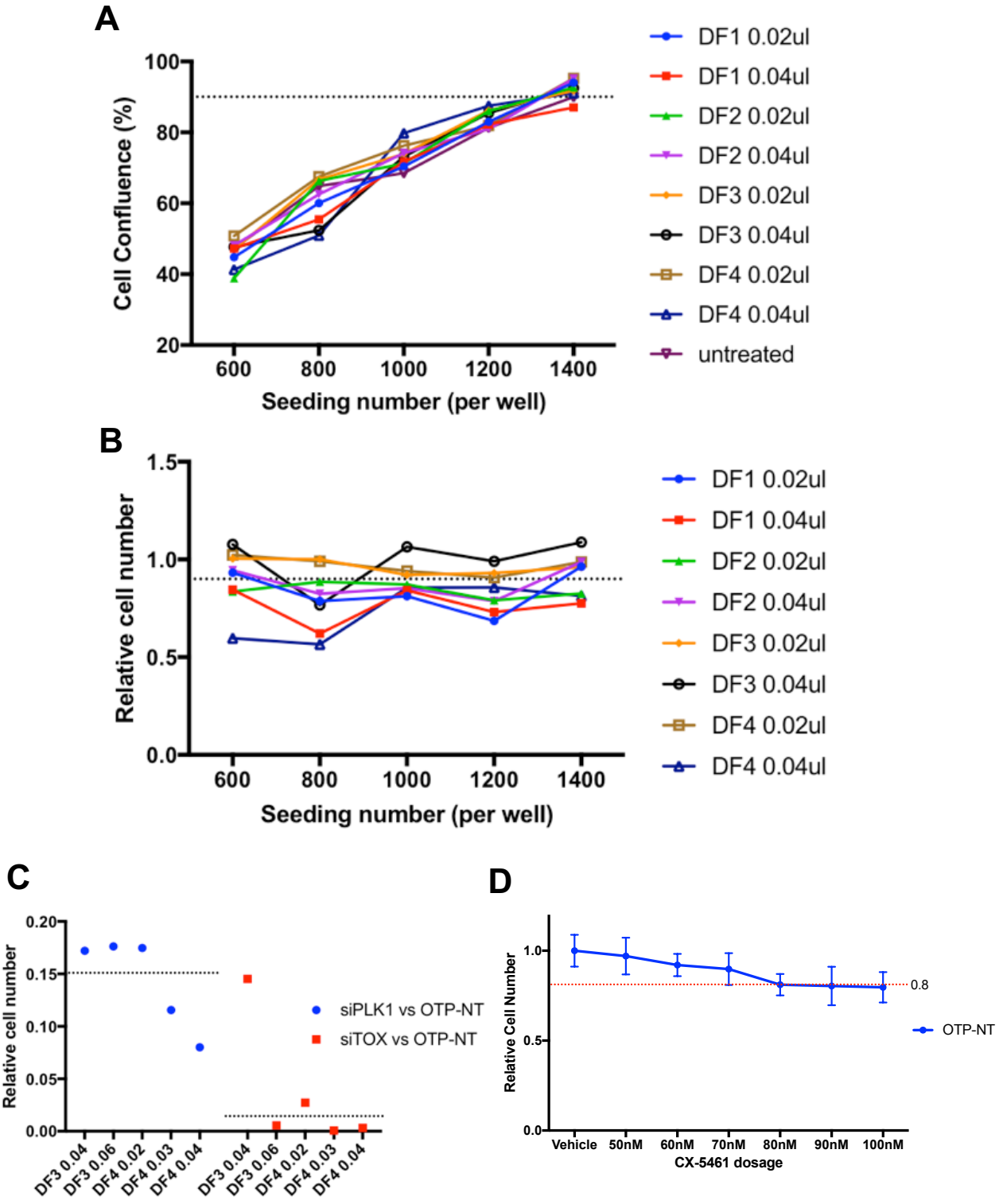
A
Cell Confluence (%)
100
80
60
40
20
600
800
1000
1200
1400
Seeding number (per well)
DF1 0.02ul
DF1 0.04ul
DF2 0.02ul
DF2 0.04ul
DF3 0.02ul
DF3 0.04ul
DF4 0.02ul
DF4 0.04ul
untreated
B
Relative cell number
1.5
1.0
0.5
0.0
600
800
1000
1200
1400
Seeding number (per well)
DF1 0.02ul
DF1 0.04ul
DF2 0.02ul
DF2 0.04ul
DF3 0.02ul
DF3 0.04ul
DF4 0.02ul
DF4 0.04ul
C
Relative cell number
0.20
0.15
0.10
0.05
0.00
DF3 0.04
DF3 0.06
DF4 0.02
DF4 0.03
DF4 0.04
DF3 0.04
DF3 0.06
DF4 0.02
DF4 0.03
DF4 0.04
siPLK1 vs OTP-NT
siTOX vs OTP-NT
D
Relative Cell Number
1.0
0.5
0.0
0.8
OTP-NT
Vehicle
50nM
60nM
70nM
80nM
90nM
100nM
CX-5461 dosage

**Figure 3.3 Quality controls of the screen**

**A.** Layout of the screen plates. Columns 1 and 24 were filled with media to prevent evaporation. Columns 2 and 23 contained randomized negative and positive controls. Columns 3-22 contained 320 randomly distributed siRNAs.
**B.** Example of Z' factors. The Z' factors of mock/PLK1 and OTP/PLK1 pairs were always larger than 0, which indicated the significant dynamic range between positive and negative controls. The Z' factors of OTP/RRN3 pair became larger after drug treatment, which was an indication of the existence of synergistic effect.
**C.** Example of health reports. %CV below 15% indicated low variation and good reproducibility between replicates of positive and negative controls. The high %CV of siPLK1 was acceptable due to the low cell numbers.
**D.** Example of LHS vs RHS report. The LHS:RHS ratio were within the range of 0.7 to 1.3 which indicated low edge effects within the plates.

**A**

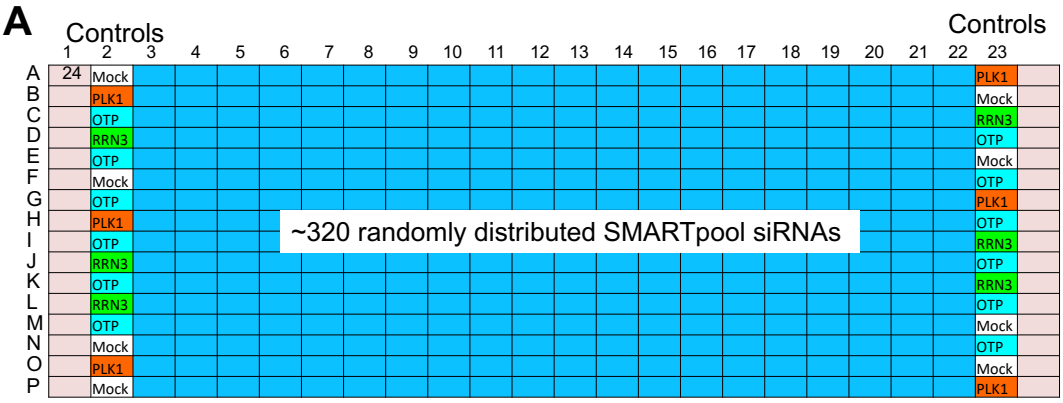


**B**

Vehicle

| plate | control.duo | REP1 | REP1.z.prime.factor | REP2 | REP2.z.prime.factor |
|---|---|---|---|---|---|
| 12013 | mock/PLK1 | 001A | 0.06 | 001B | 0.06 |
| 12014 | mock/PLK1 | 002A | 0.46 | 002B | 0.49 |
| 12013 | mock/RRN3 | 001A | -1.38 | 001B | -1.38 |
| 12014 | mock/RRN3 | 002A | -0.35 | 002B | -0.54 |
| 12013 | OTP/PLK1 | 001A | 0.07 | 001B | 0.07 |
| 12014 | OTP/PLK1 | 002A | 0.63 | 002B | 0.58 |
| 12013 | OTP/RRN3 | 001A | -1.56 | 001B | -1.56 |
| 12014 | OTP/RRN3 | 002A | 0.03 | 002B | -0.02 |

Drug

| plate | control.duo | REP1 | REP1.z.prime.factor | REP2 | REP2.z.prime.factor |
|---|---|---|---|---|---|
| 12013 | mock/PLK1 | 001C | 0.55 | 001D | 0.37 |
| 12014 | mock/PLK1 | 002C | 0.18 | 002D | 0.45 |
| 12013 | mock/RRN3 | 001C | 0.22 | 001D | -0.19 |
| 12014 | mock/RRN3 | 002C | -0.12 | 002D | 0.2 |
| 12013 | OTP/PLK1 | 001C | 0.57 | 001D | 0.35 |
| 12014 | OTP/PLK1 | 002C | 0.42 | 002D | 0.53 |
| 12013 | OTP/RRN3 | 001C | 0.31 | 001D | -0.22 |
| 12014 | OTP/RRN3 | 002C | 0.23 | 002D | 0.33 |

**C**

Vehicle

| plate | Control | Mean Cell Count | SD Cell Count | %CV |
|---|---|---|---|---|
| 1 | mock | 4722.12 | 515.92 | 10.93 |
| 1 | OTP | 5503 | 485.89 | 8.83 |
| 1 | PLK1 | 915.5 | 171.89 | 18.78 |
| 1 | RRN3 | 3130.33 | 372.23 | 11.89 |

Drug

| plate | Control | Mean Cell Count | SD Cell Count | %CV |
|---|---|---|---|---|
| 1 | mock | 4204.25 | 466.06 | 11.09 |
| 1 | OTP | 4471.75 | 665.56 | 14.88 |
| 1 | PLK1 | 899.5 | 291.88 | 32.45 |
| 1 | RRN3 | 2161 | 136.43 | 6.31 |

**D**

| screen.run | parameter | plate | rep1.average | rep1.average | rep1.RHS.LHS.ratio | rep2.average. | rep2.average. | rep2.RHS.LHS.ratio |
|---|---|---|---|---|---|---|---|---|
| 20150609 | cell.count | 12039 | 1021 | 1157 | 1.13 | 1192 | 1293 | 1.08 |
| 20150609 | cell.count | 12040 | 1350 | 1566 | 1.16 | 1337 | 1450 | 1.08 |
| 20150609 | cell.count | 12041 | 1268 | 1558 | 1.23 | 1394 | 1642 | 1.18 |
| 20150609 | cell.count | 12042 | 1405 | 1500 | 1.07 | 1322 | 1599 | 1.21 |

**Figure 3.4 Quality controls of the screen (continued)**

**A.** Example heat map report. Relative cell numbers compared to mean of OTP-NT controls were as indicated: red, very low; blue, low; green, comparable; and cyan, very high. The map shows that the four colours were randomly distributed across the plate, which indicated low edge effects within the plate. All positive controls were in red or blue, which indicated the robustness and reliability of the controls. **B.** Example of correlation report. The correlation plots measured the reproducibility between the two replicates. A Pearson correlation coefficient over 0.8 indicated good correlation between the replicates. **C, D.** Examples of scatterplots of the primary screen **(C)** before and **(D)** after normalization. The variability between plates was dramatically reduced after normalisation.

**A**

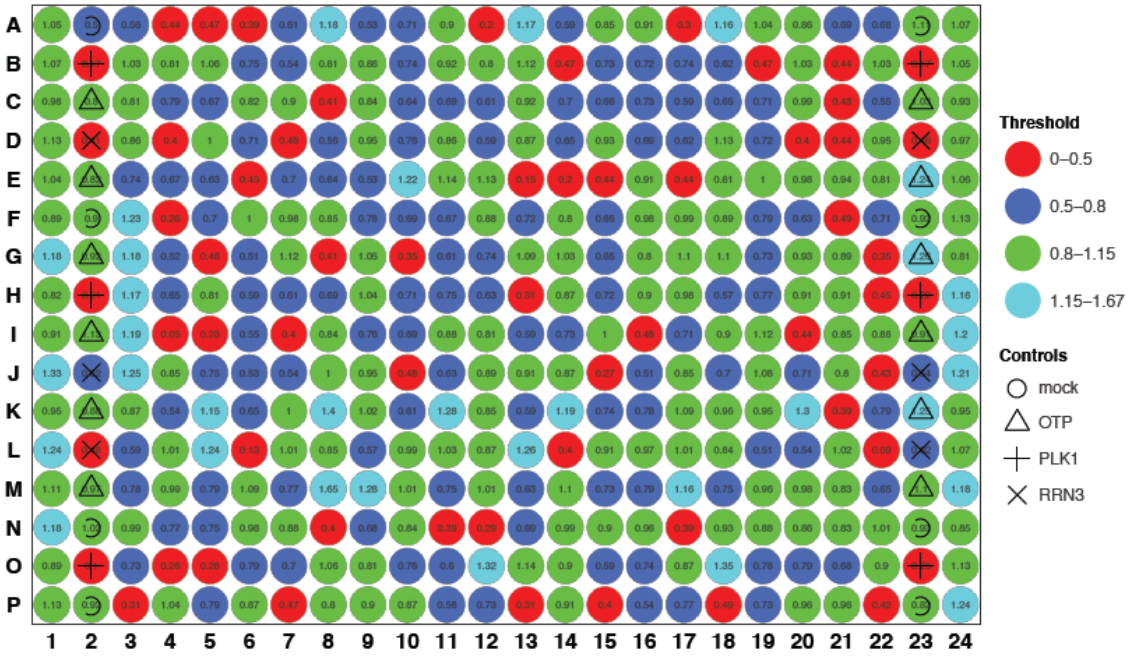
A
B
C
D
E
F
G
H
I
J
K
L
M
N
O
P
1 2 3 4 5 6 7 8 9 10 11 12 13 14 15 16 17 18 19 20 21 22 23 24
Threshold
0–0.5
0.5–0.8
0.8–1.15
1.15–1.67
Controls
mock
OTP
PLK1
RRN3

**B**

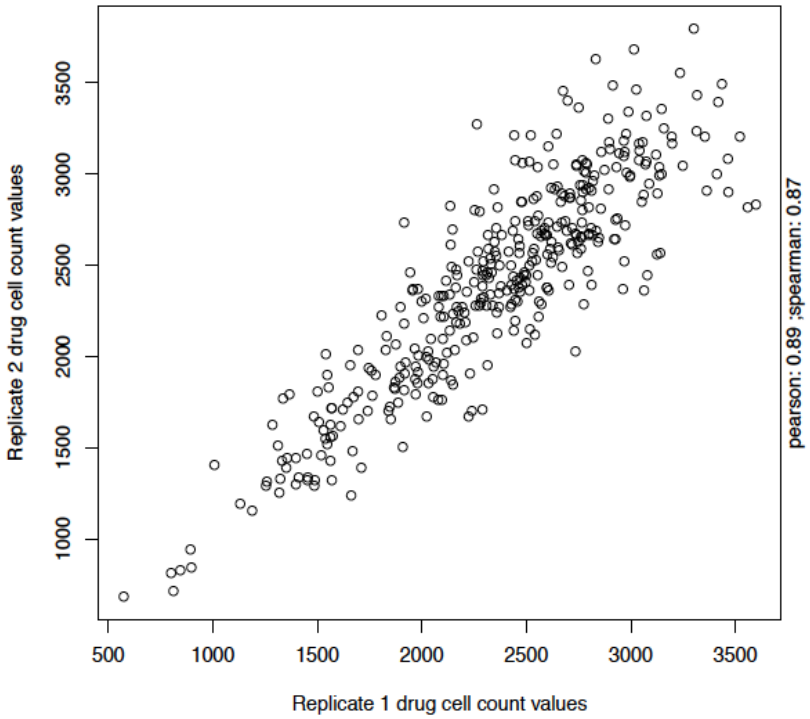
Replicate 2 drug cell count values
1000
1500
2000
2500
3000
3500
500
1000
1500
2000
2500
3000
3500
Replicate 1 drug cell count values
pearson: 0.89 ;spearman: 0.87

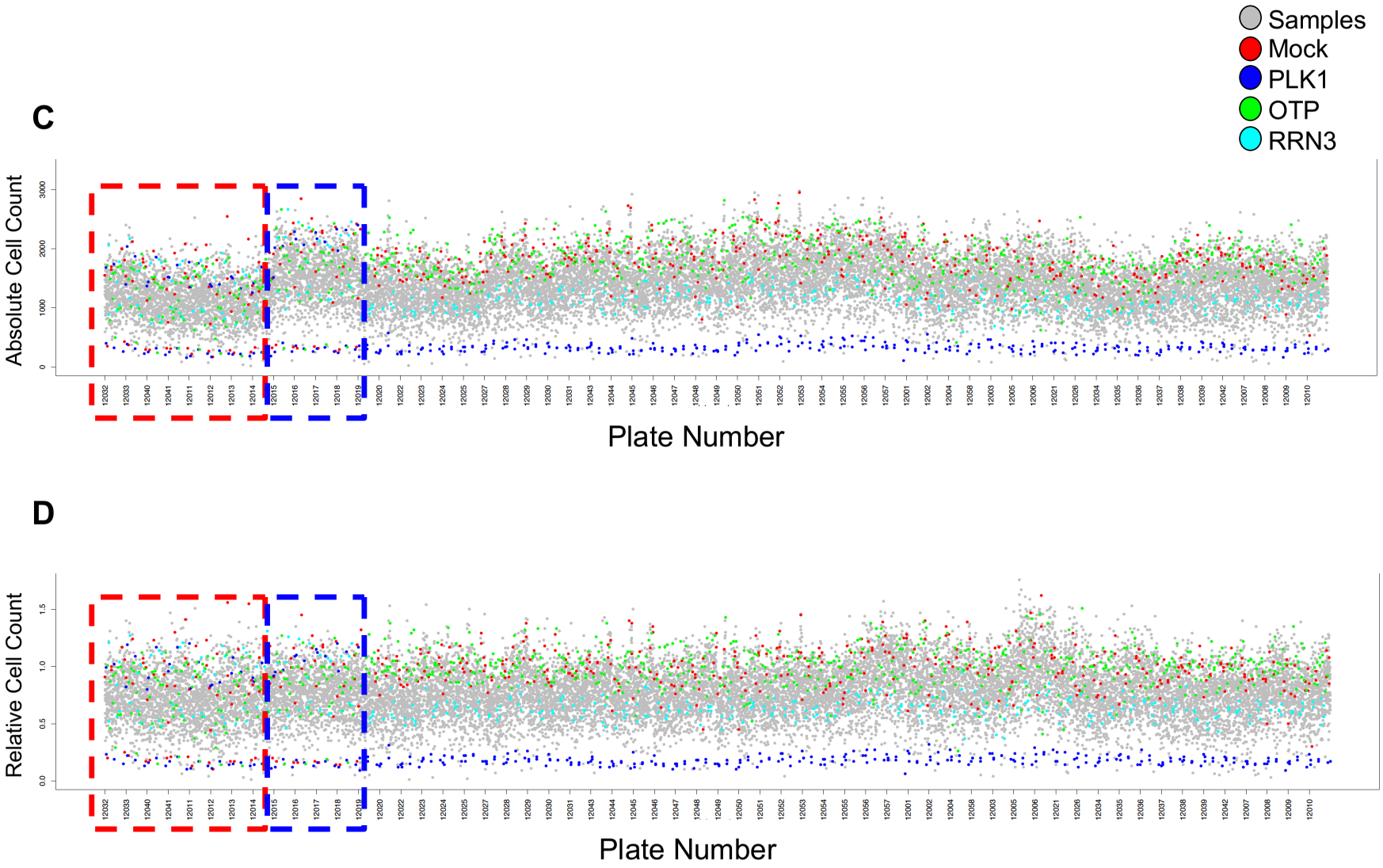
C
Samples
Mock
PLK1
OTP
RRN3
Absolute Cell Count
0
1000
2000
3000
Plate Number
D
Relative Cell Count
0.0
0.5
1.0
1.5
Plate Number

**Figure 3.5 Summary of screen criteria and siRNA screen results**

**A.** Target selection criteria. Genes with very low expression level were first excluded from the candidates list. The primary and secondary deconvolution screens were then performed and targets were selected based on the relative cell number and Bliss independence. **B.** Calculation of the Bliss independence. Generally, the Bliss independence measures the difference between the actual and the predicted drug effects on relative cell number. **C.** Pathway enrichment of primary screen candidates. Pathways with p-value lower than 0.01 were listed. Candidates were enriched in the DNA damage pathway, followed by inflammation and cell adhesion pathways. **D.** Pathway enrichment of secondary screen candidates. Pathways with p-value lower than 0.05 were listed. Candidates were enriched in the DNA damage pathway, followed by cell cycle pathways. **E.** Gene networking analysis showed that TOP1 and BRCA2 were at the hubs of the 17 genes network, which indicated the most important targets in the candidate list.

**A**

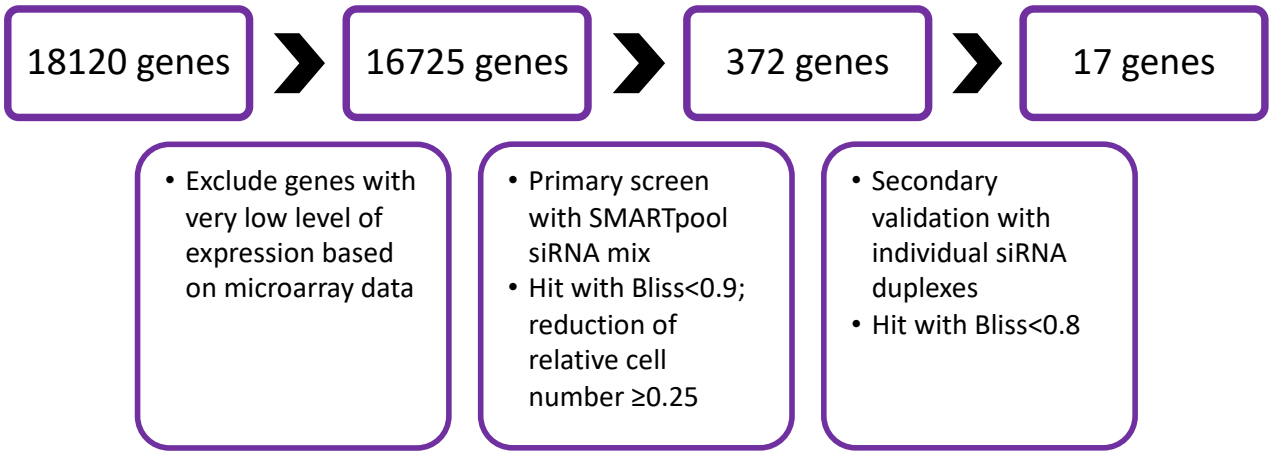


**B**

$$\text{Bliss Indep.} = \frac{\text{Relative Cell Number (siRNA+CX-5461)}}{\text{Relative Cell Number (siRNA)} \times \text{Relative Cell Number (CX-5461)}}$$

**C**

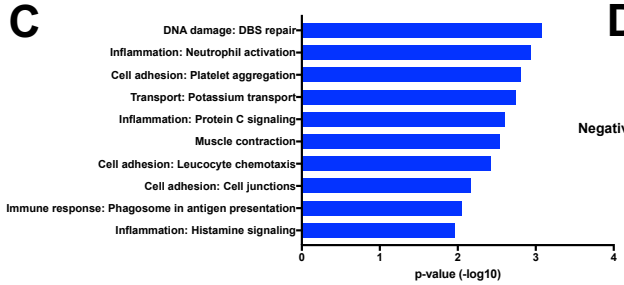


**D**

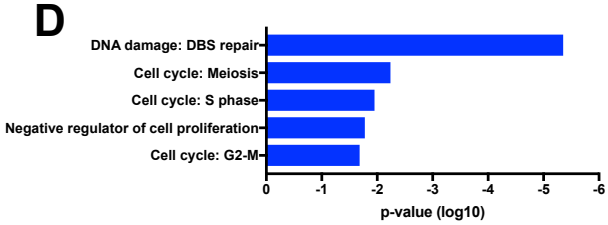


**E**

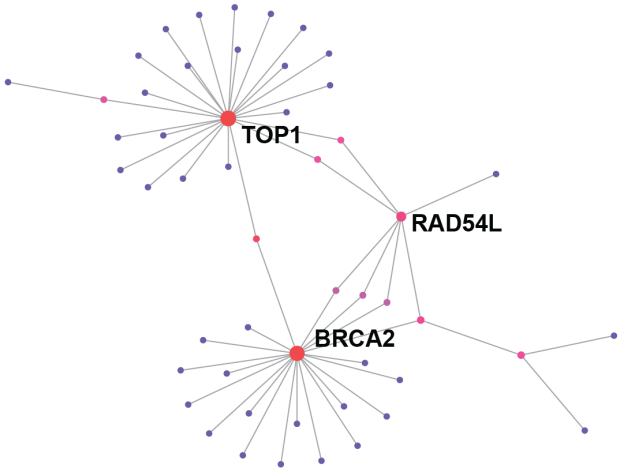

**Figure 3.6 Summary of mini chemical compound screen and results**

**A.** The workflow of the mini chemical compound screen. 450 OVCAR4 cells were seeded into 384-well plates per well on Day 0. On Day 1, the media was removed and replaced by the fresh growth media with chemical compounds either with or without 50nM CX-5461. The drug concentrations are listed in **B.** Cells were cultured for another 5 days, and were fixed, stained and counted on Day 6. **C.** The screen results were presented in a heatmap. The red and blue colours indicate low and high relative cell number, respectively. Cells with dual treatment of chemical inhibitors and CX-5461 were compared in parallel with the cells treated with chemical inhibitors only. If the co-treatment of both drugs altered the drug response pattern and sensitised the cells to the tested chemical compounds, then it indicates that the chemical compound potentially synergises with CX-5461. Drug combinations with increased sensitivity to at least two continuous dosage points are defined as potential synergistic combinations and highlighted with green boxes, which indicates that the CX-5461 can synergise with the chemical compound in a dosage window of at least 1 log. The heatmap was generated using the mean relative cell number of N=5 experiments.

**A**

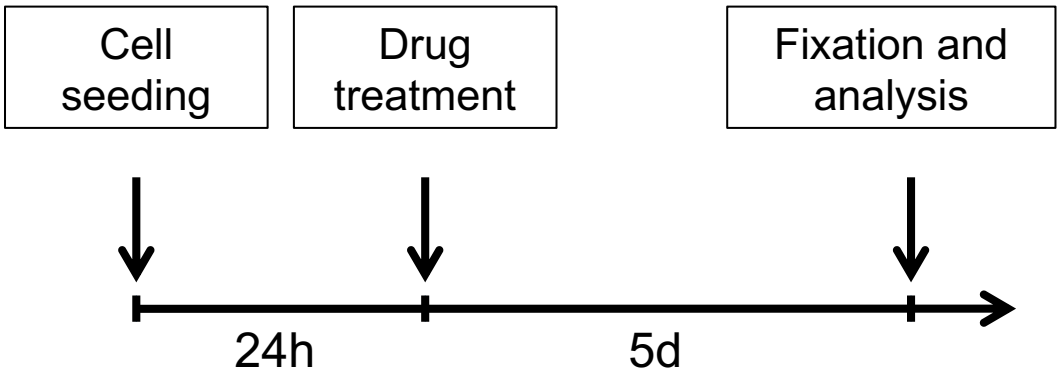


**B**

| Category | TOP1i | RAD54i | RAD51i | HSP90i | HSP90i | HRi | HRi | mTORi | | ATM/ATRi | PARPi | BCL-2i | ATMi | ATRi |
|---|---|---|---|---|---|---|---|---|---|---|---|---|---|---|
| Drug name | Topotecan | Streptonigrin | B02 | AT13387 | 17-AAG | Spironolactone | Pentoxifylline | Everolimus | Cisplatin | KU-55933 +VE-821 | BMN-673 | ABT-199 | KU-55593 | VE-821 |
| Dosages | 1000.00 nM | 100.000 nM | 100.000 uM | 1000.00 nM | 1000.00 nM | 100.000 uM | 10.0000 mM | 1000.00 nM | 10.0000 uM | 100.000 uM | 1000.00 nM | 100.000 uM | 100.000 uM | 100.000 uM |
| | 333.33 nM | 33.333 nM | 33.333 uM | 333.33 nM | 333.33 nM | 33.333 uM | 3.3333 mM | 333.33 nM | 3.3333 uM | 33.333 uM | 333.33 nM | 33.333 uM | 33.333 uM | 33.333 uM |
| 1 | 111.11 nM | 10.000 nM | 11.111 uM | 111.11 nM | 111.11 nM | 11.111 uM | 1.1111 mM | 111.11 nM | 1.1111 uM | 11.111 uM | 111.11 nM | 11.111 uM | 11.111 uM | 11.111 uM |
| 2 | 37.04 nM | 3.333 nM | 3.704 uM | 37.04 nM | 37.04 nM | 3.704 uM | 0.3704 mM | 37.04 nM | 0.3704 uM | 3.704 uM | 37.04 nM | 3.704 uM | 3.704 uM | 3.704 uM |
| 3 | 12.35 nM | 1.000 nM | 1.235 uM | 12.35 nM | 12.35 nM | 1.235 uM | 0.1235 mM | 12.35 nM | 0.1235 uM | 1.235 uM | 12.35 nM | 1.235 uM | 1.235 uM | 1.235 uM |
| 4 | 4.12 nM | 0.333 nM | 0.412 uM | 4.12 nM | 4.12 nM | 0.412 uM | 0.0412 mM | 4.12 nM | 0.0412 uM | 0.412 uM | 4.12 nM | 0.412 uM | 0.412 uM | 0.412 uM |
| 5 | 1.37 nM | 0.100 nM | 0.137 uM | 1.37 nM | 1.37 nM | 0.137 uM | 0.0137 mM | 1.37 nM | 0.0137 uM | 0.137 uM | 1.37 nM | 0.137 uM | 0.137 uM | 0.137 uM |
| 6 | 0.46 nM | 0.033 nM | 0.046 uM | 0.46 nM | 0.46 nM | 0.046 uM | 0.0046 mM | 0.46 nM | 0.0046 uM | 0.046 uM | 0.46 nM | 0.046 uM | 0.046 uM | 0.046 uM |
| 7 | 0.15 nM | 0.010 nM | 0.015 uM | 0.15 nM | 0.15 nM | 0.015 uM | 0.0015 mM | 0.15 nM | 0.0015 uM | 0.015 uM | 0.15 nM | 0.015 uM | 0.015 uM | 0.015 uM |
| 8 | 0.05 nM | 0.003 nM | 0.005 uM | 0.05 nM | 0.05 nM | 0.005 uM | 0.0005 mM | 0.05 nM | 0.0005 uM | 0.005 uM | 0.05 nM | 0.005 uM | 0.005 uM | 0.005 uM |

**C**

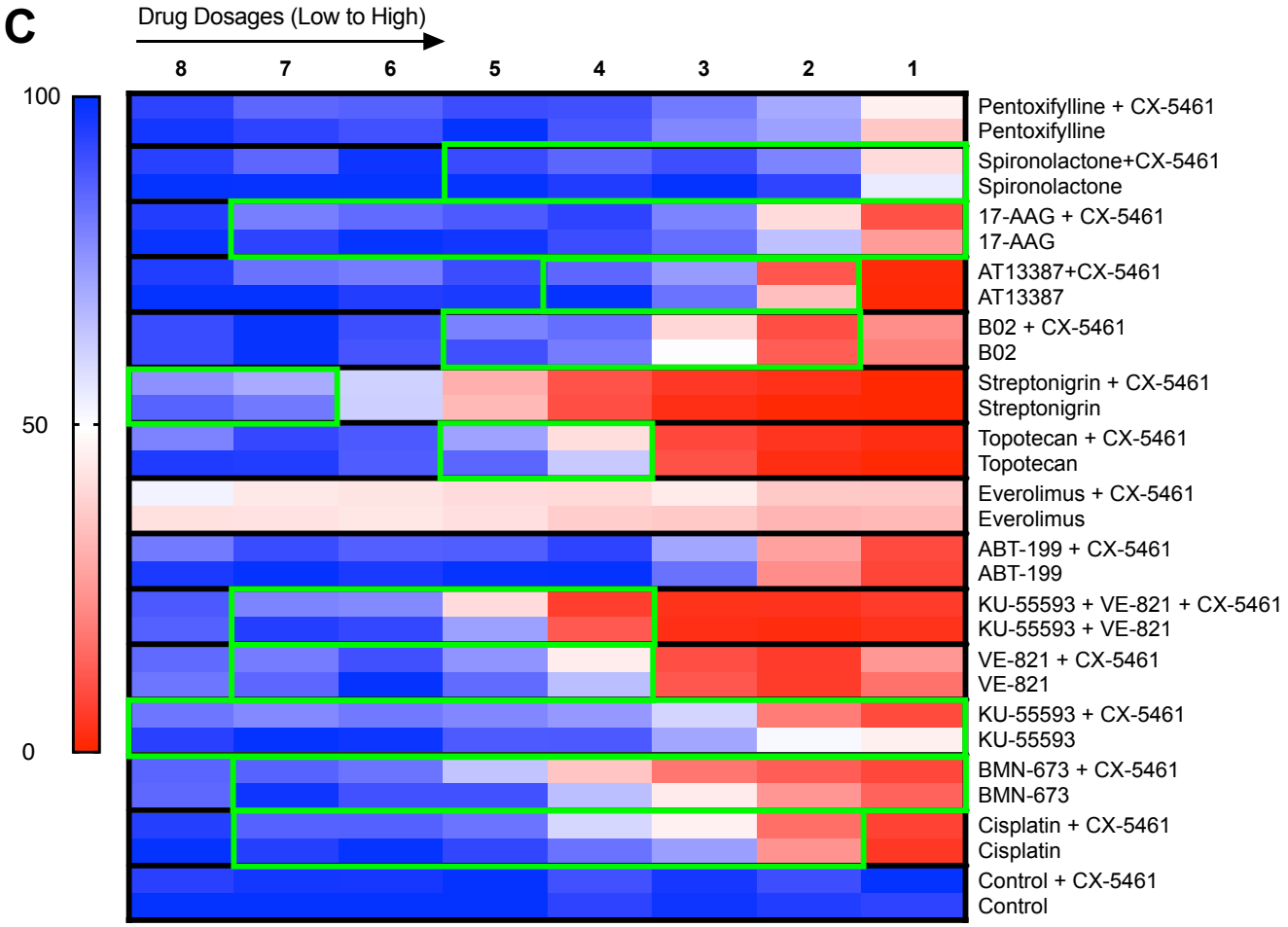

# Chapter 4. Homologous recombination deficiency sensitises ovarian cancer cells to CX-5461 treatment

## 4.1. Introduction

As a key component of the HR pathway, BRCA2 mutation is associated with improved survival and chemotherapy response in ovarian cancer [475]. However, its relationship with CX-5461 sensitivity remained unclear until 2017 when a study reported that CX-5461 demonstrates selective lethality in BRCA1/2 deficient mammary and colorectal tumours both in vivo and in vitro. The synergistic effect was attributed to the lethal level of DNA damage caused by the HR-deficient cells' incapability of repairing blocked replication forks and ssDNA gaps or breaks induced by CX-5461 [225]. This finding prompted the implementation of a phase I clinical trial l evaluating CX-5461 in 24 patients with advanced solid tumours. Among them, one BRCA2 mutant patient has obtained a partial response (PR) with a 67% reduction in disease burden while four other patients with BRCA1/2 mutations have obtained stable disease (SD) as the best response. No severe adverse effect was observed during the treatment and these results have led to the planning of a phase II study for breast cancer patients with germline HR deficiency or tumour HRD aberrations [464]. However, the therapeutic potential of CX-5461 in HR-deficient ovarian cancer has yet to be explored. Due to the high level of similarity between the breast and ovarian cancer genetics revealed by the genomic DNA copy number arrays, DNA methylation, exome sequencing, mRNA arrays, microRNA sequencing, and reverse phase protein arrays [476, 477], it is rational to expect that HR-deficient ovarian cancer, particularly with BRCA2 mutations, would show an enhanced sensitivity of CX-5461 similar to that of HR-deficient breast cancer. Three HR components, BRCA2, RAD54L and RAD51AP1 were identified from our screen to be synergistic with CX-5461 when targeted (Figure 4.1C), which further prompted us to investigate the interaction between HR and CX-5461, as well as the cellular and molecular mechanisms behind the synergistic effects. We decided to focus on BRCA2 in the following sections as the prevalence of BRCA2 mutation in ovarian

cancer (5.5~5.8%) is much higher than that of RAD54L and RAD51AP1 (<1%) [478-480]. These observations and thoughts led to the formation of following hypotheses: i) The synergistic effect we observed from the screen is valid and reproducible; ii) Cell lines with stable BRCA2 knockdown or other HR deficiencies are more sensitive to CX-5461 treatment; iii) Enhanced DNA damage and genomic instability is the cause of the synergistic effects.

To assess these hypotheses, we utilised both molecular and cellular biology tools to validate the findings obtained from the RNAi screen. A genetically modified OVCAR4 cell line containing a doxycycline-inducible BRCA2 knockdown transgenic construct was also generated to evaluate the long-term response of HR deficient cell lines to CX-5461.

## 4.2. Results

### 4.2.1 Knockdown of BRCA2 using siRNA synergises with CX-5461 in inhibiting cell proliferation

Potential off-target effects are a complicating factor in assessing the functional outcomes of RNAi [408]. In order to verify that the synergistic effects identified in the screen are the result of the on-target inhibition of BRCA2, we first performed validation experiments to confirm the knockdown of BRCA2. RT-qPCR was used to determined BRCA2 messenger RNA (mRNA) level in OVCAR4 cells transfected with SMARTpool siBRCA2 or the OTP-NT control. The results showed that the SMARTpool siBRCA2 successfully reduces the mRNA level of BRCA2 by 80%, indicating a successful knockdown of BRCA2 (Figure 4.1A).

In order to confirm the reliability and reproducibility of the synergistic effect between BRCA2 inhibition and CX-5461 treatment, we performed cell proliferation assays with CX-5461 or/and siBRCA2 using the same treatment conditions as the primary screen. Consistent synthetic lethality was observed in siBRCA2-transfected OVCAR4 cells treated with 80nM CX-5461 for 48 hours, in which the transfection of siBRCA2 or treatment of CX-5461 alone moderately reduced the cell proliferation by 10-15% compared to control while the combination treatment markedly reduced the cell counts by more than 50% (Figure 4.1B). The corresponding Bliss independence score of siBRCA+CX-5461 treatment was 0.658, indicating a strong synergistic effect, which is in accordance with the Bliss independence plots extracted from the screen (Figure 4.1C).

### 4.2.2 BRCA2 knockdown abolishes RAD51 foci formation

We next confirmed the functional inhibition of BRCA2 after siBRCA2 transfection by measuring RAD51 foci number in response to CX-5461 or doxorubicin treatment. BRCA2 is required for the recruitment of RAD51 in response to multiple types of DNA damage. Loss of BRCA2 impairs the recruitment of RAD51 to the DNA damage lesion, thus inhibiting HR function [260]. In order to assess the impact of BRCA2 knockdown on RAD51 foci formation, we performed immunofluorescence staining of RAD51 and γH2AX in BRCA2 knockdown cells treated with either doxorubicin or CX-5461. γH2AX is a marker of DNA strand breaks [358] while doxorubicin can block the re-ligation function of TOP2 which induces DNA DSBs directly [481]. As shown in Figure 4.2A and 4.2B, loss of BRCA2 abolished the formation of RAD51 foci after 1μM CX-5641 or 1μM doxorubicin treatment, but did not affect the formation of γH2AX foci, which indicates the presence of DNA strand breaks. This result demonstrates the successful inhibition of BRCA2 function by SMARTpool siBRCA2 transfection.

### 4.2.3 Combined treatment of siBRCA2 and CX-5461 induces massive genomic instability

A closer examination of the cells under microscopy revealed that the combined treatment of siBRCA2 and CX-5461 induced massive genomic instability as measured by micronuclei numbers. This phenomenon was comparable to PLK1 knockdown but was not observed with single treatment of siBRCA2, siTOP1 or CX-5461, or combined treatment of siTOP1 and CX-5461 (Figure 4.3A and 4.3B). As PLK1 (polo-like kinase 1) plays an important role in the initiation, maintenance, and completion of mitosis, and its inhibition leads to aneuploidy,

micronuclei, disorganized spindle poles and defects in chromosomal alignment [424, 425], this finding indicates that the synergistic effect between CX-5461 and loss of BRCA2 is likely to be caused by excessive, unrepairable DNA damage during mitosis (also called mitotic catastrophe). Similar phenotypes were not observed in combined treatment of siTOP1 and CX-5461, indicating the involvement of a different synergistic mechanism other than mitotic catastrophe. This provided an important clue for the mechanistic study of the combination effect between CX-5461 and TOP1 inhibition, which will be extensively discussed in Chapter 5.

### 4.2.4 Cells with stable BRCA2 knockdown are more sensitive to CX-5461 treatment

About 5.5-5.8% HGSC patients harbour an inactive BRCA2 gene [11]. While we examined the impact of short-term siRNA knockdown, in order to study the longer-term effects, we generated a genetically modified OVCAR4 cell line carrying a doxycycline-inducible BRCA2 knockdown transgenic construct. This construct contains a shRNA gene targeting BRCA2 under the control of a Tet-On transactivator. As the Tet-On transactivator is only active in the presence of doxycycline [482], we can thus control the expression of shBRCA2 by culturing cells with or without doxycycline.

To generate the cell line with inducible shBRCA2 construct, the OVCAR4 cells were infected with the lentivirus carrying the pLKO-Tet-On-shBRCA2 construct (kindly provided by Prof. Madalena Tarsounas). Cells were selected with puromycin, and the successfully transduced cells were then cultured with or without doxycycline for at least 7 days before experiments (Figure 4.4A). The BRCA2 knockdown efficiency was measured by RT-qPCR to detect the mRNA

level of BRCA2. The results showed that the mRNA level of BRCA2 was reduced by 60% in the presence of 0.2μg/ml doxycycline, indicating a successful knockdown of BRCA2 (Figure 4.4B).

To determine whether the OVCAR4 cells with stable BRCA2 knockdown are more sensitive to CX-5461 treatment, we performed the dose response assay of CX-5461 in cells with or without doxycycline induction. In a dose response assay, cells are treated with a series of drug doses and plots of drug dosages vs. cell growth inhibition are generated. We found that, compared to the cells without doxycycline induction, the dose response curve of OVCAR4 cells with BRCA2 knockdown shifts to the left, which indicates an increased sensitivity to CX-5461 treatment. The 50% inhibition of cell growth ($GI_{50}$) and total growth inhibition (TGI) dosages also decreased by 45% from 68nM to 40nM and 540nM to 284nM respectively (Figure 4.4C). These results suggest that the inhibition of BRCA2 can sensitise cells to CX-5461 treatment.

## 4.3. Discussion

The studies presented in this chapter utilised both molecular and cellular biology tools to study the interaction between homologous recombination pathway and CX-5461. Strong synergistic effects and increased sensitivity to CX-5461 treatment were observed in BRCA2 knockdown cells either with siRNA or shRNA. As mutated BRCA2 is present in 10-15% of HGSC patients, CX-5461 provides a potential therapeutic option for this patient cohort. When considering other HR pathway components, e.g. RAD51 and RAD54L, then this percentage can be up to 50%. We and others have identified a synergistic effect between CX-5461 and BRCA2 deficiency. In 2017, Xu, et al. showed that CX-5461 can induce selective lethality in BRCA1/2-deficient colorectal and triple negative breast

cancer (TNBC) xenografts [225]. Moreover, from the pharmaco-genomics data generated by Dr Karen Sheppard and Dr Elaine Sanij, gene set enrichment analysis (GSEA) also indicates a correlation between CX-5461 sensitivity and HR status in a panel of OVCA cell lines [325]. Together, these data strongly support the therapeutic potential of CX-5461 in treating HR-deficient HGSC. As the phase I/II clinical trial of CX-5461 in triple-negative breast cancer (TNBC) patients with BRCA1/2 mutation or homologous recombination deficiency (HRD) is currently underway and the activity of CX-5461 has been observed in some of these patients [464]. A clinical trial of CX-5461 in HR-deficient OVCA is planned to commence at Peter Mac in 2019.

One shortcoming of this chapter is that we did not carry out specific experiments to assess the possibility of off-target effects for some knockdown reagents, which we showed to synergise with CX-5461 [408]. We used individual siRNA duplexes in the secondary screen against BRCA2 and TOP1. For inducible shRNA BRCA2 knockdown, we utilised RT-qPCR and showed knockdown. We also utilised immunofluorescence staining for TOP1 and validated its knockdown with siRNA. However, we cannot eliminate the possibility that the synergistic phenotypes we observed could be caused off-target effects. To address this, we could introduce an RNAi-insensitive ORF of BRCA2 to test if it could rescue the synergistic effects [483, 484]. The RNAi-insensitive ORF can be generated by using synonymous mutations which abolish siRNA binding sequences but not alter the amino acid sequences, nor the function of the proteins [485]. Other methods include RNA-Seq which can be used to monitor the global mRNA level changes or using siRNA with 1 to 2-base-pair altered as negative controls [483]. However, rescue experiments would provide the best evidence for on-target effects of the knockdowns.

Another concern raised from our results regards the degree of sensitisation to CX-5461 treatment in BRCA2-deficient cells. It is possible that the 50% drop in the $GI_{50}$ and TGI dosage with BRCA2 knockdown is too small to be significant (Figure 4.4C). This argument can be addressed by the fact that the dose response assay was carried out in a shRNA knockdown background. However, due to the limited knockdown efficiency of shRNA, the mRNA level of BRCA2 was only decreased by 60% (Figure 4.4B), compared to that of siBRCA2 at 80% (Figure 4.1A). Although we do not know the exact cause of this difference, it could be associated with the design of the antisense oligos as we did not use the same sequences for the siBRCA2 and shBRCA2 construct. Another cause may involve the low Dicer expression in some ovarian cancer cell lines, which has been associated with poor silencing efficiency (See detailed description of shRNA and Dicer in section 3.2) [486]. It is possible that the remaining 40% of BRCA2 expression is functional and can provide resistance to CX-5461 treatment. The sensitisation could be more significant if BRCA2 knockout, rather than knockdown, cell lines were used. Xu, et al. used isogenic BRCA2 knockout cell lines in their study and the drop of the $GI_{50}$ and TGI dosages with CX-5461 treatment in BRCA2 knockout cell lines was 90% [225]. Similar results have also been observed by our group when the RAD51C knockout OVCAR8 cell line (another HGSC cell line [487]) was used [325]. Specifically, upon the treatment of low dose CX-5461, the RAD51C knockout cells exhibited increased sensitivity to growth inhibition compared to OVCAR8 cells, while increased cell death was observed in the RAD51C knockout cells with high dose CX-5461 treatment, both of which confirmed synthetic lethality between CX-5461 and HR deficiency.

A third question regarding our study is why BRCA1, which is frequently associated with HGSC tumorigenesis, was not identified as a target in the screen. BRCA1 did not pass the primary screen due to weak synergistic readouts. This could be caused by 1) the unsuccessful knockdown with the SMARTpool

siBRCA1, or 2) the lack of synergy between CX-5461 and BRCA1 deficiency. The second possibility is particularly interesting because a similar phenomenon has also been reported in at least three independent clinical studies [488-490]. Specifically, in these studies, significant improvements in overall survival with cytotoxic therapies was observed in HGSC patients with *BRCA2* mutation compared to those with *BRCA1* mutation. This disparity has been attributed to the closer association of BRCA2 with HR than BRCA1, which has been reviewed in detail by Liu, et al [491]. Briefly, BRCA1 acts during the initial steps of DDR, which senses and mediates the downstream DNA damage signals, while BRCA2 is directly involved in HR, which loads RAD51 to damage sites or stalled replication forks. BRCA2 is thus considered to be more directly related to HR (See details of BRCA1/2 and HR in section 1.6.1). In order words, although the BRCA mutation status is generally considered to be a prognosis marker of HGSC, BRCA2 appears to play a more significant role than BRCA1.

The results from this chapter have been incorporated into another parallel study in the laboratory led by Dr Elaine Sanij investigating the combination effects of BRCA2 gene with other HR and DDR components, including RAD51, BRCA1, ATM/ATR, CHK1/CHK2, PARP and conventional chemotherapy drug cisplatin. Significant clinical impact can be generated if CX-5461 can synergise with approved drugs which are currently used to treat HGSC. For example, in Dr Elaine Sanij's study, the individual or combined use of CX-5641 and PARP inhibitor has been tested both in vitro and in vivo with distinct HR backgrounds [325]. In OVCAR8 cells, the loss of RAD51C dramatically increased the cells' sensitivity to CX-5461 to a level similar to that of talazoparib (BMN673), and the combination of these two drugs further extended the therapeutic efficacy. When tested in PDX models, the results varied between different HR backgrounds. In a BRCA2 mutated HGSC PDX model, the individual treatment of CX-5461 and Olaparib both exhibited anti-tumoral efficacy and the combination of these two

further extended the survival of the mice. However, in a BRCA1 promoter hypermethylated, cisplatin resistant/refractory HGSC PDX model, the single treatment of Olaparib failed to show any therapeutic efficacy while significant benefit was still observed with CX-5461 single treatment. No further extension of survival was observed with the combination of these two drugs in this model. These data demonstrated the different sensitivity spectrum between CX-5461 and the PARP inhibitors, and the potential of combining these two molecules. Other possible drug combinations are also under evaluation, and hopefully more combinations could be identified to benefit HGSC patients.

**Figure 4.1 Validation of the synergistic effect between CX-5461 and BRCA2 knockdown**

**A.** RT-qPCR quantification of BRCA2 mRNA confirmed the successful knockdown of BRCA2. The mRNA level of BRCA2 decreased averagely 77% after siBRCA2 transfection. Combined data of N=3 experiments presented as mean±SEM. ****p<0.0001, student's t-test was used. **B.** Cell proliferation assay with siBRCA2 confirmed the synergistic effect between CX-5461 and BRCA2 knockdown. There was a significant decrease of cell number after treating siBRCA2 transfected OVCAR4 cells with 80nM CX-5461 for 48 hours. The siPLK1 was used as the positive control of transfection efficiency and the negative control of synergistic effect. The Bliss independence score is 0.658 which indicates strong synergistic effect. Representative data of N=3 experiments presented as mean±SD. ns: not significant, ****p<0.0001, student's t-test was used. **C.** Bliss independence extracted from the secondary screen results. Each point represented the Bliss independence score of an individual siRNA duplex. All three HR components (RAD54L, BRCA2 and RAD51AP1) showed strong synergistic effects (Bliss independence <0.8) with CX-5461. GAPDH serves as an example of an additive effect.

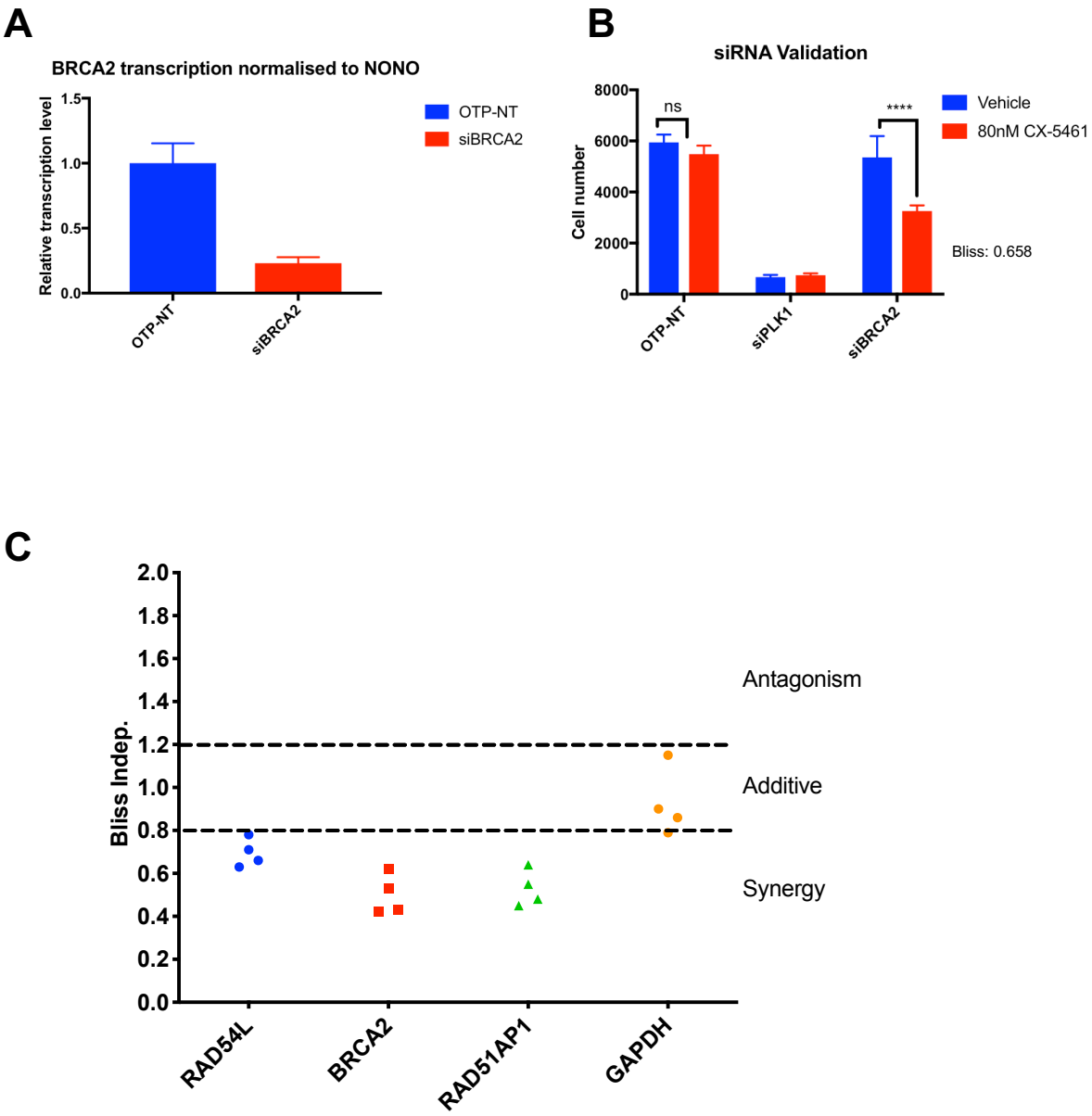
A
BRCA2 transcription normalised to NONO
Relative transcription level
1.5
1.0
0.5
0.0
OTP-NT
siBRCA2
OTP-NT
siBRCA2
B
siRNA Validation
Cell number
8000
6000
4000
2000
0
ns
****
Vehicle
80nM CX-5461
Bliss: 0.658
OTP-NT
siPLK1
siBRCA2
C
Bliss Indep.
2.0
1.8
1.6
1.4
1.2
1.0
0.8
0.6
0.4
0.2
0.0
Antagonism
Additive
Synergy
RAD54L
BRCA2
RAD51AP1
GAPDH

**Figure 4.2 Functional validation of BRCA2 knockdown**

The functional inhibition of BRCA2 by siBRCA2 was confirmed with RAD51 and γH2AX foci formation assay. BRCA2 mediates the loading of RAD51 on single-strand DNA in response to DNA damage while γH2AX is a marker of DNA DSBs. No RAD51 foci formation was detected in BRCA2 knockdown cells after 1μM doxorubicin (Doxo) **(A)** or 1μM CX-5461 **(B)** treatment for 3 hours. Representative images from N=2 experiments.

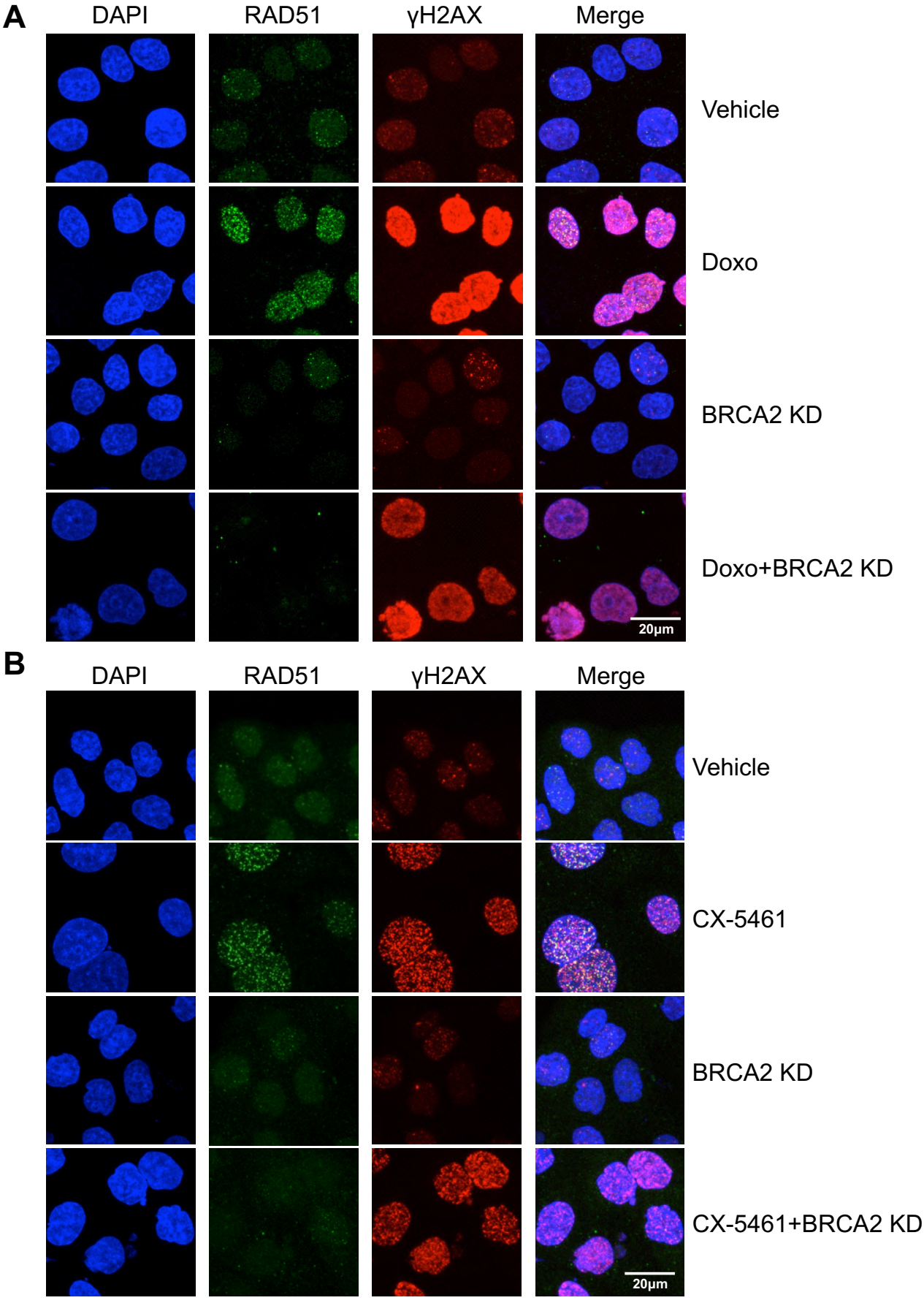
A
DAPI
RAD51
γH2AX
Merge
Vehicle
Doxo
BRCA2 KD
Doxo+BRCA2 KD
20μm
B
DAPI
RAD51
γH2AX
Merge
Vehicle
CX-5461
BRCA2 KD
CX-5461+BRCA2 KD
20μm

**Figure 4.3 Increased genomic instability in BRCA2 knockdown cells treated with CX-5461**

**A.** Increased micronucleus formation (marked by red arrows) was observed in BRCA2 but not TOP1 knockdown cells after 80nM CX-5461 treatment for 48 hours. Cells were stained with DAPI and images were captured using Arrayscan VTI high content system (Thermofisher). These are the representative images of N=3 experiments. **B.** Quantification of micronucleus formation using Cellomics software (Thermo Fisher Scientific). There is a significant increase of cells with micronuclei comparable to PLK1 knockdown after treated BRCA2 knockdown cells with 80nM CX-5461 for 48 hours. Combined data of N=3 experiments with 18 replicates (wells of cells) in each treatment group were presented as mean±SEM. ns: not significant, *$p<0.05$, ****$p<0.0001$, student's t-test was used.

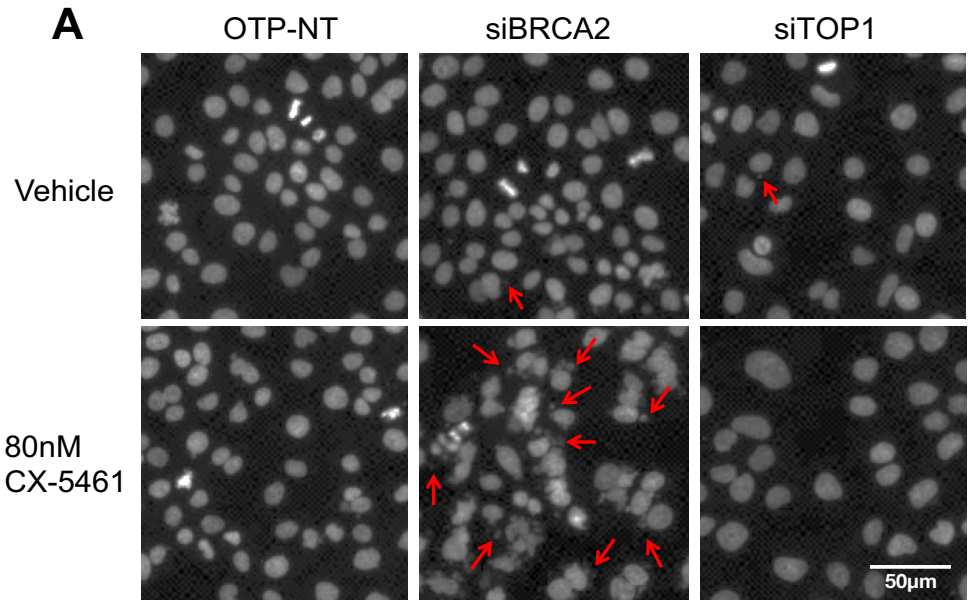
A
OTP-NT
siBRCA2
siTOP1
Vehicle
80nM
CX-5461
50µm

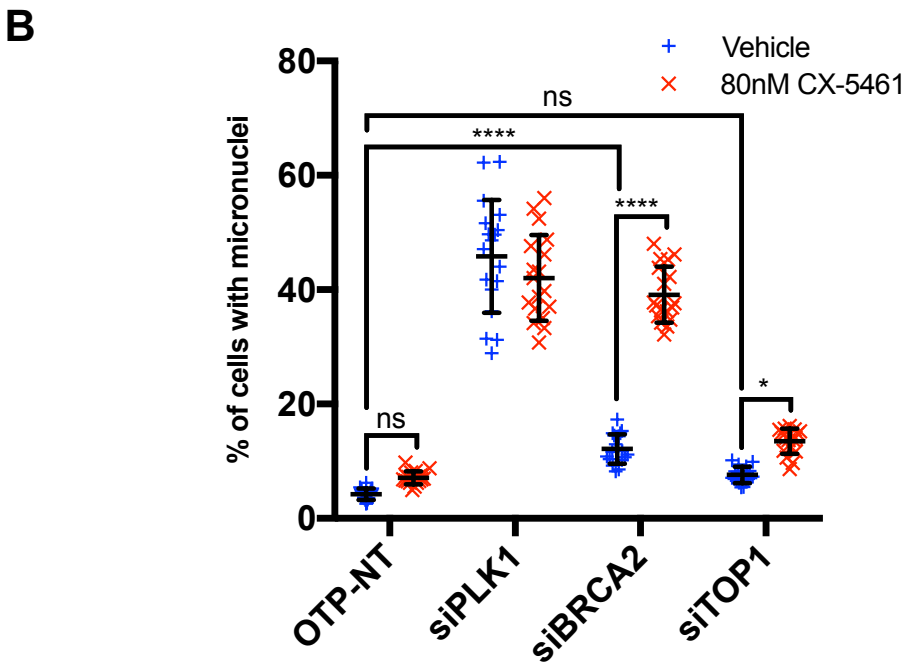
B
Vehicle
80nM CX-5461
% of cells with micronuclei
80
60
40
20
0
ns
****
****
ns
*
OTP-NT
siPLK1
siBRCA2
siTOP1

**Figure 4.4 BRCA2 knockdown sensitises HGSC cells to CX-5461 treatment**

**A.** Doxycycline-inducible BRCA2 knockdown OVCAR4 cells were generated to evaluate the cellular response of BRCA2 suppression to CX-5461 treatment. OVCAR4 cells were infected with lentivirus carrying the pLKO-TetOn-shBRCA2 (puromycin resistant) constructs, and was selected and cultured with 1μg/ml puromycin. Cells that survived the antibiotic selection were then cultured either with or without 0.2μg/ml doxycycline for at least 7 days. The CX-5461 dose response curve was then generated using these cells. **B.** The knockdown efficiency was determined by RT-qPCR. The BRCA2 mRNA level decreased approximately 60% after doxycycline induction. Combined data of N=3 experiments presented as mean ±SEM. **C**. The CX-5461 dose response curve was generated using cell counts as the readout. OVCAR4-Tet-On-shBRCA2-puro cells with or without doxycycline induction were treated with various doses of CX-5461 for 5 days. The OVCAR4-Tet-On-shBRCA2-puro cells with doxycycline induction are more sensitive to CX-5461 treatment. The $GI_{50}$ and TGI dosages decreased by 40% accordingly. Combined data of N=3 experiments presented as median±range.

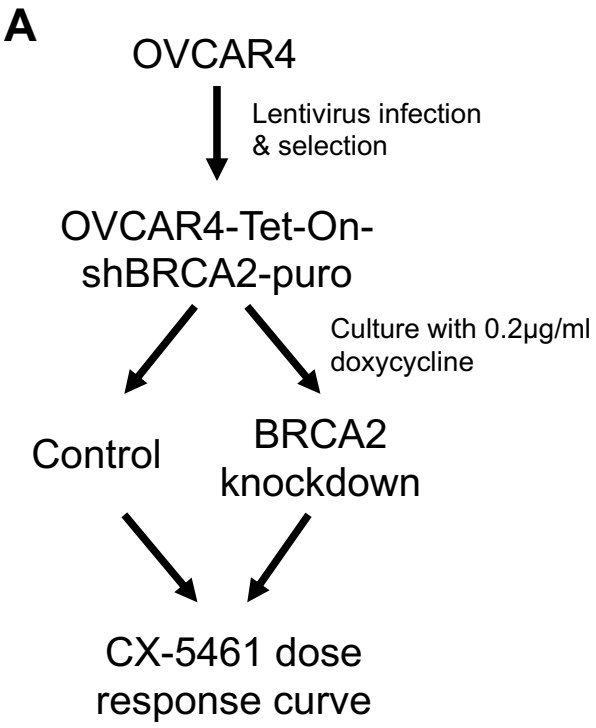


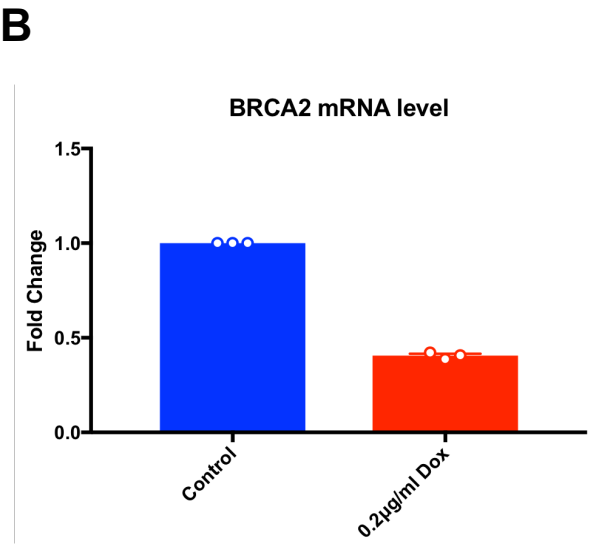


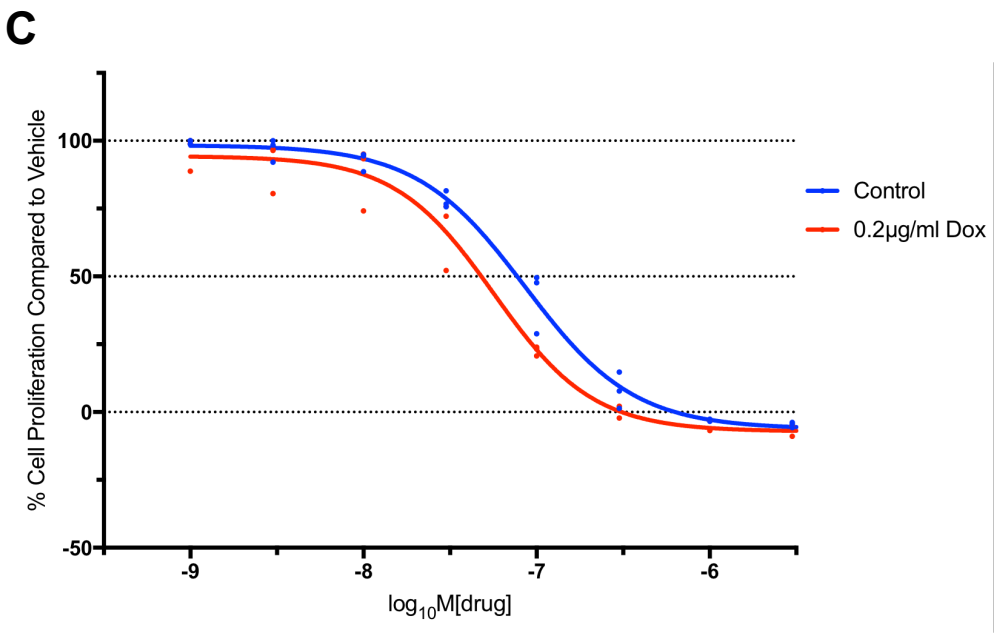


| | Control | 0.2µg/ml Dox |
|---|---|---|
| $GI_{50}$ (nM) | 67.6±10.8 | 39.7±6.7 |
| TGI (nM) | 540±58 | 284±71 |

# Chapter 5. CX-5461 can synergise with TOP1 inhibition both *in vitro* and *in vivo*

## 5.1. Introduction

In this chapter, we focussed on TOP1 which was also identified by the screen (Chapter 3) to have strong synergistic effect with CX-5461. TOP1 is attractive target as the TOP1 inhibitor, Topotecan, is currently used in clinic as a second-line treatment option to treat ovarian cancer [447]. More importantly, the synergistic effect between TOP1 inhibition and CX-5461 was observed in a HR proficient background, which suggested that this combination might be a potential approach to overcome the chemo-resistance caused by the restoration/reactivation of HR function.

### 5.1.1 Functions, structure and localisation of TOP1

TOP1 is a type of DNA topoisomerase which ubiquitously exist in all forms of life and resolve DNA topological problems, thus facilitating transcription/replication and maintaining genomic stability [492]. DNA topological problems can happen during the unwinding process of the DNA double helix during DNA replication and transcription when the DNA double-strands become too loose (negative supercoiling) or too tight (positive supercoiling), both of which can cause torsional stress and lead to genomic instability. There are three kinds of topoisomerases in mammalian cells, namely Type 1A, Type 1B and Type 2A, with shared and distinct functions (Figure 5.1A). Type 1A enzymes relieve hyper-negative supercoils by creating single-strand DNA breaks at the negative supercoiling 'bubble' and pass the intact single strand through the broken strand, while type 1B enzymes relieve both negative and positive supercoils by creating single-strand breaks and allowing controlled rotation of the broken strand around the intact strand [493]. In contrast, Type 2A enzymes relieve negative/positive supercoils and DNA knots/catenanes by

creating double-strand DNA breaks with four-base overhangs and pass the intact double-strand through the broken one. Both Type 1 and Type 2A enzymes re-ligate the DNA following the relaxation, thus keeping the genome intact. In humans, there are two Type 1B enzymes, namely TOP1 and TOP1mt. TOP1 is exclusively located in the nucleus whereas TOP1mt is located in mitochondria [494].

TOP1 is a large enzyme with a molecular weight of 90kD and can be structurally divided into four domains, namely the N-terminal domain (a.a. 1-214), the core domain (a.a. 215-635), the linker (a.a. 636-712) and the C-terminal domain (a.a. 713-765), which contains the active site at Tyr-723. The N-terminus of the TOP1 enzyme is dispensable for the DNA relaxation function but is required for the nuclear localisation [495], while the C-terminal and core domains can form a C-shaped clamp that is able to envelop the target DNA and execute enzymatic activity [496]. Once the TOP1 enzyme recognises and clamps around the supercoiled DNA, the active site at Tyr-723 attacks the DNA phosphodiester backbone by attaching the tyrosine to the 3′-phosphate end of the DNA, thus creating a single-strand break as well as a covalent connection between the nucleotide and TOP1 enzyme. After cleavage, the topological stress held by the DNA can be released by a ‘controlled rotation’ driven by the tension in the DNA when one DNA strand swivels around the other. The swivelling happens within the region containing the enzyme clamp and is slowed down by friction generated by the interaction between the enzyme and the DNA, resulting in a ‘controlled rotation’. TOP1 has a DNA sequence preference for nucleotides from positions −4 to −1 as follows: 5′-(A/T) (G/C) (A/T) (A/T)-3′, with covalent attachment (cleavage) at the −1 thymine or cytosine residues. After the relaxation step, the re-ligation of the ‘nick’ is conducted as the reverse of the cleavage reaction in which the oxygen on the 5′ terminal end of the strand overhang serves as the

nucleophile that attacks the phosphate to break the bond between the DNA and enzyme [496-498].

TOP1 is mostly localised in the nucleolus where massive torsional stress is generated during transcription of rDNA. However, TOP1 is also required for long gene transcription occurring in the nucleoplasm. The localisation of TOP1 in the nucleolus and nucleoplasm is determined by its N-terminal and core domains and can be abolished by the loss or mutation of some key amino acids. For example, the truncation of a.a. 1-67 at the far end of the N-terminal domain can cause translocation of TOP1 from the nucleolus to become evenly distributed throughout the nucleus [495, 499].

TOP1 is an indispensable housekeeping gene in higher eukaryotes as the loss (knockout) of TOP1 in both mouse and Drosophila is embryonic lethal [492]. It has also been reported that a significant proportion of TOP1 molecules colocalises with RNA polymerase I (Pol I) in the fibrillar centre of the nucleolus during the disruption of rDNA transcription, and co-migrates with Pol I to the nucleolar periphery during the disruption of rDNA transcription [500]. This colocalization is also regulated by the N-terminal domain of TOP1. In addition, TOP1 has also been reported to interact with nucleolin, a nucleolar protein crucial for the synthesis and maturation of ribosomes [501]. As rDNA genes are one of the most highly transcribed genes in cells, the role of TOP1 at the rDNA chromatin has been extensively studied, which further indicates its importance in maintaining nucleolar function and stability. In Aziz, et al.'s paper, it was revealed that the loss of Top1 in yeast results in rRNA transcriptional blockade due to the accumulation of both positive supercoils in front of Pol I, which slows down elongation and R-loop formation behind Pol I, which reduces pre-rRNA truncation and pre-rRNA synthesis [502]. In addition to its role in rRNA transcription, the loss of Top1 or treatment of CPTs in yeast also results in the

genomic instability of rDNA genes, which was demonstrated by the increased reciprocal crossover (RCO) rates (the rate measuring the inter-homolog recombination) at rDNA chromatin [503, 504]. In addition, deletions and mutations at the rDNA locus were also observed upon treatment with CPT or TOP1 overexpression, revealing the requirement of a suitable amount of TOP1 (not too much or too little) to maintain homeostasis at the rDNA [505].

Apart from its role in resolving the negative/positive supercoiling caused by transcription/replication and maintaining genomic stability at rDNA, TOP1 has been identified to be involved in chromatin remodelling, transcriptional control and even RNA splicing. In yeast, research has shown that Top1 activity is required for the maintenance of the open chromatin structure at gene promoter regions and facilitating transcription [506]. It has been reported that TOP1 is strongly regulated by BRD4 to overcome the torsional stress induced by the elongation of RNA Polymerase II (Pol II) transcription but preserves negative supercoiling that assists promoter melting at start sites (promoter melting is the unwinding of the double-stranded DNA at the promoter region to allow the access of the RNA polymerases) [507]. Additionally, the inhibition of TOP1 alters pre-mRNA splicing of the caspase-2 transcript and tissue factor (TF), which brings a novel insight into TOP1's role in gene transcription [508, 509].

### 5.1.2 TOP1 in cancer development

TOP1 has long been associated with tumourigenesis. An immunohistochemistry (IHC) study of 24,262 patients with diverse cancers revealed that the overexpression of TOP1 protein was present in 51% of the tumours [510]. The amplification of TOP1 gene copy number was also observed in over 30% of metastatic breast cancer [511]. Furthermore, high expression of TOP1 was found to be correlated with worse OS in epithelial ovarian carcinoma (EOC) patients,

particularly those having the serous subtype [512]. A similar trend was also observed in liver cancer in which elevated expression levels of TOP1 were closely associated with poorer OS and disease-free survival rates [513]. It is believed that TOP1 promotes tumour growth by suppressing tumour genomic instability and facilitating transcription. As a result, it is not surprising that some researchers have argued that TOP1 is an oncogene, thus providing a good rationale to target TOP1 as an option for cancer treatment [514].

### 5.1.3 Camptothecins as a class of TOP1 inhibitors in cancer treatment

Due to its crucial role in facilitating DNA replication and transcription, TOP1 has been regarded as a drug target for cancer treatment since the late 1980s. Two drugs, Topotecan (TPT) and irinotecan, have been approved by the FDA as second-line treatment options for ovarian cancer and metastatic colorectal cancer, respectively. Both drugs are derived from Camptothecin (CPT) with enhanced solubility and stability in the blood [515]. CPT was first isolated by Wall and Wani from the bark of *Camptotheca acuminata* in 1966, one year before they identified paclitaxel. However, CPT did not gain much attention until the late 1980s when TOP1 was identified as its sole target [516].

CPT and its derivatives (CPTs) inhibit TOP1 by integrating into the TOP1/DNA covalent complex (TOP1cc) and forming a ternary complex. Specifically, CPTs bind between the TOP1 enzyme and the intact DNA strand through hydrogen bonding, thus preventing the re-ligation of DNA nicks as well as the dissociation of TOP1 from the DNA [515]. Since S-phase cells demonstrate the highest sensitivity to CPTs, the therapeutic effect of CPTs has been mainly attributed to the irreparable replication stress caused by the collision between trapped TOP1 and replication machinery. However, recent findings indicate that CPTs can

induce apoptosis in non-mitotic neuronal cells as well, which suggests the existence of mitosis-independent pathways [517]. One proposed pathway is the inhibition of transcription caused by the accumulated torsional stress ahead of the transcription machinery [518]. Other explanations include the blockade of angiogenesis via the inhibition of hypoxia inducible factor-1α (HIF-1α) which is a main modulator of vascular endothelial growth factor (VEGF) expression [519-521]. Interestingly, this inhibition of HIF-1α is not mediated by the suppression of HIF-1α mRNA transcription but instead relies on the decreased rate of HIF-1α protein translation with the exact mechanisms remaining unknown [522].

The clinical application of CPTs depends on antitumor efficacy and dose-limiting toxicity. Several key molecules have been identified during the last two decades, which can be used as biomarkers to predict treatment response to CPTs.

**TOP1**

The expression and mutation status of the TOP1 enzyme is highly correlated to the treatment outcome of CPTs. Research has shown that while the suppression of TOP1 in lymphoma produces resistance to CPT, it also hypersensitizes the cancer cells to doxorubicin, a Type 2A topoisomerase inhibitor [523]. A similar trend was also observed in tumour cells deficient in TOP1 degradation which is highly sensitive to CPT treatment [524]. Furthermore, a number of TOP1 mutations, e.g. R621H, L617I E418K, G503S, D533G, are associated with reduced sensitivity to CPT-based therapy, which is due to the attenuated binding of CPTs to the TOP1cc [525, 526]. It is worth highlighting that in the later sections (section 5.2.7) we demonstrate that the depletion of TOP1 can indeed abolish Topotecan's ability to induce replication stress. However, it did not affect the synergistic effect between TOP1 inhibition and CX-5461, which indicated that CX-5461 is synergising with the functional inhibition of TOP1 rather than the

TOP1 trapping. It also indicated that there is a possibility that CX-5461 may be able to overcome the CPTs resistance caused by the loss of TOP1, although further studies are required to prove this conjecture.

**Membrane transporters**

Membrane transporters are a class of membrane proteins involved in the movement of ions, small molecules, or macromolecules. CPT-derived drugs are the substrates of a number of transporters, including P-glycoprotein (P-gp, also called Multi Drug Resistance, MDR1), BCRP, ABCG2 and ABCB1 [527, 528]. The hyperactivation of these 'drug pumps' effluxes CPT to reduce its concentration in the cytoplasm, thereby conferring drug resistance. Several inhibitors targeting these 'drug pumps' are currently under clinical development [529, 530].

**TDP1 and PARP**

Tyrosyl DNA phosphodiesterase 1 (TDP1) is the enzyme that catalyses the hydrolysis of the phosphodiester bond between TOP1 and the 3′-phosphate of DNA, and resolves the stalled TOP1cc induced by the internal and external TOP1 trappers such as CPTs. Loss of TDP1 is associated with defects in the repair of TOP1-associated DNA strand breaks, and confers hypersensitivity to CPTs [528, 531]. A recent paper has shown that the TDP1/TOP1 ratio can serve as a promising biomarker for the response of small cell lung cancer to TPT [532]. TOP1 has also been reported to bind Poly (ADP-ribose) polymerase (PARP), a crucial enzyme involved in single-strand DNA break repair. PARP inhibition does not provide additional sensitivity to CPTs in TDP1-deficient cells, which indicates that TDP1 and PARP are components of the same pathway [531]. As PARP inhibitor (PARPi) has recently been approved for HGSC treatment, this

finding provides rationale for combining CPTs and PARPi to treat HGSC. The clinical trial is currently underway [533].

**Other DNA repair and DDR proteins**

CPTs cause single-strand DNA breaks and replication stress, which, if not repaired, could lead to dangerous double-strand DNA breaks (DSB). Therefore, it is not surprising that CPTs can synergise with a number of deficiencies in DNA repair and DDR pathways, while the overexpression of the components in these pathways can lead to drug resistance. Typical examples include MSH2 or MLH1 genes in mismatch repair (MMR); XRCC1 in base excision repair (BER); ATM, ATR, CHK1, CHK2 in DDR; and RAD51, BRCA1, BRCA2, NBS1 in homologous recombination DNA repair [528, 531, 534].

**Apoptosis inhibitors**

CPT treatment can induce apoptosis [518, 535]. Studies have shown that proapoptotic proteins, such as p53 and BAX, are upregulated after CPT treatment, while the expression of BCL-2, an anti-apoptosis protein, is decreased [536]. Moreover, overexpression of BCL-2 is associated with CPT resistance [528].

### 5.1.4 Limitation of Camptothecins in cancer treatment

One significant issue hampering the clinical application of CPTs is the dose limiting toxicities including myelosuppression and diarrhoea. Myelosuppression (also called bone marrow suppression) is a severe side-effect with reduced production of blood cells including anaemia (reduced red blood cells), neutropenia (reduced white blood cells) and thrombocytopenia (reduced platelets), which can lead to fatigue, infection and haemorrhage, respectively. The severity

of the side effects from CPTs is dose dependent, and sometimes can be lethal [537]. It is worth highlighting that in the later part of this thesis (section 5.2.9) we demonstrated that CX-5461 is able to synergise with low dose Topotecan *in vivo* which can partially alleviate the toxicity problems of CPTs.

### 5.1.5 Emerging TOP1 inhibitors

A number of TOP1 inhibitors are under development to enhance the therapeutic efficacy of TOP1 inhibition while alleviating toxicity. A large proportion of the new TOP1 inhibitors are still Camptothecin derivatives, but with different chemical modifications aimed at increasing drug efficacy and stability and reducing toxicity. Typical examples include NKTR-102 and CRLX101, which conjugate irinotecan to a macromolecular core (PEG), thus allowing slow drug release with lower peak concentration and prolonged half-life. The usage of liposomal formulation employs a similar approach [538, 539]. In contrast, Dilomotecan (BN80915) and S39625 reduce nonspecific binding to serum albumin by modifying the E-ring of Camptothecin [534, 540]. A number of non-camptothecin TOP1 inhibitors are also under investigation, including indenoisoquinolines, indolocarbazoles and phenanthridine derivatives, all of which still inhibit the re-ligation function of TOP1 but with more favourable characteristics such as 1) enhanced stability in the blood; 2) less reversible TOP1cc trapping; and 3) not being substrates of the membrane transporters [534, 540, 541]. Apart from these, researchers have also identified several compounds that inhibit TOP1 through a different mechanism from Camptothecin, e.g. CY13II inhibits the catalytic cleavage activity of TOP1 instead of forming the TOP1cc [542]. However, while none of these candidates has been able to pass phase III clinical trial so far, a number of drug combinations with Topotecan are under investigation and the future looks promising [543, 544]. Here we demonstrated

another possible combination option, CX-5461 which is able to deliver synergistic anti-tumoural effect in HR proficient HGSC even at low doses of Topotecan.

### 5.1.6 Hypothesis and approaches

Based on our data to date, the following hypotheses were generated: i) The synergistic effect between CX-5461 and TOP1 inhibition we observed from the screen is reproducible and generally applicable in a range of cell/cancer types; ii) The synergetic effect is caused by the enhanced DDR and independent of p53; iii) The enhanced DDR is not caused by the excessive DNA damage, but instead caused by the nucleolar associated DDR as both Pol I and TOP1 are preferably localised in the nucleolus; iv) The CX-5461/Topotecan combination will be well tolerated *in vivo* and shows synergistic anti-tumour effects.

To assess these hypotheses, we utilised a number of molecular and cellular biology tools to validate the findings we obtained from the screen in multiple cell line models. We also adopted multiple proteomic/molecular quantification and imaging approaches to investigate the cellular and molecular mechanisms of the synergistic effect. For the *in vivo* assessment of the CX-5461/Topotecan combination, we generated an OVCAR3 cell-line derived xenograft mouse model to evaluate the tolerability and the therapeutic potential of the combination.

## 5.2. Results

### 5.2.1 Successful knockdown of TOP1 using TOP1 siRNAs

As studies with RNAi knockdown are frequently hampered by off-target effects, we first performed validation experiments to functionally confirm the successful knockdown of TOP1. We determined the protein level of TOP1 by performing immunofluorescent staining of TOP1 using an anti-TOP1 antibody in OVCAR4 cells transfected with either SMARTpool siRNA against TOP1 (siTOP1) or non-targeting siRNA control (OTP-NT). Immunofluorescent staining showed successful depletion of TOP1 protein 72 hours after siTOP1 transfection, while the treatment of 1 μM CX-5461 for 3 hours did not affect the expression of TOP1 (Figure 5.1B and 5.1C). We co-stained TOP1 with an antibody to UBF, a transcription factor that controls the transcription of rRNA genes (See details in section 1.4) [113, 545]. Interestingly, we found that a significant amount of TOP1 co-localised with UBF in the nucleolus, which is consistent with a previous study [541]. This co-localisation still exists after CX-5461 treatment with TOP1 co-migrating with UBF to the nucleolar periphery (Figure 5.1B). As the nucleolus is the site where the ribosomal RNA (rRNA) is transcribed and processed, the preferential localisation of TOP1 in the nucleolus and its partial colocalization with UBF support its important role in maintaining the genome integrity at the rDNA and facilitating rDNA transcription.

### 5.2.2 Combination of siTOP1 and CX-5461 synthetically inhibits cell proliferation but does not induce genomic instability

In order to confirm the synergistic effects between CX-5461 and siTOP1, we performed cell proliferation assays using the same conditions as the screen, in which siPLK1 and siBRCA2 served as comparisons. Cell counting revealed a consistent decrease in cell number after combined treatment of siTOP1/siBRCA2 and CX-5461 compared to vehicle control, siTOP1/ siBRCA2 alone and CX-5461 alone, but not with siPLK1, which confirmed the reproducibility of the synergistic effects (Figure 5.1D). The bliss independence is 0.706 indicating strong synergistic effects. Intriguingly, unlike the CX-5461/siBRCA2 dual treatment which induced strong micronuclei formation, the CX-5461/siTOP1 dual treatment inhibited cell proliferation without causing strong genomic instability, as measured by quantification of micronuclei (Figure 4.3A and 4.3B). This is a strong indication that the synergy between CX-5461 and BRCA2/TOP1 depletion occurs via distinct mechanisms. While extensive DNA damage (mitotic catastrophe) is likely to be the major cause of synergy between CX-5461 and BRCA2 depletion, it is unlikely to contribute to the combination effect of CX-5461 and TOP1 inhibition. This divergence is also a good demonstration of the potential value of testing different, rational drug combinations in disease with different genomic phenotypes (See Section 4.2.3 for details).

### 5.2.3 The combination of Topotecan and CX-5461 inhibits cell proliferation in multiple ovarian cancer cell lines

siRNAs are powerful tools in genetic studies, however, their application in the clinic is still limited by their delivery efficiency and stability issues [440, 441]. Therefore, using clinically approved drugs is a more practical way to enhance the clinical impact of our findings. From our mini chemical compound screen, we

found a potential synergistic drug combination between Topotecan and CX-5461 (Figure 3.6C). However, only one cell line (OVCAR4) and a single dosage of CX-5461 was tested in the screen. In order to assess the general applicability of the combination, we sought to verify our findings in multiple cell lines to further support the results from the screen. Two-dimensional checkerboard assays, a widely used assay for synergy testing, were used to investigate the effect of the CX-5641/Topotecan combination at different dosages in a variety of cell lines [546]. We evaluated the synergistic effects of combining CX-5461 and Topotecan in an additional three HGSC cell lines (OVCAR3, OVCAR4 and CAOV3, all of which are of high genomic similarity to HGSC [6]) and one ovarian clear cell cancer (OCCC) line SKOV3. We included the SKOV3 cell line in our panel because it has been reported to be resistant to current platinum-based chemotherapy and the newly introduced PARP inhibitors [422, 423]. Additionally, all four cell lines possess functional BRCA1/2 genes, while three out of the four cell lines (OVCAR3, OVCAR4 and CAOV3) harbour mutant p53 [6]. These are important features as our project is focusing on the BRCA1/2 proficient HGSC, while the mutant p53 supports the later conclusion that the effect of CX-5461 is not via p53-dependent pathways.

In order to better characterise the cell lines and determine the appropriate dosages to use for the checkerboard assay, we first performed dose response experiments for CX-5461, Topotecan, cisplatin and Olaparib in all these four cell lines. Cisplatin and Olaparib are both approved for the first-line treatment of OVCA [547]. We included these two drugs in order to compare the efficacy of the CX-5461/Topotecan combination to clinically approved drugs for OVCA. Consistent with previous reports, SKOV3 is the most resistant cell line to cisplatin and Olaparib treatment, with $GI_{50}$ dosages at 0.9μM and 3.8μM respectively [548, 549]. Interestingly, OVCAR4 and CAOV3 showed similar resistance to Olaparib as SKOV3 (2.1μM and 4.4μM compared to 3.8μM), but not to cisplatin (108nM

and 330nM compared to 909nM), indicating the heterogeneity of the responses of cells to different treatments. In contrast, OVCAR3 was the most sensitive cell line to both drugs, with $GI_{50}$ at 40nM and 73nM, respectively (Figure 5.2A and B). For Topotecan and CX-5461, although OVCAR3 was still the most sensitive cell line to these two drugs (1.2nM and 23nM), there was no marked difference with respect to $GI_{50}$ or TGI dosages between the other three cell lines (Figure 5.2C and D). In summary, although the four cell lines demonstrated various sensitivities to cisplatin in a wide dosage range of 1.5 logs and strong resistance to Olaparib in three of the four cell lines, their sensitivity to the combination of Topotecan and CX-5461 was similar. Thus, the cell lines' sensitivity to Topotecan and CX-5461 treatment does not correlate to that of current therapies and highlights the potential importance of this combination in treating relapsed disease.

We then utilised the data obtained from the dose response curves to setup checkerboard assays. For the two-dimensional checkerboard assay, a series of dilutions of both drugs were used against each other to identify the maximum synergistic effect and the corresponding drug concentrations [550]. Bliss independence [427, 428, 551] and combination index (CI, Chou-Talalay method) [552, 553] analyses were used to quantify the synergistic effects, and the results were visualised using Combenefit software [396]. Strikingly, we found that the combination of two drugs significantly inhibited cell proliferation in all four cell lines, especially at high doses (Figure 5.3A, B, C, D). Cells were treated with indicated doses of drugs for 9 days, and were fixed and counted. A 9-day treatment period was used as enhanced therapeutic efficacy was observed with long term drug treatment (Figure 5.4E). The results were presented in 3D plots in which the relative cell number compared to the vehicle control was plotted on the Z axis, the concentration of drugs was plotted on the X and Y axis, and the combination effects were demonstrated by different colours. The blue indicates synergistic, green additive, and red antagonistic effects. The blue colour, indicating

synergistic effects, can be observed in all cell lines with the highest doses of CX-5461 and Topotecan tested. The lowest Bliss independence obtained from OVCAR3, OVCAR4, CAOV3 and SKOV3 cell lines were 0.163, 0.251, 0.426 and 0.211, respectively, all of which indicated strong synergy, which is consistent to the results obtained by using siRNAs (Figure 5.1D). Similar conclusions were also observed using the Chou-Talalay method that low combination indices (CI<0.9) were reproducibly obtained at the 90% effect point, indicating strong synergistic effects (Figure 5.3E).

In addition to the cell proliferation inhibition phenotype, microscopic examination revealed an enlarged, flattened cell morphology after combination treatment, which is suggestive of cell cycle arrest or a senescence-like phenotype [554] (Figure 5.4A, B). We classified this phenotype as senescence-like rather than senescence due to the fact that we did not observe a strong increase in senescence-associated β-galactosidase staining, which is a widely marker of senescence [555] (data not shown). The senescence-like phenotype was further supported by clonogenic assays aimed at investigating the proliferative potential of cells after drug treatment withdrawal [556]. For the clonogenic assay, OVCAR4 cells were seeded into 6-well plates drugged with vehicle control, cisplatin, Olaparib, CX-5461, Topotecan or CX-5461/Topotecan combination for 48 hours at the $GI_{50}$ dosages at 5 days. The drugs were then washed off and the proliferation of cells was closely monitored for another 5 days (Figure 5.4C). We washed off the drugs at 48 hours so as to investigate if the cell cycle arrest is reversible or not. An irreversible cycle arrest being more favourable than the reversible one due to the long-lasting effect of tumour growth inhibition. Strikingly, the combination treatment of CX-5461/Topotecan caused a persistent irreversible cell cycle arrest even after drug withdrawal while other treatment groups resumed proliferation. Specifically, the cell confluence was at 6% at the time of drug withdrawal for all treatment groups; 5 days after drug withdrawal, the cell confluence of the CX-

5461/Topotecan groups only increased to 14%, compared to 60% for vehicle group and 40% for all other treatment groups (Figure 5.4D and E). Microscopic examination of cells in these clonogenic assays revealed enlarged, flattened cell morphology similar to Figure 5.4A, consistent with a senescence-like phenotype.

In order to further confirm the cellular senescence phenotype, we performed RT-qPCR to detect the expression level of a panel of senescence-associated secretory phenotype (SASP) genes, including IL1a, IL1β, IL6, IL8, CXCL1, p16 and p21 [557-559]. Interestingly, this interleukin signature was also observed in the primary siRNA screen results (Figure 3.5C). NONO is a housekeeping gene which served as an internal control [560] while 5'ETS (transcribed by Pol I) and 5S (transcribed by Pol III) were used as controls to evaluate the Pol I transcription rate after drug withdrawal (The Pol I transcription will be discussed in section 5.2.5). OVCAR4 cells were treated with 80nM CX-5461, 6nM Topotecan ($GI_{50}$ dosages at 5 days) or CX-5461/Topotecan combination for 48 hours. The drug-containing media was then washed off and replaced by normal cell culture media. Cells were cultured for another 48 hours before harvest. As expected, the RT-qPCR results demonstrated a significant increase in the mRNA level of IL1α, IL6, IL8 and p21 after combined treatment compared to vehicle or single drug-treated cells (Figure 5.4F), thus strongly supporting a senescence phenotype. Among them, the elevation of p21 mRNA expression is particularly interesting because 1) p21 is a potent cyclin-dependent kinase inhibitor that is capable of inhibiting all cyclin/CDK complexes, particularly CDK2, thus promoting cell cycle arrest (Figure 1.4); 2) p21 is one of the main downstream targets of p53 [561, 562]. Increased p21 expression could provide the key mechanism for the cell cycle arrest phenotype. However, as HGSC cell lines harbour mutant p53, the p53 pathway is unlikely to contribute to the activation of p21. Thus, a p53-independent mechanism is likely to be involved in promoting the transcription of p21 [563].

Furthermore, in order to investigate whether the CX-5461 and Topotecan combination is capable of treating other types of cancer in addition to OVCA, we performed the same two-dimensional checkerboard assay to evaluate the synergistic effects in two B-cell acute lymphoblastic leukaemia (B-ALL) cell lines MHH-CALL4 and SUP-B15. We chose B-ALL because both CX-5461 and Topotecan as single agents have been investigated in treating haematological malignancies, including B-ALL [564-566]. Strikingly, strong synergistic effects, indicated by the 'blue colour' in the bliss maps, were also observed in these two B-ALL cell lines, particularly in SUP-B15 cell line, probably due to the shorter doubling time (18hrs) compared to that of MHH-CALL4 (80-100hrs) which might result in a higher activity of Pol I and TOP1 enzymes (Figure 5.5A, B). This result suggests that the potential efficacy of combining CX-5461 and Topotecan is not restricted to ovarian cancer and may have the potential to be a broad-spectrum cancer therapy, e.g. in Topotecan-approved cancer types like small cell lung cancer and cervical cancer or those with high activity of Pol I and TOP1 enzymes [567, 568].

### 5.2.4 Combined treatment of CX-5461 and Topotecan induces cell cycle arrest at late S and G2 phases

Although cellular senescence has been identified to be a major driver of the synergistic effects of CX-5461 and Topotecan combination, at the cellular level, the inhibition of cell proliferation could also be caused by increased cell death via apoptosis or necrosis. In order to investigate whether cell death contributes to the combination effects, we performed cell proliferation assays measuring the change in cell number after 48 hours treatment of CX-5461, Topotecan or CX-5461/Topotecan combination in OVCAR3, OVCAR4 and CAOV3 cell lines with or without the apoptosis inhibitor Q-VD-OPh. We used 48 hours' time point to

investigate the short-term cellular responses to the treatments. Q-VD-OPh inhibits apoptosis by blocking the cleavage capacity of several caspases including caspases-3, -7, -8, -9, -10, and -12 [569, 570]. The cell proliferation assay showed a consistent reduction in cell number in all three cell lines after combination treatment compared to single drug and vehicle treatments at the dosage indicated in Figure 5.6D. The dosage was set at the 5-day's $GI_{50}$ dosage of the corresponding drugs in the corresponding cell lines (Figure 5.6B). However, although the co-treatment of Q-VD-OPh moderately increased the cell number by approximately 5% in the treatment groups, it failed to rescue the synergistic phenotype, which indicates that apoptosis does not play a major role in the synergistic effect between CX-5461 and Topotecan.

In order to further explore this conclusion, we performed flow cytometry (FACS) analysis to directly measure the proportion of dead cells as indicated by the subG1 population using the same treatment conditions as the proliferation assay. The cell cycle profiles of OVCAR3, OVCAR4 and CAOV3 cells were obtained by bromodeoxyuridine (BrdU) and propidium iodide (PI) labelling, which measures replication and DNA content, respectively. BrdU is an analogue of thymidine that can be incorporated into newly synthesized DNA during DNA replication in S phase, while PI is a fluorescent DNA intercalating agent that is commonly used to measure the DNA content [571]. Although all three cell lines showed an increased subG1 population after CX-5461/Topotecan combination treatment for 48 hours (6% to 12% for OVCAR4, 13% to 18% OVCAR3 and 25% to 35% for CAOV3), these modest increases in cell death are not sufficient to explain the observed large reductions of cell number. Furthermore, the co-treatment of Q-VD-OPh can only partially alleviated the cell death phenotype (Figure 5.6A), all of which suggest that the cell death has only a marginal contribution to the inhibition of cell proliferation and is unlikely to be the major mechanism contributing to the reduction in cell number.

In contrast, cell cycle analysis performed on the same FACS datasets showed enhanced cell cycle arrest during the late S/G2 phase in all three cell lines after 48 hours of CX-5461/Topotecan combination treatment when the late S/G2 phase population of OVCAR3, OVCAR4 and CAOV3 cells was increased from 60% to 75%, 45% to 65% and 40% to 60%, respectively (Figure 5.6C and D), indicating that the inhibition of cell proliferation was mainly caused by enhanced cell cycle arrest rather than cell death. Doxorubicin, a TOP2 inhibitor which induces double-strand DNA breaks (DSBs), was used as a comparison whose treatment demonstrated cell cycle arrest at both G1 and G2 phases (Figure 5.6D). This difference in the arrested cell phases is particularly interesting because it indicates the different mechanisms underlying the combination and doxorubicin treatments and demonstrates the preference of the combination in targeting the S/G2 phase cells (cells undergoing replication) rather than G1 phase cells (non-proliferating cells). This preference is particularly important as it may indicate that the CX-5461/Topotecan combination has the potential to selectively target the proliferating tumour cells while sparing the non-proliferating normal cells, which are also being targeted by the doxorubicin. It has been reported that the fatal cardiotoxic adverse effect of doxorubicin was largely caused by its unselectively cytotoxicity to the non-dividing cardiac cells [572, 573].

### 5.2.5 The synergistic effects of the combination are not caused by rRNA-p53 anti-proliferative responses

At the cellular level, CX-5461 has been reported to induce cell-cycle arrest, apoptosis, or senescence in various cancer cell lines via p53-dependent and independent anti-proliferative responses [208]. The p53-independent response occurs via the DDR pathway, while the p53-dependent response is induced by the

release of free ribosomal proteins (RPs), caused by the perturbations of rRNA synthesis, from the nucleolus into the nucleus to subsequently stabilise p53. The reduction in the pre-rRNA level and the increase in the p53 protein level and phospho-p53 (S15) (ATM/ATR phosphorylation site) level can be observed during this process [203, 221].

It has been reported that OVCAR4 cells possess mutant p53 [225]. However, in order to confirm that the p53 pathway in OVCAR4 cells are indeed non-functional and the synergistic effect was not a result of the rRNA-p53 mediated responses, we first analysed the protein and phosphorylation (activation) level of p53 in OVCAR4 and BJ3 cells treated with 1μM CX-5461 for 48 hours by western blots. BJ3 cells (human dermal fibroblast) were used as a positive control for p53 activation as they possess wild type p53 and an intact rRNA-p53 mediated anti-proliferative response [220]. While the accumulation of p53 protein and increased p53 phosphorylation (activation) were observed in CX-5461-treated BJ3 cells, similar trends were not observed in OVCAR4 cells (Figure 5.7A). On the other hand, increased phosphorylation of CHK2, a key component in DDR, was observed in both cell lines, suggesting that the p53-independent DDR, but not the rRNA-p53 responses, likely plays a main role in response to CX-5461 in OVCAR4 cells.

We next performed the Pol I transcription assay in OVCAR4 cells by using RT-qPCR to detect the level of the newly synthesised 45S pre-rRNA, which is rapidly processed and thus serves as a surrogate measure of rDNA transcription. The treatment of 80nM CX-5461 for 3 and 24 hours significantly decreased the 45S pre-rRNA abundance (5'ETS, ITS1 and ITS2 primers) but not 5S pre-rRNA (transcribed by Pol III) (Figure 5.7B), which confirmed CX-5461's ability to selectively inhibit Pol I transcription. 1μM CX-5461 and 5nM ActinomycinD (a low dose known to inhibit Pol I transcription) served as positive controls.

However, no further reduction of 45S pre-rDNA transcription was observed with CX-5461 and Topotecan combination treatment, which indicates that the synergistic effect is not caused by an enhanced inhibition of rDNA transcription.

In order to assess the impact of inhibition of rDNA transcription on cell proliferation, we then performed cell proliferation assays using the same conditions. Interestingly, although 5nM ActinomycinD achieved a much stronger effect in suppressing rDNA transcription compared to CX-5461/Topotecan combination treatment (Figure 5.7C), its effect on cell proliferation inhibition was not as pronounced as that of the combination treatment (Figure 5.7D). In other words, the level of acute rDNA transcription inhibition is not correlated with the inhibition of cell proliferation. Similarly, in the previous drug wash off experiments, while the inhibition of rRNA transcription was observed during the CX-5461/Topotecan combination treatment (55% reduction in 5'ETS transcription 24hrs after dual drug treatment) (Figure 5.7C), we did not observe any significant change in 5'ETS transcription (less than 10% reduction) 48 hours after drug withdrawal (Figure 5.4F). Moreover, although CX-5461 treatment alone can inhibit rRNA transcription at a comparable level as CX-5461/Topotecan combination (Figure 5.7C), it failed to demonstrated a comparable cell growth inhibition after the drug withdrawal (Figure 5.4D and E). The restoration of rRNA transcription (but not cell proliferation) after drug withdrawal (Figure 5.4E), as well as the lack of correlation between rRNA transcriptional inhibition and cell proliferation inhibition (Figure 5.7C&D), strongly indicate that the synergistic effect of the combination is not due to rRNA-p53 mediated nucleolar stress responses.

### 5.2.6 Enhanced DDR after CX-5461 and Topotecan combination treatment

The p53-independent response to CX-5461 is largely mediated by Ataxia telangiectasia mutated (ATM) and Ataxia telangiectasia and Rad3 related (ATR) kinases, both of which are part of the DDR pathway [220, 223]. ATM/ATR are activated by various forms of DNA damage, including DNA double-strand breaks (DSBs) and RPA-coated single-strand DNA (ssDNA). Protein kinases CHK1 and CHK2 are the major downstream targets of ATM/ATR, which arrest cell-cycle progression by various mechanisms [574].

In order to investigate if DDR is the cause of the synergistic effects of CX-5461 and Topotecan, we assessed the activation/phosphorylation of a number of key DDR pathway components in OVCAR3, OVCAR4 and CAOV3 cells by western blotting after 3 or 24 hours CX-5461, Topotecan or CX-5461/Topotecan combination treatment (Figure 5.8A). 1μM CX-5461 and 1μM Doxorubicin (a TOP2 inhibitor which induces DSBs) served as positive controls as they are known to induce DDR [575]. The panel of DDR components include pRPA32/RPA2(S4/S8), pRPA2(S33), pATM(S1981), pATR(T1989), pCHK1(S345), pCHK2(T68), pKAP1(S824), γH2AX(S139) and pCDC2(Y15) (See details of these components in Chapter 1.1.6 and Figure 1.4). Enhanced activation/phosphorylation of pRPA32/RPA2(S4/S8), pRPA2(S33), pCHK1(S345) and pCHK2(T68) were reproducibly observed in CX-5461 and Topotecan combination treated cells, especially at 24 hours, which indicates an enhanced DDR after combination treatment (Figure 5.8B). Similar responses were also observed in OVCAR3 and CAOV3 cell lines (Figure 5.8C). Interestingly, despite the strong activation of DDR, we did not observe enhanced phosphorylation of H2AX (γH2AX) with the CX-5461/Topotecan combination treatment, which, in contrast, was strongly activated with doxorubicin treatment.

The treatment of doxorubicin also dramatically activated pCHK2 at 3 hrs and pATM at 24 hrs, which was distinct from the CX-5461/Topotecan combination treatment (Figure 5.8B). The strong and rapid phosphorylation of γH2AX, pCHK2 and pATM is a canonical indicator of the formation of DSBs [575]. These data suggest that the CX-5461 and Topotecan combination activates the DDR in a different way from doxorubicin, which was known to activate DDR via DSBs.

### 5.2.7 Enhanced DDR does not result in DNA strand breaks, G4-DNA stabilisation or global replication stress

We then investigated the trigger of the enhanced DDR by the combination treatment. Previous studies have shown that CX-5461-induced DDR is either DNA damage-dependent or -independent [220, 225]. DNA double-strand (DSBs) and single-strand DNA breaks (SSBs) are the most common form of DNA damage. In order to investigate whether the DDR is the result of the accumulation of DNA strand breaks, we performed the alkaline comet assay, a sensitive method that detects SSBs, DSBs, alkali-labile sites, oxidative bases or DNA-DNA/DNA-protein crosslinks at the single cell level [576]. Cells were treated with 1μM CX-5461, 20nM Topotecan or 1μM CX-5461/20nM Topotecan combination for 3 hours (the drug dosages are higher due to short treatment period), and were then harvested for the assay. Doxorubicin, a DNA topoisomerase II inhibitor known to induce direct DSBs, was used as a positive control [481]. Similar to our previous observations, long comet tails indicative of extensive DNA damage, were only observed in doxorubicin-treated cells but not CX-5461, Topotecan or CX-5461/Topotecan combination-treated cells at the concentrations tested (Figure 5.9A and B) [420]. These results are consistent with the western blot analysis of γH2AX, a common marker of multiple types of DNA damage [313], in which strong phosphorylation was only observed in doxorubicin-treated cells (Fig. 5.8B

and C). These findings strongly suggest that the activation of DDR caused by the CX-5461 and Topotecan combination treatment was not the result of accumulated DNA strand breaks.

G4-DNA is a four-stranded DNA structure formed by single-stranded guanine-rich DNA sequences whose stabilisation can impede the progression of DNA polymerases and lead to replication stress, DNA damage and genomic instability [577]. As CX-5461 has been reported to be a DNA G-quadruplex (G4-DNA) stabiliser [225], we then tested if the synergy between CX-5461 and Topotecan resulted in enhanced G4-DNA stabilisation. We performed immunofluorescent (IF) cell staining in OVCAR4 cells treated with 1μM CX-5461, 20nM Topotecan, 1μM CX-5461/20nM Topotecan combination, 1μM doxorubicin or 10μM TMPyP4 for 3 hours using a G4-DNA specific antibody (1H6), which is a conventional method to evaluate the presence of G4-DNA [467]. TMPyP4 is a strong G4-DNA stabiliser that was used as a positive control [578]. Despite the fact that CX-5461 treatment resulted in a moderate stabilisation of G4-DNA in the nucleoli as marked by UBF staining, CX-5461/Topotecan combination-treated cells did not show stabilisation (Figure 5.9C and D). TMPyP4 treatment was the only treatment that showed strong stabilisation of G4-DNA [467]. Furthermore, western blot analysis of OVCAR4 cells treated with 10μM TMPyP4 for 1 or 3 hours showed no activation/phosphorylation of the key DDR components pCHK1(S345) and pCHK2(T68) compared to 1μM CX-5461 treatment (Figure 5.9E). Similarly, TMPyP4 also did not inhibit Pol I transcription, as demonstrated by RT-qPCR of 45S pre-rRNA in cells treated with 10μM TMPyP4 at various time points (Figure 5.9F). Together, these results suggest that the enhanced formation of G4-DNA structures does not result in synergy between CX-5461 and Topotecan.

CX-5461 treatment has also been reported to induce global replication stress [225]. Replication stress is a phenomenon of slow or problematic progression of replication forks. Stalled replication forks, if not properly stabilised and restarted, can lead to the generation of fork collapse and genomic instability [313, 579]. The DDR can be activated by stalled replication forks, which provide a significant contribution to DNA damage-independent DDR [313]. In order to determine whether replication stress contributes to the synergy between CX-5461 and Topotecan, we performed IF staining in OVCAR4 cells treated with 1μM CX-5461, 20nM Topotecan, 1μM CX-5461/20nM Topotecan combination, or 1μM doxorubicin for 3 hours to assess the replication-dependent γH2AX and RAD51 foci formation, both of which are markers of replication stress [225, 580, 581]. Cells were also co-treated with 5-ethynyl-2'-deoxyuridine (EdU), an analogue of thymidine that is similar to BrdU, which can be incorporated into newly synthesized DNA during DNA replication. Consistent with previous studies, increased γH2AX and RAD51 foci formation was observed in CX-5461, Topotecan and CX-5461/Topotecan combination-treated cells, and was highly correlated to EdU incorporation, indicating the existence of replication stress in replicating/S-phase cells (Figure 5.10A). However, although γH2AX and RAD51 foci formation was indeed strong in CX-5461, Topotecan or CX-5461/Topotecan combination-treated cells, there was no further enhancement compared to CX-5461 or Topotecan single treatment (Figure 5.10B and C). In fact, the level of γH2AX and RAD51 foci formation in the CX-5461/Topotecan combination-treated cells was similar to that of the Topotecan-treated cells. In contrast, doxorubicin treatment induced strong γH2AX foci, but not RAD51 foci, formation in both EdU positive and negative cells, suggesting the formation of DSBs. It has been reported that only γH2AX but not RAD51 foci are induced by the DSBs formed in G0/G1 phase [582]. This reveals a different cellular response towards different types of DNA abnormalities, which is also consistent with observations above describing the differential mechanisms underlying the

response to CX-5461/Topotecan combination and doxorubicin (section 5.2.4 and 5.2.6). Together, these data suggest that 1) CX-5461, Topotecan or CX-5461/Topotecan combination treatment induces replication-dependent formation of γH2AX and RAD51 foci, which is likely due to replication stress rather than DSBs; 2) The level of RAD51 and γH2AX foci formation is not correlated to the level of cell proliferation inhibition. The strong replication stress induced by CX-5461 and Topotecan combination treatment may contribute to the inhibition of proliferation but is not the root cause of the synergistic effect; 3) CX-5461 and Topotecan may play redundant roles in inducing replication stress.

Some RAD51/ γH2AX foci can be found in EdU negative cells in all treatment groups (Figure 10B-C, E-F). This phenomenon can be attributed to the roles played by RAD51/ γH2AX in the DDR process. RAD51 plays a central role in HR by catalysing the ssDNA crossover to its undamaged homologue to allow re-synthesis of the damaged region. As HR occurs in both S and G2 phases, our finding that RAD51 foci are present in EdU negative G2 phase cells is consistent [583]. RAD51 foci formation has also been shown in G1 phase cells with extensive DNA damage [584]. Similarly, as an early responder to DNA damage, γH2AX can be phosphorylated and activated by all three PIKKs (ATM, ATR and DNAPKs) independent of cell cycle; thus, it is not surprising to observe γH2AX in EdU negative cells, particularly in cancer cells with unstable genomes [585].

Topotecan disrupts TOP1 function by trapping TOP1 on the chromatin via its TOP1cc (reviewed in Chapter 5.1.3), which is distinct from siTOP1 which simply reduces the mRNA and protein level of TOP1. However, this TOP1 poisoning process is a strong inducer of replication stress by itself, which makes it difficult to determine the contribution of replication stress to the combination effects in our experimental system [586, 587]. In order to avoid the noise caused by TOP1 trapping and to better dissect the role of replication stress in the combination of

CX-5461 and the functional inhibition of TOP1 (without TOP1 poisoning), we performed IF staining of γH2AX and RAD51 foci in OTP-NT or siTOP1-transfected OVCAR4 cells treated with 1μM CX-5461, 20nM Topotecan, or the combination of 1μM CX-5461/20nM Topotecan together with EdU labelling. Strikingly, the RAD51 and γH2AX foci formation in EdU negative cells (G0/G1/G2 phase cells) was weak in all treatment groups, which supports our previous statement that the combination of CX-5461 and TOP1 inhibition does not cause DSBs. Doxorubicin, a TOP2 inhibitor known to cause DSBs, induced γH2AX foci formation independent of EdU incorporation (Figure 5.10A and C). For EdU positive cells (S phase cells), although strong γH2AX and RAD51 foci formation was still observed in CX-5461, Topotecan, or CX-5461/Topotecan combination-treated OTP-NT transfected cells, similar effects were not observed in siTOP1 transfected cells (Figure 5.10D). To be more specific, the level of RAD51 foci formation in TOP1 knockdown cells treated with CX-5461, Topotecan, or the CX-5461/Topotecan combination was equivalent to that of the vehicle-treated cells. In fact, all the treatment groups with TOP1 knockdown had a lower RAD51 foci formation level compared to their mock knockdown counterparts, including the Topotecan only group, which confirms the specificity of Topotecan (Figure 5.10E). We attributed the absence of RAD51 foci to the reduced level of ssDNA formation, which could be the result of alleviated TOP1 trapping, or replication stress. For γH2AX foci formation, the situation is more complex. Similar to RAD51 foci, alleviated γH2AX foci formation was observed in Topotecan or vehicle-treated TOP1 knockdown cells. However, despite of the marked decrease in RAD51 foci formation, γH2AX foci formation in CX-5461 or CX-5461/Topotecan combination-treated TOP1 knockdown cells still was maintained at a relatively high level (Figure 5.10F). We attributed this sustained strong γH2AX foci formation to the activation of ATM upon CX-5461 treatment by mechanisms other than DSBs or replication stress. It has been reported that

overactivation of ATM can induce γH2AX foci formation without the presence of actual DNA damage [588]. Moreover, we did not observe localisation of RAD51 foci in the nucleolar region (Dr Elaine Sanij's unpublished data). All these findings suggest that 1) the global replication stress induced by the CX-5461 and Topotecan combination is highly dependent on the TOP1 expression level that the depletion of TOP1 can alleviate replication stress; 2) TOP1 itself is a source of replication stress under basal conditions; 3) global replication stress is not correlated to the synergistic effects between CX-5461 and TOP1 inhibition.

### 5.2.8 CX-5461, Topotecan or combination treatment induces both replication-dependent and -independent nucleolar-associated DDR

Given that DNA strand breaks, G4-DNA structures and global replication stress likely do not contribute to the synergy between CX-5461 and Topotecan, we then hypothesised that the nucleolar-associated DDR may contribute to the synergistic effect as both RNA Pol I and TOP1 are predominantly localised in the nucleolus [100].

In order to investigate the existence of a nucleolar-associated DDR, we performed IF analysis of upstream DDR components pRPA2(S33) and pRPA32(S4/S8) together with the nucleolar marker UBF in OVCAR4 cells treated with 1μM CX-5461, 20nM Topotecan, the combination of 1μM CX-5461/20nM Topotecan, 1μM doxorubicin or 5nM ActinomycinD for 3 hours. pRPA2(S33) and pRPA32(S4/S8) are two different post-translational modifications of RPA (Reviewed in Chapter 1.1.6) [329, 589]. Surprisingly, IF staining showed a distinct staining pattern for these two RPA modifications. For pRPA32(S4/8), strong foci were observed at the centre of the nucleolus after the CX-

5461/Topotecan combination treatment, but were not observed with doxorubicin or actinomycin D treatment. These foci did not co-migrate with UBF to the nucleolar periphery upon treatment with CX-5461 and their formation was not correlated to EdU status (Figure 5.11A and C). For pRPA32(S33), strong UBF colocalising pRPA2(S33) foci formation was observed in both CX-5461/Topotecan combination-treated and doxorubicin-treated groups. However, in CX-5461/Topotecan combination treated groups, these foci only present in the EdU-positive cells; while in doxorubicin treated groups, they present in both EdU-positive and -negative cells (Figure 5.11B and D). This EdU-independent activation of pRPA2(S33) further confirmed the replication independent DNA damaging action of doxorubicin. Together, these data suggest that 1) the CX-5461 and Topotecan combination treatment induced a nucleolar-associated DDR; 2) ssDNA is present in the nucleolus upon the combination treatment; 3) the CX-5461/Topotecan combination demonstrated distinct staining pattern as doxorubicin, which further suggested the different therapeutic mechanisms followed by these two treatments; 4) multiple DDR mechanisms maybe involved in response to the combination treatment as the two groups of RPA proteins exhibited different localization and expression patterns.

As ssDNA-bound RPA32/RPA2 is known to be the platform for ATR activation/phosphorylation, we thus investigated the ATR activation status by IF staining with a phospho-ATR(T1989) antibody. The results revealed that after 3 hours treatment of 1μM CX-5461, there was a replication-independent (as defined by EdU staining) increase in pATR staining and the staining was further enhanced by the co-treatment of 20nM Topotecan. The enhanced pATR staining occurred at UBF foci, which indicates that the CX-5461/Topotecan combination treatment activates the DDR via ATR phosphorylation within the nucleoli (Figure 5.12A). A similar staining pattern was not observed with ActinomycinD or doxorubicin treatment, although enhanced pATR foci formation in other regions of the nucleus

was indeed observed in the doxorubicin group independent of EdU (Figure 5.12B), which further confirmed its replication independent DNA damaging capability [573]. It should be noted that the pATR and pRPA(S33) both colocalise with UBF in the CX-5461/Topotecan combination group. This colocalization does not exist in response to doxorubicin treatment as the pATR does not colocalise with UBF, further highlighting the distinct mechanism of action between the combination therapy and doxorubicin. Based on these results, we conclude that 1) the CX-5461 and Topotecan combination treatment induces a nucleolar-associated DDR via the RPA-ATR axis; 2) the DDR is not replication or DSB-dependent, indicating the existence of mechanisms other than the induction of replication stress or DSBs (See section 1.6); 3) the strong induction of pATR foci formation at nucleolus was not observed with doxorubicin or ActinomycinD treatment, reinforcing our previous observations above that a different mechanism was used by the CX-5461/Topotecan combination. 4) the DDR induced by the CX-5461/Topotecan combination, particularly the early responders like pATR, is restricted to the nucleolar region, which is distinct from doxorubicin which induces global DNA damage (also indicated by pATR). This specificity suggests that the CX-5461/Topotecan combination may provide a safer, more targeted therapeutic approach than doxorubicin.

As the RPA-ATR-mediated DDR induced by the combination was not exclusively dependent on DNA replication and DSBs were not detectable, we then investigated the possibility that replication-independent DDR could be involved in this process. As reviewed in Chapters 1.6.1 and 1.6.2, the DDR can also be activated via the transcription-coupled DDR mediated by the TC-NER, even in non-proliferating cells [590, 591]. RPA protein is known to be activated and involved in the TC-NER by stabilising ssDNA during the TC-NER process and activating the ATR cascade to slow down cell cycle progression [592-594], which is in accordance with the activated pRPA32/RPA2 and pATR phenotypes we have

observed. One of the main triggers of TC-NER is R-loops [595]. R-loops are three-stranded DNA secondary structures when the nascent RNA hybridises with the DNA template (the RNA-DNA hybrids), leaving the non-template DNA single-stranded [596]. RPA32/RPA2 can bind to ssDNA and protect it from DNA damage or from forming secondary DNA structures such as G4-DNA, thus serving as a sensor of R-loops [597]. R-loops naturally occur during transcription but can lead to replication stress and genomic instability if left unresolved [596, 597]. It is not surprising that the nucleolus containing the rDNA is a frequent site for R-loop formation due to its unusually high transcription rate [598]. TOP1 is also known to be involved in the prevention of R-loop formation. The transcription of RNA polymerases induces positive and negative supercoils ahead of and behind the polymerases, respectively, while the formation of negative supercoils favours R-loop formation. TOP1 can resolve these negatives supercoils, thus avoiding the formation of R-loops [598]. Indeed, the loss/inhibition of TOP1 can cause R-loop accumulation in both yeast and mammalian cells [100, 599], while the accumulation of R-loops can activate NER and induce genomic instability [600]. As Pol I transcription, TOP1 inhibition and RPA-ATR-mediated DDR converge on R-loop formation, this prompted us to test if the accumulation of R-loops is involved in the synergy between CX-5461 and Topotecan.

In order to evaluate the formation of R-loops, we utilized a widely used specific antibody against RNA-DNA hybrids [S9.6] to perform IF analysis in OVCAR4 cells treated with 1μM CX-5461, 20nM Topotecan or the combination. Consistent with a previous report, strong formation of RNA-DNA hybrids was observed in the cytoplasm in all treatment groups, which was attributed to mitochondrial R-loops and cytoplasmic tRNA [599]. However, enhanced R-loop foci formation in the nucleolus marked by UBF was only observed with the combination treatment (Figure 5.13A and B). In addition, the localization of UBF and R-loops was also altered following drug treatment. UBF and R-loops were partially colocalised

with each other in the vehicle and 20nM Topotecan-treated groups, while the addition of 1μM CX-5461 disrupted this colocalization, and UBF migrated to peripheral nucleolar caps, leaving R-loops at the centre of the nucleolus (Figure 5.13A). The R-loop staining pattern shared high similarity to that of pRPA32(S4/S8), which confirms pRPA32 role as a sensor of R-loops [597]. Taken together, we suggest that the CX-5461 and Topotecan combination treatment induces a replication-independent, nucleolar-associated DDR that can drive the formation of R-loops via the RPA-ATR axis.

In addition to the RPA-ATR axis, we also examined whether ATM is involved in the synergistic effects as our previous study has shown that the Pol I inhibition can lead to the activation of ATM signalling [420]. In order to evaluate the activation of ATM, we performed IF staining of pKAP1(S824), a major phosphorylated substrate of ATM, in OVCAR4 cells treated with 1μM CX-5461 or/and 20nM Topotecan for 3 hours [601]. A significant increase in the percentage of cells with high pKAP1 expression was observed in EdU-positive cells with combination treatment, indicating the strong activation of ATM (Figure 5.14A and B). Furthermore, KAP1 has been reported to be a suppressor of p21 gene transcription while phosphorylation of KAP1 at S824 can deactivate KAP1 suppressive function and promote the expression of p21 [602-605]. When considering the senescence-like phenotype that occurs in response to the combination (Figure 5.4F), the enhanced phosphorylation of KAP1 by ATM could be driving the elevated transcription of p21. While further experiments are necessary to test this hypothesis, it is possible that the activation of ATM-KAP1-p21 contributes to the cell cycle arrest observed with the CX-5461 and Topotecan combination treatment.

### 5.2.9 CX-5461 and Topotecan combination treatment is well tolerated in vivo and can slow tumour progression in a xenograft mouse model of HGSC

The clinical treatment of HGSC is currently hindered by the drug resistance that develops in response to treatment, particularly with respect to the restoration of HR function [24]. Very limited salvage therapeutic options are available for patients who are refractory or have developed resistant disease to conventional platinum-based chemotherapies and PARP inhibitors, and the prognosis for these patients is poor [41]. Topotecan is among the top choices of these salvage therapies, but its dose-limiting toxicity in haematological suppression restricts its long-term use [474]. As a result, if the combination of CX-5461 and Topotecan could slow down tumour progression *in vivo* while keeping side-effects minimal, it would deliver a significant impact in clinical practice.

In order to evaluate the clinical potential of the CX-5461 and Topotecan combination, we tested the combination in a pre-clinical OVCA xenograft model. We utilised the mutant p53 HR-proficient OVCAR3 cell line, which was established from a cisplatin-refractory patient and is widely used as a model system to study drug resistance in OVCA [606-608]. $5x10^6$ OVCAR3 cells were subcutaneously engrafted into 40 4-6-week-old female NOD SCID Gamma (Non-Obese Diabetic.Cg-*Prkdc*$^{scid}$ *Il2rg*$^{tm1Wjl}$/SzJ, NSG) severe immunodeficient mice and were then left to grow for approximately 3 weeks until the average tumour volume reached $100mm^3$.

Tumour-bearing mice were randomised into four groups (10 mice for each group) and administrated with 30mg/kg CX-5461 (oral gavage) or/and 5mg/kg Topotecan (intraperitoneal injection) (maximum tolerated dosages (MTD)

determined by the TRL) and the corresponding vehicles twice a week for four weeks (8 doses in total). The dosages were empirically determined based on previous studies [606, 609]. We monitored tumour growth twice a week until the tumour volume reached 1000mm$^3$ at which time the mice were culled. Mice were weighed to monitor animal health in response to the drug treatments.

CX-5461 treatment alone only had a very moderate effect in delaying tumour growth and prolonging survival, consistent with previous observations that HR-proficient xenografts are less sensitive to CX-5461 treatment compared to HR-deficient ones [225]. Alternatively, Topotecan treatment alone was more potent in inhibiting tumour growth, which further supports the rationale of its use in the clinic (Figure 5.15B). Strikingly, the combined treatment of CX-5461 and Topotecan completely stalled tumour progression during the period of treatment and extended overall survival by almost 30% compared to Topotecan only treatment (Figure 5.15C). The tolerability of the treatment was also acceptable during the treatment period with regard to change in body weight (Figure 5.15A). However, we did observe some dose-limiting toxicity related to Topotecan treatment, including body weight loss and pale limbs and lips, which are signs of anaemia and haematological suppression. These side-effects have also been observed in the clinic and are reversible after ceasing dosing [610].

To test whether the moderate side effects from the combination treatment could be reduced while retaining therapeutic efficacy, we performed a second experiment using half the MTD dose of Topotecan (2.5mg/kg twice per week). Indeed, the side-effects were largely alleviated (Figure 5.15D) and the therapy was still effective. The combined treatment of CX-5461 and Topotecan stabilised the disease (Figure 5.15E) during the treatment period and extended the overall survival by more than 50% compared to Topotecan alone (Figure 5.15F). In other words, the synergistic effect was even stronger using a lower dose of Topotecan.

In summary, our pre-clinical results strongly support the combination of CX-5461 and Topotecan as a promising therapeutic treatment option for HR-proficient, chemo-resistant HGSC. Furthermore, using a reduced dose of Topotecan while retaining efficacy indicates the possibility of longer-term treatment and hence therapeutic outcome.

## 5.3. Discussion

This chapter focussed on the validation and the mechanistic study of the synergistic effect between CX-5461 and TOP1 inhibition, which was identified by the genome-wide siRNA screen and the focussed chemical compound screen described in the previous chapters. We have also provided insight into the in vivo application of the CX-5461/TOP1 combination in the latter part of this chapter.

Specifically, we verified that TOP1 inhibition, either by siRNA knockdown or by the chemical inhibitor Topotecan, together with CX-5461 treatment can synergistically inhibit cell proliferation in HGSC cell line OVCAR4 (Figure 5.1). The effectiveness of this combination effect was confirmed by the results of the drug checkerboard assays performed in three HGSC cell lines (OVCAR3, OVCAR4 and CAOV3) and one OCCC cell line SKOV3 (Figure 5.3). The synergistic effect demonstrated in the SKOV3 cell line is particularly interesting because this cell line is known to be resistant to both cisplatin and Olaparib, which are the current standard treatment options of ovarian cancer (Figure 5.2) [422, 423]. This finding strongly suggests that the CX-5461/Topotecan combination may have the potential to overcome the resistance to standard therapies in ovarian cancer.

One caveat of our experiments is that we did not test TOP1 knockdown efficiency with individual siRNA duplexes, which raises the possibility of off-target effects. As only 2 out of the pool of 4 siTOP1 duplexes we used synergise with CX-5461 (Table 3.2), it is possible that the siTOP1 duplexes causing the synergistic effects are not the ones that downregulate TOP1 expression. To address this, we could introduce an RNAi-insensitive ORF of TOP1 to test if it rescues the synergistic effects and the expression of TOP1 protein. The details of the method as well as other ways of detecting the off-target effects have been described in section 4.3.

In addition to ovarian cancer cell lines, we have also tested the efficacy of the CX-5461/Topotecan combination in B-cell acute lymphoblastic leukaemia (B-ALL) cell lines SUP-B15 and MHH-CALL4 (Figure 5.5). Both CX-5461 and Topotecan are being evaluated in the clinic to treat B-ALL [223, 566, 611]. Strong synergistic effects were observed in both cell lines, demonstrating the broader applicability of this combination to other cancers. However, further studies are required to determine the tumours types which are more likely to be sensitive to this therapy, perhaps starting with the tumour types which Topotecan has been approved for use (e.g. small cell lung cancer and cervical cancer) or those with high activity of the Pol I and TOP1 enzymes (can be determined by immunohistochemistry or real-time PCR).

We then investigated the cellular mechanisms underlying the synergistic effect between CX-5461 and Topotecan. We found that the CX-5461/Topotecan combination induces cell growth inhibition and strong cycle arrest at late S/G2 phase in all three HGSC cell lines. In contrast, doxorubicin-treated cells were arrested at G1/G2 phases, revealing different mechanisms adopted by different drugs (Figure 5.6B, C and D). Cell death, as determined by the subG1 cell population, was moderately increased after 48hrs treatment of CX-5461 or CX-5461/Topotecan combination (Figure 5.6A), but was not comparable to that of B-cell lymphoma in which massive apoptosis was observed within just 3hrs treatment of CX-5461 [221]. It is worth highlighting that the CX-5461 dosage used to treat B-cell lymphoma was even lower than that of the HGSC cells. This dramatic difference in drug sensitivity demonstrated the heterogeneity among different types of cancer. The massive apoptosis observed in B-cell lymphoma was attributed to the activation of p53 pathways [221] (See Section 1.5 for details of the p53-dependent apoptotic pathway in lymphoma). Interestingly, we found no correlation between CX-5461 sensitivity (in terms of $GI_{50}$ dosages) and p53

status in our panel of ovarian cancer cell lines (Figure 3.1C). However, future experiments will test whether the combination of CX-5461 and Topotecan also has improved efficacy in p53 wildtype OVCA, e.g. LGSC. Also, it is possible that the absence of apoptosis was the result of the overexpression of anti-apoptotic factors, like BCL2-family proteins [612]. This hypothesis can be tested by including inhibitors of anti-apoptotic factors, like Venetoclax (ABT-199), into the treatment [613].

The cell cycle arrest phenotype induced by the CX-5461/Topotecan combination could be the result of either senescence or quiescence. Quiescence-induced cell cycle arrest is due to the withdrawal of serum growth factors and nutrients and is reversible after their replenishment. In contrast, senescence induces cell cycle arrest even with sufficient growth-stimulation [614]. Flattened and/or enlarged cell morphology, increased p21, p16 or senescence-associated β-galactosidase expression, senescence-associated secretory phenotype (SASP), and senescence-associated heterochromatic foci are often observed and used as markers of senescence. In fact, senescence is one of the main outcomes of chemotherapy or radiation therapies. However, although the senescence is an effective response to current therapeutics, it can be overcome through the inactivation of p53, p16, RB, or/and over-expression of CDC2/CDK1 and survivin [615, 616].

The cell cycle arrest phenotype presented after CX-5461/Topotecan combination treatment was identified as senescence-like, as the cell cycle arrest was persistent and irreversible even after drug withdrawal (Figure 5.4C, D and E). Microscopic examination of combination-treated cells demonstrated a typical senescence-like morphology with flattened and/or enlarged cells (Figure 5.4A). RT-qPCR of a panel of SASP-associated genes also revealed a significant increase in the transcription of IL1α, IL6, IL8 and p21 (Figure 5.4F). Among them, the elevation of p21 expression is particularly interesting because it is a well-known pan-CDK

inhibitor that is capable of promoting cell cycle arrest (Figure 1.4 and 5.8A). Thus, increased p21 expression provides an explanation of the observed cell cycle arrest phenotype. Moreover, no major changes in 5'ETS expression were observed compared to the vehicle-treated cells, indicating that restoration of rDNA transcription after drug withdrawal was insufficient to restore cell proliferation (Figure 5.4F). This argument was further supported by the results of the 45S pre-rRNA transcription assay and the cell proliferation assay with another Pol I transcription inhibitor, ActinomycinD, that no correlation was observed between rDNA transcription inhibition and inhibition of cell proliferation (Figure 5.7C and D). Together, these data suggest that the CX-5461/Topotecan combination treatment causes a persistent, irreversible cellular senescence independent of rDNA transcription inhibition. Furthermore, this induction of senescence has also provided an explanation as to why the CX-5461/Topotecan combination-treated tumours grew slower than other treatment groups (measured by the slope of the tumour growth curves) even after the stop of dosing (Figure 5.15B and E). It also prompted us to investigate the DDR pathways to determine the molecular mechanism of the combination as the DDR is frequently involved in the senescence and cell cycle arrest at S/G2 phases [614].

As expected, multiple components of the DDR pathways were found to be activated (hyperphosphorylated) by western blotting after treatment with the CX-5461/Topotecan combination, particularly pRPA32 (S4/S8), pRPA2(S33), pCHK1(S345) and pCHK2(T68), all of which are the main substrates of the three PIKKs (ATM, ATR, DNAPKcs), although the phosphorylation level of ATR and ATM themselves was not very consistent across different experiments, probably due their large molecular weight, their difficulty of processing and the sensitivity of the assay (Figure 5.8). Interestingly, no major change was seen in γH2AX phosphorylation, a common marker of multiple types of DNA damage, which was distinct from that of doxorubicin treatment in which strong γH2AX

phosphorylation was observed 24hrs after the drug treatment. Additionally, a strong and rapid phosphorylation of pCHK2(T68) was observed within just 3hrs treatment of doxorubicin, which was different from that of CX-5461/Topotecan combination treatment which followed a progressive activation pattern of the DDR components. All these data suggest that the CX-5461/Topotecan combination triggers the DDR in a different way to doxorubicin, which is known to cause direct DNA strands double-strand breaks and a rapid and strong activation of ATM [575].

We then investigated the root cause of the DDR further. We demonstrated that the DDR was not the result of DNA strand breaks as no γH2AX activation or comet tails was detected in CX-5461/Topotecan combination treated cells (Figure 5.9A & B). We also examined the possibility of G4-DNA being involved as Xu, et al. has reported that the CX-5461 is a G4-DNA stabiliser [225]. However, enhanced G4-DNA stabilisation was not observed by IF in the OVCAR4 cell line treated with CX-5461 or CX-5461/Topotecan combination, probably due to the heterogeneity between different cell types (Figure 5.9C & D). We considered replication stress as a plausible explanation for the enhanced DDR given strong RAD51 and γH2AX foci formation, a marker of replication stress, was indeed observed with CX-5461/Topotecan combination. Nevertheless, a closer examination of the results revealed the lack of correlation between cell proliferation inhibition and replication stress, and the strong RAD51 and γH2AX foci formation was likely to be a by-product of TOP1 poisoning by Topotecan (Figure 5.10).

We further interrogated if the nucleolar-associated DDR contributes to the synergistic effect as both RNA Pol I and TOP1 are predominantly localised in the nucleolus region [100]. Strong pRPA2(S33), pRPA32(S4/S8) and pATR(T1989) foci formation (activation) was observed in the nucleolus with the CX-

5461/Topotecan combination (Figure 5.11A to D), indicating the existence of ssDNA in the nucleolus [337]. Furthermore, the replication-independent activation of pRPA32(S4/S8) and pATR(T1989) suggested the involvement of the transcription-coupled DDR, which was confirmed by the enhanced R-loop foci staining in the nucleolar region (Figure 5.13A and B). Based on all these data, we generated the following rDNA transcriptional stress model to better illustrate the consequences of RNA Pol I and TOP1 dual inhibition.

Under normal rDNA transcription, each rDNA gene is simultaneously being transcribed by more than 100 RNA polymerase I molecules in tandem. Each Polymerase is in close proximity, thus preventing newly synthesised pre-rRNA from accessing the DNA. The positive supercoiling generated ahead of the transcription machinery also neutralises the negative supercoiling caused by the preceding polymerases and displaced nucleosomes. Meanwhile, TOP1 effectively removes all unwanted negative and positive supercoiling, thus ensuring the smooth and efficient progression of rDNA transcription (Figure 5.16A). However, upon treatment with CX-5641, RNA polymerase is displaced from rDNA chromatin, prolonging both the proximity of nascent RNA and the negatively supercoiled state of the DNA. The inhibition of rDNA transcription would also stimulate cells to activate more rDNA copies by removing histones from the nucleosomes, releasing the negative supercoiling stored in the nucleosomes (Figure 5.16B) [220]. On the other hand, the knockdown or trapping of TOP1 exacerbates the unwound DNA by preventing relaxation of the negative supercoils (Figure 5.16C). When combined together, the dual inhibition would increase the distance between polymerases and create excessive positive supercoiling ahead of transcription and negative supercoiling behind. The positively supercoiled DNA could activate the DDR directly via ATM and ATR [617], while negative supercoiling would promote the formation of R-loops. RPA32/RPA would bind to the stranded ssDNA in the R-loop and transactivate

the DDR via ATR or ATM [329]. Other secondary DNA structures, like G4-DNA, can also form at this region, which could further impede the resolution of R-loops, resulting in their stabilisation [596]. The activated/phosphorylated ATR/ATM could further activate the downstream CHK1/2, KAP1, p21, thereby inducing TC-NER, cell cycle arrest and senescence (Figure 5.16D).

However, some questions still remained unanswered by this model. For example, we still do not know how pRPA32(S4/S8) interacts with ATR at the rDNA as they do not colocalise perfectly with each other, as the pRPA32(S4/8) forms strong bead-like foci at the centre of the nucleolus while pRPA2(S33) and pATR(T1989) migrate with UBF to the nucleolus (Figure 5.11B and D). One possible explanation is that the protein mobility inside the nucleolus is limited and the damaged rDNA needs to move from the nucleolar interior to the periphery to access DNA repair factors [105]. We also do not understand why the activation of pRPA2(S33) and pKAP1 is replication-dependent while that of pRPA2(S4/8) and pATR(T1989) is replication-independent. Based on our observation that the pRPA2(S33) and pATR(T1989) are not colocalised with UBF upon the treatment of doxorubicin (Figure 5.11B and Figure 5.12B), it is possible that these two axes are regulated and activated separately, e.g. the pRPA(S4/8) and pATR are activated in a replication-independent manner while the pRPA2(S33), pKAP1 and pATM are activated in a replication-dependent manner. Additionally, we hypothesise that TC-NER is involved in the detection and repair of nucleolar transcriptional stress. One possible experiment to address this hypothesis is to test for unscheduled DNA synthesis during G1 and G2 phases as TC-NER requires DNA synthesis to fill the ssDNA gap. All in all, this model incorporates the data from our extensive mechanistic analyses but remains a model that will require further testing and refinement to better understand the exquisite regulation of the nucleolar DDR to allow its manipulation to treat cancer.

Additionally, we have demonstrated an increase in the phosphorylation of KAP1, a major substrate of ATM and a master regulator of p21 transcription, in the S-phase population after CX-5461/Topotecan combination treatment (Figure 5.14A and B). This finding not only suggests that ATM is activated but also links the DDR to the elevated transcription of p21, thus providing another explanation for the cell cycle arrest/senescence phenomenon we have observed in clonogenic assays (Figure 5.4C, D and E).

Strikingly, the application of the combination of CX-5461 and Topotecan in vivo results in a significant extension of overall survival in an OVCA tumour-bearing xenograft mouse model with tolerable side-effects. The side-effects can be further alleviated by reducing the dosage of Topotecan without compromising the efficacy of the therapy (Figure 5.15).

Despite the impressive therapeutic potential presented in the *in vivo* experiment, a number of publications have argued that cell line-derived ovarian tumour xenografts might not best represent the clinical setting due to genetic drift and the lack of heterogeneity [618, 619]. Therefore, in future experiments, our laboratory will test the combination using patient-derived tumour xenografts (PDXs), which provide a better resemblance to the natural growth of ovarian cancer. Moreover, the NSG mice used in our in vivo experiment are immunodeficient mice and do not possess functional immune cells. They are also reported to be less tolerant to DNA damaging agents such as chemotherapy drugs due to the loss-of-function mutation in the *Prkdc* (*DNA-PK*) gene [620]. As a result, in the future we plan to evaluate the combination in the ID8 syngeneic mouse model, a tumour-bearing mouse model with an intact immune system, to better examine the tolerability of the treatment. This would also enable investigation of the response of the immune system to the drug combination as the combination treatment can induce a strong SASP phenotype. Furthermore, it will be important for us to compare our

combination therapy approach with standard therapies, like cisplatin or Olaparib, in these models to define any improvements in efficacy.

In summary, our results demonstrate that the combination of CX-5461 and Topotecan induces a persistent, irreversible cell cycle arrest/senescence-like phenotype, which results from a replication-dependent and -independent, nucleolar-associated DDR. This DDR is restricted to the nucleolar region, suggesting it may provide therapeutic efficacy without global DNA damage, limiting side effects and providing a greater therapeutic window than conventional cytotoxic drugs like cisplatin and doxorubicin which cause non-specific DNA damage. This drug combination is well tolerated and demonstrates remarkable therapeutic efficacy *in vivo*, which provides a promising option for treating HR-proficient, chemo-resistant HGSC.

**Figure 5.1 Validation of TOP1 knockdown using siRNA**

**A.** Simplified illustrations of the working mechanisms of three types of topoisomerases. **B.** The successful knockdown of TOP1 was confirmed by immunofluorescent staining. The TOP1 protein (green) was depleted from the nucleus 72 hours after siTOP1 transfection, while the treatment of 1 μM CX-5461 for 3 hours did not affect the expression of TOP1. TOP1 significantly co-localised with the nucleolar marker UBF (red). The white dashed line outlines the cell nucleus. Representative images from N=3 experiments. **C.** Quantification of TOP1 immunofluorescent staining using CellProfiler. There was a significant decrease of TOP1 mean intensity with siTOP1 transfection, but not with CX-5461 treatment. Combined data of N=3 experiments normalised to the vehicle median are presented as median with interquartile range. At least 500 cells were analysed for each treatment group. Non-parametric one-way ANOVA was used. ns: not significant, ****p<0.0001. **D.** Cell proliferation assay with siTOP1 confirmed the synergistic effect between CX-5461 and TOP1 knockdown. There was a significant decrease in cell number after treating siTOP1 transfected OVCAR4 cells with 80nM CX-5461 for 48 hours. siPLK1 was used as the positive control for transfection efficiency and the negative control for the synergistic effects. siBRCA2 was used as a positive control of synergistic effects. The Bliss independence score is 0.706 which indicates a strong synergistic effect. Representative data of N=3 experiments are presented as mean±SD. Student's t-test was used. ns: not significant, ****p<0.0001.

*Figure 5.1A is adapted from website of Prof Joaquim Roca Bosch of the Structural Biology Unit at the Molecular Biology Institute of Barcelona in January 2019 (http://www.rocabosch.com/w_TOPOS/index_TOPOS.html) [621]. Written permission was obtained from Prof Joaquim Roca Bosch. See Appendix II for details of the permission.

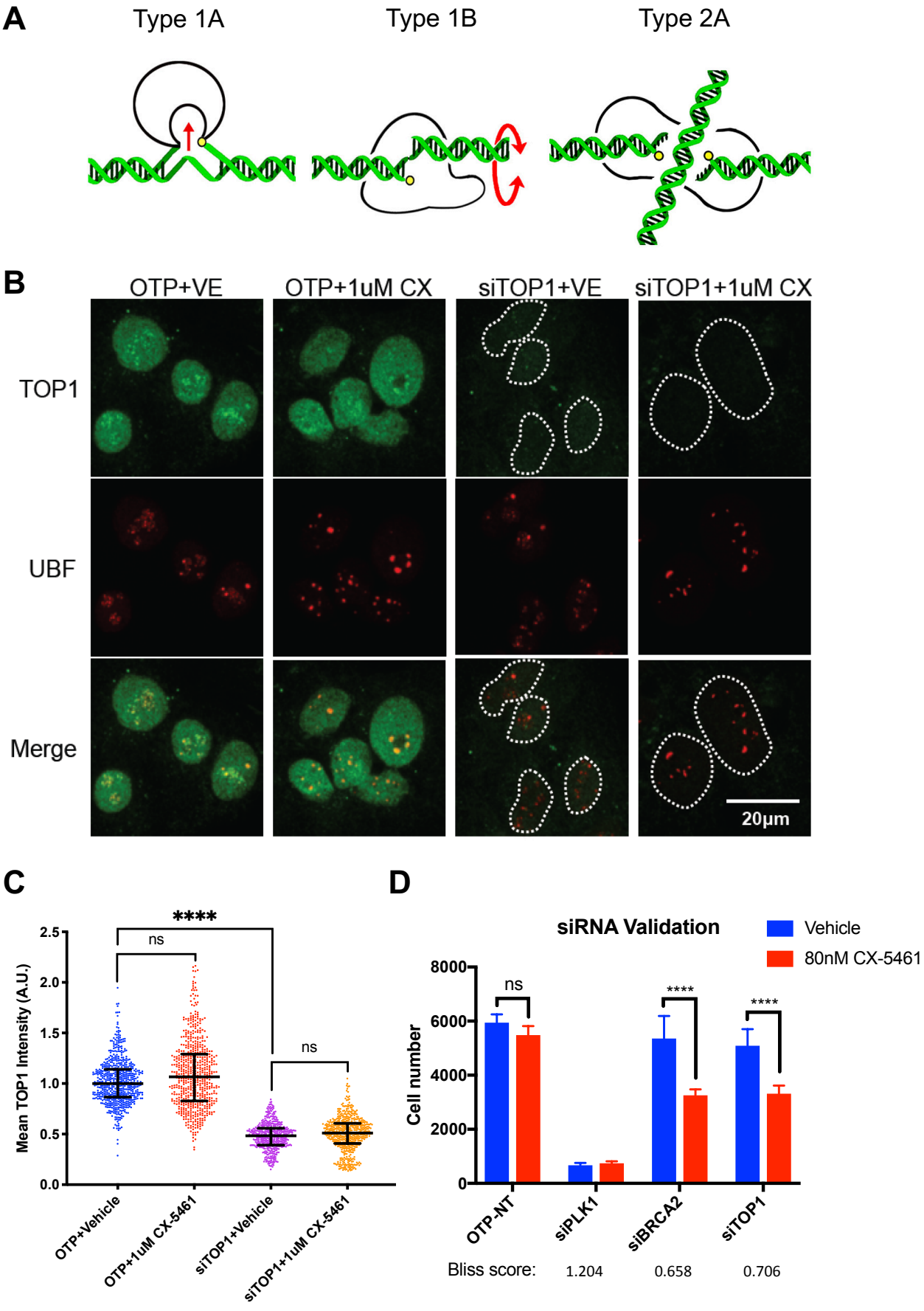
A
Type 1A
Type 1B
Type 2A
B
OTP+VE
OTP+1uM CX
siTOP1+VE
siTOP1+1uM CX
TOP1
UBF
Merge
20μm
C
****
ns
ns
Mean TOP1 Intensity (A.U.)
2.5
2.0
1.5
1.0
0.5
0.0
OTP+Vehicle
OTP+1uM CX-5461
siTOP1+Vehicle
siTOP1+1uM CX-5461
D
siRNA Validation
Vehicle
80nM CX-5461
Cell number
8000
6000
4000
2000
0
ns
****
****
OTP-NT
siPLK1
siBRCA2
siTOP1
Bliss score:
1.204
0.658
0.706

**Figure 5.2 Dose response curves of existing/emerging drugs in four ovarian cancer cell lines**

Dose response curves of **(A)** cisplatin, **(B)** Olaparib, **(C)** Topotecan and **(D)** CX-5461 in four different ovarian cancer cell lines (OVCAR3, OVCAR4, CAOV3 and SKOV3) measured by cell number (DAPI staining). The curves were generated using an ordinary nonlinear regression fit. The 50% inhibition of cell growth ($GI_{50}$) and total growth inhibition (TGI) dosages were determined by curve interpolation and were shown as median±range. The chart presents the combined results of N=3 experiments.

**A**

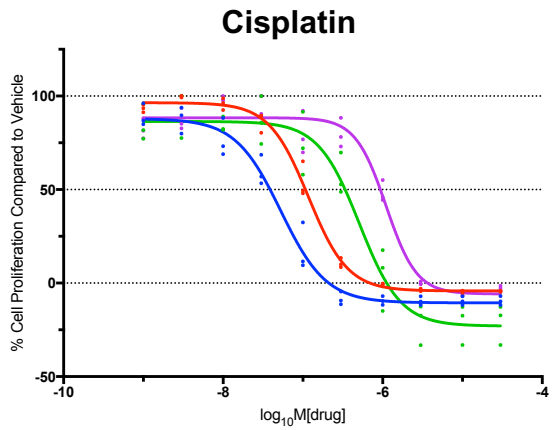


| | OVCAR3 | OVCAR4 | CAOV3 | SKOV3 |
|---|---|---|---|---|
| $GI_{50}$ (nM) | 40±8 | 108±13 | 330±89 | 909±83 |
| TGI (μM) | 0.22±0.06 | 0.68±0.38 | 1.39±0.34 | 3.76±0.13 |

**B**

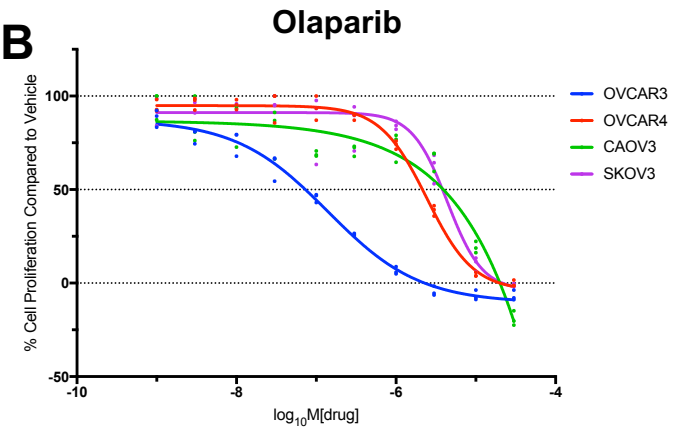


| | OVCAR3 | OVCAR4 | CAOV3 | SKOV3 |
|---|---|---|---|---|
| $GI_{50}$ (nM) | 73±11 | 2144±110 | 4405±833 | 3832±328 |
| TGI (μM) | 2.59±0.78 | 20.94±3.54 | 20.94±3.54 | 21.62±2.31 |

**C**

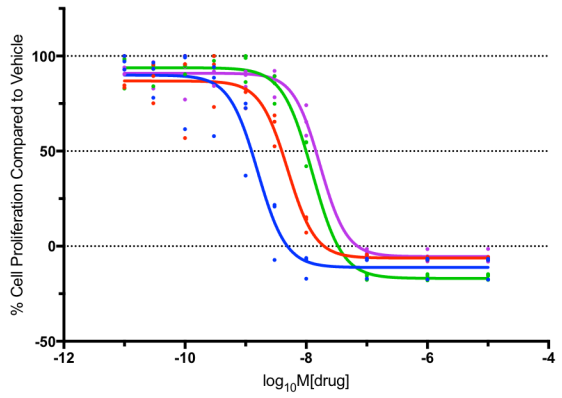


| | OVCAR3 | OVCAR4 | CAOV3 | SKOV3 |
|---|---|---|---|---|
| $GI_{50}$ (nM) | 1.2±0.4 | 4.0±0.4 | 9.9±1.0 | 14.5±1.4 |
| TGI (nM) | 5.5±0.9 | 20±2.5 | 32.6±1.3 | 71.8±13.4 |

**D**

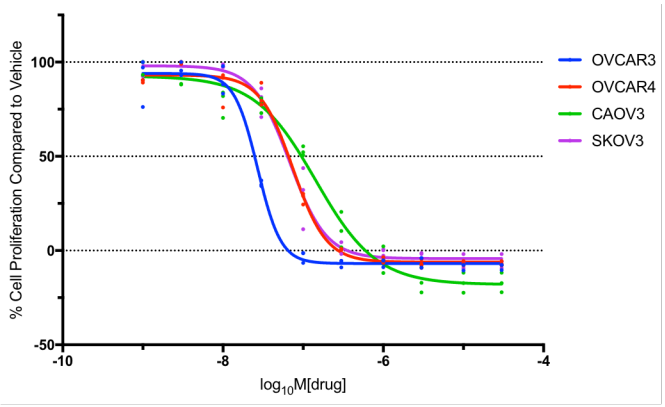


| | OVCAR3 | OVCAR4 | CAOV3 | SKOV3 |
|---|---|---|---|---|
| $GI_{50}$ (nM) | 25.2±1.7 | 65.6±4.1 | 97±8.5 | 66.4±12.1 |
| TGI (nM) | 71±18 | 279±34 | 667±183 | 371±79 |

**Figure 5.3 The combination of CX-5461 and Topotecan shows strong synergistic effects in multiple ovarian cancer cells lines**

The bliss maps of CX-5461 and Topotecan combination in **(A)** OVCAR3, **(B)** OVCAR4, **(C)** CAOV3 and **(D)** SKOV3 cell lines. The bliss maps were generated using Combenefit software (Cancer Research UK Cambridge Institute) based on the results of the two-dimensional checkerboard assay. Cells were treated with indicated doses of drugs for 9 days and counted. The Z axis represents the %control measuring the relative cell number compared to the vehicle control while the X and Y axis represent different drug dosages. The combination effects were demonstrated in different colours. Blue for synergistic, green for additive, and red for antagonistic effects. Representative charts of N=3 experiments. **E.** The combination index (CI) of CX-5461 and Topotecan combination in OVCAR3, OVCAR4, CAOV3 and SKOV3 cell lines calculated using the CalcuSyn software (Biosoft) based on the Chou-Talalay method. The plots represent the combination index at 90% effects. Combined data of N=3 experiments were presented as median±SEM

A

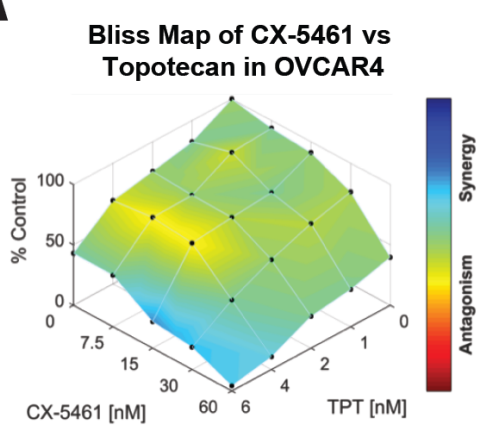
Bliss Map of CX-5461 vs Topotecan in OVCAR4
% Control
100
50
0
0
7.5
15
30
60
CX-5461 [nM]
6
4
2
1
0
TPT [nM]
Synergy
Antagonism

B

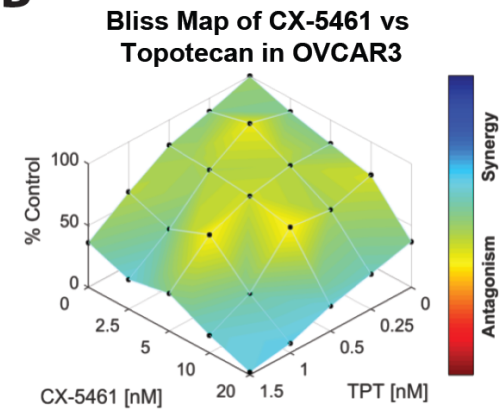
Bliss Map of CX-5461 vs Topotecan in OVCAR3
% Control
100
50
0
0
2.5
5
10
20
CX-5461 [nM]
1.5
1
0.5
0.25
0
TPT [nM]
Synergy
Antagonism

C

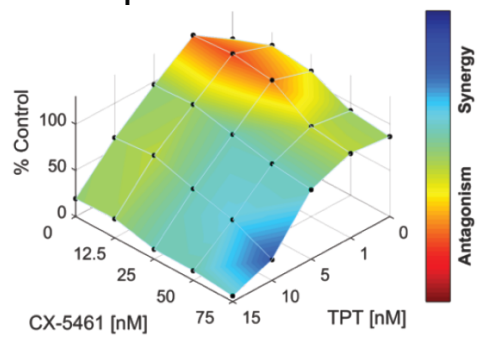
Bliss Map of CX-5461 vs Topotecan in CAOV3
% Control
100
50
0
0
12.5
25
50
75
CX-5461 [nM]
15
10
5
1
0
TPT [nM]
Synergy
Antagonism

D

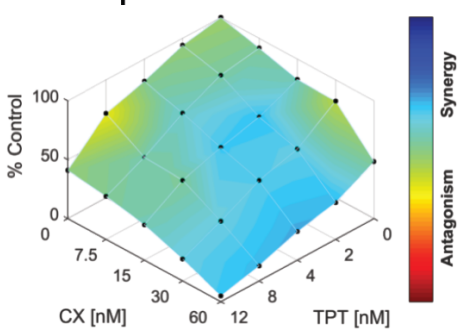
Bliss Map of CX-5461 vs Topotecan in SKOV3
% Control
100
50
0
0
7.5
15
30
60
CX [nM]
12
8
4
2
0
TPT [nM]
Synergy
Antagonism

E

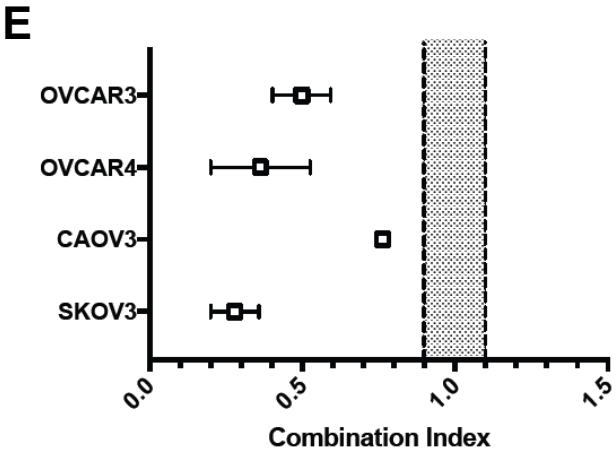
OVCAR3
OVCAR4
CAOV3
SKOV3
0.0
0.5
1.0
1.5
Combination Index

**Figure 5.4 The combined treatment of CX-5461 and Topotecan induces a senescence-like phenotype in ovarian cancer cells and inhibits clonogenicity**

**A.** Enlarged, flattened cell morphology was observed after CX-5461 and Topotecan dual treatment for 9 days, which indicates cell cycle arrest or a senescence-like phenotype. Representative images of N=5 experiments. **B.** The cell size was quantified by dividing the cell confluence with the cell number. The cells treated with CX-5461 and Topotecan were 10 times larger than the vehicle-treated cells. Combined data of N=5 experiments are presented as mean±SEM. Student's t-test was used. ns: not significant, ****p<0.0001. **C.** Workflow scheme of the clonogenic assay. Briefly, 10,000 OVCAR4 cells per well were plated into 6-welled plates (BD Falcon) on day 0. Cells were cultured for 24 hours, then treated with cisplatin, Olaparib, CX-5461 or/and Topotecan. 48 hours after drug treatment, the drugs were washed off and replaced with normal media. Cells were cultured for another 5 days, fixed and stained with crystal violet. **D.** Crystal violet staining at day8 showed a significant decrease in clonogenicity after CX-5461 and Topotecan treatment for 48 hours. Representative image of N=3 experiments. **E.** CX-5461 and Topotecan dual treatment caused persistent irreversible cell cycle arrest even after drug withdrawal. The cells were treated with the indicated drugs for 48 hours. The drug-containing media was then washed off and replaced with normal cell culture media. Cells treated with CX-5461, Topotecan, cisplatin or Olaparib as single agents resumed proliferation rapidly, but not with the CX-5641 and Topotecan combination. Enlarged, flattened cell morphology similar to Figure 5.4A was observed in CX-5641 and Topotecan dual-treated cells. Combined data of N=3 experiments are presented as mean±SEM. Two-way ANOVA was used. ****p<0.0001 compared to vehicle. **F.** RT-qPCR of a panel of SASP genes revealed increased transcription of IL1a, IL6, IL8 and p21. The median of N=3 experiments were presented in a heatmap. The reproducibility across replicates was assessed using %CV and SEM (data not shown). The white

and blue colour indicate low and high expression level compared to vehicle respectively.

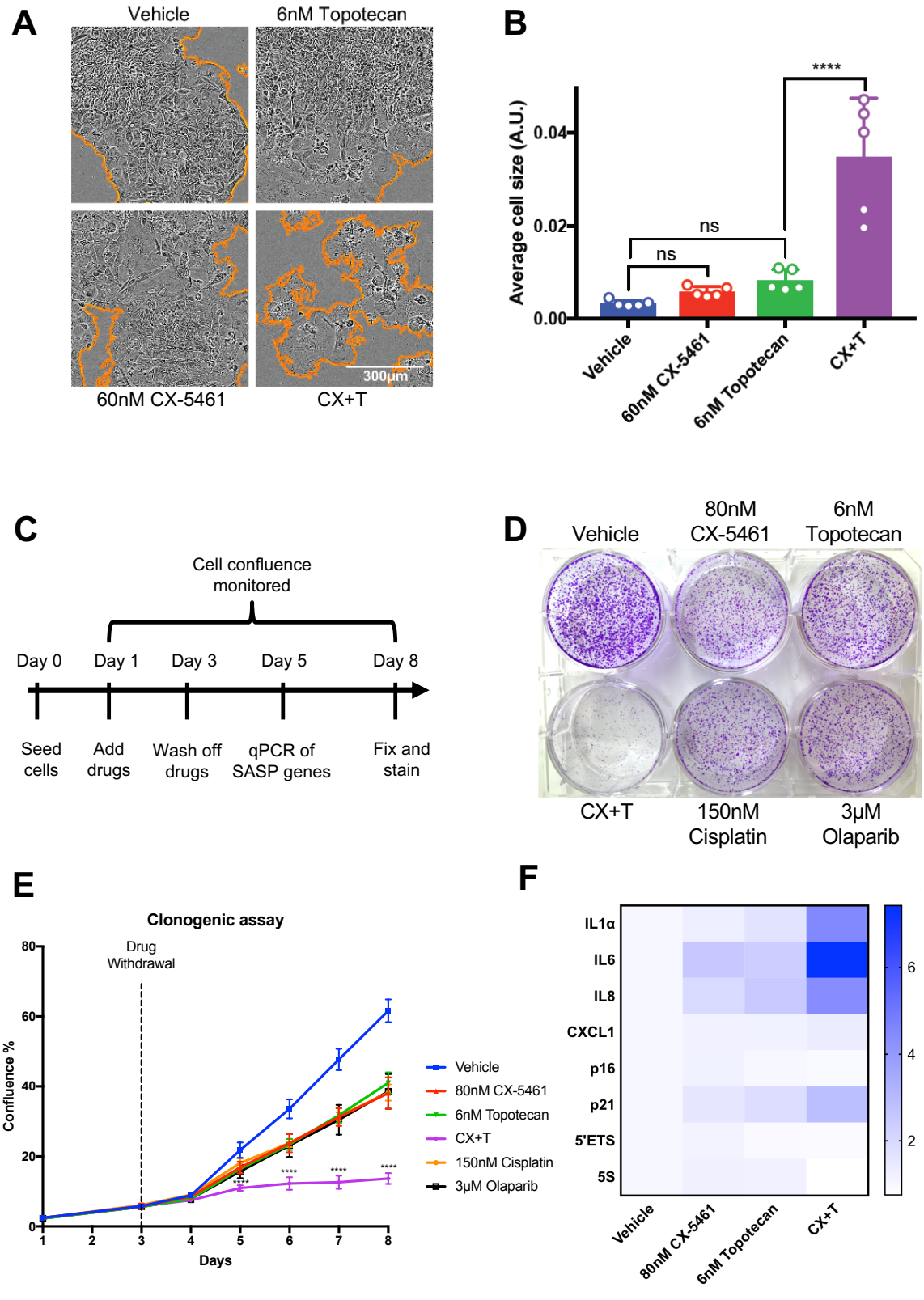
A
Vehicle
6nM Topotecan
300µm
60nM CX-5461
CX+T
B
Average cell size (A.U.)
0.00
0.02
0.04
ns
ns
****
Vehicle
60nM CX-5461
6nM Topotecan
CX+T
C
Cell confluence monitored
Day 0
Day 1
Day 3
Day 5
Day 8
Seed cells
Add drugs
Wash off drugs
qPCR of SASP genes
Fix and stain
D
Vehicle
80nM CX-5461
6nM Topotecan
CX+T
150nM Cisplatin
3µM Olaparib
E
Clonogenic assay
Drug Withdrawal
Confluence %
Days
Vehicle
80nM CX-5461
6nM Topotecan
CX+T
150nM Cisplatin
3µM Olaparib
F
IL1α
IL6
IL8
CXCL1
p16
p21
5'ETS
5S
Vehicle
80nM CX-5461
6nM Topotecan
CX+T

**Figure 5.5 The combination of CX-5461 and Topotecan shows strong synergistic effects in B-lineage acute lymphoblastic leukaemia cell lines**

The bliss maps of the CX-5461 and Topotecan combination in (A) MHH-CALL4 and (B) SUP-B15 cell lines. The bliss maps were generated using Combenefit software (Cancer Research UK Cambridge Institute) based on the results of the two-dimensional checkerboard assay. Cells were treated with indicated doses of drugs for 9 days and quantified using CellTiter-Glo. The Z axis represents the %control measuring the relative cell viability compared to the vehicle control while the X and Y axis represent different drug dosages. The combination effects were demonstrated in different colours. Blue for synergistic, green for additive, and red for antagonistic effects. Representative charts of N=3 experiments.

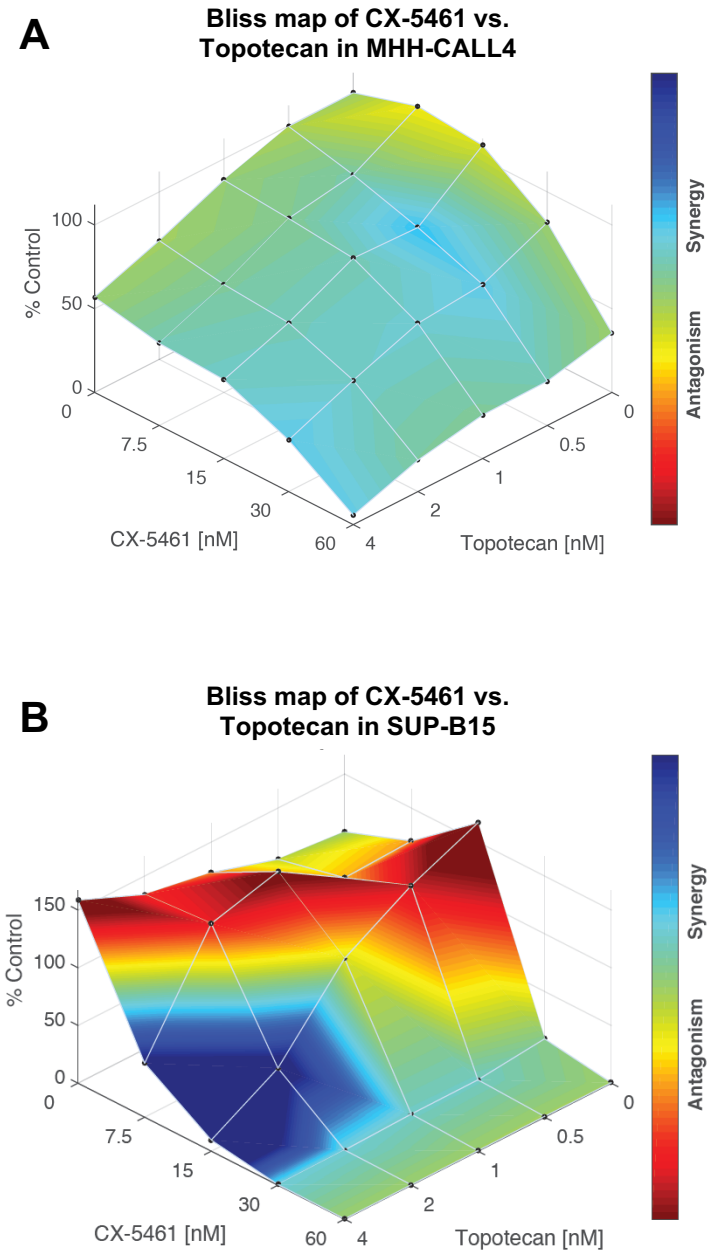
A
Bliss map of CX-5461 vs. Topotecan in MHH-CALL4
% Control
100
50
0
0
7.5
15
30
60
CX-5461 [nM]
0
0.5
1
2
4
Topotecan [nM]
Synergy
Antagonism
B
Bliss map of CX-5461 vs. Topotecan in SUP-B15
% Control
150
100
50
0
0
7.5
15
30
60
CX-5461 [nM]
0
0.5
1
2
4
Topotecan [nM]
Synergy
Antagonism

**Figure 5.6 Combined treatment of CX-5461 and Topotecan induces cell cycle arrest at late S and G2 phases**

**A.** Cell proliferation assays showed that, although the treatment of Q-VD-OPh moderately enhanced the cell proliferation in OVCAR4 and CAOV3 cells, it cannot reverse the synergistic effects. Cells were treated with indicated drugs dosages for 48 hours and counted. Representative data of N=2 experiments are presented as mean±SD. **B.** CX-5461 and Topotecan dual treatment causes a moderate increase in cell death, indicated by the subG1 population, in all three HGSC cell lines. The cell death can be partially rescued by Q-VD-OPh treatment. Cells were treated with indicated drug dosages for 48 hours. Cells were then fixed, stained with PI, and analysed by FACS. Combined data of N=3 experiments are presented as mean±SEM. Student's t-test was used. ns: not significant, **p<0.01, ***p<0.001. **C.** Representative charts and **D.** Quantification of cell cycle analysis revealed enhanced cell cycle arrest at late S and G2 phases after CX-5461 and Topotecan dual treatment in all three HGSC cell lines. Cells were treated with indicated drugs dosages for 48 hours. BrdU was added into the cell culture media 1 hour before harvest. Cells were fixed, stained with PI and anti-BrdU antibody, and analysed by FACS. Combined data of N=3 experiments are presented as mean±SEM. Student's t-test was used. *p<0.05, **p<0.01, ***p<0.001.

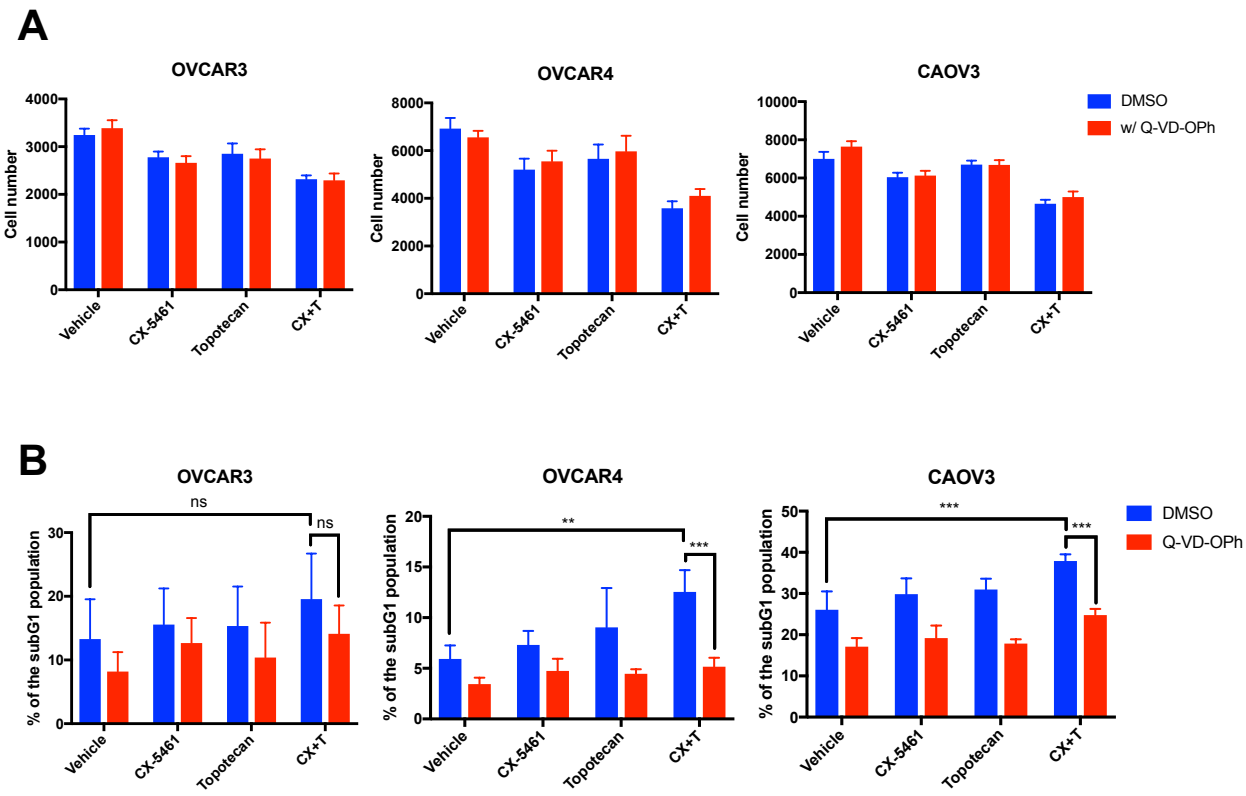
A
OVCAR3
OVCAR4
CAOV3
Cell number
4000
3000
2000
1000
0
8000
6000
4000
2000
10000
8000
6000
4000
2000
0
Vehicle
CX-5461
Topotecan
CX+T
DMSO
w/ Q-VD-OPh
B
OVCAR3
OVCAR4
CAOV3
% of the subG1 population
ns
ns
**
***
***
***
30
20
10
0
20
15
10
5
0
50
40
30
20
10
0
Vehicle
CX-5461
Topotecan
CX+T
DMSO
Q-VD-OPh

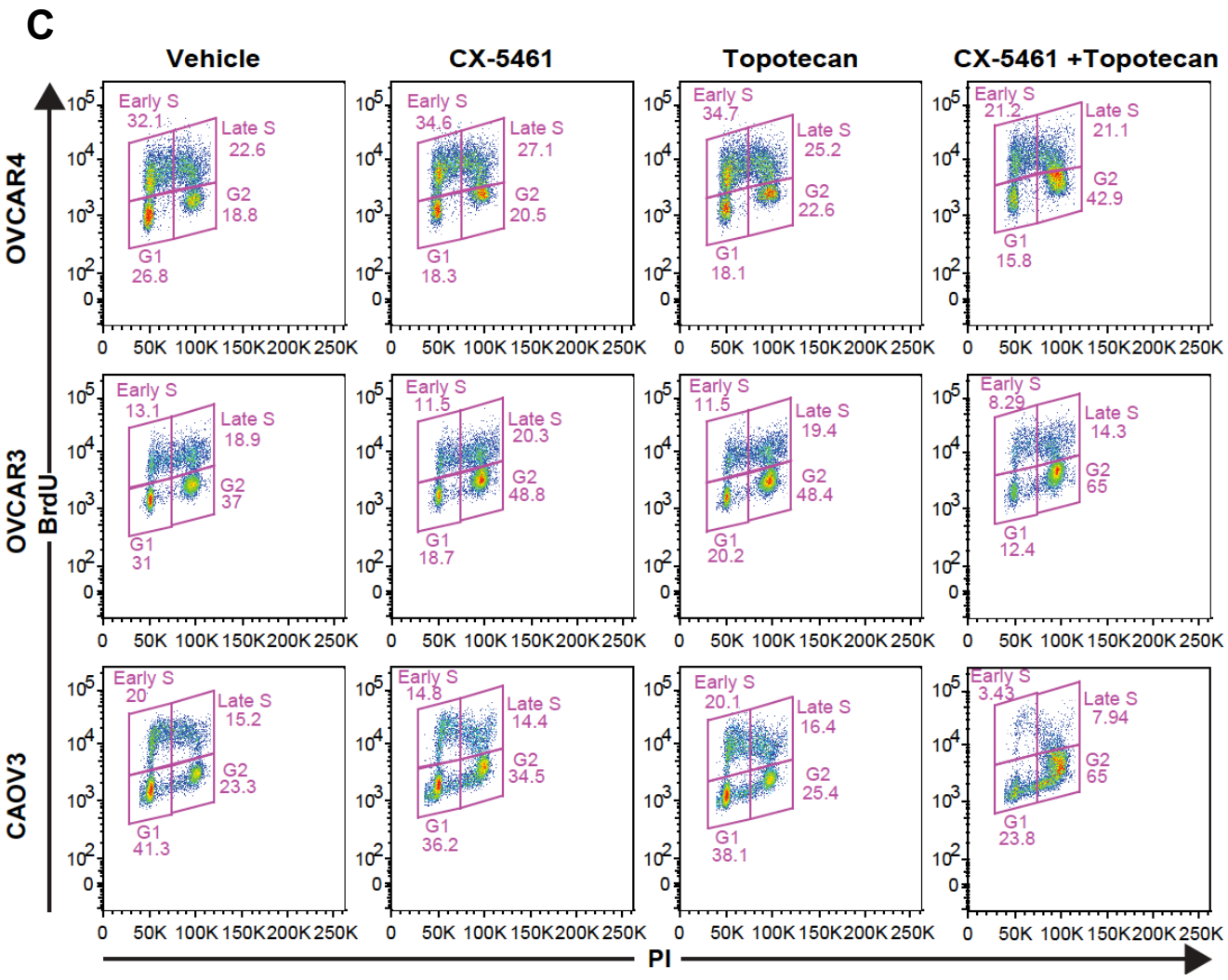
C
Vehicle
CX-5461
Topotecan
CX-5461 +Topotecan
OVCAR4
OVCAR3
CAOV3
BrdU
PI
Early S 32.1
Late S 22.6
G2 18.8
G1 26.8
Early S 34.6
Late S 27.1
G2 20.5
G1 18.3
Early S 34.7
Late S 25.2
G2 22.6
G1 18.1
Early S 21.2
Late S 21.1
G2 42.9
G1 15.8
Early S 13.1
Late S 18.9
G2 37
G1 31
Early S 11.5
Late S 20.3
G2 48.8
G1 18.7
Early S 11.5
Late S 19.4
G2 48.4
G1 20.2
Early S 8.29
Late S 14.3
G2 65
G1 12.4
Early S 20
Late S 15.2
G2 23.3
G1 41.3
Early S 14.8
Late S 14.4
G2 34.5
G1 36.2
Early S 20.1
Late S 16.4
G2 25.4
G1 38.1
Early S 3.43
Late S 7.94
G2 65
G1 23.8
0 50K 100K 150K200K 250K

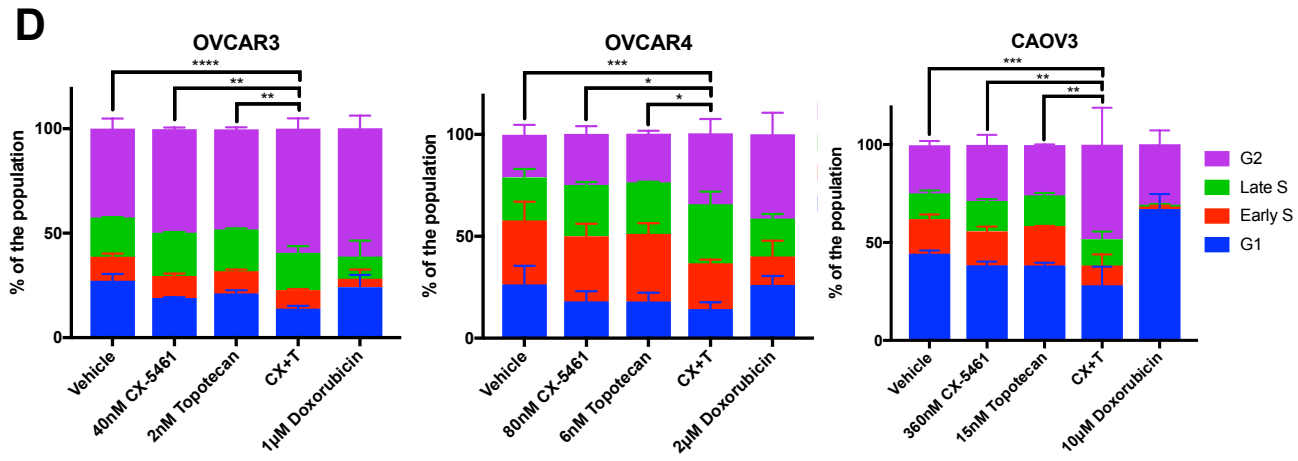
D
OVCAR3
OVCAR4
CAOV3
% of the population
Vehicle
40nM CX-5461
2nM Topotecan
CX+T
1μM Doxorubicin
80nM CX-5461
6nM Topotecan
2μM Doxorubicin
360nM CX-5461
15nM Topotecan
10μM Doxorubicin
G2
Late S
Early S
G1

**Figure 5.7 rRNA transcriptional suppression is not correlated with proliferation inhibition**

**A.** Western blots of p53, p-p53 and p-CHK2 in BJ3 and OVCAR4 cells treated with 1μM CX-5461 for 48 hours. Enhanced p53 and p-p53 were observed in BJ3 cells but not OVCAR4 cells, while enhanced p-CHK2 was observed in both cell lines. Representative image of N=3 experiments. **B.** The primer set used for 45S pre-rRNA detection. **C.** The Pol I transcription assay was used to evaluate pre-rDNA transcription inhibition after drug treatment for 3 and 24 hours. There was a very significant reduction in 45S rDNA transcription with 1μM CX-5461 or 5nM ActinomycinD treatment, but only moderate change with 80nM CX-5461 treatment, and there was no further reduction when combined with 6nM Topotecan. No significant change was observed in 5S pre-rDNA transcription, which demonstrates the selectivity of CX-5461 for inhibiting Pol I transcription. Combined data of N=3 experiments are presented as mean±SEM. Student's t-test was used. *p<0.05, **p<0.01, ***p<0.001, ****p<0.0001 compared to vehicle. **D.** Cell proliferation assay was performed for 48 hours using the same drug dosages as the Pol I transcription assay. There is a significant decrease in cell number in CX-5461 and Topotecan combination-treated cells. However, the level of cell proliferation inhibition caused by the 5nM ActinomycinD was not as significant as it was with CX-5461. Combined data of N=3 experiments with 18 replicates/wells of cells in each treatment group are presented as mean±SEM. Student's t-test was used. ****p<0.0001.

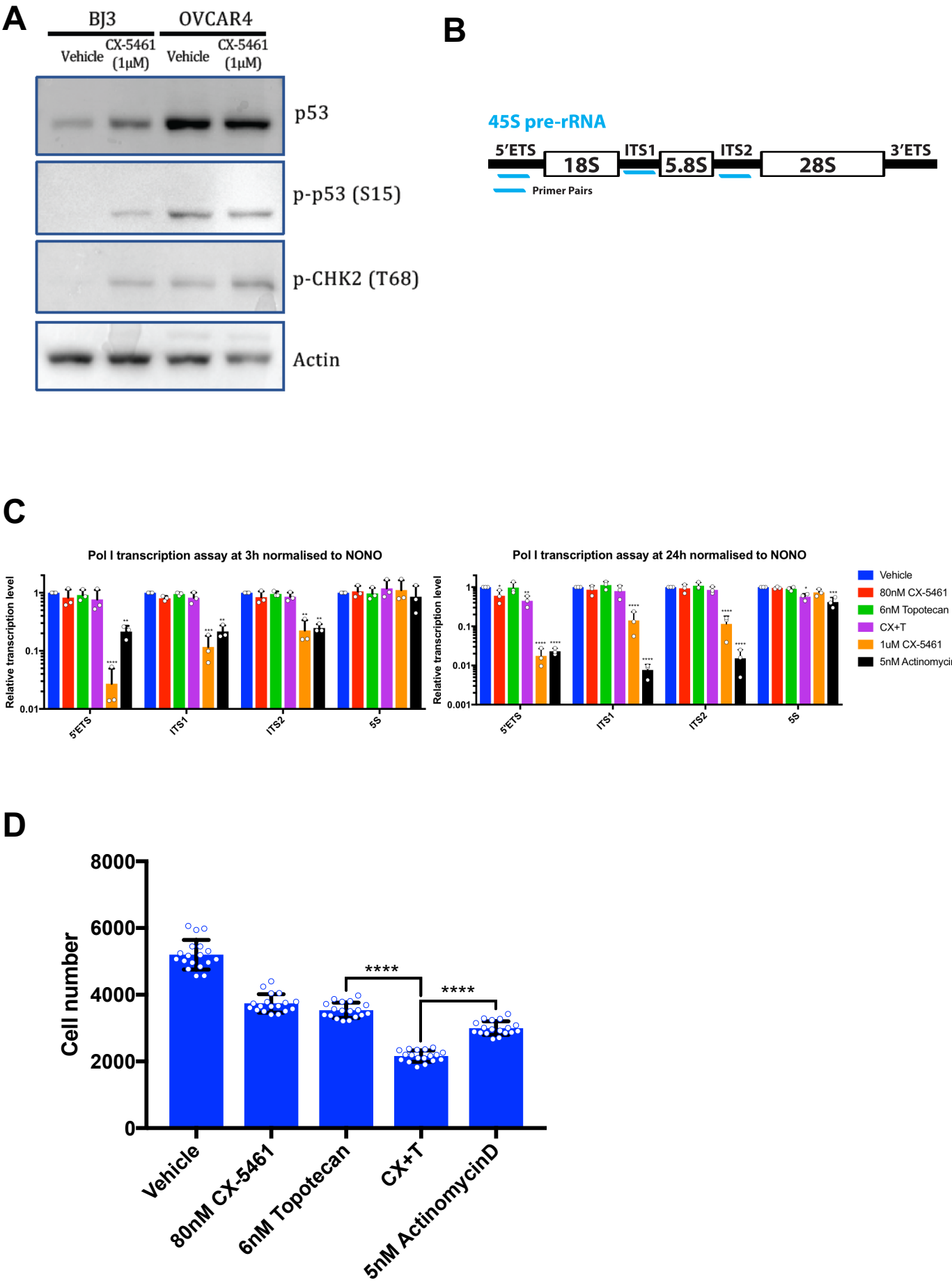
A
BJ3
OVCAR4
Vehicle
CX-5461 (1μM)
Vehicle
CX-5461 (1μM)
p53
p-p53 (S15)
p-CHK2 (T68)
Actin
B
45S pre-rRNA
5'ETS
18S
ITS1
5.8S
ITS2
28S
3'ETS
Primer Pairs
C
Pol I transcription assay at 3h normalised to NONO
Pol I transcription assay at 24h normalised to NONO
Relative transcription level
5'ETS
ITS1
ITS2
5S
Vehicle
80nM CX-5461
6nM Topotecan
CX+T
1uM CX-5461
5nM Actinomycin D
D
Cell number
8000
6000
4000
2000
0
****
****
Vehicle
80nM CX-5461
6nM Topotecan
CX+T
5nM ActinomycinD

**Figure 5.8 Enhanced DDR after combined treatment of CX-5461 and Topotecan**

**A**. Schematic diagram of the DDR pathway. **B.** Western blot analysis of the DDR in OVCAR4 cells treated with vehicle, 80nM CX-5461or/and 6nM Topotecan, 1μM CX-5461, 1μM doxorubicin for 3 or 24 hours. The expression and phosphorylation level of key DDR components was measured, including pATR(T1989), pATM(S1961), pCHK1(S345), pCHK2(T68), pRPA32(S4/S8), pRPA2 (S33), γH2AX (S139). The level of tubulin was used as an internal control. Enhanced activation/phosphorylation of pRPA32(S4/S8), pRPA2(S33), pCHK1(S345) and pCHK2(T68) was reproducibly observed in CX-5461 and Topotecan combination-treated cells, especially at 24 hours. Representative images of N=4 experiments. **C.** Western blot analysis of the DDR in OVCAR3 and CAOV3 cells treated with indicated drugs and dosages for 24 hours. Representative images of N=3 experiments.

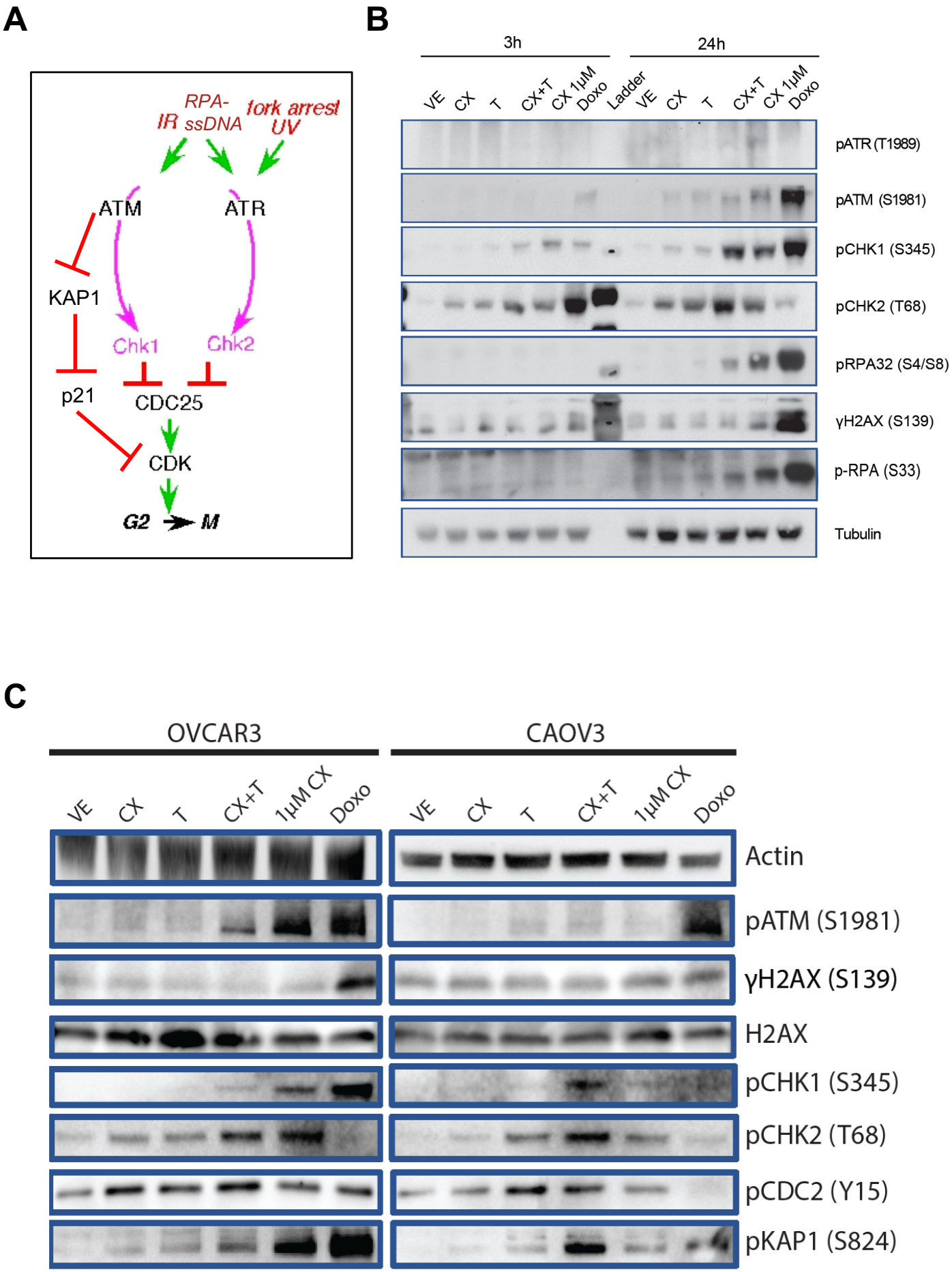
A
RPA-ssDNA
IR
fork arrest
UV
ATM
ATR
KAP1
Chk1
Chk2
p21
CDC25
CDK
G2
M
B
3h
24h
VE
CX
T
CX+T
CX 1µM
Doxo
Ladder
pATR (T1989)
pATM (S1981)
pCHK1 (S345)
pCHK2 (T68)
pRPA32 (S4/S8)
γH2AX (S139)
p-RPA (S33)
Tubulin
C
OVCAR3
CAOV3
VE
CX
T
CX+T
1µM CX
Doxo
Actin
pATM (S1981)
γH2AX (S139)
H2AX
pCHK1 (S345)
pCHK2 (T68)
pCDC2 (Y15)
pKAP1 (S824)

**Figure 5.9 Enhanced DDR is not caused by accumulation of DNA strand breaks or G4-DNA stabilisation**

**A.** Alkaline comet assay of OVCAR4 cells treated with 1μM CX-5461, 20nM Topotecan, CX-5461 and Topotecan, 1μM doxorubicin for 3 hours. Long comet tails were only observed in doxorubicin-treated cells. Representative images of N=3 experiments. **B.** Quantification of the alkaline comet assay. The olive tail moment was calculated using FIJI software with the OpenComet plugin. Combined data of N=3 experiments are presented as median with interquartile range. At least 120 cells were analysed for each treatment group. Non-parametric one-way ANOVA was used. ****$p<0.0001$. **C.** IF staining of OVCAR4 cells treated with 1μM CX-5461 or/and 20nM Topotecan, 1μM doxorubicin or 10μM TMPyP4 for 3 hours using a G4-DNA specific antibody (1H6). Strong IF staining was only observed with TMPyP4 treatment. Representative images of N=3 experiments. **D.** Quantification of G4-DNA immunofluorescent staining was performed using CellProfiler. Combined data of N=3 experiments normalised to the median of the TMPyP4 group are presented as median with interquartile range. At least 500 cells were analysed for each treatment group. Non-parametric one-way ANOVA was used. ****$p<0.0001$ compared to vehicle. **E.** Western blot analysis of OVCAR4 cells treated with 1μM CX-5461 or 10μM TMPyP4 for 1 hour or 3 hours. Strong phosphorylation of pCHK1(S345) and pCHK2(T68) was observed with CX-5461 treatment but not with TMPyP4. Representative images of N=3 experiments. **F.** The Pol I transcription assay showed no decrease in 45S pre-rDNA transcription with 10μM TMPyP4 at 0.5-, 1-, 3-, 6- and 24-hours' time points. 1μM CX-5461 served as the positive control. Combined data of N=2 experiments are presented as mean±SEM.

**A**

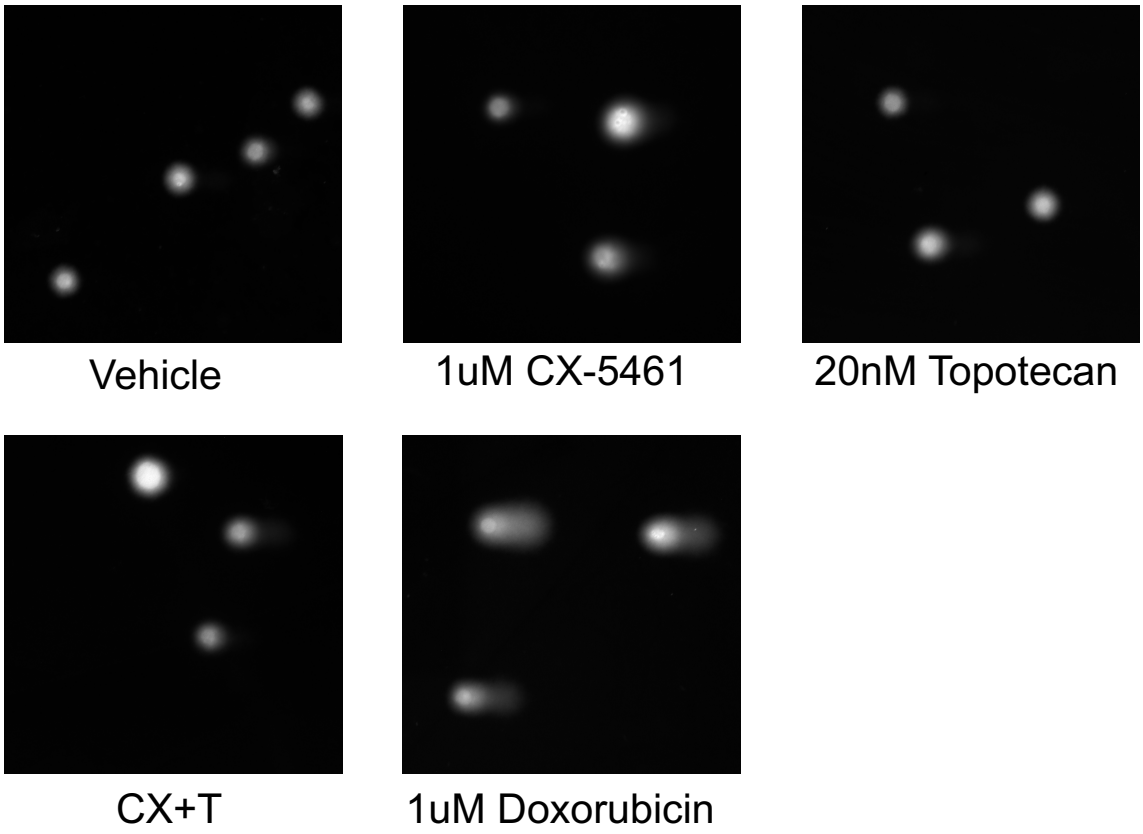
Vehicle
1uM CX-5461
20nM Topotecan
CX+T
1uM Doxorubicin

**B**

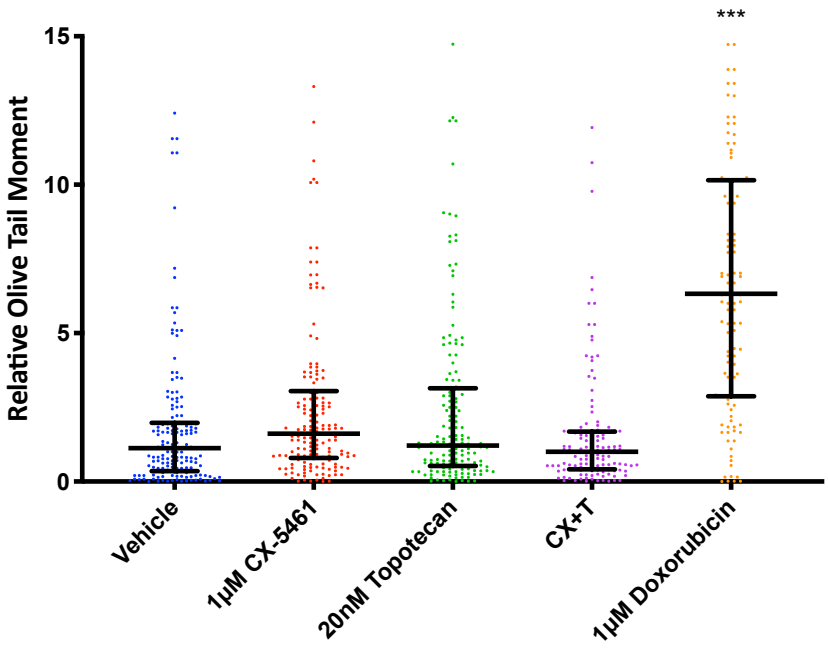
Relative Olive Tail Moment
15
10
5
0
***
Vehicle
1μM CX-5461
20nM Topotecan
CX+T
1μM Doxorubicin

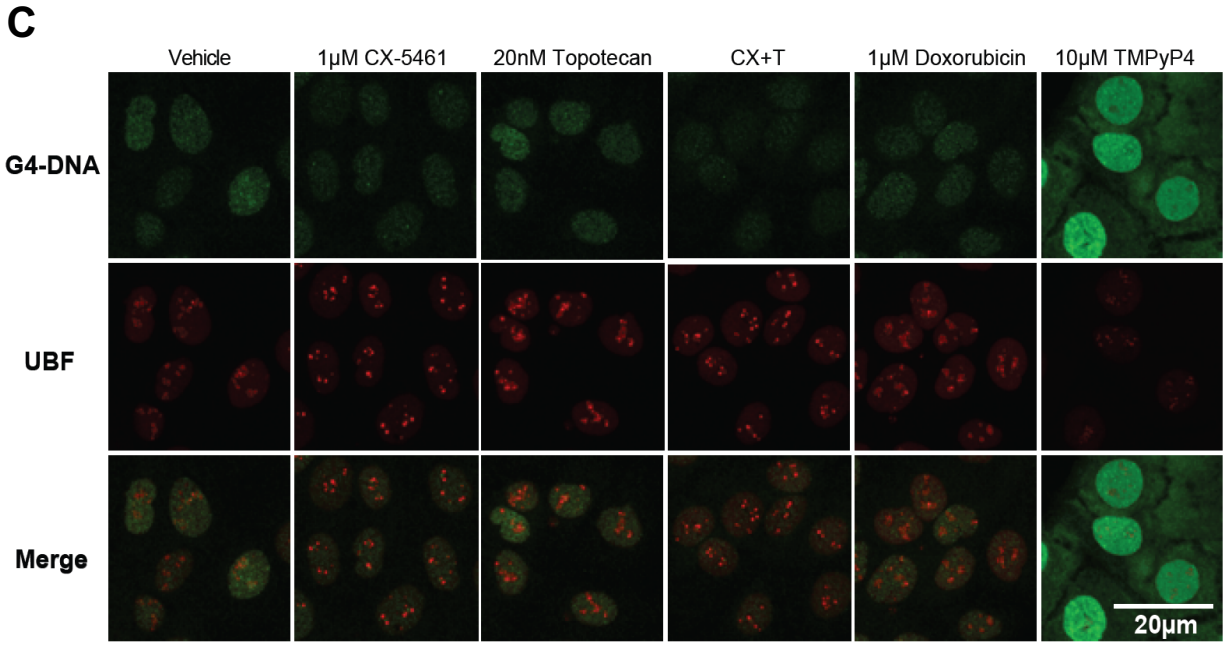
C
Vehicle
1μM CX-5461
20nM Topotecan
CX+T
1μM Doxorubicin
10μM TMPyP4
G4-DNA
UBF
Merge
20μm

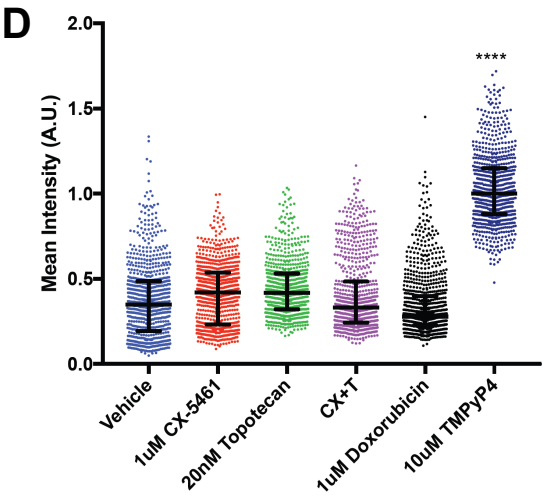
D
Mean Intensity (A.U.)
2.0
1.5
1.0
0.5
0.0
****
Vehicle
1uM CX-5461
20nM Topotecan
CX+T
1uM Doxorubicin
10uM TMPyP4

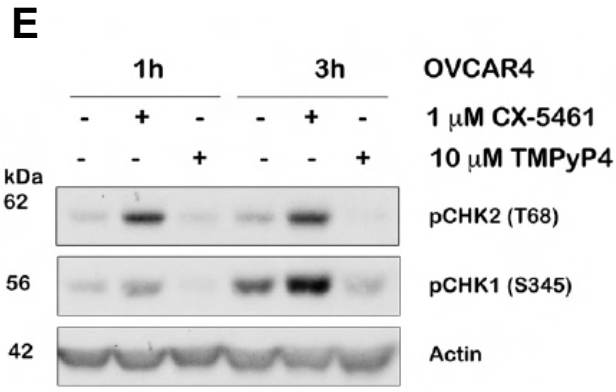
E
1h
3h
OVCAR4
1 μM CX-5461
10 μM TMPyP4
kDa
62
56
42
pCHK2 (T68)
pCHK1 (S345)
Actin

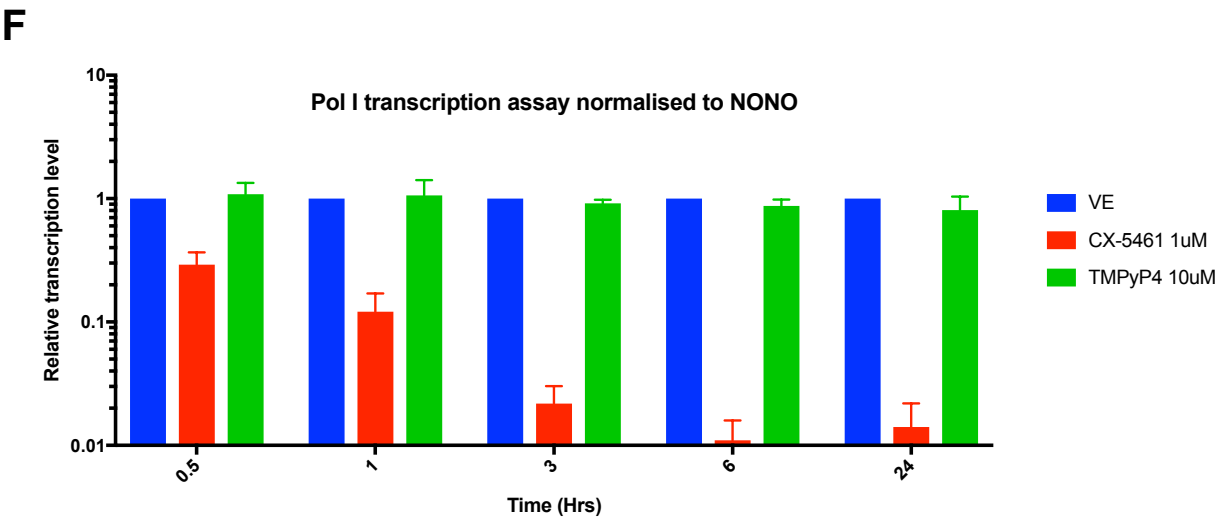
F
Pol I transcription assay normalised to NONO
Relative transcription level
10
1
0.1
0.01
0.5
1
3
6
24
Time (Hrs)
VE
CX-5461 1uM
TMPyP4 10uM

**Figure 5.10 Enhanced DDR is not correlated with global replication stress**

**A.** IF staining of γH2AX and RAD51 foci in OVCAR4 cells treated with 1μM CX-5461 or/and 20nM Topotecan or 1μM doxorubicin for 3 hours. Cells undergoing DNA replication were labelled with 10μM EdU. Representative images of N=3 experiments. RAD51 foci **(B)** and γH2AX foci **(C)** were identified and quantified using CellProfiler. Combined data of N=3 experiment was represented as median with interquartile range. At least 300 cells were analysed for each treatment group. Non-parametric one-way ANOVA was used. ns: not significant, ****p<0.0001. **D.** IF staining of γH2AX and RAD51 foci in OTP-NT or siTOP1 transfected OVCAR4 cells treated with 1μM CX-5461, 20nM Topotecan or the combination for 3 hours. Cells under DNA replication were labelled with 10μM EdU. Representative images of N=3 experiments. RAD51 foci **(E)** and γH2AX foci **(F)** were identified and quantified using CellProfiler. Combined data of N=3 experiments are presented as median with interquartile range. At least 240 cells were analysed for each treatment group. Non-parametric one-way ANOVA was used. VE: vehicle, CX: 1μM CX-5461, T: 20nM Topotecan, ns: not significant, **<p<0.01, ****p<0.0001.

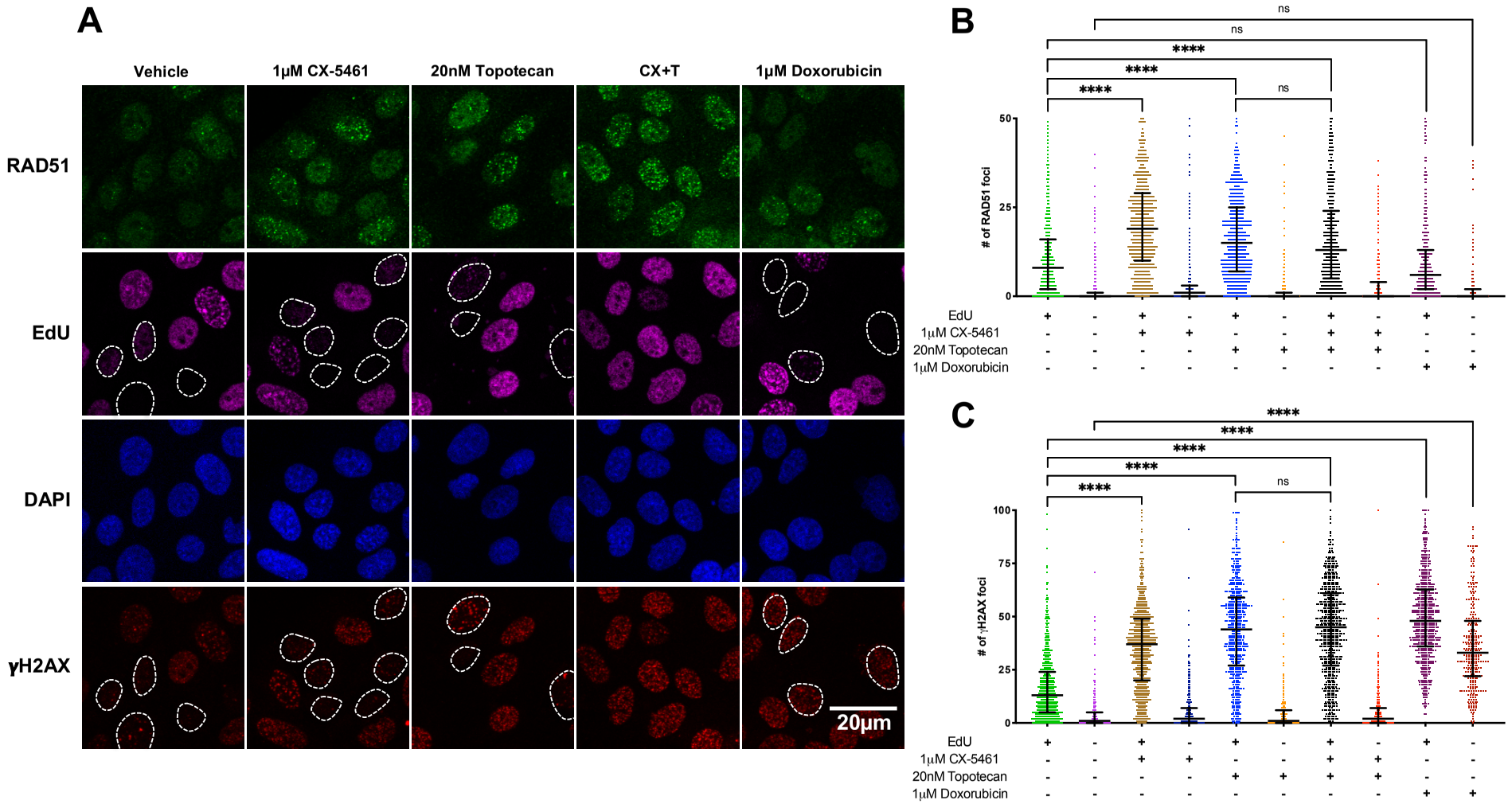
A
Vehicle
1μM CX-5461
20nM Topotecan
CX+T
1μM Doxorubicin
RAD51
EdU
DAPI
γH2AX
20μm
B
ns
ns
****
****
****
ns
# of RAD51 foci
50
25
0
EdU
1μM CX-5461
20nM Topotecan
1μM Doxorubicin
C
****
****
****
****
****
ns
# of γH2AX foci
100
75
50
25
0
EdU
1μM CX-5461
20nM Topotecan
1μM Doxorubicin

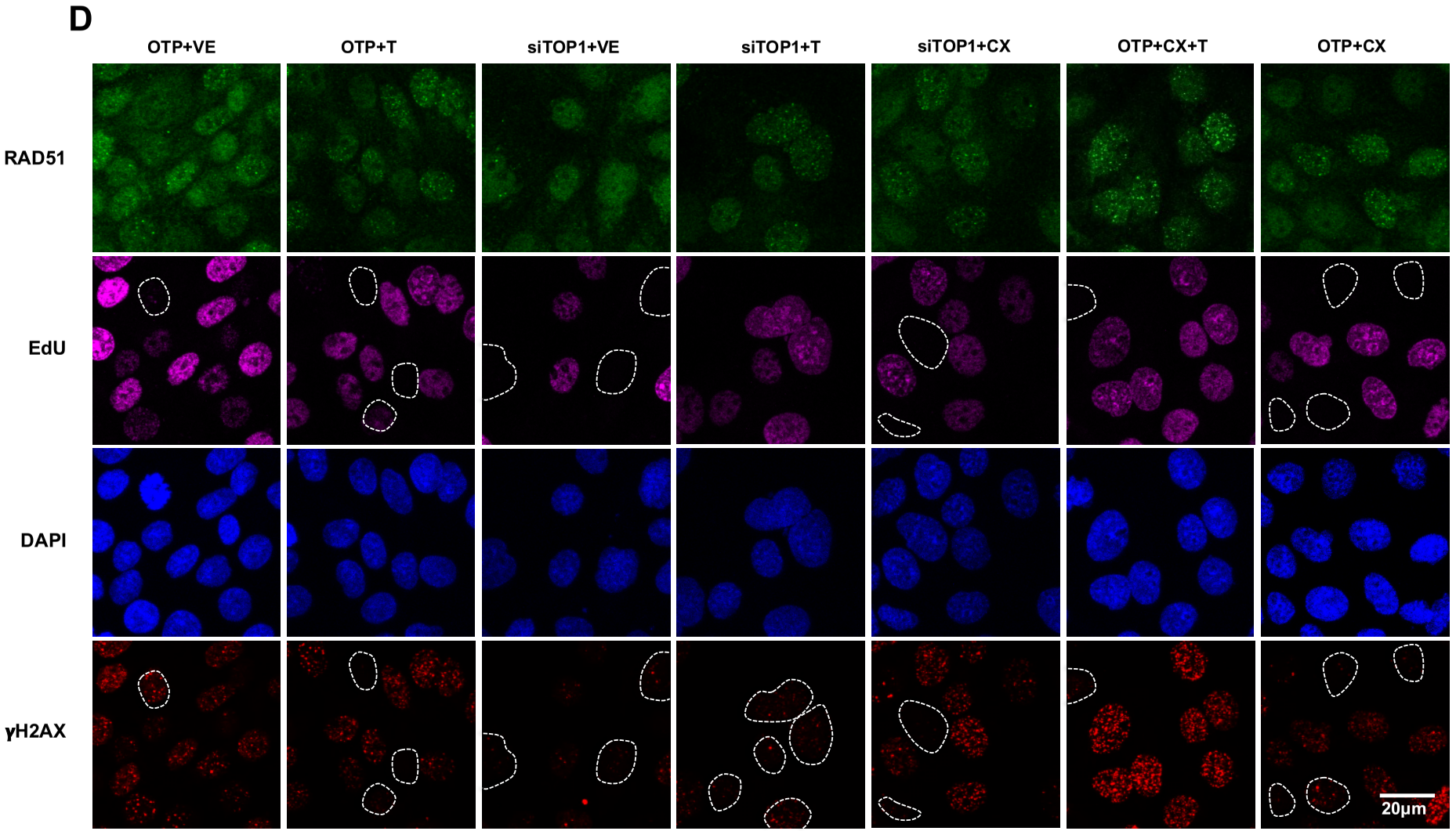
D
OTP+VE
OTP+T
siTOP1+VE
siTOP1+T
siTOP1+CX
OTP+CX+T
OTP+CX
RAD51
EdU
DAPI
γH2AX
20μm

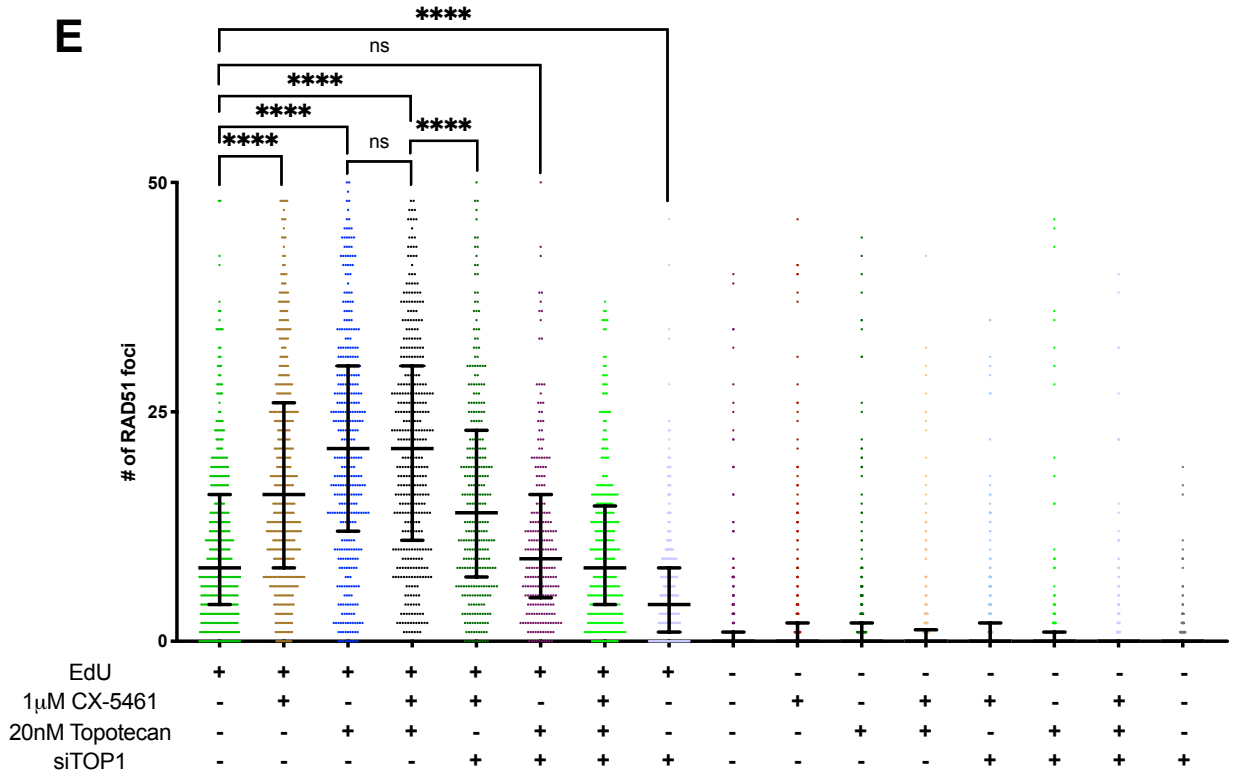
E
****
ns
****
****
****
ns
****
50
25
0
# of RAD51 foci
EdU + + + + + + + + - - - - - - - -
1μM CX-5461 - + - + + - + - - + - + + - + -
20nM Topotecan - - + + - + + - - - + + - + + -
siTOP1 - - - - + + + + - - - - + + + +

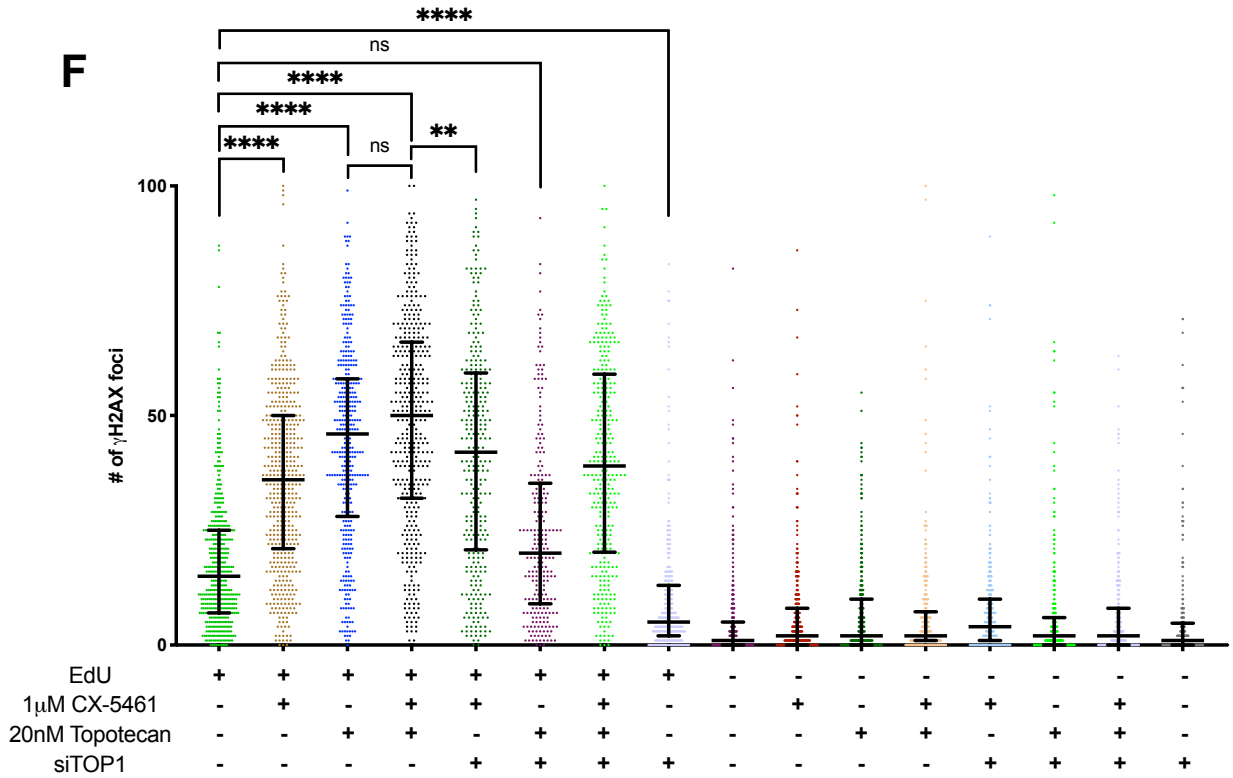
F
****
ns
****
****
****
ns
**
100
50
0
# of γH2AX foci
EdU + + + + + + + + - - - - - - - -
1μM CX-5461 - + - + + - + - - + - + + - + -
20nM Topotecan - - + + - + + - - - + + - + + -
siTOP1 - - - - + + + + - - - - + + + +

**Figure 5.11 CX-5461 and Topotecan combination treatment induces strong RPA phosphorylation in the nucleolus**

IF staining of pRPA32(S4/S8) **(A)** and pRPA2(S33) **(B)** in OVCAR4 cells treated with 1μM CX-5461, 20nM Topotecan, CX-5461 and Topotecan, 1μM doxorubicin or 5nM ActinomycinD for 3 hours. UBF was used as a nucleolar marker. Cells undergoing DNA replication were labelled with 10μM EdU. Representative images of N=3 experiments. pRPA32(S4/S8) **(C)** and pRPA2(S33) **(D)** mean intensity colocalising with UBF were identified and quantified using CellProfiler. Combined data of N=3 experiments (The pRPA32 S4/S8 data is N=2) normalised to the vehicle median are presented as median with interquartile range. For pRPA32(S4/S8), at least 160 cells were analysed for each treatment group. For pRPA2(S33), at least 240 cells were analysed for each treatment group. Non-parametric one-way ANOVA was used. ns: not significant, ***$p<0.001$, ****$p<0.0001$.

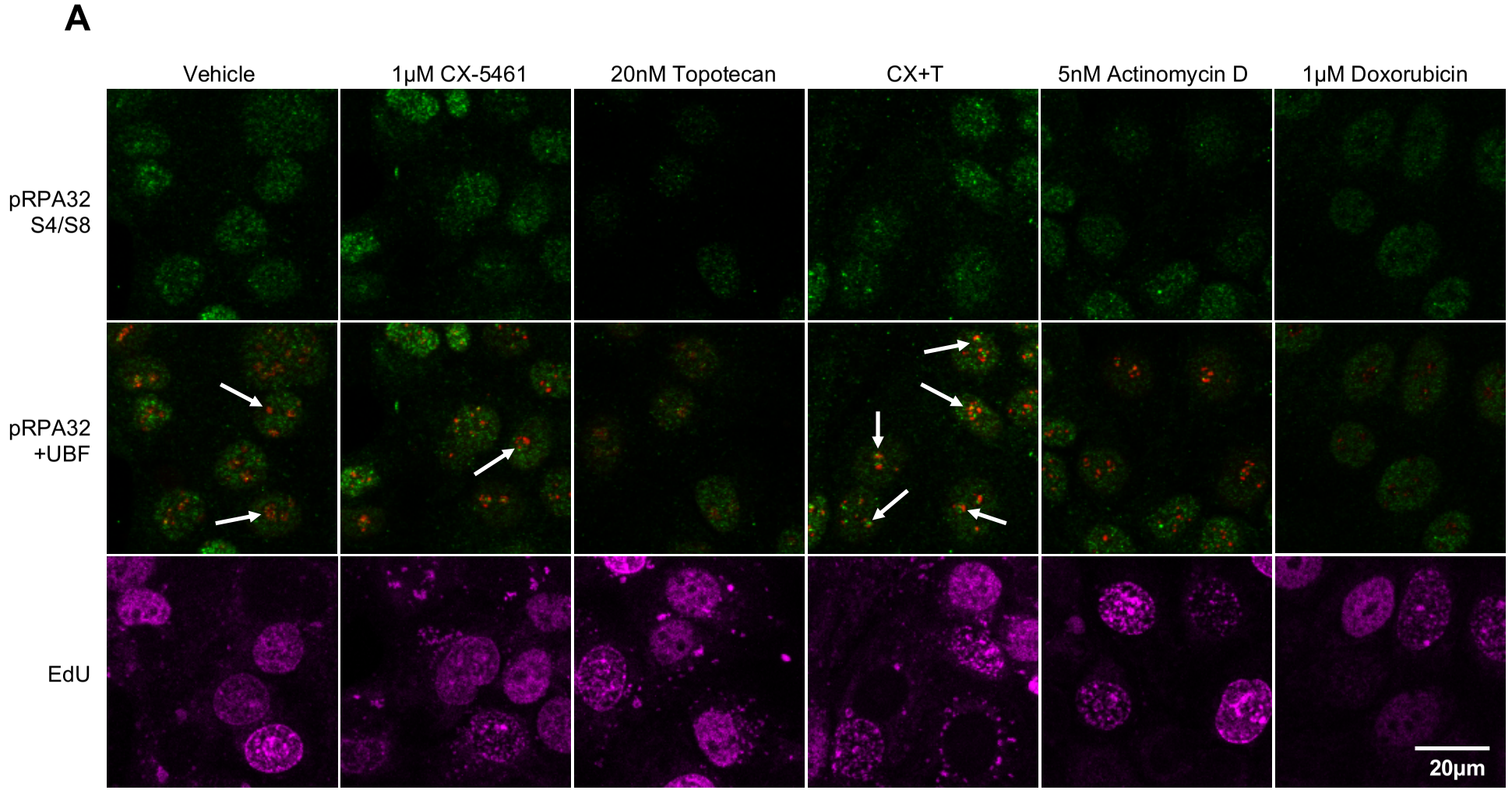
A
Vehicle
1μM CX-5461
20nM Topotecan
CX+T
5nM Actinomycin D
1μM Doxorubicin
pRPA32 S4/S8
pRPA32 +UBF
EdU
20μm

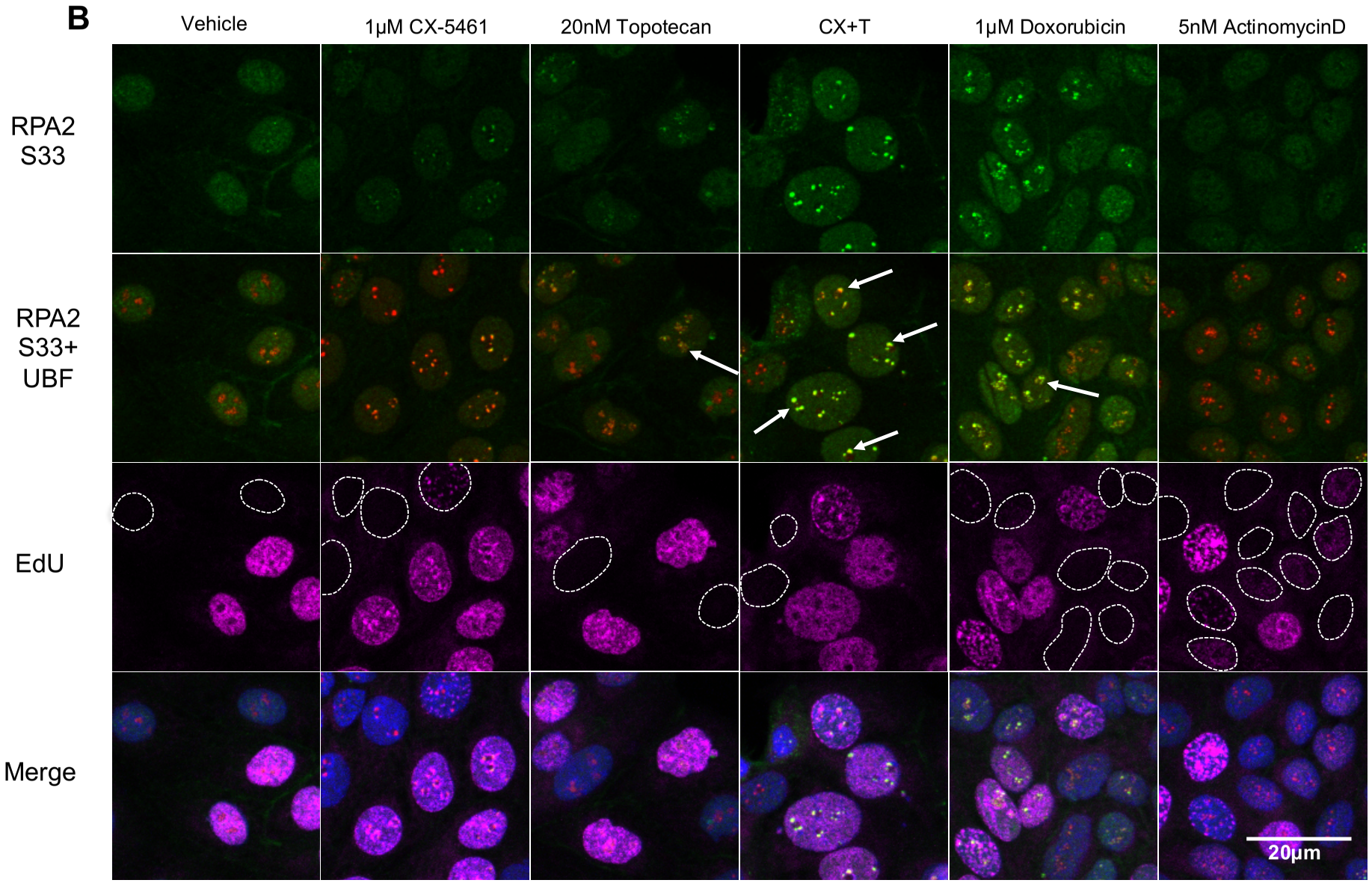
B
Vehicle
1μM CX-5461
20nM Topotecan
CX+T
1μM Doxorubicin
5nM ActinomycinD
RPA2 S33
RPA2 S33+ UBF
EdU
Merge
20μm

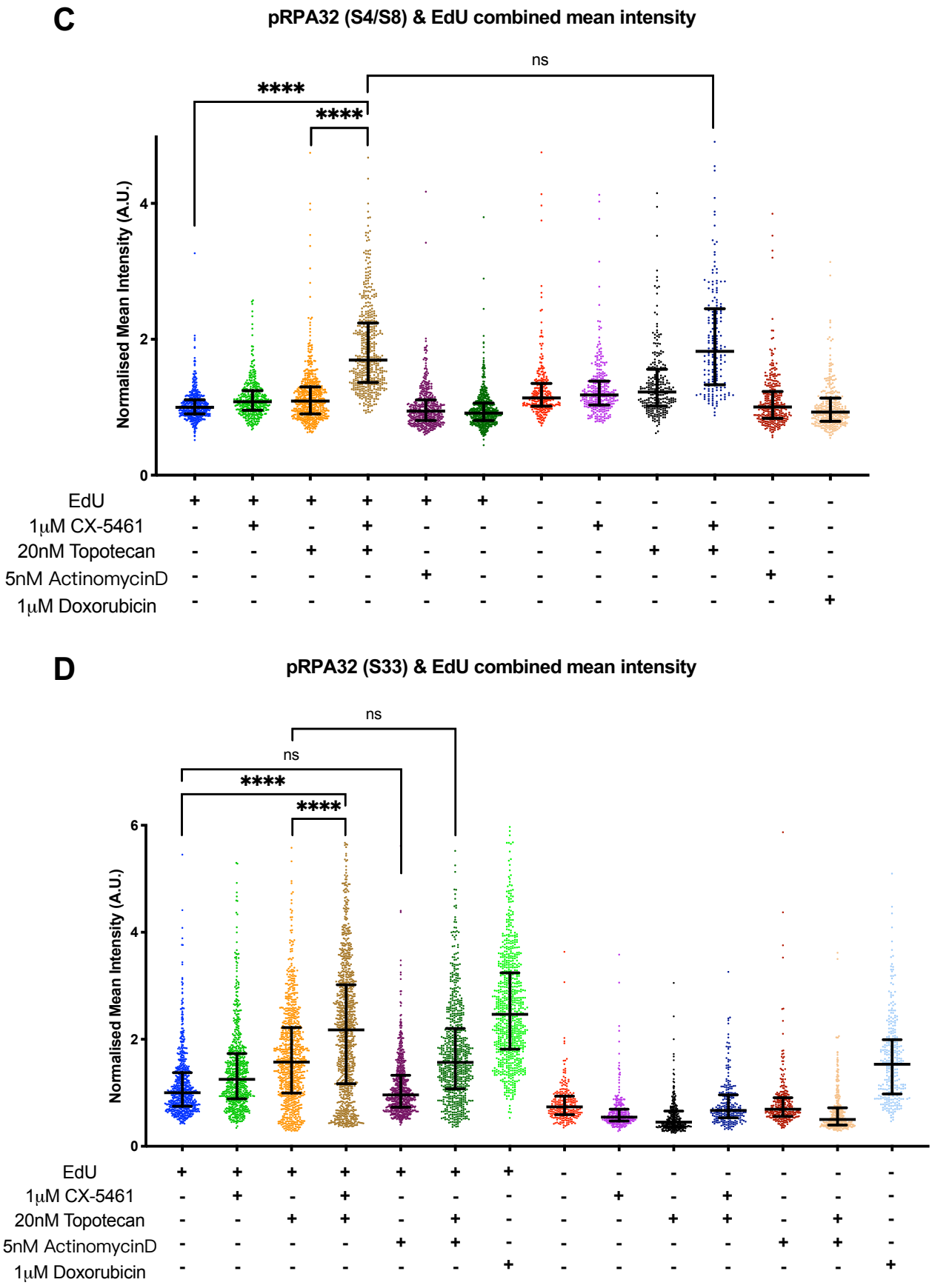
C
pRPA32 (S4/S8) & EdU combined mean intensity
ns
****
****
Normalised Mean Intensity (A.U.)
0
2
4
EdU + + + + + + - - - - - -
1μM CX-5461 - + - + - - - + - + - -
20nM Topotecan - - + + - - - - + + - -
5nM ActinomycinD - - - - + - - - - - + -
1μM Doxorubicin - - - - - - - - - - - +
D
pRPA32 (S33) & EdU combined mean intensity
ns
ns
****
****
Normalised Mean Intensity (A.U.)
0
2
4
6
EdU + + + + + + + - - - - - - -
1μM CX-5461 - + - + - - - - + - + - - -
20nM Topotecan - - + + - + - - - + + - + -
5nM ActinomycinD - - - - + + - - - - - + + -
1μM Doxorubicin - - - - - - + - - - - - - +

**Figure 5.12 CX-5461 and Topotecan combination treatment induces strong ATR phosphorylation in the nucleolus**

**A.** IF staining of pATR (T1989) in OVCAR4 cells treated with 1μM CX-5461 or/and 20nM Topotecan, 1μM doxorubicin or 5nM ActinomycinD for 3 hours. UBF was used as a nucleolar marker. Cells undergoing DNA replication were labelled with 10μM EdU. Representative images of N=3 experiments. **B.** pATR mean intensity co-localising with UBF was identified and quantified using CellProfiler. Combined data of N=3 experiment normalised to the vehicle median are presented as median with interquartile range. At least 180 cells were analysed for each treatment group. Non-parametric one-way ANOVA was used. ns: not significant, *p<0.05, ***p<0.001, ****p<0.0001.

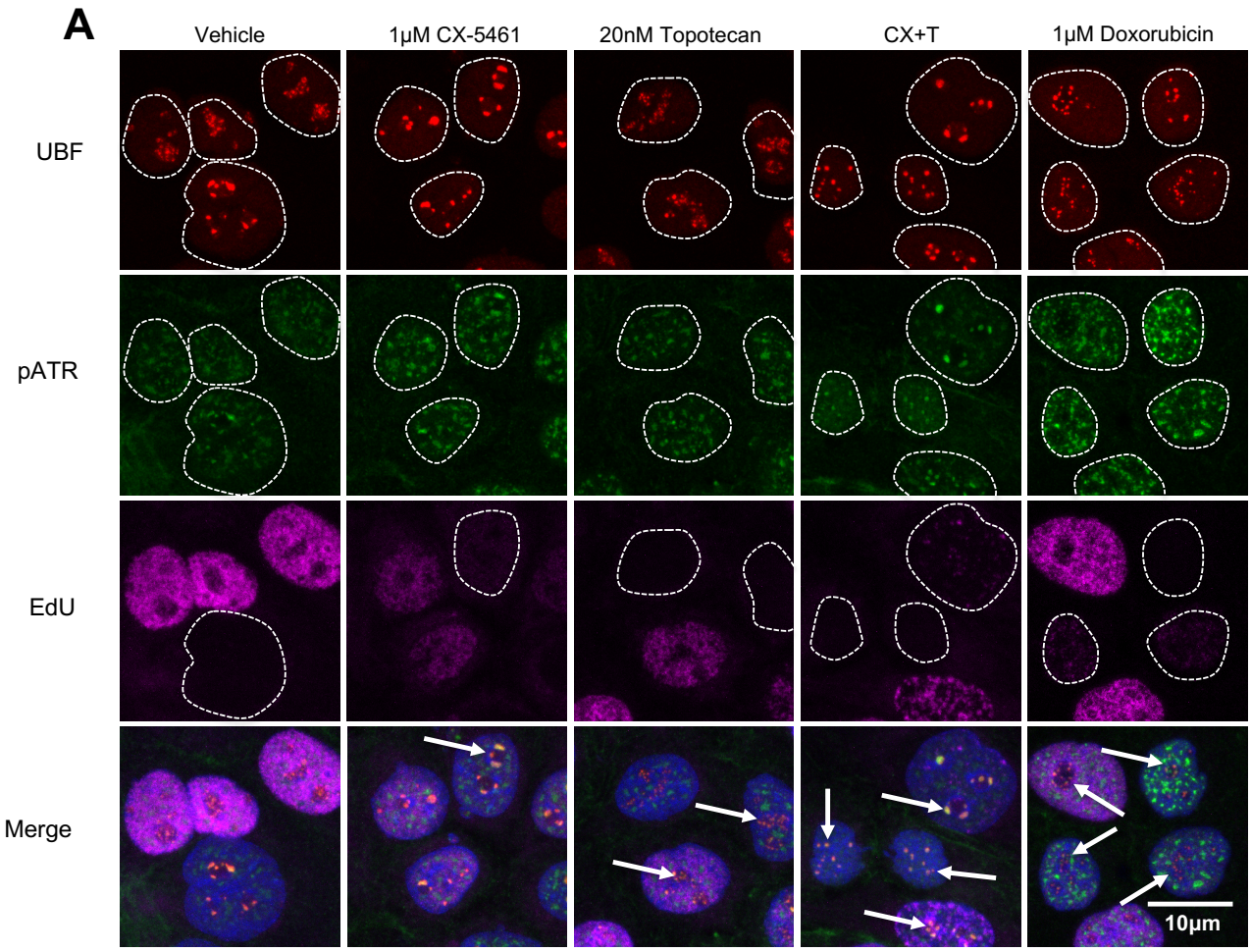
A
Vehicle
1μM CX-5461
20nM Topotecan
CX+T
1μM Doxorubicin
UBF
pATR
EdU
Merge
10μm

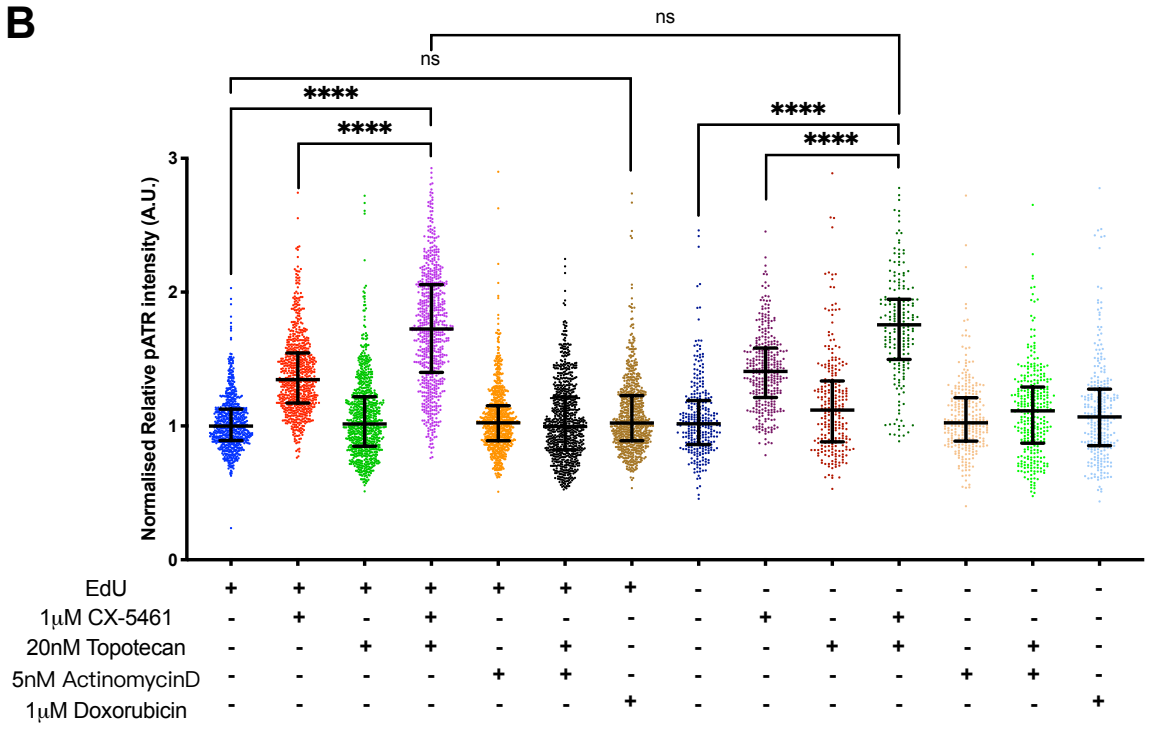
B
ns
ns
****
****
****
****
Normalised Relative pATR intensity (A.U.)
0
1
2
3
EdU
1μM CX-5461
20nM Topotecan
5nM ActinomycinD
1μM Doxorubicin

**Figure 5.13 CX-5461 and Topotecan combination treatment induces strong R-loop formation in the nucleolus**

**A.** IF staining of R-loops using an RNA-DNA hybrid-specific antibody (S9.6) in OVCAR4 cells treated with 1μM CX-5461 or/and 20nM Topotecan for 3 hours. UBF was used as a nucleolar marker. Representative images of N=3 experiments. Strong R-loop foci was observed in the nucleolus centre after CX-5461 and Topotecan combination treatment (marked by the red arrows). **B.** The R-loop mean intensity in the nucleus was identified and quantified using CellProfiler. Combined data of N=3 experiment normalised to the vehicle median are presented as median with interquartile range. At least 600 cells were analysed for each treatment group. Non-parametric one-way ANOVA was used. ****$p<0.0001$.

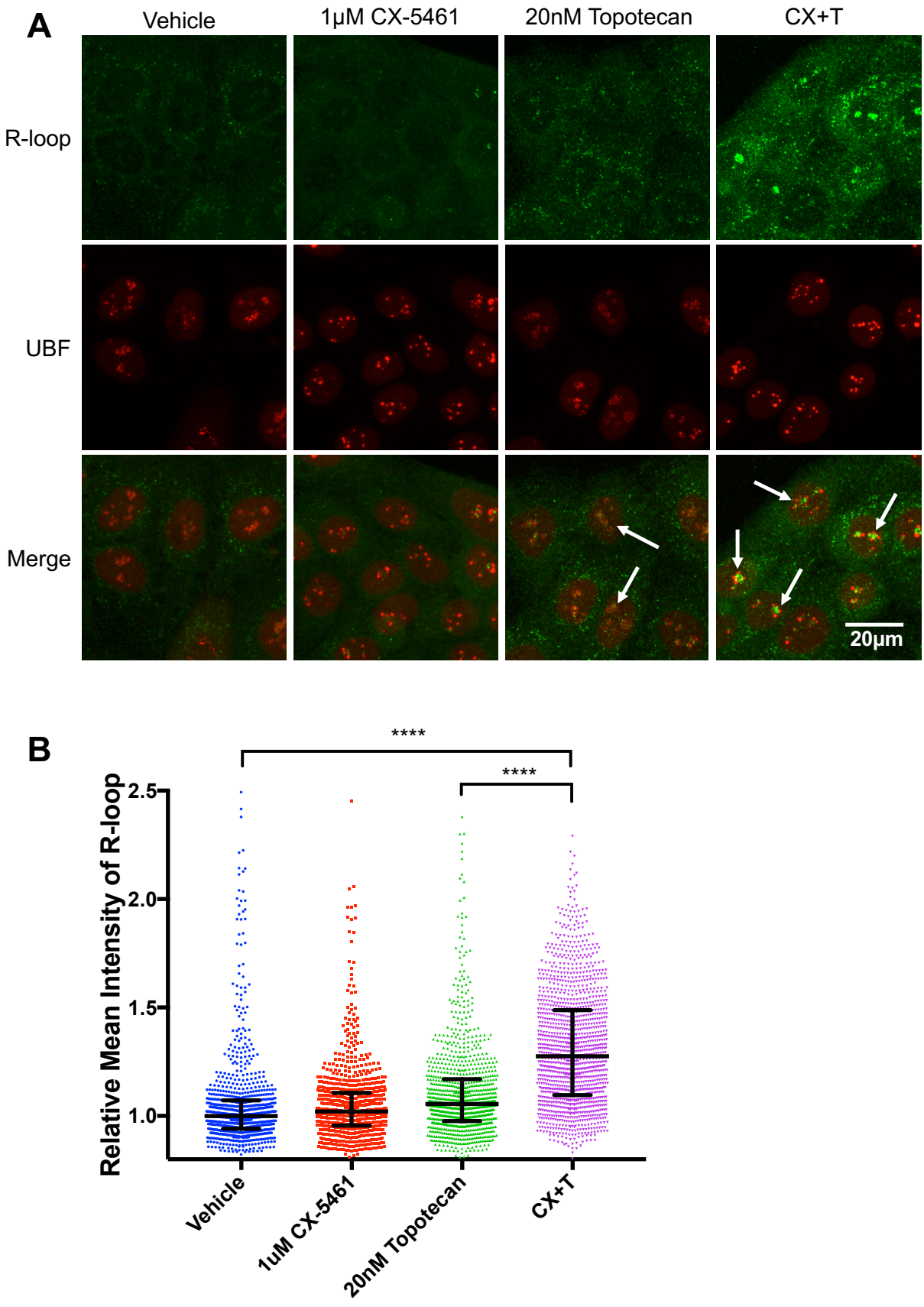
A
Vehicle
1μM CX-5461
20nM Topotecan
CX+T
R-loop
UBF
Merge
20μm
B
****
****
Relative Mean Intensity of R-loop
2.5
2.0
1.5
1.0
Vehicle
1uM CX-5461
20nM Topotecan
CX+T

**Figure 5.14 CX-5461 and Topotecan combination treatment increases the percentage of cells with a high level of KAP1 phosphorylation**

**A.** IF staining of pKAP1(S824) in OVCAR4 cells treated with 1μM CX-5461 or/and 20nM Topotecan for 3 hours. There is a significant increase in the percentage of cells with high pKAP1 expression. Representative images of N=3 experiments. **B.** Quantification of the pKAP1 IF staining using CellProfiler. Combined data of N=3 experiments normalised to the median of vehicle group are presented as median with interquartile range. At least 360 cells were analysed for each treatment group. Non-parametric one-way ANOVA was used. ****$p<0.0001$ compared to vehicle.

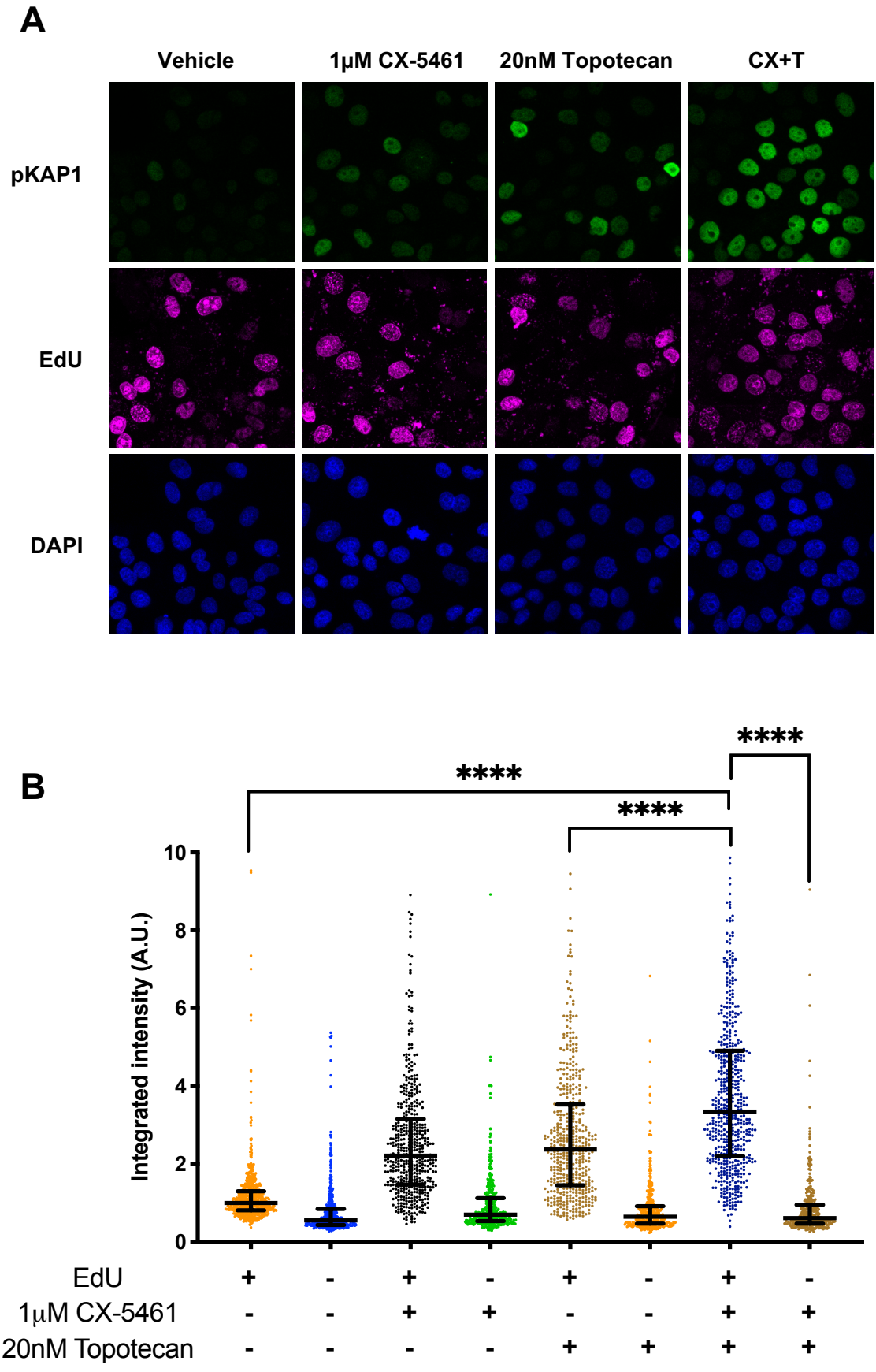
A
Vehicle
1μM CX-5461
20nM Topotecan
CX+T
pKAP1
EdU
DAPI
B
****
****
****
Integrated intensity (A.U.)
0
2
4
6
8
10
EdU + - + - + - + -
1μM CX-5461 - - + + - - + +
20nM Topotecan - - - - + + + +

**Figure 5.15 CX-5461 and Topotecan combination treatment is well tolerated *in vivo* and can reduce tumour progression in xenografts**

The OVCAR3 cell line was utilized in xenografts to evaluate the safety and therapeutic efficacy of the combination treatment *in vivo.* Two independent trials were conducted with same doses of CX-5461 but different doses of Topotecan. Briefly, $5x10^6$ OVCAR3 cells were subcutaneously engrafted into 40 4-6-week-old female immunodeficient NOD SCID Gamma (NSG) mice and were then left to grow for approximate 3 weeks until the average tumour volume reached $100mm^3$. The tumour bearing mice were randomised into four groups (10 mice for each group) and administrated with 30mg/kg CX-5461(oral gavage) or/and 5mg/kg (2.5mg/kg for the second trial) Topotecan (intraperitoneal injection) and the corresponding vehicles twice a week for four weeks (8 doses in total, indicated by dashes in **A, B, C, D**). The body weight (**A, D**) and tumour volume (**B, E**) were closely monitored twice a week until the tumour volume reached $1000mm^3$ when the mice were euthanised for ethical reasons. The dates of euthanasia were recorded and used to plot the survival curve (**C, F**). The body weight (**A, D**) and tumour volume (**B, E**) were presented as mean±SEM. The Mantel-Cox test was used for the survival curve. *p<0.05, ***p<0.01, ****p<0.0001.

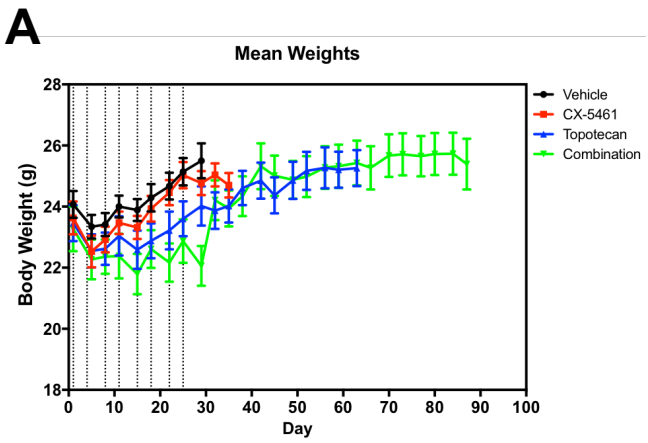


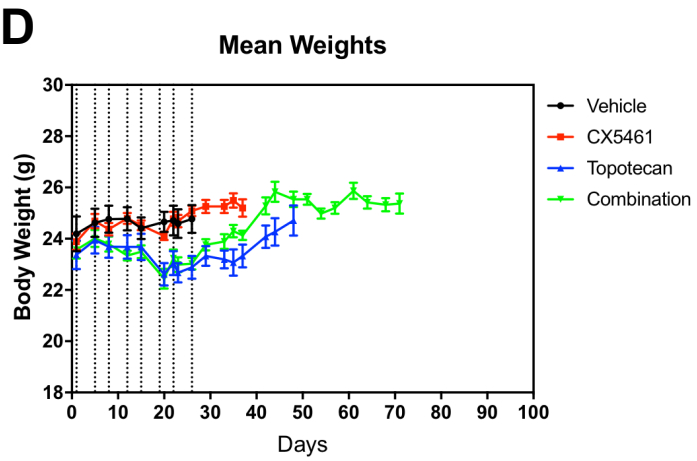


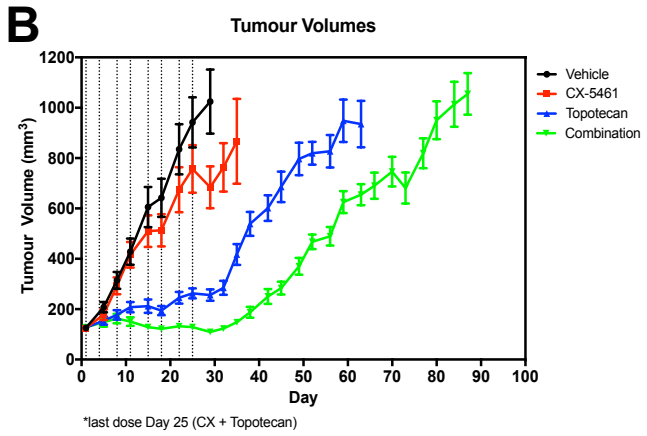


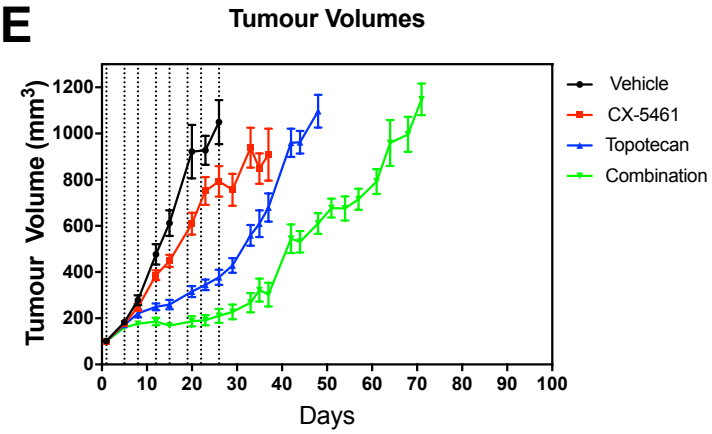


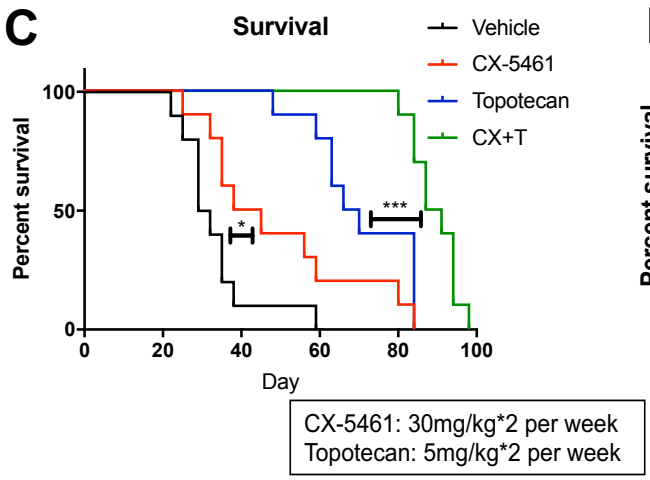


CX-5461: 30mg/kg*2 per week
Topotecan: 5mg/kg*2 per week

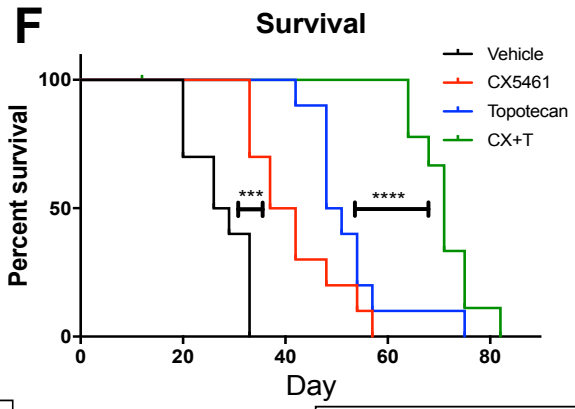


CX-5461: 30mg/kg*2 per week
Topotecan: 2.5mg/kg*2 per week

**Figure 5.16 Schematic of the proposed mechanism of the synergy between CX-5461 and Topotecan**

Model of the rRNA transcription under different treatment conditions. Pol I is represented in red circles, TOP1 in blue circles and the newly synthesized rRNA in red curves. Under normal rDNA transcription without drug treatment **(A)** or with Topotecan treatment **(C)**, the Pol I enzymes transcribes rDNA in close proximity which naturally prevents the formation of topological stress induced by positive (+) and negative (-) supercoiling. Upon the treatment of CX-5461 **(B)**, fewer Pol I enzymes are loaded onto the rDNA chromatin, which facilitates the formation of positive and negative supercoiling, while TOP1 removes this topological stress. When treated with the CX-5461/Topotecan combination **(D)**, the positive and negative supercoiling caused by Pol I transcription can no longer be resolved by TOP1, leading to the formation of R-loops and ssDNA. RPA (yellow oval) and ATR (green oval) respond to the ssDNA and activate the downstream DDR and cellular responses.

**A** Normal State of rDNA Transcription

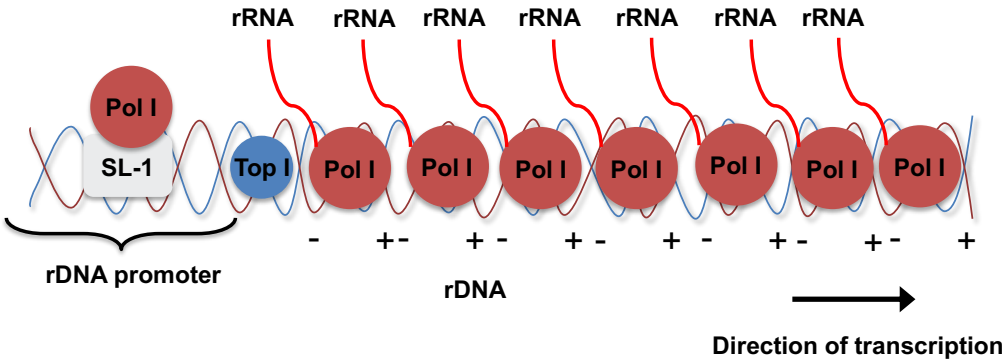


**B** CX-5461 treatment

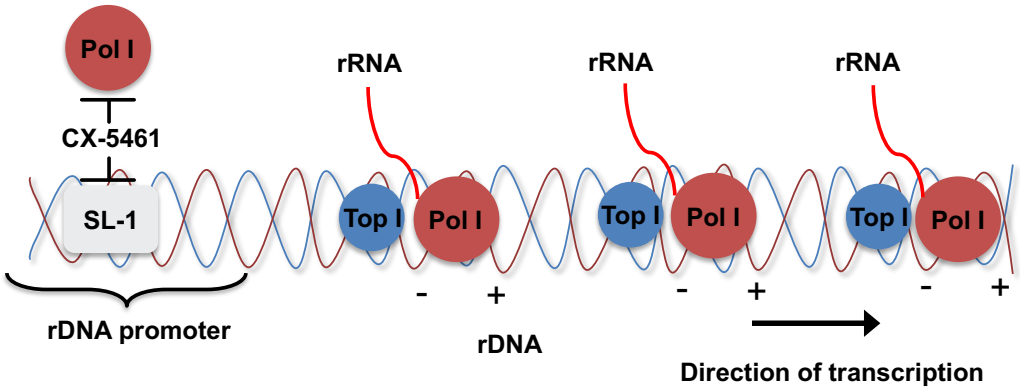


**C** Topotecan treatment

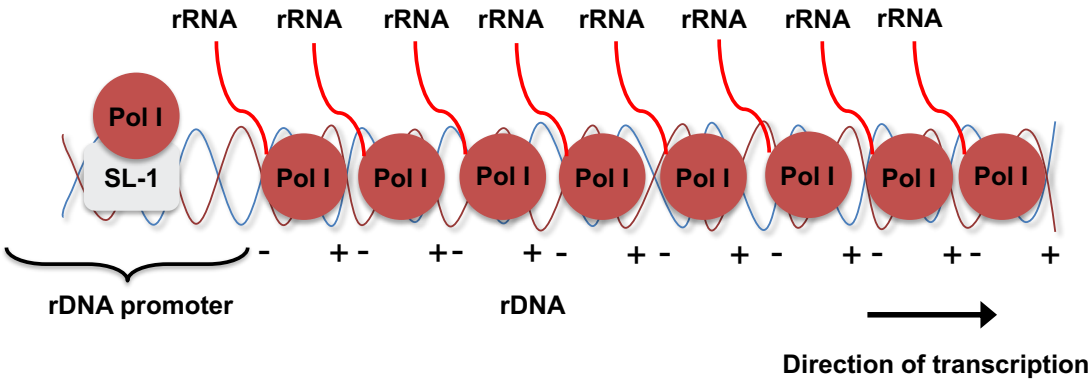

**D**

**CX-5461+Topotecan treatment**

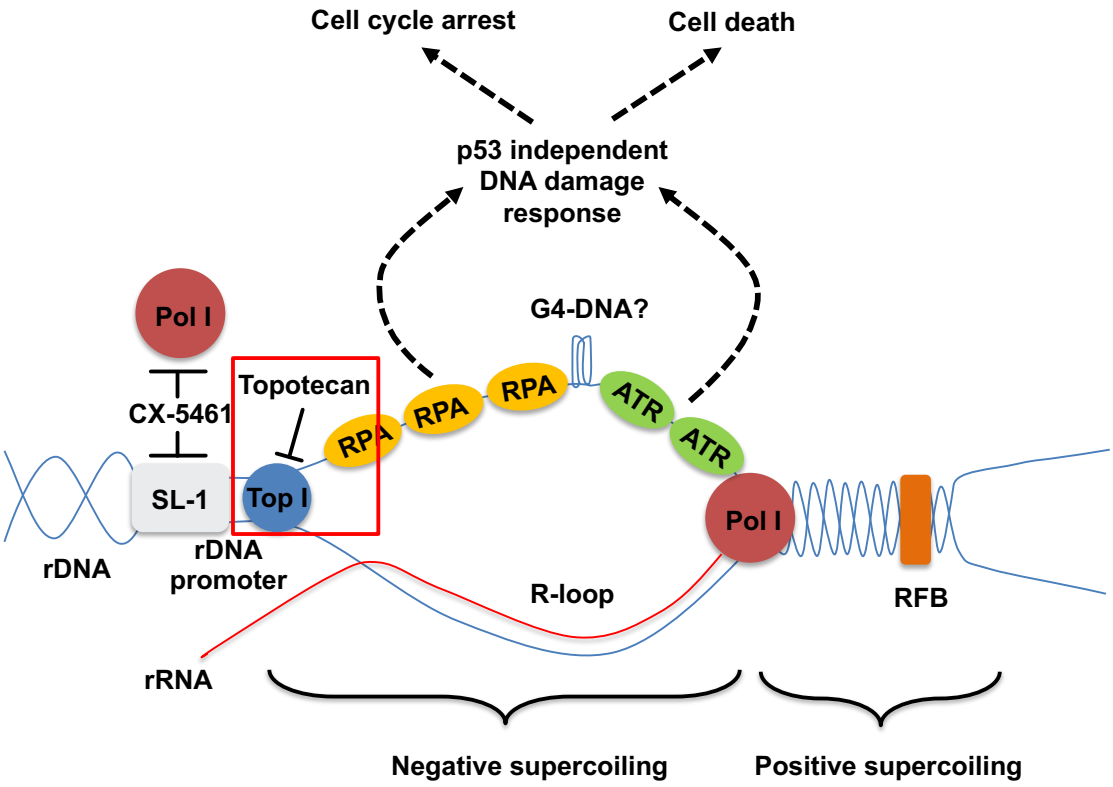

# Chapter 6. Discussion

## 6.1. Summary and key findings

HGSC is common with poor prognosis, particularly for patients with HR-proficient disease. We hypothesised that combining CX-5461 with the inhibition of specific gene products would lead to cooperative therapeutic efficacy in treating HR-proficient HGSC. In order to address this hypothesis, we performed a genome-wide RNAi screen to identify genes whose knockdown could cause synthetic lethality with low dose CX-5461 in a HR-proficient HGSC cell line. After the primary and secondary deconvolution screens, 17 candidates were identified. Gene pathway analysis of these 17 genes revealed enrichment in the HR pathway, which consisted of BRCA2, RAD54L and RAD51AP1 from the list [622-624], while gene network analysis identified BRCA2 and TOP1 as the most important genes in the list. Based on this information, we performed a focussed chemical compound screen consisting of a number of approved or potential HR, TOP1 and DNA damage repair (DDR) inhibitors to identify drug combinations that could cause synthetic lethality with low dose CX-5461 in the HGSC cell line OVCAR4. A significant number of chemical compounds were identified synergising with CX-5461, including HR inhibitors spironolactone, 17-AAG, AT13387 and B02; DNA damage signalling inhibitors KU-55593 (ATM inhibitor) and VE-821 (ATR inhibitor); as well as approved/emerging drugs for ovarian cancer including cisplatin, Topotecan (TOP1 inhibitor) and BMN-673 (PARP inhibitor). We focussed on the combination of CX-5461 and BRCA2/TOP1 inhibition in this thesis, while some other drug combinations, including ATM/ATR inhibitors, PARP inhibitors and cisplatin are being investigated in another collaborative project led by Dr Elaine Sanij.

BRCA2 is a crucial component of the HR pathway, which is responsible for the loading of RAD51 onto RPA-coated ssDNA at damaged sites, thus promoting HR repair [625]. CX-5461 has demonstrated selective lethality in BRCA1/2-deficient

mammary and colorectal cancer cells both *in vivo* and *in vitro* [225]. As a result, it was encouraging that we identified knockdown of BRCA2 to be synthetically lethal with CX-5461 in the screen. In fact, the identification of BRCA2 served as a good demonstration of the efficacy and reliability of the screen. In our follow-up studies, strong synergistic effects in growth inhibition and increased sensitivity to CX-5461 treatment were observed in ovarian cancer cells made BRCA2 deficient using either siRNA or shRNA. Massive genomic instability, as measured by micronuclei formation, was observed following CX-5461 treatment of siBRCA2 knockdown cells, which was proposed to be the mechanism of synergy for CX-5461 and BRCA2 inhibition. Increased sensitivity to CX-5461 was also observed in a BRCA2 stable knockdown cell line. Further examination of HR deficiency and defects in DDR components, including RAD51, BRCA1, ATM/ATR and CHK1/CHK2 as predictors of sensitivity to CX-5461 is being performed as part of Dr Elaine Sanij's ongoing studies.

On the other hand, the identification of TOP1 in the screen was intriguing as it is plays an essential role in DNA repair including resolving topological transcription and DNA replication stress [626]. TOP1 inhibitors, such as Topotecan and irinotecan, are currently used in the clinic as a second-line treatment option for ovarian cancer [447, 474, 627, 628]. A number of clinical trials are also underway to evaluate the potential of combining Topotecan with other conventional chemotherapies (e.g. Doxorubicin) or targeted therapies (e.g. Bevacizumab and Pazopanib) [629-631]. We tested the efficacy of combining CX-5461 and Topotecan in multiple HR-proficient ovarian cancer cell lines and found strong synergistic effects. More interestingly, there was no correlation between sensitivity of CX-5461/Topotecan to that of cisplatin/Olaparib, suggesting a different mode of action of this combination compared to the first-line therapies and providing a novel effective therapeutic option for patients with chemotherapy- and PARPi-resistant disease. This feature is particularly important

as both cisplatin and Olaparib-based therapies demonstrated selective efficacy in the BRCA-mutant patient cohort but not in the BRCA-wildtype group [632]. Our data clearly demonstrated the efficacy of the CX-5461/Topotecan in HR-proficient context, thus providing a broader efficacy spectrum compared to first-line therapy. Further, the development of resistant disease is almost inevitable in both platinum and PARP inhibitor-treated patients. Even though patients treated with PARP inhibitors have a longer PFS than the platinum group, probably due to the enhanced selectivity of PARP inhibitors [633], clinical resistance to PARPi is common. Approximately 50% of HRD HGSC eventually become HR-proficient due to secondary somatic mutations in HR genes that restore HR proficiency in platinum and PARPi-resistant disease [634]. Thus, by utilising distinct mechanisms of action from platinum and PARP inhibitors independent of BRCA status, the CX-5461/Topotecan combination brings new hope for patients with platinum/PARPi-resistant or refractory ovarian cancer.

In terms of the cellular and molecular mechanisms underlying the synergistic effects, we identified that CX-5461 synergises with the loss of TOP1 function rather than TOP1 trapping. The CX-5461/Topotecan combination treatment causes a persistent, irreversible cell cycle arrest/senescence independent of sustained rDNA transcription inhibition, but potentially caused by the initial transient inhibition of rDNA transcription. The cell cycle arrest was coupled with the upregulated transcription of p21, even in a p53-mutant background, and enhanced DDR specific to the nucleolus. We attributed the activation of the DDR to a nucleolar-associated transcription-coupled topological stress, which could lead to the enhanced formation of R-loops and ssDNA at the rDNA loci. The TOP1i/CX-5461 combination exacerbates nucleolar DDR in the absence of global DNA damage, which is distinct from doxorubicin and other DNA-damaging therapies.

Using an ovarian cancer xenograft mouse model, we demonstrated that the combined treatment is well tolerated, can significantly slow down tumour growth and extends survival. Our findings provide evidence for a novel strategy to treat HR-proficient HGSC, which brings new hope to ovarian cancer patients.

**Key findings**

1) CX-5461 exhibits synthetic lethality with TOP1 inhibition in HR-proficient HGSC, which is commonly resistant to chemotherapy.
2) CX-5461/Topotecan combination therapy induces persistent, irreversible cell cycle arrest (senescence) at late S/G2 phases, suggesting the preference of targeting proliferating cells.
3) The therapy activates cell cycle-independent nucleolar-specific DDR without causing excessive DNA damage, suggesting a safer therapeutic profile compared to conventional chemotherapies like doxorubicin, which is known to cause excessive DNA damage in normal cells that may result in severe side effects or even secondary tumours.
4) The therapy is well tolerated and extends the survival of tumour-bearing mice.
As currently there is no effective therapy to treat HR-proficient, chemo-resistant HGSC, and prognosis of patients in this cohort is poor, the CX-5461 and Topotecan combination could bring new hope to these patients and improve outcome.

## 6.2. The rationale of using the CX-5461 and Topotecan combination

Malignant cells are highly reliant on ribosomes to produce proteins for cell proliferation. Therefore, it is not surprising that the rDNA repeats are the most highly transcribed genes in actively growing and proliferating cells which can contribute to up to 60% of the global cellular transcription levels, and is frequently

associated with poor prognosis [83, 635, 636]. This phenomenon has also been observed in ovarian cancer, in which and low rDNA CpG methylation level (high transcription level of rDNA) was associated with shorter PFS [390, 391]. Inhibiting Pol I transcription using the Pol I specific inhibitor CX-5461 has demonstrated striking efficacy in a number of cancers both *in vitro* and *in vivo*, and is currently under clinical trial in haematological malignancies at the Peter MacCallum Cancer Centre [218, 221, 226-228, 230, 420, 637]. Therefore, there was sufficient rationale to test the possibility of exploiting the therapeutic potential of CX-5461 to treat ovarian cancer. Despite the fact that the p53-dependent pathway plays a key role in killing the B-lymphoma cells, we found that there was no correlation between CX-5461 sensitivity and p53 mutation status in our panel of ovarian cancer cell lines (Figure 3.1C) [221]. In fact, we demonstrated in our most recent work (Sanij et al., manuscript under revision) that CX-5461 sensitivity in ovarian cancer is linked to HR deficiency rather than p53. However, CX-5461 only has moderate efficacy in HR-proficient ovarian cancer cell lines, and improving its efficacy in this cohort was the main focus of my studies.

TOP1 facilitates DNA replication and transcription by relieving DNA of supercoiling and torsional stress [472]. TOP1 inhibitors such as Topotecan and Irinotecan have been used as anti-neoplastic medicines since 1985 [534]. High expression of TOP1 has been correlated with the poor prognosis of HGSC [512, 638]. Hence, there has been a clear rationale for using TOP1 inhibitors to treat ovarian cancer. TOP1 inhibitors were traditionally considered as a conventional DNA-damaging reagents as all approved TOP1 inhibitors block the re-ligation function of TOP1, which results in trapping of TOP1 on chromatin and creating single-strand DNA breaks [534]. However, Topotecan has consistently shown therapeutic effects in HR-proficient platinum-resistant ovarian cancer [639, 640], which has garnered attention to its DNA damage-independent therapeutic

potential. A number of studies have attributed these effects to TOP1's role in relaxing DNA negative supercoiling, which prevents the formation of R-loops, especially during rDNA transcription [100, 502, 599, 641]. Our results support this argument as CX-5461 synergised with both TOP1 knockdown and trapping agents. We also confirmed the nucleolar localisation of TOP1, which has been previously reported [500, 599]. As both RNA Pol I and TOP1 are present within the nucleoli to facilitate the active transcription of rDNA genes, it was rational to investigate how the inhibition of both enzymes could affect the process of transcription and the chromatin configuration at rDNA, and how these could further affect cell proliferation.

## 6.3. Mechanistic insight

### The transcription-coupled topological stress model

We provide a hypothetical model that explains the cellular response to the combination of CX-5461 and Topotecan and its distinction from conventional DNA damage or replication stress models, which includes 1) the DNA damage-independent DDR; 2) the replication-independent DDR; 3) the accumulation of nucleolar R-loops and pRPA32/RPA2 foci; 4) the loss of nucleosome protection against MNase at the rDNA promoter after CX-5461 treatment implicating combination therapy-induced open chromatin defects and strongly localised DDR at the rDNA loci [220]. The nucleolus has recently been described as 'an emerging hub in maintenance of genomic stability' [642]. However, little is known about how the DDR is activated and regulated in this region [598]. Our model, at least in part, provides the missing pieces of this DDR puzzle, which can be a stepping stone for the future exploitation of the nucleolar DDR pathway as a method of cancer treatment.

This model is supported by the findings of 1) replication-independent recruitment of phosphorylated ATR at the nucleolar periphery; 2) replication-independent formation of phosphorylated RPA32/RPA2 foci at the nucleolus; 3) activation of the DDR without excessive DNA damage. Despite this evidence, future experiments will be aimed at demonstrating the existence of negative supercoiling including the direct visualisation of negative supercoiling using electron microscopy (EM) [100] and the identification of the direct binding sites of pATR and pRPA32/RPA2 using chromatin immune-precipitation sequencing (ChIP-seq).

Furthermore, we hypothesise that the Transcription-Coupled Nucleotide Excision Repair (TC-NER) may be involved in the replication-independent nucleolar-associated transcription-coupled DDR. To investigate the involvement of TC-NER, components of TC-NER, like XPG or CSB, can be targeted to see if this could confer sensitivity to CX-5461 [643]. Alternatively, TC-NER can be indirectly measured by EdU incorporation during the G1 or G2 cell cycle phases as TC-NER involves DNA synthesis outside S phase [644, 645]. This can be done in cells expressing Fluorescent Ubiquitination-based Cell Cycle Indicator (FUCCI) which is a powerful tool to indicate the cell cycle phases [646]. If TC-NER is indeed involved in the replication-independent nucleolar-associated DDR, then we should observe increased incorporation of EdU at the nucleolus during G1 or G2 cell cycle phases, which could further confirm the existence of transcription-coupled DDR at the nucleolus [647].

**The interaction between replication stress and transcriptional stress**

CX-5461 has been reported to induce global replication stress [225]. However, our results suggest that global replication stress does not correlate with the

therapeutic effect of the CX-5461 and Topotecan combination treatment. It has been reported that the conflicts between transcription and replication are particularly frequent at rDNA repeat clusters due to the extraordinary transcription rate at rDNA, which can contribute to the formation of R-loops and replication stress [598]. However, we did not observe enrichment of RAD51 or γH2AX foci formation at the nucleolus, which makes it difficult to associate replication stress with the nucleolar-associated DDR we have observed. The staining pattern of RAD51 or γH2AX foci after CX-5461 and Topotecan treatment is also distinct from that of I-PpoI, a homing endonuclease that introduces DNA DSBs at rDNA repeats in human cells, although some reports argue that the response to DSBs is different from that of CX-5461-mediated replication stress [105, 420]. It is possible that the replication stress and transcriptional stress observed with the CX-5461/Topotecan combination are distinct events, and different DDRs are induced to cope with these stresses, e.g. the replication-dependent pRPA2(S33), pKAP1 and perhaps pATM are sensors of replication stress while the replication-independent pRPA2(S4/8) and pATR(T1989) are responders to transcriptional stress. This independent activation of DDR pathways can be further studied by testing the effects of specific inhibition of ATM or ATR, which could reveal therapeutic synergy between the CX-5461/Topotecan combination and ATM or ATR inhibitors. Indeed, ATR inhibitors are currently in clinical trials for the treatment of ovarian cancer [648, 649]. The combination may also be used to treat HR-deficient tumours as HR is crucial for resolving replication stress, or combined with WEE1 inhibitors which could override the cell cycle arrest induced by DDR, thus causing irreparable DNA damage. It has already been reported that the treatment of the WEE1 inhibitor, AZD1775, can sensitise small cell lung cancer and pancreatic cancer to PARP inhibitors like Olaparib [650, 651].

## 6.4. The translational impact of the CX-5461 and Topotecan combination studies

For over 40 years, there has been little progress in the treatment of HR-proficient HGSC. However, our results demonstrate that the combined treatment of CX-5461 and TOP1 inhibitors shows striking efficacy in inhibiting tumour growth and extending overall survival *in vivo*, and is well tolerated during the treatment period, providing strong evidence for a novel strategy to treat HR-proficient HGSC patients. We did not address the possibility of applying this combination therapy in HR-deficient HGSC in the current study. However, given the evidence that BRCA1 and BRCA2 are also known to preserve genomic integrity by repairing R-loop-associated DNA damage [308, 652-654], we strongly believe that this combination will also work in HR-deficient HGSC. Our study provides a clear example of combining an emerging drug candidate with a conventional drug to provide a potential new option for HGSC patients.

One major advantage of the combination therapy is that it activates cell cycle-independent nucleolus-specific DDR without causing excessive DNA damage, suggesting a safer therapeutic profile compared to conventional chemotherapies like doxorubicin, which is known to cause excessive DNA damage in normal cells that may result in severe side effects or even secondary tumours [655]. The therapy is also well tolerated and extends the survival of tumour-bearing mice. As there has been no effective therapy to treat HR-proficient, chemo-resistant HGSC, and prognosis of patients in this cohort is poor, the emergence of the CX-5461 and Topotecan combination could bring new hope to these patients. Additionally, the broad therapeutic efficacy of the CX-5461 and Topotecan combination in multiple ovarian cancer cell lines and tumour types reveal its potential of overcoming tumour heterogeneity. Intra- and inter-tumoural heterogeneity are considered to be a major challenge in cancer treatment given their role in driving

drug resistance and disease progression [656, 657]. As the CX-5461 and Topotecan combination is effective in multiple HGSC cell lines, it is possible that the combined treatment is insensitive to the genetic variance between tumour cells and may partially overcome tumour heterogeneity.

Regarding the clinical indication of the CX-5461/TOP1 combination, BRCA-wildtype, platinum/PARPi-resistant patients might be a suitable starting point because 1) currently there is no effective standard treatment option for this patient cohort; 2) the CX-5461/TOP1 combination uses a different mechanism as platinum/PARPi does which does not rely on HR deficiency; 3) the CX-5461/TOP1 combination is effective in HR-proficient OVCA. An initial trial could be designed to enrich for patients with high Pol I and TOP1 activity, determined by immunohistochemistry or RT-qPCR of biopsied samples, to potentially enhance the selectivity of the CX-5461 and Topotecan. In addition to OVCA, other Topotecan-approved diseases, like lung cancer, cervical cancer and haematological malignancies can also be considered. However, all these patient selection strategies are still hypothetical and need to be tested by extensive investigation.

## 6.5. The future development of the CX-5461 and Topotecan combination therapy

Our data clearly demonstrated the promise of the therapeutic development of the CX-5461 and Topotecan combination. Both CX-5461 and Topotecan have been developed to treat various types of cancer, and the mechanism of the synergistic effect does not restrict its application to ovarian cancer. As a result, it is rational to expand the application of this combination to other cancer types. We have tested this combination in acute lymphoblastic leukaemia (ALL) cell lines MHH-

CALL4 and SUP-B15, showing strong synergistic effects in both cell lines. This provides a strong rationale for testing the CX-5461 and Topotecan combination in a larger panel of cancer cell lines. Furthermore, although we demonstrate that CX-5461/Topotecan combination works in HR-proficient OVCA, we do not know whether its sensitivity is associated with other genetic backgrounds, e.g. amplified MYC signalling. Indeed, recent studies, including Dr Elaine Sanij's study in ovarian cancer (manuscript under revision), have demonstrated that the induced MYC target gene expression signature correlates with the sensitivity to CX-5461 [227, 658]. Thus, more research is required to identify the biomarkers that can help us to predict the response to the CX-5461/Topotecan combination and distinguish patients who are most likely to benefit.

Moreover, some measures could also be taken to increase Topotecan's specificity and alleviate its side effects. In addition to the development of novel TOP1 inhibitors, antibody drug conjugates (ADCs) with CPTs are also under evaluation. ADCs are conjugated molecules composed of an antibody linked to biologically active cytotoxic small molecules (also called 'payloads'). The ADCs combine the advantages of the specificity of monoclonal antibodies with the cancer-killing ability of cytotoxic drugs, thus delivering a tumour-specific cytotoxic effect like a guided missile with a nuclear warhead [659]. Two ADCs with CPTs, Labetuzumab govitecan (IMMU-130) and Sacituzumab govitecan (IMMU-132), are under clinical development to treat epithelial ovarian cancer [660, 661]. It would be rational to combine CX-5461 with these HGSC-targeted CPTs-conjugated ADCs when available to achieve better therapeutic outcome in vivo.

# References

1. Ferlay, J., et al., *Cancer incidence and mortality worldwide: Sources, methods and major patterns in GLOBOCAN 2012.* International Journal of Cancer, 2015. **136**(5): p. E359-E386.
2. Lokadasan, R., et al., *Targeted agents in epithelial ovarian cancer: review on emerging therapies and future developments.* ecancermedicalscience, 2016. **10**: p. 626.
3. *Australian Cancer Incidence and Mortality (ACIM) books*. 2015: Australian Institute of Health and Welfare.
4. DiSaia, P.J. and W.T. Creasman, *Clinical gynecologic oncology*. 2012: Elsevier Health Sciences.
5. Anglesio, M.S., et al., *Type-specific cell line models for type-specific ovarian cancer research.* PLoS One, 2013. **8**(9): p. e72162.
6. Domcke, S., et al., *Evaluating cell lines as tumour models by comparison of genomic profiles.* Nat Commun, 2013. **4**: p. 2126.
7. Vang, R., I.-M. Shih, and R.J. Kurman, *OVARIAN LOW-GRADE AND HIGH-GRADE SEROUS CARCINOMA: Pathogenesis, Clinicopathologic and Molecular Biologic Features, and Diagnostic Problems.* Advances in anatomic pathology, 2009. **16**(5): p. 267-282.
8. Labidi-Galy, S.I., et al., *High grade serous ovarian carcinomas originate in the fallopian tube.* Nature Communications, 2017. **8**(1): p. 1093.
9. Ahmed, A.A., et al., *Driver mutations in TP53 are ubiquitous in high grade serous carcinoma of the ovary.* J Pathol, 2010. **221**(1): p. 49-56.
10. Bowtell, D.D., *The genesis and evolution of high-grade serous ovarian cancer.* Nat Rev Cancer, 2010. **10**(11): p. 803-8.
11. Bowtell, D.D.L., *The genesis and evolution of high-grade serous ovarian cancer.* Nat Rev Cancer, 2010. **10**(11): p. 803-808.
12. Ledermann, J.A., Y. Drew, and R.S. Kristeleit, *Homologous recombination deficiency and ovarian cancer.* European Journal of Cancer, 2016. **60**: p. 49-58.
13. Walsh, C.S., *Two decades beyond BRCA1/2: Homologous recombination, hereditary cancer risk and a target for ovarian cancer therapy.* Gynecologic Oncology, 2015. **137**(2): p. 343-350.
14. Rosen, D.G., et al., *Ovarian cancer: pathology, biology, and disease models.* Front Biosci (Landmark Ed), 2009. **14**: p. 2089-102.
15. Cheaib, B., A. Auguste, and A. Leary, *The PI3K/Akt/mTOR pathway in ovarian cancer: therapeutic opportunities and challenges.* Chin J Cancer, 2015. **34**(1): p. 4-16.
16. Tothill, R.W., et al., *Novel molecular subtypes of serous and endometrioid ovarian cancer linked to clinical outcome.* Clin Cancer Res, 2008. **14**(16): p. 5198-208.
17. Tan, T.Z., et al., *Functional genomics identifies five distinct molecular subtypes with clinical relevance and pathways for growth control in epithelial ovarian cancer.* EMBO Mol Med, 2013. **5**(7): p. 1051-66.
18. Koshiyama, M., N. Matsumura, and I. Konishi, *Recent concepts of ovarian carcinogenesis: type I and type II.* Biomed Res Int, 2014. **2014**: p. 934261.
19. Shih Ie, M. and R.J. Kurman, *Ovarian tumorigenesis: a proposed model based on morphological and molecular genetic analysis.* Am J Pathol, 2004. **164**(5): p. 1511-8.
20. Cepeda, V., et al., *Biochemical mechanisms of cisplatin cytotoxicity.* Anticancer Agents Med Chem, 2007. **7**(1): p. 3-18.

21. Jordan, M.A. and L. Wilson, *Microtubules as a target for anticancer drugs.* Nat Rev Cancer, 2004. **4**(4): p. 253-265.
22. Conklin, C.M. and C.B. Gilks, *Differential diagnosis and clinical relevance of ovarian carcinoma subtypes.* Expert Review of Obstetrics & Gynecology, 2014.
23. Chetrit, A., et al., *Effect of BRCA1/2 mutations on long-term survival of patients with invasive ovarian cancer: the national Israeli study of ovarian cancer.* J Clin Oncol, 2008. **26**(1): p. 20-5.
24. Bolton, K.L., et al., *Association between brca1 and brca2 mutations and survival in women with invasive epithelial ovarian cancer.* JAMA, 2012. **307**(4): p. 382-389.
25. Luvero, D., A. Milani, and J.A. Ledermann, *Treatment options in recurrent ovarian cancer: latest evidence and clinical potential.* Therapeutic Advances in Medical Oncology, 2014. **6**(5): p. 229-239.
26. Meehan, R.S. and A.P. Chen, *New treatment option for ovarian cancer: PARP inhibitors.* Gynecologic Oncology Research and Practice, 2016. **3**(1): p. 3.
27. Clamp, A. and G. Jayson, *PARP inhibitors in BRCA mutation-associated ovarian cancer.* Lancet Oncol, 2015. **16**(1): p. 10-2.
28. Jones, P., *Niraparib: a poly(ADP-ribose) polymerase (PARP) inhibitor for the treatment of tumors with defective homologous recombination.* J Med Chem, 2015. **58**.
29. Pommier, Y., M.J. O'Connor, and J. de Bono, *Laying a trap to kill cancer cells: PARP inhibitors and their mechanisms of action.* Sci Transl Med, 2016. **8**(362): p. 362ps17.
30. Murai, J., *Trapping of PARP1 and PARP2 by clinical PARP inhibitors.* Cancer Res, 2012. **72**.
31. Rouleau, M., et al., *PARP inhibition: PARP1 and beyond.* Nat Rev Cancer, 2010. **10**(4): p. 293-301.
32. McCabe, N., et al., *Deficiency in the repair of DNA damage by homologous recombination and sensitivity to poly(ADP-ribose) polymerase inhibition.* Cancer Res, 2006. **66**(16): p. 8109-15.
33. Coleman, R.L., *A phase II evaluation of the potent, highly selective PARP inhibitor veliparib in the treatment of persistent or recurrent epithelial ovarian, fallopian tube, or primary peritoneal cancer in patients who carry a germline BRCA1 or BRCA2 mutation—an NRG oncology/gynecologic oncology group study.* Gynecol Oncol, 2015. **137**.
34. Murai, J., et al., *Trapping of PARP1 and PARP2 by Clinical PARP Inhibitors.* Cancer Res, 2012. **72**(21): p. 5588-99.
35. Murai, J., et al., *Stereospecific PARP trapping by BMN 673 and comparison with olaparib and rucaparib.* Mol Cancer Ther, 2014. **13**(2): p. 433-43.
36. Moore, K., et al., *Maintenance Olaparib in Patients with Newly Diagnosed Advanced Ovarian Cancer.* N Engl J Med, 2018. **379**(26): p. 2495-2505.
37. Clark, C.C., J.N. Weitzel, and T.R. O'Connor, *Enhancement of synthetic lethality via combinations of ABT-888, a PARP inhibitor, and carboplatin in vitro and in vivo using BRCA1 and BRCA2 isogenic models.* Mol Cancer Ther, 2012. **11**(9): p. 1948-58.
38. Rottenberg, S., *High sensitivity of BRCA1-deficient mammary tumors to the PARP inhibitor AZD2281 alone and in combination with platinum drugs.* Proc Natl Acad Sci U S A, 2008. **105**.
39. Oza, A.M., *Olaparib combined with chemotherapy for recurrent platinum-sensitive ovarian cancer: a randomised phase 2 trial.* Lancet Oncol, 2015. **16**.

40. Coward, J.I., K. Middleton, and F. Murphy, *New perspectives on targeted therapy in ovarian cancer.* Int J Womens Health, 2015. **7**: p. 189-203.
41. Agarwal, R. and S.B. Kaye, *Ovarian cancer: strategies for overcoming resistance to chemotherapy.* Nat Rev Cancer, 2003. **3**(7): p. 502-16.
42. Christie, E.L., et al., *Reversion of BRCA1/2 Germline Mutations Detected in Circulating Tumor DNA From Patients With High-Grade Serous Ovarian Cancer.* J Clin Oncol, 2017. **35**(12): p. 1274-1280.
43. Patch, A.M., et al., *Whole-genome characterization of chemoresistant ovarian cancer.* Nature, 2015. **521**(7553): p. 489-94.
44. Fojo, T. and S. Bates, *Mechanisms of resistance to PARP inhibitors--three and counting.* Cancer Discov, 2013. **3**(1): p. 20-3.
45. D'Andrea, A.D., *Mechanisms of PARP inhibitor sensitivity and resistance.* DNA Repair (Amst), 2018.
46. Pettitt, S.J., et al., *Genome-wide and high-density CRISPR-Cas9 screens identify point mutations in PARP1 causing PARP inhibitor resistance.* Nature Communications, 2018. **9**(1): p. 1849.
47. Edwards, S.L., et al., *Resistance to therapy caused by intragenic deletion in BRCA2.* Nature, 2008. **451**(7182): p. 1111-5.
48. Mayor, P., et al., *BRCA1 reversion mutation acquired after treatment identified by liquid biopsy.* Gynecol Oncol Rep, 2017. **21**: p. 57-60.
49. Jaspers, J.E., et al., *Loss of 53BP1 causes PARP inhibitor resistance in Brca1-mutated mouse mammary tumors.* Cancer Discov, 2013. **3**(1): p. 68-81.
50. Choi, Young E., et al., *Platinum and PARP Inhibitor Resistance Due to Overexpression of MicroRNA-622 in BRCA1-Mutant Ovarian Cancer.* Cell Reports, 2016. **14**(3): p. 429-439.
51. Ding, X., et al., *Synthetic viability by BRCA2 and PARP1/ARTD1 deficiencies.* Nat Commun, 2016. **7**: p. 12425.
52. Bitler, B.G., et al., *PARP inhibitors: Clinical utility and possibilities of overcoming resistance.* Gynecol Oncol, 2017. **147**(3): p. 695-704.
53. Mirza, M.R., et al., *Niraparib Maintenance Therapy in Platinum-Sensitive, Recurrent Ovarian Cancer.* N Engl J Med, 2016. **375**(22): p. 2154-2164.
54. Kim, D.S., et al., *Activation of PARP-1 by snoRNAs Controls Ribosome Biogenesis and Cell Growth via the RNA Helicase DDX21.* Mol Cell, 2019.
55. Ledermann, J.A. and R.S. Kristeleit, *Optimal treatment for relapsing ovarian cancer.* Ann Oncol, 2010. **21 Suppl 7**: p. vii218-22.
56. Mantia-Smaldone, G.M., R.P. Edwards, and A.M. Vlad, *Targeted treatment of recurrent platinum-resistant ovarian cancer: current and emerging therapies.* Cancer Manag Res, 2011. **3**: p. 25-38.
57. Markman, M., *Second-Line Treatment of Ovarian Cancer.* The Oncologist, 2000. **5**(1): p. 26-35.
58. Colon-Otero, G., et al., *Phase 2 trial of everolimus and letrozole in relapsed estrogen receptor-positive high-grade ovarian cancers.* Gynecol Oncol, 2017. **146**(1): p. 64-68.
59. Emons, G., et al., *Temsirolimus in women with platinum-refractory/resistant ovarian cancer or advanced/recurrent endometrial carcinoma. A phase II study of the AGO-study group (AGO-GYN8).* Gynecol Oncol, 2016. **140**(3): p. 450-6.
60. Behbakht, K., et al., *Phase II trial of the mTOR inhibitor, temsirolimus and evaluation of circulating tumor cells and tumor biomarkers in persistent and*

*recurrent epithelial ovarian and primary peritoneal malignancies: a Gynecologic Oncology Group study.* Gynecol Oncol, 2011. **123**(1): p. 19-26.
61. Pardoll, D.M., *The blockade of immune checkpoints in cancer immunotherapy.* Nat Rev Cancer, 2012. **12**(4): p. 252-64.
62. Gaillard, S.L., A.A. Secord, and B. Monk, *The role of immune checkpoint inhibition in the treatment of ovarian cancer.* Gynecol Oncol Res Pract, 2016. **3**: p. 11.
63. Mu, C.-Y., et al., *High expression of PD-L1 in lung cancer may contribute to poor prognosis and tumor cells immune escape through suppressing tumor infiltrating dendritic cells maturation.* Medical Oncology, 2011. **28**(3): p. 682-688.
64. Kim, R., M. Emi, and K. Tanabe, *Cancer immunoediting from immune surveillance to immune escape.* Immunology, 2007. **121**(1): p. 1-14.
65. Mandai, M., et al., *Anti-PD-L1/PD-1 immune therapies in ovarian cancer: basic mechanism and future clinical application.* Int J Clin Oncol, 2016. **21**(3): p. 456-61.
66. De Felice, F., et al., *Immunotherapy of Ovarian Cancer: The Role of Checkpoint Inhibitors.* J Immunol Res, 2015. **2015**: p. 191832.
67. Hamanishi, J., M. Mandai, and I. Konishi, *Immune checkpoint inhibition in ovarian cancer.* Int Immunol, 2016. **28**(7): p. 339-48.
68. Postow, M.A., M.K. Callahan, and J.D. Wolchok, *Immune Checkpoint Blockade in Cancer Therapy.* J Clin Oncol, 2015. **33**(17): p. 1974-82.
69. Rizvi, N.A., et al., *Activity and safety of nivolumab, an anti-PD-1 immune checkpoint inhibitor, for patients with advanced, refractory squamous non-small-cell lung cancer (CheckMate 063): a phase 2, single-arm trial.* Lancet Oncol, 2015. **16**(3): p. 257-65.
70. Borghaei, H., et al., *Nivolumab versus Docetaxel in Advanced Nonsquamous Non-Small-Cell Lung Cancer.* N Engl J Med, 2015. **373**(17): p. 1627-39.
71. Hamanishi, J., et al., *Safety and Antitumor Activity of Anti-PD-1 Antibody, Nivolumab, in Patients With Platinum-Resistant Ovarian Cancer.* J Clin Oncol, 2015. **33**(34): p. 4015-22.
72. Emens, L.A., M. Kok, and L.S. Ojalvo, *Targeting the programmed cell death-1 pathway in breast and ovarian cancer.* Curr Opin Obstet Gynecol, 2016. **28**(2): p. 142-7.
73. Homicsko, K. and G. Coukos, *Targeting Programmed Cell Death 1 in Ovarian Cancer.* J Clin Oncol, 2015. **33**(34): p. 3987-9.
74. Heong, V., N. Ngoi, and D.S. Tan, *Update on immune checkpoint inhibitors in gynecological cancers.* J Gynecol Oncol, 2017. **28**(2): p. e20.
75. Duraiswamy, J., et al., *Dual blockade of PD-1 and CTLA-4 combined with tumor vaccine effectively restores T-cell rejection function in tumors.* Cancer Res, 2013. **73**(12): p. 3591-603.
76. Collazo-Lorduy, A. and M.D. Galsky, *Combining chemotherapy and immune checkpoint blockade.* Current Opinion in Urology, 2016. **26**(6): p. 508-513.
77. Pfirschke, C., et al., *Immunogenic Chemotherapy Sensitizes Tumors to Checkpoint Blockade Therapy.* Immunity, 2016. **44**(2): p. 343-54.
78. Weir, G.M., R.S. Liwski, and M. Mansour, *Immune modulation by chemotherapy or immunotherapy to enhance cancer vaccines.* Cancers (Basel), 2011. **3**(3): p. 3114-42.
79. Fransson, A., et al., *Strong synergy with APR-246 and DNA-damaging drugs in primary cancer cells from patients with TP53 mutant High-Grade Serous ovarian cancer.* J Ovarian Res, 2016. **9**(1): p. 27.

80. Mohell, N., et al., *APR-246 overcomes resistance to cisplatin and doxorubicin in ovarian cancer cells.* Cell Death Dis, 2015. **6**: p. e1794.
81. Bykov, V.J., et al., *Targeting of Mutant p53 and the Cellular Redox Balance by APR-246 as a Strategy for Efficient Cancer Therapy.* Front Oncol, 2016. **6**: p. 21.
82. Goodfellow, S.J. and J.C. Zomerdijk, *Basic mechanisms in RNA polymerase I transcription of the ribosomal RNA genes.* Subcell Biochem, 2013. **61**: p. 211-36.
83. Russell, J. and J.C. Zomerdijk, *The RNA polymerase I transcription machinery.* Biochem Soc Symp, 2006(73): p. 203-16.
84. Rossetti, S., A.J. Wierzbicki, and N. Sacchi, *Undermining ribosomal RNA transcription in both the nucleolus and mitochondrion: an offbeat approach to target MYC-driven cancer.* Oncotarget, 2017. **9**(4): p. 5016-5031.
85. White, R.J., *RNA polymerases I and III, growth control and cancer.* Nat Rev Mol Cell Biol, 2005. **6**(1): p. 69-78.
86. Montanaro, L., D. Treré, and M. Derenzini, *Nucleolus, Ribosomes, and Cancer.* The American Journal of Pathology, 2008. **173**(2): p. 301-310.
87. Liebhaber, S.A., S. Wolf, and D. Schlessinger, *Differences in rRNA metabolism of primary and SV40-transformed human fibroblasts.* Cell, 1978. **13**: p. 121-127.
88. Zhao, J., et al., *ERK-dependent phosphorylation of the transcription initiation factor TIF-IA is required for RNA polymerase I transcription and cell growth.* Mol. Cell, 2003. **11**: p. 405-413.
89. Belin, S., et al., *Dysregulation of Ribosome Biogenesis and Translational Capacity Is Associated with Tumor Progression of Human Breast Cancer Cells.* PLoS ONE, 2009. **4**(9): p. e7147.
90. Wang, H.D., A. Trivedi, and D.L. Johnson, *Regulation of RNA polymerase I-dependent promoters by the hepatitis B virus X protein via activated Ras and TATA-binding protein.* Mol Cell Biol, 1998. **18**(12): p. 7086-94.
91. Kao, C.F., S.Y. Chen, and Y.H. Lee, *Activation of RNA polymerase I transcription by hepatitis C virus core protein.* J Biomed Sci, 2004. **11**(1): p. 72-94.
92. Diesch, J., R.D. Hannan, and E. Sanij, *Perturbations at the ribosomal genes loci are at the centre of cellular dysfunction and human disease.* Cell & Bioscience, 2014. **4**(1): p. 43.
93. Ueshima, S., K. Nagata, and M. Okuwaki, *Internal Associations of the Acidic Region of Upstream Binding Factor Control Its Nucleolar Localization.* Mol Cell Biol, 2017. **37**(22).
94. Drygin, D., W.G. Rice, and I. Grummt, *The RNA polymerase I transcription machinery: an emerging target for the treatment of cancer.* Annu Rev Pharmacol Toxicol, 2010. **50**: p. 131-56.
95. Grummt, I., *Life on a planet of its own: regulation of RNA polymerase I transcription in the nucleolus.* Genes Dev., 2003. **17**: p. 1691-1702.
96. Sanij, E. and R.D. Hannan, *The role of UBF in regulating the structure and dynamics of transcriptionally active rDNA chromatin.* Epigenetics, 2009. **4**(6): p. 374-82.
97. Tuan, J.C., W. Zhai, and L. Comai, *Recruitment of TATA-binding protein-TAFI complex SL1 to the human ribosomal DNA promoter is mediated by the carboxy-terminal activation domain of upstream binding factor (UBF) and is regulated by UBF phosphorylation.* Molecular and cellular biology, 1999. **19**(4): p. 2872-2879.
98. Zhang, Y., et al., *The Paf1 complex is required for efficient transcription elongation by RNA polymerase I.* Proceedings of the National Academy of Sciences, 2009. **106**(7): p. 2153.

99. Kusnadi, E.P., et al., *Regulation of rDNA transcription in response to growth factors, nutrients and energy.* Gene, 2015. **556**(1): p. 27-34.
100. French, S.L., et al., *Distinguishing the roles of Topoisomerases I and II in relief of transcription-induced torsional stress in yeast rRNA genes.* Mol Cell Biol, 2011. **31**(3): p. 482-94.
101. Suja, J.A., et al., *Relative distribution of rDNA and proteins of the RNA polymerase I transcription machinery at chromosomal NORs.* Chromosoma, 1997. **105**(7-8): p. 459-69.
102. Ray, S., et al., *Topoisomerase IIalpha promotes activation of RNA polymerase I transcription by facilitating pre-initiation complex formation.* Nat Commun, 2013. **4**: p. 1598.
103. Bywater, M.J., et al., *Dysregulation of the basal RNA polymerase transcription apparatus in cancer.* Nat Rev Cancer, 2013. **13**(5): p. 299-314.
104. Nadkarni, A., et al., *Nucleotide Excision Repair and Transcription-coupled DNA Repair Abrogate the Impact of DNA Damage on Transcription.* J Biol Chem, 2016. **291**(2): p. 848-61.
105. van Sluis, M. and B. McStay, *A localized nucleolar DNA damage response facilitates recruitment of the homology-directed repair machinery independent of cell cycle stage.* Genes Dev, 2015. **29**(11): p. 1151-63.
106. Li, P., et al., *ABH2 couples regulation of ribosomal DNA transcription with DNA alkylation repair.* Cell Rep, 2013. **4**(4): p. 817-29.
107. Hanawalt, P.C. and G. Spivak, *Transcription-coupled DNA repair: two decades of progress and surprises.* Nat Rev Mol Cell Biol, 2008. **9**(12): p. 958-70.
108. Stefanovsky, V., et al., *Growth factor signaling regulates elongation of RNA polymerase I transcription in mammals via UBF phosphorylation and r-chromatin remodeling.* Mol Cell, 2006. **21**(5): p. 629-39.
109. Diesch, J., R.D. Hannan, and E. Sanij, *Genome wide mapping of UBF binding-sites in mouse and human cell lines.* Genom Data, 2015. **3**: p. 103-5.
110. Sanij, E., et al., *A novel role for the Pol I transcription factor UBTF in maintaining genome stability through the regulation of highly transcribed Pol II genes.* Genome Res, 2015. **25**(2): p. 201-12.
111. Kermekchiev, M., J.L. Workman, and C.S. Pikaard, *Nucleosome binding by the polymerase I transactivator upstream binding factor displaces linker histone H1.* Mol Cell Biol, 1997. **17**(10): p. 5833-42.
112. Sanij, E., et al., *UBF levels determine the number of active ribosomal RNA genes in mammals.* The Journal of Cell Biology, 2008. **183**(7): p. 1259-1274.
113. Hamdane, N., et al., *Conditional inactivation of Upstream Binding Factor reveals its epigenetic functions and the existence of a somatic nucleolar precursor body.* PLoS Genet, 2014. **10**(8): p. e1004505.
114. Xie, W., et al., *The chromatin remodeling complex NuRD establishes the poised state of rRNA genes characterized by bivalent histone modifications and altered nucleosome positions.* Proc Natl Acad Sci U S A, 2012. **109**(21): p. 8161-6.
115. Studitsky, V.M., et al., *Chromatin remodeling by RNA polymerases.* Trends Biochem Sci, 2004. **29**(3): p. 127-35.
116. Diermeier, S.D., et al., *Chromatin-specific regulation of mammalian rDNA transcription by clustered TTF-I binding sites.* PLoS genetics, 2013. **9**(9): p. e1003786-e1003786.

117. Jansa, P., et al., *The transcript release factor PTRF augments ribosomal gene transcription by facilitating reinitiation of RNA polymerase I.* Nucleic acids research, 2001. **29**(2): p. 423-429.
118. West, S., N. Gromak, and N.J. Proudfoot, *Human 5′ → 3′ exonuclease Xrn2 promotes transcription termination at co-transcriptional cleavage sites.* Nature, 2004. **432**(7016): p. 522-525.
119. Mischo, H.E., et al., *Yeast Sen1 helicase protects the genome from transcription-associated instability.* Mol Cell, 2011. **41**(1): p. 21-32.
120. Sanij, E., et al., *UBF levels determine the number of active ribosomal RNA genes in mammals.* J Cell Biol, 2008. **183**(7): p. 1259-74.
121. Xu, B., et al., *Ribosomal DNA copy number loss and sequence variation in cancer.* PLoS Genet, 2017. **13**(6): p. e1006771.
122. Wang, M. and B. Lemos, *Ribosomal DNA copy number amplification and loss in human cancers is linked to tumor genetic context, nucleolus activity, and proliferation.* PLoS Genetics, 2017. **13**(9): p. e1006994.
123. Zhou, H., et al., *Overexpression of Ribosomal RNA in the Development of Human Cervical Cancer Is Associated with rDNA Promoter Hypomethylation.* PLOS ONE, 2016. **11**(10): p. e0163340.
124. Ghoshal, K., et al., *Role of human ribosomal RNA (rRNA) promoter methylation and of methyl-CpG-binding protein MBD2 in the suppression of rRNA gene expression.* J Biol Chem, 2004. **279**(8): p. 6783-93.
125. Raval, A., et al., *Reduced rRNA expression and increased rDNA promoter methylation in CD34+ cells of patients with myelodysplastic syndromes.* Blood, 2012. **120**(24): p. 4812-8.
126. Kochanek, S., et al., *DNA methylation in the promoter of ribosomal RNA genes in human cells as determined by genomic sequencing.* FEBS Letters, 1996. **388**(2-3): p. 192-194.
127. Lawrence, R.J., et al., *A concerted DNA methylation/histone methylation switch regulates rRNA gene dosage control and nucleolar dominance.* Mol Cell, 2004. **13**(4): p. 599-609.
128. Zentner, G.E., et al., *Integrative genomic analysis of human ribosomal DNA.* Nucleic Acids Res, 2011. **39**(12): p. 4949-60.
129. Brandenburger, Y., et al., *Increased expression of UBF is a critical determinant for rRNA synthesis and hypertrophic growth of cardiac myocytes.* FASEB J., 2001. **15**: p. 2051-2053.
130. Yu, F., et al., *Analysis of histone modifications at human ribosomal DNA in liver cancer cell.* Scientific Reports, 2015. **5**: p. 18100.
131. Strohner, R., et al., *Recruitment of the nucleolar remodeling complex NoRC establishes ribosomal DNA silencing in chromatin.* Mol Cell Biol, 2004. **24**(4): p. 1791-8.
132. Yang, L., et al., *Regulation of SirT1-nucleomethylin binding by rRNA coordinates ribosome biogenesis with nutrient availability.* Mol Cell Biol, 2013. **33**(19): p. 3835-48.
133. Grummt, I., *The nucleolus-guardian of cellular homeostasis and genome integrity.* Chromosoma, 2013. **122**(6): p. 487-97.
134. Lempiäinen, H. and D. Shore, *Growth control and ribosome biogenesis.* Current Opinion in Cell Biology, 2009. **21**(6): p. 855-863.

135. Poortinga, G., et al., *c-MYC coordinately regulates ribosomal gene chromatin remodeling and Pol I availability during granulocyte differentiation.* Nucleic Acids Res, 2011. **39**(8): p. 3267-81.
136. van Riggelen, J., A. Yetil, and D.W. Felsher, *MYC as a regulator of ribosome biogenesis and protein synthesis.* Nat Rev Cancer, 2010. **10**(4): p. 301-9.
137. Grandori, C., et al., *c-Myc binds to human ribosomal DNA and stimulates transcription of rRNA genes by RNA polymerase I.* Nat Cell Biol, 2005. **7**(3): p. 311-8.
138. Arabi, A., et al., *c-Myc associates with ribosomal DNA and activates RNA polymerase I transcription.* Nat Cell Biol, 2005. **7**(3): p. 303-10.
139. White, R.J., *RNA polymerases I and III, non-coding RNAs and cancer.* Trends Genet, 2008. **24**(12): p. 622-9.
140. Hannan, K.M., et al., *Signaling to the ribosome in cancer--It is more than just mTORC1.* IUBMB Life, 2011. **63**(2): p. 79-85.
141. McCubrey, J.A., et al., *Roles of the Raf/MEK/ERK pathway in cell growth, malignant transformation and drug resistance.* Biochim Biophys Acta, 2007. **1773**(8): p. 1263-84.
142. Kim, E.K. and E.J. Choi, *Pathological roles of MAPK signaling pathways in human diseases.* Biochim Biophys Acta, 2010. **1802**(4): p. 396-405.
143. Sears, R., et al., *Ras enhances Myc protein stability.* Mol Cell, 1999. **3**(2): p. 169-79.
144. Stefanovsky, V.Y., *An immediate response of ribosomal transcription to growth factor stimulation in mammals is mediated by ERK phosphorylation of UBF.* Mol. Cell, 2001. **8**: p. 1063-1073.
145. Stefanovsky, V.Y. and T. Moss, *The splice variants of UBF differentially regulate RNA polymerase I transcription elongation in response to ERK phosphorylation.* Nucleic Acids Res, 2008. **36**(15): p. 5093-101.
146. Voit, R., M. Hoffmann, and I. Grummt, *Phosphorylation by G1-specific cdk-cyclin complexes activates the nucleolar transcription factor UBF.* EMBO J, 1999. **18**(7): p. 1891-9.
147. Porta, C., C. Paglino, and A. Mosca, *Targeting PI3K/Akt/mTOR Signaling in Cancer.* Front Oncol, 2014. **4**: p. 64.
148. Sheppard, K., et al., *Targeting PI3 kinase/AKT/mTOR signaling in cancer.* Crit Rev Oncog, 2012. **17**(1): p. 69-95.
149. Wang, Y., et al., *The predictive role of phosphatase and tensin homolog (PTEN) loss, phosphoinositol-3 (PI3) kinase (PIK3CA) mutation, and PI3K pathway activation in sensitivity to trastuzumab in HER2-positive breast cancer: a meta-analysis.* Curr Med Res Opin, 2013. **29**(6): p. 633-42.
150. Chalhoub, N. and S.J. Baker, *PTEN and the PI3-kinase pathway in cancer.* Annu Rev Pathol, 2009. **4**: p. 127-50.
151. Chen, Z., et al., *Crucial role of p53-dependent cellular senescence in suppression of Pten-deficient tumorigenesis.* Nature, 2005. **436**(7051): p. 725-30.
152. Populo, H., J.M. Lopes, and P. Soares, *The mTOR signalling pathway in human cancer.* Int J Mol Sci, 2012. **13**(2): p. 1886-918.
153. Devlin, J.R., et al., *AKT signalling is required for ribosomal RNA synthesis and progression of Emu-Myc B-cell lymphoma in vivo.* FEBS J, 2013. **280**(21): p. 5307-16.
154. Hannan, K.M., *mTOR-dependent regulation of ribosomal gene transcription requires S6K1 and is mediated by phosphorylation of the carboxy-terminal*

*activation domain of the nucleolar transcription factor UBF.* Mol. Cell. Biol., 2003. **23**: p. 8862-8877.
155. Jastrzebski, K., et al., *Coordinate regulation of ribosome biogenesis and function by the ribosomal protein S6 kinase, a key mediator of mTOR function.* Growth Factors, 2007. **25**(4): p. 209-26.
156. Chan, J.C., et al., *AKT promotes rRNA synthesis and cooperates with c-MYC to stimulate ribosome biogenesis in cancer.* Sci Signal, 2011. **4**(188): p. ra56.
157. Nguyen le, X.T. and B.S. Mitchell, *Akt activation enhances ribosomal RNA synthesis through casein kinase II and TIF-IA.* Proc Natl Acad Sci U S A, 2013. **110**(51): p. 20681-6.
158. Ruzzene, M., et al., *Cross-talk between the CK2 and AKT signaling pathways in cancer.* Advances in Biological Regulation, 2017. **64**: p. 1-8.
159. Zhang, C., L. Comai, and D.L. Johnson, *PTEN represses RNA Polymerase I transcription by disrupting the SL1 complex.* Mol Cell Biol, 2005. **25**(16): p. 6899-911.
160. Vincent, T., et al., *The glycogen synthase kinase (GSK) 3beta represses RNA polymerase I transcription.* Oncogene, 2008. **27**(39): p. 5254-9.
161. Golomb, L., S. Volarevic, and M. Oren, *p53 and ribosome biogenesis stress: the essentials.* FEBS Lett, 2014. **588**(16): p. 2571-9.
162. Zhai, W. and L. Comai, *Repression of RNA polymerase I transcription by the tumor suppressor p53.* Mol Cell Biol, 2000. **20**(16): p. 5930-8.
163. Voit, R., K. Schafer, and I. Grummt, *Mechanism of repression of RNA polymerase I transcription by the retinoblastoma protein.* Mol Cell Biol, 1997. **17**(8): p. 4230-7.
164. Cavanaugh, A.H., et al., *Activity of RNA polymerase I transcription factor UBF blocked by Rb gene product.* Nature, 1995. **374**(6518): p. 177-80.
165. Hannan, K.M., *Rb and p130 regulate RNA polymerase I transcription: Rb disrupts the interaction between UBF and SL-1.* Oncogene, 2000. **19**: p. 4988-4999.
166. Ho, J.S., et al., *p53-Dependent transcriptional repression of c-myc is required for G1 cell cycle arrest.* Mol Cell Biol, 2005. **25**(17): p. 7423-31.
167. Stambolic, V., et al., *Regulation of PTEN transcription by p53.* Mol Cell, 2001. **8**(2): p. 317-25.
168. Feng, Z., et al., *The coordinate regulation of the p53 and mTOR pathways in cells.* Proc Natl Acad Sci U S A, 2005. **102**(23): p. 8204-9.
169. Hannan, K.M., *RNA polymerase I transcription in confluent cells: Rb downregulates rDNA transcription during confluence-induced cell cycle arrest.* Oncogene, 2000. **19**: p. 3487-3497.
170. Ayrault, O., et al., *Human tumor suppressor p14ARF negatively regulates rRNA transcription and inhibits UBF1 transcription factor phosphorylation.* Oncogene, 2006. **25**(58): p. 7577-86.
171. Le, X., et al., *Systematic Functional Characterization of Resistance to PI3K Inhibition in Breast Cancer.* Cancer Discov, 2016. **6**(10): p. 1134-1147.
172. Leroy, C., R.J. Amante, and M. Bentires-Alj, *Anticipating mechanisms of resistance to PI3K inhibition in breast cancer: a challenge in the era of precision medicine.* Biochem Soc Trans, 2014. **42**(4): p. 733-41.
173. Sheppard, K.E., et al., *Synergistic inhibition of ovarian cancer cell growth by combining selective PI3K/mTOR and RAS/ERK pathway inhibitors.* Eur J Cancer, 2013. **49**(18): p. 3936-44.
174. Maik-Rachline, G. and R. Seger, *The ERK cascade inhibitors: Towards overcoming resistance.* Drug Resist Updat, 2016. **25**: p. 1-12.

175. Hatzivassiliou, G., et al., *ERK inhibition overcomes acquired resistance to MEK inhibitors.* Mol Cancer Ther, 2012. **11**(5): p. 1143-54.
176. Cornelison, R., et al., *Targeting Rna-Polymerase I in Both Chemosensitive and Chemoresistant Populations in Epithelial Ovarian Cancer.* Clin Cancer Res, 2017.
177. Cancer Genome Atlas Research, N., *Integrated genomic analyses of ovarian carcinoma.* Nature, 2011. **474**(7353): p. 609-15.
178. Wojnarowicz, P.M., et al., *The genomic landscape of TP53 and p53 annotated high grade ovarian serous carcinomas from a defined founder population associated with patient outcome.* PLoS One, 2012. **7**(9): p. e45484.
179. Zhang, Y., et al., *TP53 mutations in epithelial ovarian cancer.* Transl Cancer Res, 2016. **5**(6): p. 650-663.
180. Mandilaras, V., et al., *TP53 mutations in high grade serous ovarian cancer and impact on clinical outcomes: a comparison of next generation sequencing and bioinformatics analyses.* Int J Gynecol Cancer, 2019.
181. Cole, A.J., et al., *Assessing mutant p53 in primary high-grade serous ovarian cancer using immunohistochemistry and massively parallel sequencing.* 2016. **6**: p. 26191.
182. Quartuccio, S.M., et al., *Mutant p53 expression in fallopian tube epithelium drives cell migration.* Int J Cancer, 2015. **137**(7): p. 1528-38.
183. Yue, X., et al., *Mutant p53 in Cancer: Accumulation, Gain-of-Function, and Therapy.* J Mol Biol, 2017. **429**(11): p. 1595-1606.
184. Oren, M. and V. Rotter, *Mutant p53 gain-of-function in cancer.* Cold Spring Harb Perspect Biol, 2010. **2**(2): p. a001107.
185. Popp, M.W. and L.E. Maquat, *Nonsense-mediated mRNA Decay and Cancer.* Curr Opin Genet Dev, 2018. **48**: p. 44-50.
186. Li, S., et al., *The Novel Pathogenic Mutation c.849dupT in BRCA2 Contributes to the Nonsense-Mediated mRNA Decay of BRCA2 in Familial Breast Cancer.* J Breast Cancer, 2018. **21**(3): p. 330-333.
187. Johnson, J.K., et al., *The application of nonsense-mediated mRNA decay inhibition to the identification of breast cancer susceptibility genes.* BMC Cancer, 2012. **12**: p. 246.
188. Ivanov, I., et al., *Identifying candidate colon cancer tumor suppressor genes using inhibition of nonsense-mediated mRNA decay in colon cancer cells.* Oncogene, 2007. **26**(20): p. 2873-84.
189. Hu, Z., C. Yau, and A.A. Ahmed, *A pan-cancer genome-wide analysis reveals tumour dependencies by induction of nonsense-mediated decay.* Nat Commun, 2017. **8**: p. 15943.
190. Zhu, J., et al., *Gain-of-function p53 mutants co-opt chromatin pathways to drive cancer growth.* Nature, 2015. **525**(7568): p. 206-11.
191. Zhang, Y., et al., *TP53 mutations in epithelial ovarian cancer.* Translational Cancer Research, 2016. **5**(6): p. 650-663.
192. Hanrahan, A.J., et al., *Genomic complexity and AKT dependence in serous ovarian cancer.* Cancer Discov, 2012. **2**(1): p. 56-67.
193. Corney, D.C., et al., *Role of p53 and Rb in ovarian cancer.* Adv Exp Med Biol, 2008. **622**: p. 99-117.
194. Leary, A., et al., *The PI3K/Akt/mTOR Pathway in Ovarian Cancer: Biological Rationale and Therapeutic Opportunities*, in *Ovarian Cancer - A Clinical and Translational Update*, I.n. Díaz-Padilla, Editor. 2013, InTech: Rijeka. p. Ch. 13.
195. Musa, F. and R. Schneider, *Targeting the PI3K/AKT/mTOR pathway in ovarian cancer.* Translational Cancer Research, 2015. **4**(1): p. 97-106.

196. Bollag, G., et al., *Loss of NF1 results in activation of the Ras signaling pathway and leads to aberrant growth in haematopoietic cells.* Nat Genet, 1996. **12**(2): p. 144-8.
197. Hew, K.E., et al., *MAPK Activation Predicts Poor Outcome and the MEK Inhibitor, Selumetinib, Reverses Antiestrogen Resistance in ER-Positive High-Grade Serous Ovarian Cancer.* Clin Cancer Res, 2016. **22**(4): p. 935-47.
198. Gruosso, T., et al., *MAP3K8/TPL-2/COT is a potential predictive marker for MEK inhibitor treatment in high-grade serous ovarian carcinomas.* Nature Communications, 2015. **6**: p. 8583.
199. Mittempergher, L., *Genomic Characterization of High-Grade Serous Ovarian Cancer: Dissecting Its Molecular Heterogeneity as a Road Towards Effective Therapeutic Strategies.* Current Oncology Reports, 2016. **18**(7): p. 44.
200. Karst, A.M., K. Levanon, and R. Drapkin, *Modeling high-grade serous ovarian carcinogenesis from the fallopian tube.* Proc Natl Acad Sci U S A, 2011. **108**(18): p. 7547-52.
201. Hein, N., et al., *The nucleolus: an emerging target for cancer therapy.* Trends Mol Med, 2013. **19**(11): p. 643-54.
202. Hung, S.S., et al., *Cell cycle and growth stimuli regulate different steps of RNA polymerase I transcription.* Gene, 2017. **612**: p. 36-48.
203. Woods, S.J., et al., *The nucleolus as a fundamental regulator of the p53 response and a new target for cancer therapy.* Biochim Biophys Acta, 2015. **1849**(7): p. 821-9.
204. Quin, J.E., et al., *Targeting the nucleolus for cancer intervention.* Biochim Biophys Acta, 2014. **1842**(6): p. 802-16.
205. Hannan, R.D., D. Drygin, and R.B. Pearson, *Targeting RNA polymerase I transcription and the nucleolus for cancer therapy.* Expert opinion on therapeutic targets, 2013. **17**(8): p. 873-878.
206. Hannan, K.M., et al., *Dysregulation of RNA polymerase I transcription during disease.* Biochim Biophys Acta, 2013. **1829**(3-4): p. 342-60.
207. Bywater, M.J., et al., *Inhibition of RNA polymerase I as a therapeutic strategy to promote cancer-specific activation of p53.* Cancer Cell, 2012. **22**(1): p. 51-65.
208. Yan, S., et al., *The Potential of Targeting Ribosome Biogenesis in High-Grade Serous Ovarian Cancer.* Int J Mol Sci, 2017. **18**(1).
209. Sobell, H.M., *Actinomycin and DNA transcription.* Proc Natl Acad Sci U S A, 1985. **82**(16): p. 5328-31.
210. Harris, C.C., *The carcinogenicity of anticancer drugs: a hazard in man.* Cancer, 1976. **37**(2 Suppl): p. 1014-23.
211. Peltonen, K., et al., *Identification of novel p53 pathway activating small-molecule compounds reveals unexpected similarities with known therapeutic agents.* PLoS One, 2010. **5**(9): p. e12996.
212. Peltonen, K., et al., *A Targeting Modality for Destruction of RNA Polymerase I that Possesses Anticancer Activity.* Cancer Cell, 2014. **25**(1): p. 77-90.
213. Wei, T., et al., *Small-Molecule Targeting of RNA Polymerase I Activates a Conserved Transcription Elongation Checkpoint.* Cell Rep, 2018. **23**(2): p. 404-414.
214. Fu, X., et al., *BMH-21 inhibits viability and induces apoptosis by p53-dependent nucleolar stress responses in SKOV3 ovarian cancer cells.* Oncol Rep, 2017. **38**(2): p. 859-865.
215. Colis, L., et al., *DNA intercalator BMH-21 inhibits RNA polymerase I independent of DNA damage response.* Oncotarget, 2014. **5**(12): p. 4361-9.

216. Drygin, D., et al., *Targeting RNA polymerase I with an oral small molecule CX-5461 inhibits ribosomal RNA synthesis and solid tumor growth.* Cancer Res, 2011. **71**(4): p. 1418-30.
217. Haddach, M., et al., *Discovery of CX-5461, the first direct and selective inhibitor of RNA polymerase I, for cancer therapeutics.* ACS Medicinal Chemistry Letters, 2012. **3**(7): p. 602-606.
218. Drygin, D., et al., *Targeting RNA Polymerase I with an Oral Small Molecule CX-5461 Inhibits Ribosomal RNA Synthesis and Solid Tumor Growth.* Cancer Research, 2011. **71**(4): p. 1418-1430.
219. Khot, A., et al., *First-in-Human RNA Polymerase I Transcription Inhibitor CX-5461 in Patients with Advanced Hematologic Cancers: Results of a Phase I Dose-Escalation Study.* Cancer Discovery, 2019. **9**(8): p. 1036.
220. Quin, J., et al., *Inhibition of RNA polymerase I transcription initiation by CX-5461 activates non-canonical ATM/ATR signaling.* Oncotarget, 2016.
221. Bywater, M.J., et al., *Inhibition of RNA polymerase I as a therapeutic strategy to promote cancer-specific activation of p53.* Cancer cell, 2012. **22**(1): p. 51-65.
222. Macias, E., et al., *An ARF-independent c-MYC-activated tumor suppression pathway mediated by ribosomal protein-Mdm2 Interaction.* Cancer Cell, 2010. **18**(3): p. 231-43.
223. Negi, S.S. and P. Brown, *rRNA synthesis inhibitor, CX-5461, activates ATM/ATR pathway in acute lymphoblastic leukemia, arrests cells in G2 phase and induces apoptosis.* Oncotarget, 2015. **6**(20): p. 18094-104.
224. Negi, S.S. and P. Brown, *Transient rRNA synthesis inhibition with CX-5461 is sufficient to elicit growth arrest and cell death in acute lymphoblastic leukemia cells.* Oncotarget, 2015. **6**(33): p. 34846-34858.
225. Xu, H., et al., *CX-5461 is a DNA G-quadruplex stabilizer with selective lethality in BRCA1/2 deficient tumours.* Nat Commun, 2017. **8**: p. 14432.
226. Rebello, R.J., et al., *The Dual Inhibition of RNA Pol I Transcription and PIM Kinase as a New Therapeutic Approach to Treat Advanced Prostate Cancer.* Clin Cancer Res, 2016. **22**(22): p. 5539-5552.
227. Lee, H.C., et al., *RNA Polymerase I Inhibition with CX-5461 as a Novel Therapeutic Strategy to Target MYC in Multiple Myeloma.* Br J Haematol, 2017. **177**(1): p. 80-94.
228. Hein, N., et al., *Inhibition of Pol I transcription treats murine and human AML by targeting the leukemia-initiating cell population.* Blood, 2017.
229. Li, L., et al., *CX-5461 induces autophagy and inhibits tumor growth via mammalian target of rapamycin-related signaling pathways in osteosarcoma.* Onco Targets Ther, 2016. **9**: p. 5985-5997.
230. Devlin, J.R., et al., *Combination therapy targeting ribosome biogenesis and mRNA translation synergistically extends survival in MYC-driven lymphoma.* Cancer Discovery, 2015.
231. Jackson, S.P. and J. Bartek, *The DNA-damage response in human biology and disease.* Nature, 2009. **461**(7267): p. 1071-8.
232. Brown, J.S., et al., *Targeting DNA Repair in Cancer: Beyond PARP Inhibitors.* Cancer Discov, 2017. **7**(1): p. 20-37.
233. O'Connor, M.J., *Targeting the DNA Damage Response in Cancer.* Mol Cell, 2015. **60**(4): p. 547-60.
234. Seluanov, A., Z. Mao, and V. Gorbunova, *Analysis of DNA double-strand break (DSB) repair in mammalian cells.* J Vis Exp, 2010(43).

235. Mahaney, B.L., K. Meek, and S.P. Lees-Miller, *Repair of ionizing radiation-induced DNA double-strand breaks by non-homologous end-joining.* Biochem J, 2009. **417**(3): p. 639-50.
236. Alvarez-Quilon, A., et al., *ATM specifically mediates repair of double-strand breaks with blocked DNA ends.* Nat Commun, 2014. **5**: p. 3347.
237. Saleh-Gohari, N., et al., *Spontaneous Homologous Recombination Is Induced by Collapsed Replication Forks That Are Caused by Endogenous DNA Single-Strand Breaks.* Molecular and Cellular Biology, 2005. **25**(16): p. 7158.
238. Jekimovs, C., et al., *Chemotherapeutic compounds targeting the DNA double-strand break repair pathways: the good, the bad, and the promising.* Front Oncol, 2014. **4**: p. 86.
239. Mao, Z., et al., *DNA repair by nonhomologous end joining and homologous recombination during cell cycle in human cells.* Cell Cycle, 2008. **7**(18): p. 2902-6.
240. Goldstein, M. and M.B. Kastan, *The DNA damage response: implications for tumor responses to radiation and chemotherapy.* Annu Rev Med, 2015. **66**: p. 129-43.
241. Mao, Z., et al., *Comparison of nonhomologous end joining and homologous recombination in human cells.* DNA Repair (Amst), 2008. **7**(10): p. 1765-71.
242. Chang, H.H.Y., et al., *Non-homologous DNA end joining and alternative pathways to double-strand break repair.* Nat Rev Mol Cell Biol, 2017. **18**(8): p. 495-506.
243. Boboila, C., et al., *Alternative end-joining catalyzes class switch recombination in the absence of both Ku70 and DNA ligase 4.* The Journal of experimental medicine, 2010. **207**(2): p. 417-427.
244. Lee-Theilen, M., et al., *CtIP promotes microhomology-mediated alternative end joining during class-switch recombination.* Nature Structural &Amp; Molecular Biology, 2010. **18**: p. 75.
245. Rass, E., et al., *Role of Mre11 in chromosomal nonhomologous end joining in mammalian cells.* Nature Structural &Amp; Molecular Biology, 2009. **16**: p. 819.
246. Bennardo, N., et al., *Alternative-NHEJ is a mechanistically distinct pathway of mammalian chromosome break repair.* PLoS genetics, 2008. **4**(6): p. e1000110-e1000110.
247. Bétermier, M., P. Bertrand, and B.S. Lopez, *Is non-homologous end-joining really an inherently error-prone process?* PLoS genetics, 2014. **10**(1): p. e1004086-e1004086.
248. Jasin, M. and R. Rothstein, *Repair of strand breaks by homologous recombination.* Cold Spring Harb Perspect Biol, 2013. **5**(11): p. a012740.
249. Prakash, R., et al., *Homologous recombination and human health: the roles of BRCA1, BRCA2, and associated proteins.* Cold Spring Harb Perspect Biol, 2015. **7**(4): p. a016600.
250. Schiller, C.B., et al., *Structure of Mre11–Nbs1 complex yields insights into ataxia-telangiectasia–like disease mutations and DNA damage signaling.* Nature Structural &Amp; Molecular Biology, 2012. **19**: p. 693.
251. Feng, L., et al., *Cell cycle-dependent inhibition of 53BP1 signaling by BRCA1.* Cell Discovery, 2015. **1**: p. 15019.
252. Bunting, S.F., et al., *53BP1 inhibits homologous recombination in Brca1-deficient cells by blocking resection of DNA breaks.* Cell, 2010. **141**(2): p. 243-254.
253. Smith, J., et al., *Chapter 3 - The ATM–Chk2 and ATR–Chk1 Pathways in DNA Damage Signaling and Cancer*, in *Advances in Cancer Research*, G.F. Vande Woude and G. Klein, Editors. 2010, Academic Press. p. 73-112.

254. Ma, C.J., et al., *Protein dynamics of human RPA and RAD51 on ssDNA during assembly and disassembly of the RAD51 filament.* Nucleic Acids Res, 2017. **45**(2): p. 749-761.
255. Haahr, P., et al., *Activation of the ATR kinase by the RPA-binding protein ETAA1.* Nature Cell Biology, 2016. **18**: p. 1196.
256. Short, J.M., et al., *High-resolution structure of the presynaptic RAD51 filament on single-stranded DNA by electron cryo-microscopy.* Nucleic Acids Research, 2016. **44**(19): p. 9017-9030.
257. Zhao, W., et al., *Promotion of BRCA2-Dependent Homologous Recombination by DSS1 via RPA Targeting and DNA Mimicry.* Molecular Cell, 2015. **59**(2): p. 176-187.
258. Ceballos, S.J. and W.D. Heyer, *Functions of the Snf2/Swi2 family Rad54 motor protein in homologous recombination.* Biochim Biophys Acta, 2011. **1809**(9): p. 509-23.
259. Solinger, J.A., K. Kiianitsa, and W.D. Heyer, *Rad54, a Swi2/Snf2-like recombinational repair protein, disassembles Rad51:dsDNA filaments.* Mol Cell, 2002. **10**(5): p. 1175-88.
260. Forget, A.L. and S.C. Kowalczykowski, *Single-molecule imaging brings Rad51 nucleoprotein filaments into focus.* Trends in Cell Biology, 2010. **20**(5): p. 269-276.
261. Jackson, S.P., *Sensing and repairing DNA double-strand breaks.* Carcinogenesis, 2002. **23**(5): p. 687-96.
262. Lieber, M.R., *The Mechanism of Double-Strand DNA Break Repair by the Nonhomologous DNA End Joining Pathway.* Annual review of biochemistry, 2010. **79**: p. 181-211.
263. Zhang, F., Y. Wen, and X. Guo, *CRISPR/Cas9 for genome editing: progress, implications and challenges.* Hum Mol Genet, 2014. **23**(R1): p. R40-6.
264. Zhao, X., et al., *Cell cycle-dependent control of homologous recombination.* Acta Biochim Biophys Sin (Shanghai), 2017. **49**(8): p. 655-668.
265. Hunter, N., *Meiotic Recombination: The Essence of Heredity.* Cold Spring Harb Perspect Biol, 2015. **7**(12).
266. Sharma, V., et al., *A BRCA1-interacting lncRNA regulates homologous recombination.* EMBO Rep, 2015. **16**(11): p. 1520-34.
267. Ledermann, J.A., Y. Drew, and R.S. Kristeleit, *Homologous recombination deficiency and ovarian cancer.* Eur J Cancer, 2016. **60**: p. 49-58.
268. Kelley, M.R., D. Logsdon, and M.L. Fishel, *Targeting DNA repair pathways for cancer treatment: what's new?* Future Oncol, 2014. **10**(7): p. 1215-37.
269. Quintas-Cardama, A. and J. Cortes, *Molecular biology of bcr-abl1-positive chronic myeloid leukemia.* Blood, 2009. **113**(8): p. 1619-30.
270. Krokan, H.E., R. Standal, and G. Slupphaug, *DNA glycosylases in the base excision repair of DNA.* The Biochemical journal, 1997. **325 ( Pt 1)**(Pt 1): p. 1-16.
271. Parsons, J.L., I.I. Dianova, and G.L. Dianov, *APE1 is the major 3'-phosphoglycolate activity in human cell extracts.* Nucleic acids research, 2004. **32**(12): p. 3531-3536.
272. Fortini, P., et al., *The type of DNA glycosylase determines the base excision repair pathway in mammalian cells.* J Biol Chem, 1999. **274**(21): p. 15230-6.
273. Pascucci, B., et al., *Long patch base excision repair with purified human proteins. DNA ligase I as patch size mediator for DNA polymerases delta and epsilon.* J Biol Chem, 1999. **274**(47): p. 33696-702.

274. Sukhanova, M.V., et al., *Human base excision repair enzymes apurinic/apyrimidinic endonuclease1 (APE1), DNA polymerase beta and poly(ADP-ribose) polymerase 1: interplay between strand-displacement DNA synthesis and proofreading exonuclease activity.* Nucleic Acids Res, 2005. **33**(4): p. 1222-9.
275. Curtin, N.J., *DNA repair dysregulation from cancer driver to therapeutic target.* Nat Rev Cancer, 2012. **12**(12): p. 801-17.
276. Caldecott, K.W., *Single-strand break repair and genetic disease.* Nat Rev Genet, 2008. **9**(8): p. 619-31.
277. Reynolds, P., et al., *Disruption of PARP1 function inhibits base excision repair of a sub-set of DNA lesions.* Nucleic acids research, 2015. **43**(8): p. 4028-4038.
278. Li, G.-M., *Mechanisms and functions of DNA mismatch repair.* Cell Research, 2007. **18**: p. 85.
279. Nakagawa, T., A. Datta, and R.D. Kolodner, *Multiple functions of MutS-and MutL-related heterocomplexes.* Proceedings of the National Academy of Sciences, 1999. **96**(25): p. 14186-14188.
280. Nielsen, F.C., et al., *Characterization of human exonuclease 1 in complex with mismatch repair proteins, subcellular localization and association with PCNA.* Oncogene, 2004. **23**(7): p. 1457-68.
281. Spry, M., et al., *DNA repair pathways and hereditary cancer susceptibility syndromes.* Front Biosci, 2007. **12**: p. 4191-207.
282. Pommier, Y., et al., *Tyrosyl-DNA-phosphodiesterases (TDP1 and TDP2).* DNA Repair (Amst), 2014. **19**: p. 114-29.
283. Murai, J., et al., *Tyrosyl-DNA phosphodiesterase 1 (TDP1) repairs DNA damage induced by topoisomerases I and II and base alkylation in vertebrate cells.* The Journal of biological chemistry, 2012. **287**(16): p. 12848-12857.
284. Pouliot, J.J., et al., *Yeast Gene for a Tyr-DNA Phosphodiesterase that Repairs Topoisomerase I Complexes.* Science, 1999. **286**(5439): p. 552.
285. Berthelot, V., et al., *The human DNA ends proteome uncovers an unexpected entanglement of functional pathways.* Nucleic acids research, 2016. **44**(10): p. 4721-4733.
286. Cai, Y., N.E. Geacintov, and S. Broyde, *Nucleotide Excision Repair Efficiencies of Bulky Carcinogen–DNA Adducts Are Governed by a Balance between Stabilizing and Destabilizing Interactions.* Biochemistry, 2012. **51**(7): p. 1486-1499.
287. Wood, R.D., *Mammalian nucleotide excision repair proteins and interstrand crosslink repair.* Environ Mol Mutagen, 2010. **51**(6): p. 520-6.
288. Marteijn, J.A., et al., *Understanding nucleotide excision repair and its roles in cancer and ageing.* Nature Reviews Molecular Cell Biology, 2014. **15**: p. 465.
289. de Waard, H., et al., *Different effects of CSA and CSB deficiency on sensitivity to oxidative DNA damage.* Molecular and cellular biology, 2004. **24**(18): p. 7941-7948.
290. Neher, T.M., et al., *Photo-cross-linking of XPC-Rad23B to cisplatin-damaged DNA reveals contacts with both strands of the DNA duplex and spans the DNA adduct.* Biochemistry, 2010. **49**(4): p. 669-678.
291. Kokic, G., et al., *Structural basis of TFIIH activation for nucleotide excision repair.* Nature Communications, 2019. **10**(1): p. 2885.
292. Saijo, M., et al., *Inhibition of nucleotide excision repair by anti-XPA monoclonal antibodies which interfere with binding to RPA, ERCC1, and TFIIH.* Biochemical and Biophysical Research Communications, 2004. **321**(4): p. 815-822.

293. Fadda, E., *Role of the XPA protein in the NER pathway: A perspective on the function of structural disorder in macromolecular assembly.* Computational and Structural Biotechnology Journal, 2016. **14**: p. 78-85.
294. McNeil, E.M. and D.W. Melton, *DNA repair endonuclease ERCC1-XPF as a novel therapeutic target to overcome chemoresistance in cancer therapy.* Nucleic acids research, 2012. **40**(20): p. 9990-10004.
295. Graf, N., et al., *Role of endonucleases XPF and XPG in nucleotide excision repair of platinated DNA and cisplatin/oxaliplatin cytotoxicity.* Chembiochem : a European journal of chemical biology, 2011. **12**(7): p. 1115-1123.
296. Roy, U. and O.D. Schärer, *Involvement of translesion synthesis DNA polymerases in DNA interstrand crosslink repair.* DNA Repair, 2016. **44**: p. 33-41.
297. Jones, M.J. and T.T. Huang, *The Fanconi anemia pathway in replication stress and DNA crosslink repair.* Cell Mol Life Sci, 2012. **69**(23): p. 3963-74.
298. Deans, A.J. and S.C. West, *DNA interstrand crosslink repair and cancer.* Nature Reviews Cancer, 2011. **11**: p. 467.
299. Rodríguez, A. and A. D'Andrea, *Fanconi anemia pathway.* Current Biology, 2017. **27**(18): p. R986-R988.
300. Yang, H., et al., *Structural insights into the functions of the FANCM-FAAP24 complex in DNA repair.* Nucleic acids research, 2013. **41**(22): p. 10573-10583.
301. Singh, T.R., et al., *ATR-dependent phosphorylation of FANCM at serine 1045 is essential for FANCM functions.* Cancer research, 2013. **73**(14): p. 4300-4310.
302. Collins, N.B., et al., *ATR-dependent phosphorylation of FANCA on serine 1449 after DNA damage is important for FA pathway function.* Blood, 2009. **113**(10): p. 2181.
303. Guervilly, J.H., G. Mace-Aime, and F. Rosselli, *Loss of CHK1 function impedes DNA damage-induced FANCD2 monoubiquitination but normalizes the abnormal G2 arrest in Fanconi anemia.* Hum Mol Genet, 2008. **17**(5): p. 679-89.
304. Liang, C.-C., et al., *The FANCD2–FANCI complex is recruited to DNA interstrand crosslinks before monoubiquitination of FANCD2.* Nature Communications, 2016. **7**: p. 12124.
305. Longerich, S., et al., *Regulation of FANCD2 and FANCI monoubiquitination by their interaction and by DNA.* Nucleic Acids Research, 2014. **42**(9): p. 5657-5670.
306. Klein Douwel, D., et al., *XPF-ERCC1 Acts in Unhooking DNA Interstrand Crosslinks in Cooperation with FANCD2 and FANCP/SLX4.* Molecular Cell, 2014. **54**(3): p. 460-471.
307. Raschle, M., et al., *Mechanism of replication-coupled DNA interstrand crosslink repair.* Cell, 2008. **134**(6): p. 969-80.
308. Michl, J., J. Zimmer, and M. Tarsounas, *Interplay between Fanconi anemia and homologous recombination pathways in genome integrity.* The EMBO Journal, 2016. **35**(9): p. 909-923.
309. Kottemann, M.C. and A. Smogorzewska, *Fanconi anemia and the repair of Watson and Crick crosslinks.* Nature, 2013. **493**(7432): p. 356-363.
310. Kim, H. and A.D. D'Andrea, *Regulation of DNA cross-link repair by the Fanconi anemia/BRCA pathway.* Genes & Development, 2012. **26**(13): p. 1393-1408.
311. Deans, A.J. and S.C. West, *DNA interstrand crosslink repair and cancer.* Nat Rev Cancer, 2011. **11**(7): p. 467-80.
312. Moriwaki, S., *Hereditary Disorders with Defective Repair of UV-Induced DNA Damage.* Jpn Clin Med, 2013. **4**: p. 29-35.
313. Zeman, M.K. and K.A. Cimprich, *Causes and consequences of replication stress.* Nat Cell Biol, 2014. **16**(1): p. 2-9.

314. Vassin, V.M., et al., *Human RPA phosphorylation by ATR stimulates DNA synthesis and prevents ssDNA accumulation during DNA-replication stress.* Journal of Cell Science, 2009. **122**(22): p. 4070.
315. Toledo, Luis I., et al., *ATR Prohibits Replication Catastrophe by Preventing Global Exhaustion of RPA.* Cell, 2013. **155**(5): p. 1088-1103.
316. Moiseeva, T.N., et al., *An ATR and CHK1 kinase signaling mechanism that limits origin firing during unperturbed DNA replication.* Proceedings of the National Academy of Sciences, 2019. **116**(27): p. 13374.
317. Iyer, D.R. and N. Rhind, *The Intra-S Checkpoint Responses to DNA Damage.* Genes (Basel), 2017. **8**(2).
318. Taylor, M.R.G. and J.T.P. Yeeles, *Dynamics of Replication Fork Progression Following Helicase–Polymerase Uncoupling in Eukaryotes.* Journal of Molecular Biology, 2019. **431**(10): p. 2040-2049.
319. Acevedo, J., S. Yan, and W.M. Michael, *Direct Binding to Replication Protein A (RPA)-coated Single-stranded DNA Allows Recruitment of the ATR Activator TopBP1 to Sites of DNA Damage.* J Biol Chem, 2016. **291**(25): p. 13124-31.
320. Lindsey-Boltz, L.A., et al., *In vitro analysis of the role of replication protein A (RPA) and RPA phosphorylation in ATR-mediated checkpoint signaling.* J Biol Chem, 2012. **287**(43): p. 36123-31.
321. Choi, J.H., et al., *Reconstitution of RPA-covered single-stranded DNA-activated ATR-Chk1 signaling.* Proc Natl Acad Sci U S A, 2010. **107**(31): p. 13660-5.
322. Marechal, A. and L. Zou, *DNA damage sensing by the ATM and ATR kinases.* Cold Spring Harb Perspect Biol, 2013. **5**(9).
323. Lemaçon, D., et al., *MRE11 and EXO1 nucleases degrade reversed forks and elicit MUS81-dependent fork rescue in BRCA2-deficient cells.* Nature Communications, 2017. **8**(1): p. 860.
324. Mehta, A. and J.E. Haber, *Sources of DNA double-strand breaks and models of recombinational DNA repair.* Cold Spring Harb Perspect Biol, 2014. **6**(9): p. a016428.
325. Sanij, E., et al., *Inhibition of RNA Polymerase I Transcription Activates Targeted DNA Damage Response and Enhances the Efficacy of PARP Inhibitors in High-Grade Serous Ovarian Cancer.* bioRxiv, 2019: p. 621623.
326. Rhind, N. and P. Russell, *Signaling pathways that regulate cell division.* Cold Spring Harbor perspectives in biology, 2012. **4**(10): p. a005942.
327. So, S., A.J. Davis, and D.J. Chen, *Autophosphorylation at serine 1981 stabilizes ATM at DNA damage sites.* The Journal of Cell Biology, 2009. **187**(7): p. 977.
328. Liu, S., et al., *ATR autophosphorylation as a molecular switch for checkpoint activation.* Molecular cell, 2011. **43**(2): p. 192-202.
329. Liu, S., et al., *Distinct roles for DNA-PK, ATM and ATR in RPA phosphorylation and checkpoint activation in response to replication stress.* Nucleic Acids Res, 2012. **40**(21): p. 10780-94.
330. Shrivastav, M., L.P. De Haro, and J.A. Nickoloff, *Regulation of DNA double-strand break repair pathway choice.* Cell Res, 2008. **18**(1): p. 134-47.
331. Zhou, Y., et al., *Regulation of the DNA Damage Response by DNA-PKcs Inhibitory Phosphorylation of ATM.* Mol Cell, 2017. **65**(1): p. 91-104.
332. Shang, Z., et al., *DNA-PKcs activates the Chk2-Brca1 pathway during mitosis to ensure chromosomal stability.* Oncogenesis, 2014. **3**: p. e85.

333. DiTullio, R.A., Jr., et al., *53BP1 functions in an ATM-dependent checkpoint pathway that is constitutively activated in human cancer.* Nat Cell Biol, 2002. **4**(12): p. 998-1002.
334. Fernandez-Capetillo, O., et al., *DNA damage-induced G2-M checkpoint activation by histone H2AX and 53BP1.* Nat Cell Biol, 2002. **4**(12): p. 993-7.
335. White, D.E., et al., *KAP1, a Novel Substrate for PIKK Family Members, Colocalizes with Numerous Damage Response Factors at DNA Lesions.* Cancer Research, 2006. **66**(24): p. 11594.
336. Bochkareva, E., et al., *The RPA32 Subunit of Human Replication Protein A Contains a Single-stranded DNA-binding Domain.* Journal of Biological Chemistry, 1998. **273**(7): p. 3932-3936.
337. Chen, R. and M.S. Wold, *Replication protein A: single-stranded DNA's first responder: dynamic DNA-interactions allow replication protein A to direct single-strand DNA intermediates into different pathways for synthesis or repair.* Bioessays, 2014. **36**(12): p. 1156-61.
338. Derheimer, F.A., et al., *RPA and ATR link transcriptional stress to p53.* Proceedings of the National Academy of Sciences of the United States of America, 2007. **104**(31): p. 12778-12783.
339. Liu, S., et al., *Distinct roles for DNA-PK, ATM and ATR in RPA phosphorylation and checkpoint activation in response to replication stress.* Nucleic acids research, 2012. **40**(21): p. 10780-10794.
340. Vassin, V.M., et al., *Human RPA phosphorylation by ATR stimulates DNA synthesis and prevents ssDNA accumulation during DNA-replication stress.* Journal of cell science, 2009. **122**(Pt 22): p. 4070-4080.
341. Maréchal, A. and L. Zou, *RPA-coated single-stranded DNA as a platform for post-translational modifications in the DNA damage response.* Cell research, 2015. **25**(1): p. 9-23.
342. Callen, E., et al., *53BP1 mediates productive and mutagenic DNA repair through distinct phosphoprotein interactions.* Cell, 2013. **153**(6): p. 1266-80.
343. Jowsey, P., et al., *Characterisation of the sites of DNA damage-induced 53BP1 phosphorylation catalysed by ATM and ATR.* DNA Repair (Amst), 2007. **6**(10): p. 1536-44.
344. Wilson, K.A. and D.F. Stern, *NFBD1/MDC1, 53BP1 and BRCA1 have both redundant and unique roles in the ATM pathway.* Cell Cycle, 2008. **7**(22): p. 3584-94.
345. Mirza-Aghazadeh-Attari, M., et al., *53BP1: A key player of DNA damage response with critical functions in cancer.* DNA Repair (Amst), 2019. **73**: p. 110-119.
346. Bunting, S.F., et al., *53BP1 inhibits homologous recombination in Brca1-deficient cells by blocking resection of DNA breaks.* Cell, 2010. **141**(2): p. 243-54.
347. Bouwman, P., et al., *53BP1 loss rescues BRCA1 deficiency and is associated with triple-negative and BRCA-mutated breast cancers.* Nat Struct Mol Biol, 2010. **17**(6): p. 688-95.
348. Scully, R., et al., *DNA double-strand break repair-pathway choice in somatic mammalian cells.* Nat Rev Mol Cell Biol, 2019.
349. Escribano-Diaz, C., et al., *A cell cycle-dependent regulatory circuit composed of 53BP1-RIF1 and BRCA1-CtIP controls DNA repair pathway choice.* Mol Cell, 2013. **49**(5): p. 872-83.
350. Sartori, A.A., et al., *Human CtIP promotes DNA end resection.* Nature, 2007. **450**(7169): p. 509-14.

351. Capasso, H., et al., *Phosphorylation activates Chk1 and is required for checkpoint-mediated cell cycle arrest.* Journal of Cell Science, 2002. **115**(23): p. 4555.
352. Donzelli, M. and G.F. Draetta, *Regulating mammalian checkpoints through Cdc25 inactivation.* EMBO reports, 2003. **4**(7): p. 671-677.
353. Xiao, Z., et al., *Chk1 Mediates S and G2 Arrests through Cdc25A Degradation in Response to DNA-damaging Agents.* Journal of Biological Chemistry, 2003. **278**(24): p. 21767-21773.
354. Saini, P., Y. Li, and M. Dobbelstein, *Wee1 is required to sustain ATR/Chk1 signaling upon replicative stress.* Oncotarget, 2015. **6**(15): p. 13072-13087.
355. O'Connell, M.J., et al., *Chk1 is a wee1 kinase in the G2 DNA damage checkpoint inhibiting cdc2 by Y15 phosphorylation.* The EMBO Journal, 1997. **16**(3): p. 545-554.
356. Shang, Z.-F., et al., *Inactivation of DNA-Dependent Protein Kinase Leads to Spindle Disruption and Mitotic Catastrophe with Attenuated Checkpoint Protein 2 Phosphorylation in Response to DNA Damage.* Cancer Research, 2010. **70**(9): p. 3657.
357. Matsuoka, S., et al., *Ataxia telangiectasia-mutated phosphorylates Chk2 in vivo and in vitro.* Proceedings of the National Academy of Sciences of the United States of America, 2000. **97**(19): p. 10389-10394.
358. Connell, M.J., et al., *Chk1 is a wee1 kinase in the G<sub>2</sub> DNA damage checkpoint inhibiting cdc2 by Y15 phosphorylation.* The EMBO Journal, 1997. **16**(3): p. 545.
359. Agarwal, C., A. Tyagi, and R. Agarwal, *Gallic acid causes inactivating phosphorylation of cdc25A/cdc25C-cdc2 via ATM-Chk2 activation, leading to cell cycle arrest, and induces apoptosis in human prostate carcinoma DU145 cells.* Molecular Cancer Therapeutics, 2006. **5**(12): p. 3294.
360. Qin, J.L., et al., *Oxoaporphine Metal Complexes (Co(II), Ni(II), Zn(II)) with High Antitumor Activity by Inducing Mitochondria-Mediated Apoptosis and S-phase Arrest in HepG2.* Sci Rep, 2017. **7**: p. 46056.
361. Haupt, S., et al., *Apoptosis - the p53 network.* J Cell Sci, 2003. **116**(Pt 20): p. 4077-85.
362. Turenne, G.A., et al., *Activation of p53 transcriptional activity requires ATM's kinase domain and multiple N-terminal serine residues of p53.* Oncogene, 2001. **20**(37): p. 5100-10.
363. Cheng, Q. and J. Chen, *Mechanism of p53 stabilization by ATM after DNA damage.* Cell Cycle, 2010. **9**(3): p. 472-8.
364. Donehower, L.A., *Phosphatases reverse p53-mediated cell cycle checkpoints.* Proc Natl Acad Sci U S A, 2014. **111**(20): p. 7172-3.
365. Hu, C., et al., *Roles of Kruppel-associated Box (KRAB)-associated Co-repressor KAP1 Ser-473 Phosphorylation in DNA Damage Response.* J Biol Chem, 2012. **287**(23): p. 18937-52.
366. Burma, S., et al., *ATM phosphorylates histone H2AX in response to DNA double-strand breaks.* J Biol Chem, 2001. **276**(45): p. 42462-7.
367. Podhorecka, M., A. Skladanowski, and P. Bozko, *H2AX Phosphorylation: Its Role in DNA Damage Response and Cancer Therapy.* J Nucleic Acids, 2010. **2010**.
368. Ward, I.M. and J. Chen, *Histone H2AX Is Phosphorylated in an ATR-dependent Manner in Response to Replicational Stress.* Journal of Biological Chemistry, 2001. **276**(51): p. 47759-47762.

369. Stucki, M., et al., *MDC1 directly binds phosphorylated histone H2AX to regulate cellular responses to DNA double-strand breaks.* Cell, 2005. **123**(7): p. 1213-26.
370. Mailand, N., et al., *RNF8 Ubiquitylates Histones at DNA Double-Strand Breaks and Promotes Assembly of Repair Proteins.* Cell, 2007. **131**(5): p. 887-900.
371. Huen, M.S.Y., et al., *RNF8 Transduces the DNA-Damage Signal via Histone Ubiquitylation and Checkpoint Protein Assembly.* Cell, 2007. **131**(5): p. 901-914.
372. Thorslund, T., et al., *Histone H1 couples initiation and amplification of ubiquitin signalling after DNA damage.* Nature, 2015. **527**: p. 389.
373. Mattiroli, F., et al., *RNF168 Ubiquitinates K13-15 on H2A/H2AX to Drive DNA Damage Signaling.* Cell, 2012. **150**(6): p. 1182-1195.
374. Fradet-Turcotte, A., et al., *53BP1 is a reader of the DNA-damage-induced H2A Lys 15 ubiquitin mark.* Nature, 2013. **499**: p. 50.
375. Chen, Q., L. Sun, and Z.J. Chen, *Regulation and function of the cGAS-STING pathway of cytosolic DNA sensing.* Nat Immunol, 2016. **17**(10): p. 1142-9.
376. Li, T. and Z.J. Chen, *The cGAS–cGAMP–STING pathway connects DNA damage to inflammation, senescence, and cancer.* The Journal of Experimental Medicine, 2018. **215**(5): p. 1287.
377. Dunphy, G., et al., *Non-canonical Activation of the DNA Sensing Adaptor STING by ATM and IFI16 Mediates NF-κB Signaling after Nuclear DNA Damage.* Molecular cell, 2018. **71**(5): p. 745-760.e5.
378. Lengauer, C., K.W. Kinzler, and B. Vogelstein, *Genetic instabilities in human cancers.* Nature, 1998. **396**(6712): p. 643-9.
379. Pikor, L., et al., *The detection and implication of genome instability in cancer.* Cancer Metastasis Rev, 2013. **32**(3-4): p. 341-52.
380. Civril, F., et al., *Structural mechanism of cytosolic DNA sensing by cGAS.* Nature, 2013. **498**: p. 332.
381. Tanaka, Y. and Z.J. Chen, *STING Specifies IRF3 Phosphorylation by TBK1 in the Cytosolic DNA Signaling Pathway.* Science Signaling, 2012. **5**(214): p. ra20.
382. Yanai, H., et al., *Revisiting the role of IRF3 in inflammation and immunity by conditional and specifically targeted gene ablation in mice.* Proceedings of the National Academy of Sciences, 2018. **115**(20): p. 5253.
383. Li, T. and Z.J. Chen, *The cGAS-cGAMP-STING pathway connects DNA damage to inflammation, senescence, and cancer.* J Exp Med, 2018. **215**(5): p. 1287-1299.
384. Yang, H., et al., *cGAS is essential for cellular senescence.* Proceedings of the National Academy of Sciences, 2017. **114**(23): p. E4612.
385. Dou, Z., et al., *Cytoplasmic chromatin triggers inflammation in senescence and cancer.* Nature, 2017. **550**: p. 402.
386. Takaoka, A., et al., *Integration of interferon-alpha/beta signalling to p53 responses in tumour suppression and antiviral defence.* Nature, 2003. **424**(6948): p. 516-23.
387. Kuilman, T., et al., *Oncogene-induced senescence relayed by an interleukin-dependent inflammatory network.* Cell, 2008. **133**(6): p. 1019-31.
388. Acosta, J.C., et al., *Chemokine signaling via the CXCR2 receptor reinforces senescence.* Cell, 2008. **133**(6): p. 1006-18.
389. Coppe, J.P., et al., *The senescence-associated secretory phenotype: the dark side of tumor suppression.* Annu Rev Pathol, 2010. **5**: p. 99-118.
390. Chan, M.W., et al., *Hypermethylation of 18S and 28S ribosomal DNAs predicts progression-free survival in patients with ovarian cancer.* Clin Cancer Res, 2005. **11**(20): p. 7376-83.

391. Powell, M.A., et al., *Ribosomal DNA methylation in patients with endometrial carcinoma: an independent prognostic marker.* Cancer, 2002. **94**(11): p. 2941-52.
392. Zimmer, J., et al., *Targeting BRCA1 and BRCA2 Deficiencies with G-Quadruplex-Interacting Compounds.* Mol Cell, 2016. **61**(3): p. 449-460.
393. Schindelin, J., et al., *Fiji: an open-source platform for biological-image analysis.* Nat Methods, 2012. **9**(7): p. 676-82.
394. Carpenter, A.E., et al., *CellProfiler: image analysis software for identifying and quantifying cell phenotypes.* Genome Biol, 2006. **7**(10): p. R100.
395. Gyori, B.M., et al., *OpenComet: an automated tool for comet assay image analysis.* Redox Biol, 2014. **2**: p. 457-65.
396. Di Veroli, G.Y., et al., *Combenefit: an interactive platform for the analysis and visualization of drug combinations.* Bioinformatics, 2016. **32**(18): p. 2866-8.
397. Chou, T.-C., *The combination index (CI < 1) as the definition of synergism and of synergy claims.* Synergy, 2018.
398. Pereira, D.A. and J.A. Williams, *Origin and evolution of high throughput screening.* Br J Pharmacol, 2007. **152**(1): p. 53-61.
399. Macarron, R., et al., *Impact of high-throughput screening in biomedical research.* Nat Rev Drug Discov, 2011. **10**(3): p. 188-95.
400. Powell, D.J., R.P. Hertzberg, and R. Macarromicronn, *Design and Implementation of High-Throughput Screening Assays.* Methods Mol Biol, 2016. **1439**: p. 1-32.
401. Gao, S., et al., *Applications of RNA interference high-throughput screening technology in cancer biology and virology.* Protein Cell, 2014. **5**(11): p. 805-15.
402. Shalem, O., N.E. Sanjana, and F. Zhang, *High-throughput functional genomics using CRISPR-Cas9.* Nat Rev Genet, 2015. **16**(5): p. 299-311.
403. Fire, A., et al., *Potent and specific genetic interference by double-stranded RNA in Caenorhabditis elegans.* Nature, 1998. **391**(6669): p. 806-11.
404. Rao, D.D., et al., *siRNA vs. shRNA: similarities and differences.* Adv Drug Deliv Rev, 2009. **61**(9): p. 746-59.
405. Rand, T.A., et al., *Argonaute2 Cleaves the Anti-Guide Strand of siRNA during RISC Activation.* Cell, 2005. **123**(4): p. 621-629.
406. Wei, J.-X., et al., *Both Strands of siRNA Have Potential to Guide Posttranscriptional Gene Silencing in Mammalian Cells.* PLOS ONE, 2009. **4**(4): p. e5382.
407. Zhang, J., et al., *Modification of the siRNA passenger strand by 5-nitroindole dramatically reduces its off-target effects.* Chembiochem, 2012. **13**(13): p. 1940-5.
408. Jackson, A.L. and P.S. Linsley, *Recognizing and avoiding siRNA off-target effects for target identification and therapeutic application.* Nat Rev Drug Discov, 2010. **9**(1): p. 57-67.
409. Macarron, R. and R.P. Hertzberg, *Design and implementation of high throughput screening assays.* Mol Biotechnol, 2011. **47**(3): p. 270-85.
410. Wang, T., et al., *Genetic Screens in Human Cells Using the CRISPR-Cas9 System.* Science, 2014. **343**(6166): p. 80.
411. Ran, F.A., et al., *Genome engineering using the CRISPR-Cas9 system.* Nature Protocols, 2013. **8**: p. 2281.
412. Hsu, P.D., E.S. Lander, and F. Zhang, *Development and applications of CRISPR-Cas9 for genome engineering.* Cell, 2014. **157**(6): p. 1262-78.
413. Boettcher, M. and M.T. McManus, *Choosing the Right Tool for the Job: RNAi, TALEN, or CRISPR.* Mol Cell, 2015. **58**(4): p. 575-85.
414. Morgens, D.W., et al., *Systematic comparison of CRISPR/Cas9 and RNAi screens for essential genes.* Nat Biotechnol, 2016. **34**(6): p. 634-6.

415. Zhang, X.H., et al., *Off-target Effects in CRISPR/Cas9-mediated Genome Engineering.* Mol Ther Nucleic Acids, 2015. **4**: p. e264.
416. Schaefer, K.A., et al., *Unexpected mutations after CRISPR-Cas9 editing in vivo.* Nat Methods, 2017. **14**(6): p. 547-548.
417. Eggert, U.S., C.M. Field, and T.J. Mitchison, *Small molecules in an RNAi world.* Mol Biosyst, 2006. **2**(2): p. 93-6.
418. Fellmann, C., et al., *Cornerstones of CRISPR-Cas in drug discovery and therapy.* Nature reviews. Drug discovery, 2017. **16**(2): p. 89-100.
419. Haapaniemi, E., et al., *CRISPR–Cas9 genome editing induces a p53-mediated DNA damage response.* Nature Medicine, 2018. **24**(7): p. 927-930.
420. Quin, J., et al., *Inhibition of RNA polymerase I transcription initiation by CX-5461 activates non-canonical ATM/ATR signaling.* Oncotarget, 2016. **7**(31): p. 49800-49818.
421. Cowley, G.S., et al., *Parallel genome-scale loss of function screens in 216 cancer cell lines for the identification of context-specific genetic dependencies.* Sci Data, 2014. **1**: p. 140035.
422. Ratner, E.S., et al., *Triapine potentiates platinum-based combination therapy by disruption of homologous recombination repair.* Br J Cancer, 2016. **114**(7): p. 777-86.
423. Ihnen, M., et al., *Therapeutic potential of the poly(ADP-ribose) polymerase inhibitor rucaparib for the treatment of sporadic human ovarian cancer.* Mol Cancer Ther, 2013. **12**(6): p. 1002-15.
424. Driscoll, D.L., et al., *Plk1 inhibition causes post-mitotic DNA damage and senescence in a range of human tumor cell lines.* PLoS One, 2014. **9**(11): p. e111060.
425. Liu, Z., Q. Sun, and X. Wang, *PLK1, A Potential Target for Cancer Therapy.* Transl Oncol, 2017. **10**(1): p. 22-32.
426. Spankuch-Schmitt, B., et al., *Effect of RNA silencing of polo-like kinase-1 (PLK1) on apoptosis and spindle formation in human cancer cells.* J Natl Cancer Inst, 2002. **94**(24): p. 1863-77.
427. Zhao, W., et al., *A New Bliss Independence Model to Analyze Drug Combination Data.* J Biomol Screen, 2014. **19**(5): p. 817-21.
428. Petraitis, V., et al., *Combination therapy in treatment of experimental pulmonary aspergillosis: in vitro and in vivo correlations of the concentration- and dose-dependent interactions between anidulafungin and voriconazole by Bliss independence drug interaction analysis.* Antimicrob Agents Chemother, 2009. **53**(6): p. 2382-91.
429. Modesti, M., et al., *RAD51AP1 Is a Structure-Specific DNA Binding Protein that Stimulates Joint Molecule Formation during RAD51-Mediated Homologous Recombination.* Molecular Cell, 2007. **28**(3): p. 468-481.
430. Goyal, N., et al., *RAD54 N-terminal domain is a DNA sensor that couples ATP hydrolysis with branch migration of Holliday junctions.* Nature Communications, 2018. **9**(1): p. 34.
431. Mazin, A.V., et al., *Rad54, the motor of homologous recombination.* DNA Repair (Amst), 2010. **9**(3): p. 286-302.
432. Heyer, W.D., et al., *Rad54: the Swiss Army knife of homologous recombination?* Nucleic Acids Res, 2006. **34**(15): p. 4115-25.
433. Holloman, W.K., *Unraveling the mechanism of BRCA2 in homologous recombination.* Nat Struct Mol Biol, 2011. **18**(7): p. 748-54.

434. Venkitaraman, A.R., *Functions of BRCA1 and BRCA2 in the biological response to DNA damage.* J Cell Sci, 2001. **114**.
435. Bebek, G., *Identifying Gene Interaction Networks.* Methods in molecular biology (Clifton, N.J.), 2012. **850**: p. 483-494.
436. Vallabhajosyula, R.R., et al., *Identifying hubs in protein interaction networks.* PLoS One, 2009. **4**(4): p. e5344.
437. He, X. and J. Zhang, *Why Do Hubs Tend to Be Essential in Protein Networks?* PLOS Genetics, 2006. **2**(6): p. e88.
438. Fan, P., et al., *The PPI network analysis of mRNA expression profile of uterus from primary dysmenorrheal rats.* Sci Rep, 2018. **8**(1): p. 351.
439. Xia, J., M.J. Benner, and R.E.W. Hancock, *NetworkAnalyst - integrative approaches for protein–protein interaction network analysis and visual exploration.* Nucleic Acids Research, 2014. **42**(Web Server issue): p. W167-W174.
440. Aagaard, L. and J.J. Rossi, *RNAi Therapeutics: Principles, Prospects and Challenges.* Advanced drug delivery reviews, 2007. **59**(2-3): p. 75-86.
441. Tiemann, K. and J.J. Rossi, *RNAi-based therapeutics–current status, challenges and prospects.* EMBO Molecular Medicine, 2009. **1**(3): p. 142-151.
442. Scherman, D., et al., *Genetic pharmacology: progresses in siRNA delivery and therapeutic applications.* Gene Ther, 2017. **24**(3): p. 151-156.
443. Tatiparti, K., et al., *siRNA Delivery Strategies: A Comprehensive Review of Recent Developments.* Nanomaterials (Basel), 2017. **7**(4).
444. Veschi, V., et al., *Epigenetic siRNA and Chemical Screens Identify SETD8 Inhibition as a Therapeutic Strategy for p53 Activation in High-Risk Neuroblastoma.* Cancer Cell, 2017. **31**(1): p. 50-63.
445. Lin, Y.L., et al., *Synergistic combination of small molecule inhibitor and RNA interference against antiapoptotic Bcl-2 protein in head and neck cancer cells.* Mol Pharm, 2013. **10**(7): p. 2730-8.
446. Cormio, G., et al., *Long-term topotecan therapy in recurrent or persistent ovarian cancer.* Eur J Gynaecol Oncol, 2011. **32**(2): p. 153-5.
447. Herzog, T.J., *Update on the role of topotecan in the treatment of recurrent ovarian cancer.* Oncologist, 2002. **7 Suppl 5**: p. 3-10.
448. Mason, J.M., et al., *RAD54 family translocases counter genotoxic effects of RAD51 in human tumor cells.* Nucleic Acids Res, 2015. **43**(6): p. 3180-96.
449. Deakyne, J.S., et al., *Analysis of the activities of RAD54, a SWI2/SNF2 protein, using a specific small-molecule inhibitor.* J Biol Chem, 2013. **288**(44): p. 31567-80.
450. Huang, F. and A.V. Mazin, *A small molecule inhibitor of human RAD51 potentiates breast cancer cell killing by therapeutic agents in mouse xenografts.* PLoS One, 2014. **9**(6): p. e100993.
451. Wagner, A.J., et al., *Dose-escalation study of a second-generation non-ansamycin HSP90 inhibitor, onalespib (AT13387), in combination with imatinib in patients with metastatic gastrointestinal stromal tumour.* Eur J Cancer, 2016. **61**: p. 94-101.
452. Spiegelberg, D., et al., *The novel HSP90 inhibitor AT13387 potentiates radiation effects in squamous cell carcinoma and adenocarcinoma cells.* Oncotarget, 2015. **6**(34): p. 35652-66.
453. Shapiro, G.I., et al., *First-in-human phase I dose escalation study of a second-generation non-ansamycin HSP90 inhibitor, AT13387, in patients with advanced solid tumors.* Clin Cancer Res, 2015. **21**(1): p. 87-97.

454. Smyth, T., et al., *The HSP90 inhibitor, AT13387, is effective against imatinib-sensitive and -resistant gastrointestinal stromal tumor models.* Mol Cancer Ther, 2012. **11**(8): p. 1799-808.
455. Wang, H., et al., *Effects of treatment with an Hsp90 inhibitor in tumors based on 15 phase II clinical trials.* Mol Clin Oncol, 2016. **5**(3): p. 326-334.
456. Newman, B., et al., *HSP90 inhibitor 17-AAG selectively eradicates lymphoma stem cells.* Cancer Res, 2012. **72**(17): p. 4551-61.
457. Yao, Q., B. Weigel, and J. Kersey, *Synergism between etoposide and 17-AAG in leukemia cells: critical roles for Hsp90, FLT3, topoisomerase II, Chk1, and Rad51.* Clin Cancer Res, 2007. **13**(5): p. 1591-600.
458. Shahar, O.D., et al., *A high-throughput chemical screen with FDA approved drugs reveals that the antihypertensive drug Spironolactone impairs cancer cell survival by inhibiting homology directed repair.* Nucleic Acids Research, 2014. **42**(9): p. 5689-5701.
459. Bohm, L., *Inhibition of homologous recombination repair with Pentoxifylline targets G2 cells generated by radiotherapy and induces major enhancements of the toxicity of cisplatin and melphalan given after irradiation.* Radiat Oncol, 2006. **1**: p. 12.
460. Li, Y. and D.Q. Yang, *The ATM inhibitor KU-55933 suppresses cell proliferation and induces apoptosis by blocking Akt in cancer cells with overactivated Akt.* Mol Cancer Ther, 2010. **9**(1): p. 113-25.
461. Josse, R., et al., *ATR inhibitors VE-821 and VX-970 sensitize cancer cells to topoisomerase i inhibitors by disabling DNA replication initiation and fork elongation responses.* Cancer Res, 2014. **74**(23): p. 6968-79.
462. Zabludoff, S.D., et al., *AZD7762, a novel checkpoint kinase inhibitor, drives checkpoint abrogation and potentiates DNA-targeted therapies.* Mol Cancer Ther, 2008. **7**(9): p. 2955-66.
463. Neff, R.T., L. Senter, and R. Salani, *BRCA mutation in ovarian cancer: testing, implications and treatment considerations.* Ther Adv Med Oncol, 2017. **9**(8): p. 519-531.
464. Hilton, J., et al., *44OCCTG IND.231: A phase 1 trial evaluating CX-5461 in patients with advanced solid tumors.* Annals of Oncology, 2018. **29**(suppl_3): p. mdy048.003-mdy048.003.
465. Khot, A., et al., *RNA Polymerase 1 Transcription Inhibitor CX-5461 in Patients with Advanced Hematologic Malignancies: Results of a Phase I First in Human Study.* Blood, 2017. **130**(Suppl 1): p. 3835.
466. Rhodes, D. and H.J. Lipps, *G-quadruplexes and their regulatory roles in biology.* Nucleic Acids Res, 2015. **43**(18): p. 8627-37.
467. Henderson, A., et al., *Detection of G-quadruplex DNA in mammalian cells.* Nucleic Acids Res, 2014. **42**(2): p. 860-9.
468. Balasubramanian, S., L.H. Hurley, and S. Neidle, *Targeting G-quadruplexes in gene promoters: a novel anticancer strategy?* Nat Rev Drug Discov, 2011. **10**(4): p. 261-75.
469. Min, J., et al., *The Breast Cancer Susceptibility Gene BRCA2 Is Required for the Maintenance of Telomere Homeostasis.* Journal of Biological Chemistry, 2012. **287**(7): p. 5091-5101.
470. van Kregten, M. and M. Tijsterman, *The repair of G-quadruplex-induced DNA damage.* Exp Cell Res, 2014. **329**(1): p. 178-83.

471. Zimmer, J., et al., *Targeting BRCA1 and BRCA2 Deficiencies with G-Quadruplex-Interacting Compounds.* Mol Cell, 2016. **61**(3): p. 449-60.
472. Champoux, J.J., *DNA topoisomerases: structure, function, and mechanism.* Annu Rev Biochem, 2001. **70**: p. 369-413.
473. Pommier, Y., *Drugging topoisomerases: lessons and challenges.* ACS Chem Biol, 2013. **8**(1): p. 82-95.
474. Armstrong, D.K., *Topotecan dosing guidelines in ovarian cancer: reduction and management of hematologic toxicity.* Oncologist, 2004. **9**(1): p. 33-42.
475. McLaughlin, J.R., et al., *Long-term ovarian cancer survival associated with mutation in BRCA1 or BRCA2.* J Natl Cancer Inst, 2013. **105**(2): p. 141-8.
476. Longacre, M., et al., *A Comparative Analysis of Genetic and Epigenetic Events of Breast and Ovarian Cancer Related to Tumorigenesis.* Int J Mol Sci, 2016. **17**(5).
477. Mayor, S., *Aggressive breast cancer genetically similar to ovarian cancer.* The Lancet Oncology, 2012. **13**(11): p. e466.
478. Soegaard, M., et al., *BRCA1 and BRCA2 mutation prevalence and clinical characteristics of a population-based series of ovarian cancer cases from Denmark.* Clin Cancer Res, 2008. **14**(12): p. 3761-7.
479. Zhao, Q., et al., *Germline and somatic mutations in homologous recombination genes among Chinese ovarian cancer patients detected using next-generation sequencing.* Journal of gynecologic oncology, 2017. **28**(4): p. e39-e39.
480. Pelttari, L.M., et al., *A Finnish founder mutation in RAD51D: analysis in breast, ovarian, prostate, and colorectal cancer.* J Med Genet, 2012. **49**(7): p. 429-32.
481. Yang, F., C.J. Kemp, and S. Henikoff, *Anthracyclines induce double-strand DNA breaks at active gene promoters.* Mutation research, 2015. **773**: p. 9-15.
482. Das, A.T., L. Tenenbaum, and B. Berkhout, *Tet-On Systems For Doxycycline-inducible Gene Expression.* Curr Gene Ther, 2016. **16**(3): p. 156-67.
483. *Whither RNAi?* Nat Cell Biol, 2003. **5**(6): p. 489-90.
484. Echeverri, C.J., et al., *Minimizing the risk of reporting false positives in large-scale RNAi screens.* Nat Methods, 2006. **3**(10): p. 777-9.
485. Lassus, P., J. Rodriguez, and Y. Lazebnik, *Confirming specificity of RNAi in mammalian cells.* Sci STKE, 2002. **2002**(147): p. pl13.
486. Merritt, W.M., et al., *Dicer, Drosha, and outcomes in patients with ovarian cancer.* N Engl J Med, 2008. **359**(25): p. 2641-50.
487. Mitra, A.K., et al., *In vivo tumor growth of high-grade serous ovarian cancer cell lines.* Gynecol Oncol, 2015. **138**(2): p. 372-7.
488. Yang, D., et al., *Association of BRCA1 and BRCA2 mutations with survival, chemotherapy sensitivity, and gene mutator phenotype in patients with ovarian cancer.* JAMA, 2011. **306**(14): p. 1557-65.
489. Hyman, D.M., et al., *Improved survival for BRCA2-associated serous ovarian cancer compared with both BRCA-negative and BRCA1-associated serous ovarian cancer.* Cancer, 2012. **118**(15): p. 3703-3709.
490. Bolton, K.L., et al., *Association Between BRCA1 and BRCA2 Mutations and Survival in Women With Invasive Epithelial Ovarian Cancer.* JAMA, 2012. **307**(4): p. 382-389.
491. Liu, G., et al., *Differing clinical impact of BRCA1 and BRCA2 mutations in serous ovarian cancer.* Pharmacogenomics, 2012. **13**(13): p. 1523-35.
492. Pommier, Y., et al., *Roles of eukaryotic topoisomerases in transcription, replication and genomic stability.* Nat Rev Mol Cell Biol, 2016. **17**(11): p. 703-721.

493. Chen, S.H., N.L. Chan, and T.S. Hsieh, *New mechanistic and functional insights into DNA topoisomerases.* Annu Rev Biochem, 2013. **82**: p. 139-70.
494. Zhang, H., et al., *Human mitochondrial topoisomerase I.* Proceedings of the National Academy of Sciences, 2001. **98**(19): p. 10608.
495. Christensen, M.O., et al., *The N-terminal domain anchors human topoisomerase I at fibrillar centers of nucleoli and nucleolar organizer regions of mitotic chromosomes.* J Biol Chem, 2002. **277**(39): p. 35932-8.
496. Baker, N.M., R. Rajan, and A. Mondragon, *Structural studies of type I topoisomerases.* Nucleic Acids Res, 2009. **37**(3): p. 693-701.
497. Leppard, J.B. and J.J. Champoux, *Human DNA topoisomerase I: relaxation, roles, and damage control.* Chromosoma, 2005. **114**(2): p. 75-85.
498. Stewart, L., et al., *A Model for the Mechanism of Human Topoisomerase I.* Science, 1998. **279**(5356): p. 1534.
499. Girstun, A., et al., *Subnuclear Localization of Human Topoisomerase I.* J Cell Biochem, 2017. **118**(2): p. 407-419.
500. Christensen, M.O., et al., *Distinct effects of topoisomerase I and RNA polymerase I inhibitors suggest a dual mechanism of nucleolar/nucleoplasmic partitioning of topoisomerase I.* J Biol Chem, 2004. **279**(21): p. 21873-82.
501. Bharti, A.K., et al., *Identification of a nucleolin binding site in human topoisomerase I.* J Biol Chem, 1996. **271**(4): p. 1993-7.
502. El Hage, A., et al., *Loss of Topoisomerase I leads to R-loop-mediated transcriptional blocks during ribosomal RNA synthesis.* Genes Dev, 2010. **24**(14): p. 1546-58.
503. Andersen, S.L., et al., *Genome-destabilizing effects associated with top1 loss or accumulation of top1 cleavage complexes in yeast.* PLoS Genet, 2015. **11**(4): p. e1005098.
504. Christman, M.F., F.S. Dietrich, and G.R. Fink, *Mitotic recombination in the rDNA of S. cerevisiae is suppressed by the combined action of DNA topoisomerases I and II.* Cell, 1988. **55**(3): p. 413-425.
505. Sloan, R., et al., *Effects of camptothecin or TOP1 overexpression on genetic stability in Saccharomyces cerevisiae.* DNA Repair (Amst), 2017. **59**: p. 69-75.
506. Durand-Dubief, M., et al., *Topoisomerase I regulates open chromatin and controls gene expression in vivo.* EMBO J, 2010. **29**(13): p. 2126-34.
507. Baranello, L., et al., *RNA Polymerase II Regulates Topoisomerase 1 Activity to Favor Efficient Transcription.* Cell, 2016. **165**(2): p. 357-71.
508. Solier, S., et al., *Topoisomerase I and II inhibitors control caspase-2 pre-messenger RNA splicing in human cells.* Mol Cancer Res, 2004. **2**(1): p. 53-61.
509. Eisenreich, A., et al., *Cdc2-like kinases and DNA topoisomerase I regulate alternative splicing of tissue factor in human endothelial cells.* Circ Res, 2009. **104**(5): p. 589-99.
510. Heestand, G.M., et al., *Topoisomerase expression and amplification in solid tumours: Analysis of 24,262 patients.* Eur J Cancer, 2017. **83**: p. 80-87.
511. Kumler, I., et al., *Topoisomerase-1 gene copy aberrations are frequent in patients with breast cancer.* Int J Cancer, 2015. **137**(8): p. 2000-6.
512. Bai, Y., et al., *Targeting of topoisomerases for prognosis and drug resistance in ovarian cancer.* J Ovarian Res, 2016. **9**(1): p. 35.
513. Liu, L.-M., et al., *DNA topoisomerase 1 and 2A function as oncogenes in liver cancer and may be direct targets of nitidine chloride.* International journal of oncology, 2018.

514. Li, M. and Y. Liu, *Topoisomerase I in Human Disease Pathogenesis and Treatments.* Genomics Proteomics Bioinformatics, 2016. **14**(3): p. 166-171.
515. Li, F., et al., *Camptothecin (CPT) and its derivatives are known to target topoisomerase I (Top1) as their mechanism of action: did we miss something in CPT analogue molecular targets for treating human disease such as cancer?* Am J Cancer Res, 2017. **7**(12): p. 2350-2394.
516. Venditto, V.J. and E.E. Simanek, *Cancer therapies utilizing the camptothecins: a review of the in vivo literature.* Mol Pharm, 2010. **7**(2): p. 307-49.
517. Legarza, K. and L.X. Yang, *New molecular mechanisms of action of camptothecin-type drugs.* Anticancer Res, 2006. **26**(5A): p. 3301-5.
518. Morris, E.J. and H.M. Geller, *Induction of neuronal apoptosis by camptothecin, an inhibitor of DNA topoisomerase-I: evidence for cell cycle-independent toxicity.* The Journal of Cell Biology, 1996. **134**(3): p. 757.
519. McCrudden, K.W., et al., *Topotecan is anti-angiogenic in experimental hepatoblastoma.* Journal of Pediatric Surgery, 2002. **37**(6): p. 857-861.
520. Rapisarda, A., et al., *Identification of small molecule inhibitors of hypoxia-inducible factor 1 transcriptional activation pathway.* Cancer Res, 2002. **62**(15): p. 4316-24.
521. Beppu, K., et al., *Topotecan Blocks Hypoxia-Inducible Factor-1α and Vascular Endothelial Growth Factor Expression Induced by Insulin-Like Growth Factor-I in Neuroblastoma Cells.* Cancer Research, 2005. **65**(11): p. 4775.
522. Rapisarda, A., et al., *Topoisomerase I-Mediated Inhibition of Hypoxia-Inducible Factor 1.* Cancer Research, 2004. **64**(4): p. 1475.
523. Burgess, D.J., et al., *Topoisomerase levels determine chemotherapy response in vitro and in vivo.* Proc Natl Acad Sci U S A, 2008. **105**(26): p. 9053-8.
524. Desai, S.D., et al., *Ubiquitin/26S proteasome-mediated degradation of topoisomerase I as a resistance mechanism to camptothecin in tumor cells.* Cancer Res, 2001. **61**(15): p. 5926-32.
525. Pan, P., et al., *Molecular principle of topotecan resistance by topoisomerase I mutations through molecular modeling approaches.* J Chem Inf Model, 2013. **53**(4): p. 997-1006.
526. Gongora, C., et al., *New Topoisomerase I mutations are associated with resistance to camptothecin.* Mol Cancer, 2011. **10**: p. 64.
527. Klejewski, A., et al., *New and Old Genes Associated with Topotecan Resistance Development in Ovarian Cancer Cell Lines.* Anticancer Res, 2017. **37**(4): p. 1625-1636.
528. Rasheed, Z.A. and E.H. Rubin, *Mechanisms of resistance to topoisomerase I-targeting drugs.* Oncogene, 2003. **22**(47): p. 7296-304.
529. Santos, S.A. and A. Paulo, *Small molecule inhibitors of multidrug resistance gene (MDR1) expression: preclinical evaluation and mechanisms of action.* Curr Cancer Drug Targets, 2013. **13**(8): p. 814-28.
530. Callaghan, R., F. Luk, and M. Bebawy, *Inhibition of the multidrug resistance P-glycoprotein: time for a change of strategy?* Drug Metab Dispos, 2014. **42**(4): p. 623-31.
531. Gilbert, D.C., A.J. Chalmers, and S.F. El-Khamisy, *Topoisomerase I inhibition in colorectal cancer: biomarkers and therapeutic targets.* Br J Cancer, 2012. **106**(1): p. 18-24.
532. Meisenberg, C., et al., *TDP1/TOP1 Ratio as a Promising Indicator for the Response of Small Cell Lung Cancer to Topotecan.* Journal of cancer science & therapy, 2014. **6**(7): p. 258-267.

533. Benafif, S. and M. Hall, *An update on PARP inhibitors for the treatment of cancer.* Onco Targets Ther, 2015. **8**: p. 519-28.
534. Pommier, Y., *Topoisomerase I inhibitors: camptothecins and beyond.* Nat Rev Cancer, 2006. **6**(10): p. 789-802.
535. Bergeron, S., M. Beauchemin, and R. Bertrand, *Camptothecin- and etoposide-induced apoptosis in human leukemia cells is independent of cell death receptor-3 and -4 aggregation but accelerates tumor necrosis factor–related apoptosis-inducing ligand–mediated cell death.* Molecular Cancer Therapeutics, 2004. **3**(12): p. 1659.
536. Zhang, X.W. and B. Xu, *Differential regulation of P53, c-Myc, Bcl-2, Bax and AFP protein expression, and caspase activity during 10-hydroxycamptothecin-induced apoptosis in Hep G2 cells.* Anticancer Drugs, 2000. **11**(9): p. 747-56.
537. Pizzolato, J.F. and L.B. Saltz, *The camptothecins.* Lancet, 2003. **361**(9376): p. 2235-42.
538. Perez, E.A., et al., *Etirinotecan pegol (NKTR-102) versus treatment of physician's choice in women with advanced breast cancer previously treated with an anthracycline, a taxane, and capecitabine (BEACON): a randomised, open-label, multicentre, phase 3 trial.* Lancet Oncol, 2015. **16**(15): p. 1556-1568.
539. Tian, X., et al., *CRLX101, a nanoparticle-drug conjugate containing camptothecin, improves rectal cancer chemoradiotherapy by inhibiting DNA repair and HIF-1α.* Cancer research, 2017. **77**(1): p. 112-122.
540. Pommier, Y., *DNA topoisomerase I inhibitors: chemistry, biology, and interfacial inhibition.* Chem Rev, 2009. **109**(7): p. 2894-902.
541. Pommier, Y., *Drugging topoisomerases: lessons and challenges.* ACS Chem Biol, 2013. **8**.
542. Wu, N., et al., *A novel DNA topoisomerase I inhibitor with different mechanism from camptothecin induces G2/M phase cell cycle arrest to K562 cells.* Biochemistry, 2010. **49**(47): p. 10131-6.
543. Thomas, A., et al., *Phase I Study of ATR Inhibitor M6620 in Combination With Topotecan in Patients With Advanced Solid Tumors.* J Clin Oncol, 2018. **36**(16): p. 1594-1602.
544. Zhang, L., et al., *Combined Antitumor Therapy with Metronomic Topotecan and Hypoxia-Activated Prodrug, Evofosfamide, in Neuroblastoma and Rhabdomyosarcoma Preclinical Models.* Clin Cancer Res, 2016. **22**(11): p. 2697-708.
545. Kwon, H. and M.R. Green, *The RNA polymerase I transcription factor, upstream binding factor, interacts directly with the TATA box-binding protein.* J Biol Chem, 1994. **269**(48): p. 30140-6.
546. Martinez-Irujo, J.J., et al., *A checkerboard method to evaluate interactions between drugs.* Biochemical Pharmacology, 1996. **51**(5): p. 635-644.
547. Ledermann, J., et al., *Olaparib maintenance therapy in platinum-sensitive relapsed ovarian cancer.* N Engl J Med, 2012. **366**(15): p. 1382-92.
548. Rytelewski, M., et al., *Reciprocal positive selection for weakness - preventing olaparib resistance by inhibiting BRCA2.* Oncotarget, 2016. **7**(15): p. 20825-39.
549. Mon, M.T., et al., *Alkaloids from Stephania venosa as Chemo-Sensitizers in SKOV3 Ovarian Cancer Cells via Akt/NF-κB Signaling.* Chemical and Pharmaceutical Bulletin, 2018. **66**(2): p. 162-169.
550. Hsieh, M.H., et al., *Synergy assessed by checkerboard. A critical analysis.* Diagn Microbiol Infect Dis, 1993. **16**(4): p. 343-9.

551. Niepel, M., et al., *Common and cell-type specific responses to anti-cancer drugs revealed by high throughput transcript profiling.* Nature Communications, 2017. **8**(1).
552. Foucquier, J. and M. Guedj, *Analysis of drug combinations: current methodological landscape.* Pharmacology Research & Perspectives, 2015. **3**(3): p. e00149.
553. Chou, T.-C., *Drug Combination Studies and Their Synergy Quantification Using the Chou-Talalay Method.* Cancer Research, 2010. **70**(2): p. 440.
554. Joselow, A., et al., *Senescence-Like Phenotypes in Human Nevi.* Methods Mol Biol, 2017. **1534**: p. 175-184.
555. Rodier, F. and J. Campisi, *Four faces of cellular senescence.* J Cell Biol, 2011. **192**(4): p. 547-56.
556. Franken, N.A., et al., *Clonogenic assay of cells in vitro.* Nat Protoc, 2006. **1**(5): p. 2315-9.
557. Orjalo, A.V., et al., *Cell surface-bound IL-1α is an upstream regulator of the senescence-associated IL-6/IL-8 cytokine network.* Proceedings of the National Academy of Sciences, 2009. **106**(40): p. 17031.
558. Acosta, J.C. and J. Gil, *A Role for CXCR2 in Senescence, but What about in Cancer?* Cancer Research, 2009. **69**(6): p. 2167.
559. Noren Hooten, N. and M.K. Evans, *Techniques to Induce and Quantify Cellular Senescence.* J Vis Exp, 2017(123).
560. Eisenberg, E. and E.Y. Levanon, *Human housekeeping genes, revisited.* Trends Genet, 2013. **29**(10): p. 569-74.
561. Karimian, A., Y. Ahmadi, and B. Yousefi, *Multiple functions of p21 in cell cycle, apoptosis and transcriptional regulation after DNA damage.* DNA Repair (Amst), 2016. **42**: p. 63-71.
562. Abbas, T. and A. Dutta, *p21 in cancer: intricate networks and multiple activities.* Nat Rev Cancer, 2009. **9**(6): p. 400-14.
563. Macleod, K.F., et al., *p53-dependent and independent expression of p21 during cell growth, differentiation, and DNA damage.* Genes Dev, 1995. **9**(8): p. 935-44.
564. Jones, L., et al., *A review of new agents evaluated against pediatric acute lymphoblastic leukemia by the Pediatric Preclinical Testing Program.* Leukemia, 2016. **30**(11): p. 2133-2141.
565. Furman, W.L., et al., *Protracted intermittent schedule of topotecan in children with refractory acute leukemia: a pediatric oncology group study.* J Clin Oncol, 2002. **20**(6): p. 1617-24.
566. Saif, M.W., et al., *Open-label, dose-escalation, safety, pharmacokinetic, and pharmacodynamic study of intravenously administered CNF1010 (17-(allylamino)-17-demethoxygeldanamycin [17-AAG]) in patients with solid tumors.* Cancer Chemother Pharmacol, 2013. **71**(5): p. 1345-55.
567. Ardizzoni, A., *Topotecan in the treatment of recurrent small cell lung cancer: an update.* Oncologist, 2004. **9 Suppl 6**: p. 4-13.
568. Fiorica, J.V., *Update on the treatment of cervical and uterine carcinoma: focus on topotecan.* Oncologist, 2002. **7 Suppl 5**: p. 36-45.
569. Caserta, T.M., et al., *Q-VD-OPh, a broad spectrum caspase inhibitor with potent antiapoptotic properties.* Apoptosis, 2003. **8**(4): p. 345-52.
570. Keoni, C.L. and T.L. Brown, *Inhibition of Apoptosis and Efficacy of Pan Caspase Inhibitor, Q-VD-OPh, in Models of Human Disease.* J Cell Death, 2015. **8**: p. 1-7.
571. Cecchini, M.J., M. Amiri, and F.A. Dick, *Analysis of cell cycle position in mammalian cells.* J Vis Exp, 2012(59).

572. Yang, F., et al., *Doxorubicin, DNA torsion, and chromatin dynamics.* Biochim Biophys Acta, 2014. **1845**(1): p. 84-9.
573. Henriksen, P.A., *Anthracycline cardiotoxicity: an update on mechanisms, monitoring and prevention.* Heart, 2018. **104**(12): p. 971-977.
574. Jackson, S.P. and J. Bartek, *The DNA-damage response in human biology and disease.* Nature, 2009. **461**(7267): p. 1071-1078.
575. Kurz, E.U., P. Douglas, and S.P. Lees-Miller, *Doxorubicin activates ATM-dependent phosphorylation of multiple downstream targets in part through the generation of reactive oxygen species.* J Biol Chem, 2004. **279**(51): p. 53272-81.
576. Pu, X., Z. Wang, and J.E. Klaunig, *Alkaline Comet Assay for Assessing DNA Damage in Individual Cells.* Curr Protoc Toxicol, 2015. **65**: p. 3 12 1-11.
577. Hansel-Hertsch, R., M. Di Antonio, and S. Balasubramanian, *DNA G-quadruplexes in the human genome: detection, functions and therapeutic potential.* Nat Rev Mol Cell Biol, 2017. **18**(5): p. 279-284.
578. Han, F.X., R.T. Wheelhouse, and L.H. Hurley, *Interactions of TMPyP4 and TMPyP2 with Quadruplex DNA. Structural Basis for the Differential Effects on Telomerase Inhibition.* Journal of the American Chemical Society, 1999. **121**(15): p. 3561-3570.
579. Mazouzi, A., G. Velimezi, and J.I. Loizou, *DNA replication stress: causes, resolution and disease.* Exp Cell Res, 2014. **329**(1): p. 85-93.
580. Zellweger, R., et al., *Rad51-mediated replication fork reversal is a global response to genotoxic treatments in human cells.* The Journal of Cell Biology, 2015. **208**(5): p. 563-579.
581. Chanoux, R.A., et al., *ATR and H2AX cooperate in maintaining genome stability under replication stress.* J Biol Chem, 2009. **284**(9): p. 5994-6003.
582. Tsvetkova, A., et al., *gammaH2AX, 53BP1 and Rad51 protein foci changes in mesenchymal stem cells during prolonged X-ray irradiation.* Oncotarget, 2017. **8**(38): p. 64317-64329.
583. Yamane, A., et al., *RPA accumulation during class switch recombination represents 5′-3′ DNA-end resection during the S-G2/M phase of the cell cycle.* Cell reports, 2013. **3**(1): p. 138-147.
584. Köcher, S., et al., *Radiation-induced double-strand breaks require ATM but not Artemis for homologous recombination during S-phase.* Nucleic acids research, 2012. **40**(17): p. 8336-8347.
585. Nakamura, A.J., et al., *The complexity of phosphorylated H2AX foci formation and DNA repair assembly at DNA double-strand breaks.* Cell Cycle, 2010. **9**(2): p. 389-397.
586. O'Connell, B.C., et al., *A genome-wide camptothecin sensitivity screen identifies a mammalian MMS22L-NFKBIL2 complex required for genomic stability.* Mol Cell, 2010. **40**(4): p. 645-57.
587. Murai, J., *Targeting DNA repair and replication stress in the treatment of ovarian cancer.* Int J Clin Oncol, 2017. **22**(4): p. 619-628.
588. McManus, K.J. and M.J. Hendzel, *ATM-dependent DNA damage-independent mitotic phosphorylation of H2AX in normally growing mammalian cells.* Mol Biol Cell, 2005. **16**(10): p. 5013-25.
589. Anantha, R.W. and J.A. Borowiec, *Mitotic crisis: the unmasking of a novel role for RPA.* Cell Cycle, 2009. **8**(3): p. 357-61.

590. Vrouwe, M.G., et al., *UV-induced photolesions elicit ATR-kinase-dependent signaling in non-cycling cells through nucleotide excision repair-dependent and -independent pathways.* J Cell Sci, 2011. **124**(Pt 3): p. 435-46.
591. Kozmin, S.G. and S. Jinks-Robertson, *The mechanism of nucleotide excision repair-mediated UV-induced mutagenesis in nonproliferating cells.* Genetics, 2013. **193**(3): p. 803-17.
592. Auclair, Y., R. Rouget, and E.A. Drobetsky, *ATR kinase as master regulator of nucleotide excision repair during S phase of the cell cycle.* Cell Cycle, 2009. **8**(12): p. 1865-71.
593. Petruseva, I.O., A.N. Evdokimov, and O.I. Lavrik, *Molecular mechanism of global genome nucleotide excision repair.* Acta Naturae, 2014. **6**(1): p. 23-34.
594. Marini, F., et al., *DNA nucleotide excision repair-dependent signaling to checkpoint activation.* Proc Natl Acad Sci U S A, 2006. **103**(46): p. 17325-30.
595. Iyama, T. and D.M. Wilson, 3rd, *DNA repair mechanisms in dividing and non-dividing cells.* DNA Repair (Amst), 2013. **12**(8): p. 620-36.
596. Skourti-Stathaki, K. and N.J. Proudfoot, *A double-edged sword: R loops as threats to genome integrity and powerful regulators of gene expression.* Genes Dev, 2014. **28**(13): p. 1384-96.
597. Nguyen, H.D., et al., *Functions of Replication Protein A as a Sensor of R Loops and a Regulator of RNaseH1.* Mol Cell, 2017. **65**(5): p. 832-847 e4.
598. Lindstrom, M.S., et al., *Nucleolus as an emerging hub in maintenance of genome stability and cancer pathogenesis.* Oncogene, 2018.
599. Shen, W., et al., *Dynamic nucleoplasmic and nucleolar localization of mammalian RNase H1 in response to RNAP I transcriptional R-loops.* Nucleic Acids Res, 2017. **45**(18): p. 10672-10692.
600. Sollier, J., et al., *Transcription-coupled nucleotide excision repair factors promote R-loop-induced genome instability.* Mol Cell, 2014. **56**(6): p. 777-85.
601. White, D., et al., *The ATM substrate KAP1 controls DNA repair in heterochromatin: regulation by HP1 proteins and serine 473/824 phosphorylation.* Mol Cancer Res, 2012. **10**(3): p. 401-14.
602. Kubota, S., et al., *Phosphorylation of KRAB-associated protein 1 (KAP1) at Tyr-449, Tyr-458, and Tyr-517 by nuclear tyrosine kinases inhibits the association of KAP1 and heterochromatin protein 1alpha (HP1alpha) with heterochromatin.* J Biol Chem, 2013. **288**(24): p. 17871-83.
603. Bolderson, E., et al., *Kruppel-associated Box (KRAB)-associated co-repressor (KAP-1) Ser-473 phosphorylation regulates heterochromatin protein 1beta (HP1-beta) mobilization and DNA repair in heterochromatin.* J Biol Chem, 2012. **287**(33): p. 28122-31.
604. Addison, J.B., et al., *KAP1 promotes proliferation and metastatic progression of breast cancer cells.* Cancer Res, 2015. **75**(2): p. 344-55.
605. Li, X., et al., *Role for KAP1 serine 824 phosphorylation and sumoylation/desumoylation switch in regulating KAP1-mediated transcriptional repression.* J Biol Chem, 2007. **282**(50): p. 36177-89.
606. Guichard, S., et al., *Schedule-dependent activity of topotecan in OVCAR-3 ovarian carcinoma xenograft: pharmacokinetic and pharmacodynamic evaluation.* Clin Cancer Res, 2001. **7**(10): p. 3222-8.
607. Tortora, G., et al., *Preclinical and phase I study of oxaliplatin and topotecan in combination in human cancer.* Ann Oncol, 2002. **13**(3): p. 392-8.

608. Sakhare, S.S., et al., *Transcriptome profile of OVCAR3 cisplatin-resistant ovarian cancer cell line.* BMC Bioinformatics, 2014. **15**(Suppl 10): p. P21-P21.
609. Shah, D.K. and J.P. Balthasar, *Physiologically based pharmacokinetic model for topotecan in mice.* J Pharmacokinet Pharmacodyn, 2011. **38**(1): p. 121-42.
610. Ardizzoni, A., et al., *European Organization for Research and Treatment of Cancer (EORTC) 08957 Phase II Study of Topotecan in Combination with Cisplatin as Second-Line Treatment of Refractory and Sensitive Small Cell Lung Cancer.* Clinical Cancer Research, 2003. **9**(1): p. 143.
611. Uckun, F.M., et al., *In vitro and in vivo activity of topotecan against human B-lineage acute lymphoblastic leukemia cells.* Blood, 1995. **85**(10): p. 2817-28.
612. Shamas-Din, A., et al., *Mechanisms of action of Bcl-2 family proteins.* Cold Spring Harb Perspect Biol, 2013. **5**(4): p. a008714.
613. Ashkenazi, A., et al., *From basic apoptosis discoveries to advanced selective BCL-2 family inhibitors.* Nat Rev Drug Discov, 2017. **16**(4): p. 273-284.
614. Blagosklonny, M.V., *Cell cycle arrest is not senescence.* Aging (Albany NY), 2011. **3**(2): p. 94-101.
615. Kuilman, T., et al., *The essence of senescence.* Genes Dev, 2010. **24**(22): p. 2463-79.
616. Shweta, C., W.E. Lynne, and A.G. David, *Is Senescence Reversible?* Current Drug Targets, 2016. **17**(4): p. 460-466.
617. Burgess, R.C., et al., *Activation of DNA damage response signaling by condensed chromatin.* Cell Rep, 2014. **9**(5): p. 1703-1717.
618. Tentler, J.J., et al., *Patient-derived tumour xenografts as models for oncology drug development.* Nat Rev Clin Oncol, 2012. **9**(6): p. 338-50.
619. Hidalgo, M., et al., *Patient-derived xenograft models: an emerging platform for translational cancer research.* Cancer Discov, 2014. **4**(9): p. 998-1013.
620. Shultz, L.D., et al., *Human lymphoid and myeloid cell development in NOD/LtSz-scid IL2R gamma null mice engrafted with mobilized human hemopoietic stem cells.* J Immunol, 2005. **174**(10): p. 6477-89.
621. Roca, J., *The torsional state of DNA within the chromosome.* Chromosoma, 2011. **120**(4): p. 323-34.
622. Spies, J., et al., *Nek1 Regulates Rad54 to Orchestrate Homologous Recombination and Replication Fork Stability.* Mol Cell, 2016.
623. Huang, F. and A.V. Mazin, *Targeting the homologous recombination pathway by small molecule modulators.* Bioorg Med Chem Lett, 2014. **24**(14): p. 3006-13.
624. Parplys, A.C., et al., *NUCKS1 is a novel RAD51AP1 paralog important for homologous recombination and genome stability.* Nucleic Acids Res, 2015. **43**(20): p. 9817-34.
625. Roy, R., J. Chun, and S.N. Powell, *BRCA1 and BRCA2: different roles in a common pathway of genome protection.* Nat Rev Cancer, 2011. **12**(1): p. 68-78.
626. Bermejo, R., M.S. Lai, and M. Foiani, *Preventing replication stress to maintain genome stability: resolving conflicts between replication and transcription.* Mol Cell, 2012. **45**(6): p. 710-8.
627. Gore, M., et al., *A randomised trial of oral versus intravenous topotecan in patients with relapsed epithelial ovarian cancer.* Eur J Cancer, 2002. **38**(1): p. 57-63.
628. Markman, M., *Topotecan as Second-Line Therapy for Ovarian Cancer: Dosage Versus Toxicity.* The Oncologist, 2005. **10**(9): p. 695-697.
629. Patankar, N.A., et al., *Topotecan and doxorubicin combination to treat recurrent ovarian cancer: the influence of drug exposure time and delivery systems to achieve optimum therapeutic activity.* Clin Cancer Res, 2013. **19**(4): p. 865-77.

630. Turner, D.C., et al., *Combination metronomic oral topotecan and pazopanib: a pharmacokinetic study in patients with gynecological cancer.* Anticancer Res, 2013. **33**(9): p. 3823-9.
631. McGonigle, K.F., et al., *Combined weekly topotecan and biweekly bevacizumab in women with platinum-resistant ovarian, peritoneal, or fallopian tube cancer: results of a phase 2 study.* Cancer, 2011. **117**(16): p. 3731-40.
632. Chen, Y. and H. Du, *The promising PARP inhibitors in ovarian cancer therapy: From Olaparib to others.* Biomed Pharmacother, 2018. **99**: p. 552-560.
633. Lim, J.S.J. and D.S.P. Tan, *Understanding Resistance Mechanisms and Expanding the Therapeutic Utility of PARP Inhibitors.* Cancers (Basel), 2017. **9**(8).
634. Konstantinopoulos, P.A., et al., *Homologous Recombination Deficiency: Exploiting the Fundamental Vulnerability of Ovarian Cancer.* Cancer Discov, 2015. **5**(11): p. 1137-54.
635. Williamson, D., et al., *Nascent pre-rRNA overexpression correlates with an adverse prognosis in alveolar rhabdomyosarcoma.* Genes Chromosomes Cancer, 2006. **45**(9): p. 839-45.
636. Tsoi, H., et al., *Pre-45s rRNA promotes colon cancer and is associated with poor survival of CRC patients.* Oncogene, 2017. **36**: p. 6109.
637. Haddach, M., et al., *Discovery of CX-5461, the First Direct and Selective Inhibitor of RNA Polymerase I, for Cancer Therapeutics.* ACS Med Chem Lett, 2012. **3**(7): p. 602-6.
638. Lee, Y.C., et al., *Targeting of Topoisomerase I for Prognoses and Therapeutics of Camptothecin-Resistant Ovarian Cancer.* PLoS One, 2015. **10**(7): p. e0132579.
639. Greggi, S., et al., *Topotecan and gemcitabine in platinum/paclitaxel-resistant ovarian cancer.* Oncology, 2001. **60**(1): p. 19-23.
640. Swisher, E.M., et al., *Topotecan in platinum- and paclitaxel-resistant ovarian cancer.* Gynecol Oncol, 1997. **66**(3): p. 480-6.
641. Masse, E. and M. Drolet, *Escherichia coli DNA topoisomerase I inhibits R-loop formation by relaxing transcription-induced negative supercoiling.* J Biol Chem, 1999. **274**(23): p. 16659-64.
642. Lindstrom, M.S., et al., *Nucleolus as an emerging hub in maintenance of genome stability and cancer pathogenesis.* Oncogene, 2018. **37**(18): p. 2351-2366.
643. Fousteri, M. and L.H. Mullenders, *Transcription-coupled nucleotide excision repair in mammalian cells: molecular mechanisms and biological effects.* Cell Res, 2008. **18**(1): p. 73-84.
644. Latimer, J.J. and C.M. Kelly, *Unscheduled DNA synthesis: the clinical and functional assay for global genomic DNA nucleotide excision repair.* Methods Mol Biol, 2014. **1105**: p. 511-32.
645. Limsirichaikul, S., et al., *A rapid non-radioactive technique for measurement of repair synthesis in primary human fibroblasts by incorporation of ethynyl deoxyuridine (EdU).* Nucleic Acids Res, 2009. **37**(4): p. e31.
646. Sakaue-Sawano, A., et al., *Visualizing spatiotemporal dynamics of multicellular cell-cycle progression.* Cell, 2008. **132**(3): p. 487-98.
647. Wienholz, F., W. Vermeulen, and J.A. Marteijn, *Amplification of unscheduled DNA synthesis signal enables fluorescence-based single cell quantification of transcription-coupled nucleotide excision repair.* Nucleic Acids Res, 2017. **45**(9): p. e68.
648. O'Carrigan, B., et al., *Phase I trial of a first-in-class ATR inhibitor VX-970 as monotherapy (mono) or in combination (combo) with carboplatin (CP)*

*incorporating pharmacodynamics (PD) studies.* Journal of Clinical Oncology, 2016. **34**(15_suppl): p. 2504-2504.
649. Dillon, M.T., et al., *PATRIOT: A phase I study to assess the tolerability, safety and biological effects of a specific ataxia telangiectasia and Rad3-related (ATR) inhibitor (AZD6738) as a single agent and in combination with palliative radiation therapy in patients with solid tumours.* Clin Transl Radiat Oncol, 2018. **12**: p. 16-20.
650. Lallo, A., et al., *The Combination of the PARP Inhibitor Olaparib and the WEE1 Inhibitor AZD1775 as a New Therapeutic Option for Small Cell Lung Cancer.* Clinical Cancer Research, 2018. **24**(20): p. 5153.
651. Karnak, D., et al., *Combined inhibition of Wee1 and PARP1/2 for radiosensitization in pancreatic cancer.* Clin Cancer Res, 2014. **20**(19): p. 5085-96.
652. Wahba, L., S.K. Gore, and D. Koshland, *The homologous recombination machinery modulates the formation of RNA-DNA hybrids and associated chromosome instability.* Elife, 2013. **2**: p. e00505.
653. Bhatia, V., et al., *BRCA2 prevents R-loop accumulation and associates with TREX-2 mRNA export factor PCID2.* Nature, 2014. **511**(7509): p. 362-5.
654. Zhang, X., et al., *Attenuation of RNA polymerase II pausing mitigates BRCA1-associated R-loop accumulation and tumorigenesis.* Nat Commun, 2017. **8**: p. 15908.
655. Kaldor, J.M., et al., *Leukemia following chemotherapy for ovarian cancer.* N Engl J Med, 1990. **322**(1): p. 1-6.
656. Meacham, C.E. and S.J. Morrison, *Tumour heterogeneity and cancer cell plasticity.* Nature, 2013. **501**(7467): p. 328-337.
657. Dagogo-Jack, I. and A.T. Shaw, *Tumour heterogeneity and resistance to cancer therapies.* Nat Rev Clin Oncol, 2018. **15**(2): p. 81-94.
658. Hald, O.H., et al., *Inhibitors of ribosome biogenesis repress the growth of MYCN-amplified neuroblastoma.* Oncogene, 2018.
659. Mullard, A., *Maturing antibody-drug conjugate pipeline hits 30.* Nat Rev Drug Discov, 2013. **12**(5): p. 329-32.
660. Starodub, A.N., et al., *First-in-Human Trial of a Novel Anti-Trop-2 Antibody-SN-38 Conjugate, Sacituzumab Govitecan, for the Treatment of Diverse Metastatic Solid Tumors.* Clin Cancer Res, 2015. **21**(17): p. 3870-8.
661. Dotan, E., et al., *Abstract CT065: Labetuzumab govitecan (IMMU-130), an anti-CEACAM5/SN-38 antibody-drug conjugate, is active in patients (pts) with heavily pretreated metastatic colorectal cancer (mCRC): phase II results.* Cancer Research, 2016. **76**(14 Supplement): p. CT065.

## Appendix I The 372 candidates identified from the primary screen and the 17 candidates identified from the secondary screen (highlighted in bold)

| Gene.name | Description | Bliss Indep. | Reduction of relative cell number |
|---|---|---|---|
| BLK | B lymphoid tyrosine kinase | 0.48 | 63 |
| EVC | Ellis van Creveld syndrome | 0.5 | 50 |
| FAM3D | family with sequence similarity 3, member D | 0.51 | 54 |
| CACNA1G | calcium channel, voltage-dependent, T type, alpha 1G subunit | 0.51 | 50 |
| DNAJC24 | DnaJ (Hsp40) homolog, subfamily C, member 24 | 0.51 | 54 |
| FAM167B | family with sequence similarity 167, member B | 0.52 | 40 |
| CTNNBIP1 | catenin, beta interacting protein 1 | 0.53 | 52 |
| KBTBD2 | kelch repeat and BTB (POZ) domain containing 2 | 0.53 | 55 |
| POT1 | protection of telomeres 1 homolog (S. pombe) | 0.53 | 42 |
| GBGT1 | globoside alpha-1,3-N-acetylgalactosaminyltransferase 1 | 0.57 | 49 |
| DLGAP2 | discs, large (Drosophila) homolog-associated protein 2 | 0.57 | 43 |
| SLC38A5 | solute carrier family 38, member 5 | 0.57 | 41 |
| EHD2 | EH-domain containing 2 | 0.58 | 54 |
| CLIC5 | chloride intracellular channel 5 | 0.58 | 49 |
| PRRG3 | proline rich Gla (G-carboxyglutamic acid) 3 (transmembrane) | 0.59 | 38 |
| TMEM150A | transmembrane protein 150A | 0.59 | 36 |
| PUM2 | pumilio homolog 2 (Drosophila) | 0.59 | 39 |
| SPIN2B | spindlin family, member 2B | 0.6 | 45 |
| DDX39B | DEAD (Asp-Glu-Ala-Asp) box polypeptide 39B | 0.6 | 40 |
| C1QTNF3 | C1q and tumor necrosis factor related protein 3 | 0.6 | 39 |
| ACY3 | aspartoacylase (aminocyclase) 3 | 0.6 | 37 |
| **ANKRD36** | **ankyrin repeat domain 36** | **0.61** | **62** |
| MYF5 | myogenic factor 5 | 0.61 | 46 |
| TMEM179 | transmembrane protein 179 | 0.61 | 51 |
| EVC2 | Ellis van Creveld syndrome 2 | 0.61 | 40 |
| **RAD54L** | **RAD54-like (S. cerevisiae)** | **0.61** | **39** |

| | | | |
|---|---|---|---|
| CPNE7 | copine VII | 0.61 | 35 |
| HOXB1 | homeobox B1 | 0.62 | 35 |
| PTX4 | pentraxin 4, long | 0.62 | 33 |
| GMPR | guanosine monophosphate reductase | 0.63 | 43 |
| UNC5C | unc-5 homolog C (C. elegans) | 0.63 | 35 |
| NUDT9 | nudix (nucleoside diphosphate linked moiety X)-type motif 9 | 0.64 | 39 |
| FCRL6 | Fc receptor-like 6 | 0.64 | 36 |
| TRMT12 | tRNA methyltransferase 12 homolog (S. cerevisiae) | 0.64 | 33 |
| DUSP23 | dual specificity phosphatase 23 | 0.64 | 35 |
| C12orf59 | chromosome 12 open reading frame 59 | 0.64 | 30 |
| VTI1A | vesicle transport through interaction with t-SNAREs homolog 1A (yeast) | 0.64 | 29 |
| ZC3H11A | zinc finger CCCH-type containing 11A | 0.65 | 48 |
| CDKAL1 | CDK5 regulatory subunit associated protein 1-like 1 | 0.65 | 49 |
| ZNF296 | zinc finger protein 296 | 0.65 | 43 |
| AP1AR | adaptor-related protein complex 1 associated regulatory protein | 0.65 | 31 |
| O3FAR1 | omega-3 fatty acid receptor 1 | 0.65 | 40 |
| STRADA | STE20-related kinase adaptor alpha | 0.65 | 31 |
| GPC1 | glypican 1 | 0.65 | 33 |
| **LHFPL2** | **lipoma HMGIC fusion partner-like 2** | **0.65** | **36** |
| SIDT1 | SID1 transmembrane family, member 1 | 0.65 | 37 |
| KHDC1 | KH homology domain containing 1 | 0.65 | 28 |
| CARKD | carbohydrate kinase domain containing | 0.65 | 36 |
| UNCX | UNC homeobox | 0.65 | 35 |
| ARFGAP2 | ADP-ribosylation factor GTPase activating protein 2 | 0.65 | 30 |
| CCL11 | chemokine (C-C motif) ligand 11 | 0.65 | 30 |
| DAPP1 | dual adaptor of phosphotyrosine and 3-phosphoinositides | 0.65 | 28 |
| TMOD3 | tropomodulin 3 (ubiquitous) | 0.66 | 40 |
| PTPN7 | protein tyrosine phosphatase, non-receptor type 7 | 0.66 | 39 |
| DNAJC21 | DnaJ (Hsp40) homolog, subfamily C, member 21 | 0.66 | 34 |
| HLA-DPB1 | major histocompatibility complex, class II, DP beta 1 | 0.66 | 41 |
| ZNF274 | zinc finger protein 274 | 0.66 | 38 |
| MT1M | metallothionein 1M | 0.66 | 28 |
| CCDC24 | coiled-coil domain containing 24 | 0.66 | 29 |

| | | | |
|---|---|---|---|
| NAGPA | N-acetylglucosamine-1-phosphodiester alpha-N-acetylglucosaminidase | 0.66 | 31 |
| MLLT10 | myeloid/lymphoid or mixed-lineage leukaemia (trithorax homolog, Drosophila); translocated to, 10 | 0.67 | 41 |
| HLA-DPA1 | major histocompatibility complex, class II, DP alpha 1 | 0.67 | 40 |
| NES | nestin | 0.67 | 35 |
| PALLD | palladin, cytoskeletal associated protein | 0.67 | 29 |
| ZNF673 | zinc finger family member 673 | 0.67 | 31 |
| CD83 | CD83 molecule | 0.67 | 28 |
| GRIK5 | glutamate receptor, ionotropic, kainate 5 | 0.68 | 35 |
| ESRP1 | epithelial splicing regulatory protein 1 | 0.68 | 32 |
| ANXA13 | annexin A13 | 0.68 | 39 |
| FOXN4 | forkhead box N4 | 0.68 | 31 |
| CT47A4 | cancer/testis antigen family 47, member A4 | 0.68 | 38 |
| AKR7A2 | aldo-keto reductase family 7, member A2 (aflatoxin aldehyde reductase) | 0.68 | 30 |
| UFC1 | ubiquitin-fold modifier conjugating enzyme 1 | 0.68 | 27 |
| HHIPL1 | HHIP-like 1 | 0.68 | 33 |
| SLK | STE20-like kinase | 0.68 | 28 |
| CNNM4 | cyclin M4 | 0.68 | 34 |
| GALNT14 | UDP-N-acetyl-alpha-D-galactosamine:polypeptide N-acetylgalactosaminyltransferase 14 (GalNAc-T14) | 0.68 | 30 |
| EMR1 | egf-like module containing, mucin-like, hormone receptor-like 1 | 0.68 | 29 |
| CHD7 | chromodomain helicase DNA binding protein 7 | 0.68 | 30 |
| ALPK1 | alpha-kinase 1 | 0.69 | 32 |
| GIF | gastric intrinsic factor (vitamin B synthesis) | 0.69 | 34 |
| PRAMEF3 | PRAME family member 3 | 0.69 | 28 |
| PPP1CB | protein phosphatase 1, catalytic subunit, beta isozyme | 0.69 | 35 |
| **ZNF77** | **zinc finger protein 77** | **0.69** | **35** |
| CBX8 | chromobox homolog 8 | 0.69 | 29 |
| KCNA6 | potassium voltage-gated channel, shaker-related subfamily, member 6 | 0.69 | 33 |
| MAGEB4 | melanoma antigen family B, 4 | 0.69 | 27 |
| SPIN1 | spindlin 1 | 0.69 | 28 |
| SCGN | secretagogin, EF-hand calcium binding protein | 0.69 | 25 |
| DENND5B | DENN/MADD domain containing 5B | 0.69 | 34 |

| | | | |
|---|---|---|---|
| CPM | carboxypeptidase M | 0.69 | 32 |
| OR5M8 | olfactory receptor, family 5, subfamily M, member 8 | 0.7 | 46 |
| KCNJ14 | potassium inwardly-rectifying channel, subfamily J, member 14 | 0.7 | 36 |
| ROCK1 | Rho-associated, coiled-coil containing protein kinase 1 | 0.7 | 38 |
| KRTAP13-3 | keratin associated protein 13-3 | 0.7 | 35 |
| MORC4 | MORC family CW-type zinc finger 4 | 0.7 | 28 |
| UBE2H | ubiquitin-conjugating enzyme E2H | 0.7 | 40 |
| SCYL1 | SCY1-like 1 (S. cerevisiae) | 0.7 | 29 |
| SPRR2B | small proline-rich protein 2B | 0.7 | 31 |
| TSPAN16 | tetraspanin 16 | 0.7 | 32 |
| KCNE1 | potassium voltage-gated channel, Isk-related family, member 1 | 0.7 | 29 |
| WWP2 | WW domain containing E3 ubiquitin protein ligase 2 | 0.7 | 38 |
| SIRT2 | sirtuin 2 | 0.7 | 36 |
| C22orf36 | chromosome 22 open reading frame 36 | 0.7 | 33 |
| NOMO3 | NODAL modulator 3 | 0.7 | 38 |
| C20orf152 | chromosome 20 open reading frame 152 | 0.7 | 32 |
| EID3 | EP300 interacting inhibitor of differentiation 3 | 0.7 | 28 |
| CT47A9 | cancer/testis antigen family 47, member A9 | 0.7 | 29 |
| FAM190B | family with sequence similarity 190, member B | 0.71 | 33 |
| AGMO | alkylglycerol monooxygenase | 0.71 | 27 |
| ZNF227 | zinc finger protein 227 | 0.71 | 39 |
| TSKU | tsukushi small leucine rich proteoglycan homolog (Xenopus laevis) | 0.71 | 32 |
| HK1 | hexokinase 1 | 0.71 | 34 |
| FZD6 | frizzled family receptor 6 | 0.71 | 36 |
| GALNT4 | UDP-N-acetyl-alpha-D-galactosamine:polypeptide N-acetylgalactosaminyltransferase 4 (GalNAc-T4) | 0.71 | 35 |
| PARP2 | poly (ADP-ribose) polymerase 2 | 0.71 | 34 |
| MC4R | melanocortin 4 receptor | 0.71 | 34 |
| TRADD | TNFRSF1A-associated via death domain | 0.71 | 30 |
| PLA2G12A | phospholipase A2, group XIIA | 0.71 | 25 |
| L3MBTL1 | l(3)mbt-like 1 (Drosophila) | 0.71 | 33 |
| TYROBP | TYRO protein tyrosine kinase binding protein | 0.71 | 30 |

| | | | |
|---|---|---|---|
| SERPINH1 | serpin peptidase inhibitor, clade H (heat shock protein 47), member 1, (collagen binding protein 1) | 0.71 | 33 |
| **C18orf19** | **chromosome 18 open reading frame 19** | **0.71** | **31** |
| C14orf43 | chromosome 14 open reading frame 43 | 0.71 | 25 |
| PLCB1 | phospholipase C, beta 1 (phosphoinositide-specific) | 0.71 | 28 |
| RNF24 | ring finger protein 24 | 0.71 | 29 |
| **RAD51AP1** | **RAD51 associated protein 1** | **0.71** | **37** |
| DCAF12 | DDB1 and CUL4 associated factor 12 | 0.71 | 30 |
| CORO1A | coronin, actin binding protein, 1A | 0.71 | 25 |
| FHOD1 | formin homology 2 domain containing 1 | 0.71 | 25 |
| RALY | RNA binding protein, autoantigenic (hnRNP-associated with lethal yellow homolog (mouse)) | 0.71 | 29 |
| CD22 | CD22 molecule | 0.71 | 27 |
| CSF3 | colony stimulating factor 3 (granulocyte) | 0.71 | 30 |
| GJB5 | gap junction protein, beta 5, 31.1kDa | 0.72 | 37 |
| OR7D2 | olfactory receptor, family 7, subfamily D, member 2 | 0.72 | 35 |
| BCORL1 | BCL6 corepressor-like 1 | 0.72 | 27 |
| CCT8L2 | chaperonin containing TCP1, subunit 8 (theta)-like 2 | 0.72 | 28 |
| DLK2 | delta-like 2 homolog (Drosophila) | 0.72 | 27 |
| CDX2 | caudal type homeobox 2 | 0.72 | 33 |
| FLAD1 | FAD1 flavin adenine dinucleotide synthetase homolog (S. cerevisiae) | 0.72 | 34 |
| SLCO3A1 | solute carrier organic anion transporter family, member 3A1 | 0.72 | 27 |
| BEND6 | BEN domain containing 6 | 0.72 | 26 |
| HOXA11 | homeobox A11 | 0.72 | 30 |
| **MYO18B** | **myosin XVIIIB** | **0.72** | **30** |
| C2orf88 | chromosome 2 open reading frame 88 | 0.72 | 26 |
| DKFZp761E198 | uncharacterized protein DKFZp761E198 | 0.72 | 26 |
| UBR1 | ubiquitin protein ligase E3 component n-recognin 1 | 0.72 | 30 |
| THAP11 | THAP domain containing 11 | 0.72 | 28 |
| PRMT3 | protein arginine methyltransferase 3 | 0.72 | 29 |
| GTF3C2 | general transcription factor IIIC, polypeptide 2, beta 110kDa | 0.72 | 26 |
| MPP3 | membrane protein, palmitoylated 3 (MAGUK p55 subfamily member 3) | 0.72 | 26 |
| ADO | 2-aminoethanethiol (cysteamine) dioxygenase | 0.72 | 26 |

| | | | |
|---|---|---|---|
| HMX2 | H6 family homeobox 2 | 0.73 | 52 |
| HOXA13 | homeobox A13 | 0.73 | 36 |
| GDPD1 | glycerophosphodiester phosphodiesterase domain containing 1 | 0.73 | 33 |
| DNAJC2 | DnaJ (Hsp40) homolog, subfamily C, member 2 | 0.73 | 32 |
| TWIST2 | twist homolog 2 (Drosophila) | 0.73 | 34 |
| NLN | neurolysin (metallopeptidase M3 family) | 0.73 | 35 |
| OR5D16 | olfactory receptor, family 5, subfamily D, member 16 | 0.73 | 26 |
| ADCY6 | adenylate cyclase 6 | 0.73 | 27 |
| **SACS** | **spastic ataxia of Charlevoix-Saguenay (sacsin)** | **0.73** | **30** |
| NXNL2 | nucleoredoxin-like 2 | 0.73 | 27 |
| **SELE** | **selectin E** | **0.73** | **27** |
| MESP1 | mesoderm posterior 1 homolog (mouse) | 0.73 | 25 |
| ARHGAP35 | Rho GTPase activating protein 35 | 0.74 | 38 |
| ZNF691 | zinc finger protein 691 | 0.74 | 35 |
| ANO4 | anoctamin 4 | 0.74 | 35 |
| ARIH1 | ariadne homolog, ubiquitin-conjugating enzyme E2 binding protein, 1 (Drosophila) | 0.74 | 33 |
| YAF2 | YY1 associated factor 2 | 0.74 | 38 |
| KCNMB4 | potassium large conductance calcium-activated channel, subfamily M, beta member 4 | 0.74 | 27 |
| EAF2 | ELL associated factor 2 | 0.74 | 28 |
| CCL27 | chemokine (C-C motif) ligand 27 | 0.74 | 28 |
| **ATP9B** | **ATPase, class II, type 9B** | **0.74** | **31** |
| EPN2 | epsin 2 | 0.74 | 25 |
| NKPD1 | NTPase, KAP family P-loop domain containing 1 | 0.74 | 28 |
| MRGPRG | MAS-related GPR, member G | 0.74 | 26 |
| METTL7B | methyltransferase like 7B | 0.74 | 26 |
| BCOR | BCL6 corepressor | 0.74 | 26 |
| EDDM3A | epididymal protein 3A | 0.74 | 25 |
| YTHDF1 | YTH domain family, member 1 | 0.75 | 40 |
| TFB1M | transcription factor B1, mitochondrial | 0.75 | 32 |
| CALCB | calcitonin-related polypeptide beta | 0.75 | 30 |
| TRIM23 | tripartite motif containing 23 | 0.75 | 33 |
| AGAP6 | ArfGAP with GTPase domain, ankyrin repeat and PH domain 6 | 0.75 | 29 |
| CNKSR3 | CNKSR family member 3 | 0.75 | 31 |
| RHOXF1 | Rhox homeobox family, member 1 | 0.75 | 30 |

| | | | |
|---|---|---|---|
| SERPINA11 | serpin peptidase inhibitor, clade A (alpha-1 antiproteinase, antitrypsin), member 11 | 0.75 | 28 |
| TNFRSF14 | tumor necrosis factor receptor superfamily, member 14 | 0.75 | 27 |
| POLRMT | polymerase (RNA) mitochondrial (DNA directed) | 0.75 | 30 |
| GPR143 | G protein-coupled receptor 143 | 0.75 | 32 |
| NEUROD1 | neurogenic differentiation 1 | 0.75 | 28 |
| RENBP | renin binding protein | 0.75 | 26 |
| RAB39B | RAB39B, member RAS oncogene family | 0.75 | 27 |
| RALA | v-ral simian leukaemia viral oncogene homolog A (ras related) | 0.75 | 29 |
| B3GNT2 | UDP-GlcNAc:betaGal beta-1,3-N-acetylglucosaminyltransferase 2 | 0.75 | 29 |
| FER | fer (fps/fes related) tyrosine kinase | 0.75 | 25 |
| PET112 | PET112 homolog (yeast) | 0.75 | 25 |
| UBE2QL1 | ubiquitin-conjugating enzyme E2Q family-like 1 | 0.75 | 31 |
| C10orf10 | chromosome 10 open reading frame 10 | 0.75 | 25 |
| AFAP1 | actin filament associated protein 1 | 0.75 | 26 |
| NUB1 | negative regulator of ubiquitin-like proteins 1 | 0.75 | 26 |
| P4HA3 | prolyl 4-hydroxylase, alpha polypeptide III | 0.75 | 25 |
| KLK13 | kallikrein-related peptidase 13 | 0.76 | 37 |
| DNASE1L1 | deoxyribonuclease I-like 1 | 0.76 | 31 |
| LRRC41 | leucine rich repeat containing 41 | 0.76 | 31 |
| KCNAB3 | potassium voltage-gated channel, shaker-related subfamily, beta member 3 | 0.76 | 27 |
| PTPRA | protein tyrosine phosphatase, receptor type, A | 0.76 | 35 |
| YIPF6 | Yip1 domain family, member 6 | 0.76 | 38 |
| FAM122C | family with sequence similarity 122C | 0.76 | 36 |
| KCNK17 | potassium channel, subfamily K, member 17 | 0.76 | 27 |
| **USH1G** | **Usher syndrome 1G (autosomal recessive)** | **0.76** | **30** |
| C3orf75 | chromosome 3 open reading frame 75 | 0.76 | 28 |
| FGF11 | fibroblast growth factor 11 | 0.76 | 26 |
| TUBGCP6 | tubulin, gamma complex associated protein 6 | 0.76 | 26 |
| CYP2S1 | cytochrome P450, family 2, subfamily S, polypeptide 1 | 0.76 | 27 |
| FZD1 | frizzled family receptor 1 | 0.76 | 27 |
| C6orf62 | chromosome 6 open reading frame 62 | 0.76 | 26 |
| SPINK13 | serine peptidase inhibitor, Kazal type 13 (putative) | 0.76 | 26 |
| ERF | Ets2 repressor factor | 0.76 | 25 |
| PER2 | period homolog 2 (Drosophila) | 0.76 | 25 |

| | | | |
|---|---|---|---|
| ENO3 | enolase 3 (beta, muscle) | 0.76 | 28 |
| CD2AP | CD2-associated protein | 0.76 | 25 |
| ZMYND17 | zinc finger, MYND-type containing 17 | 0.76 | 28 |
| C20orf118 | chromosome 20 open reading frame 118 | 0.77 | 31 |
| CXCL3 | chemokine (C-X-C motif) ligand 3 | 0.77 | 27 |
| KCNJ11 | potassium inwardly-rectifying channel, subfamily J, member 11 | 0.77 | 27 |
| RPL17 | ribosomal protein L17 | 0.77 | 25 |
| GAPDH | glyceraldehyde-3-phosphate dehydrogenase | 0.77 | 34 |
| CMA1 | chymase 1, mast cell | 0.77 | 28 |
| OR5B17 | olfactory receptor, family 5, subfamily B, member 17 | 0.77 | 25 |
| ESM1 | endothelial cell-specific molecule 1 | 0.77 | 27 |
| CLCN3 | chloride channel 3 | 0.77 | 25 |
| LDHAL6A | lactate dehydrogenase A-like 6A | 0.77 | 29 |
| STAT4 | signal transducer and activator of transcription 4 | 0.77 | 31 |
| BRD1 | bromodomain containing 1 | 0.77 | 26 |
| PRSS22 | protease, serine, 22 | 0.77 | 32 |
| DDT | D-dopachrome tautomerase | 0.77 | 25 |
| TRUB1 | TruB pseudouridine (psi) synthase homolog 1 (E. coli) | 0.77 | 28 |
| KRTAP6-2 | keratin associated protein 6-2 | 0.77 | 26 |
| GGT2 | gamma-glutamyltransferase 2 | 0.77 | 27 |
| OR6N2 | olfactory receptor, family 6, subfamily N, member 2 | 0.77 | 30 |
| KCNG3 | potassium voltage-gated channel, subfamily G, member 3 | 0.78 | 30 |
| RASSF10 | Ras association (RalGDS/AF-6) domain family (N-terminal) member 10 | 0.78 | 38 |
| RAB20 | RAB20, member RAS oncogene family | 0.78 | 25 |
| GCET2 | germinal centre expressed transcript 2 | 0.78 | 27 |
| LYG1 | lysozyme G-like 1 | 0.78 | 26 |
| USP35 | ubiquitin specific peptidase 35 | 0.78 | 26 |
| CALD1 | caldesmon 1 | 0.78 | 28 |
| FLJ45831 | uncharacterized FLJ45831 | 0.78 | 35 |
| TYSND1 | trypsin domain containing 1 | 0.78 | 28 |
| **BCL2L13** | **BCL2-like 13 (apoptosis facilitator)** | **0.78** | **29** |
| PCGF2 | polycomb group ring finger 2 | 0.78 | 26 |
| LPGAT1 | lysophosphatidylglycerol acyltransferase 1 | 0.78 | 27 |
| PCYT2 | phosphate cytidylyltransferase 2, ethanolamine | 0.78 | 28 |
| **TOP1** | **topoisomerase (DNA) I** | **0.78** | **26** |

| | | | |
|---|---|---|---|
| PLSCR5 | phospholipid scramblase family, member 5 | 0.78 | 30 |
| COL24A1 | collagen, type XXIV, alpha 1 | 0.78 | 29 |
| ZDHHC21 | zinc finger, DHHC-type containing 21 | 0.78 | 28 |
| ABCC10 | ATP-binding cassette, sub-family C (CFTR/MRP), member 10 | 0.78 | 25 |
| WDYHV1 | WDYHV motif containing 1 | 0.78 | 27 |
| EDC4 | enhancer of mRNA decapping 4 | 0.78 | 26 |
| KCNMA1 | potassium large conductance calcium-activated channel, subfamily M, alpha member 1 | 0.79 | 33 |
| DDIT4 | DNA-damage-inducible transcript 4 | 0.79 | 40 |
| TJP3 | tight junction protein 3 (zona occludens 3) | 0.79 | 35 |
| RGAG4 | retrotransposon gag domain containing 4 | 0.79 | 26 |
| PPP2R4 | protein phosphatase 2A activator, regulatory subunit 4 | 0.79 | 32 |
| USP37 | ubiquitin specific peptidase 37 | 0.79 | 29 |
| PSG5 | pregnancy specific beta-1-glycoprotein 5 | 0.79 | 30 |
| **FUCA1** | **fucosidase, alpha-L- 1, tissue** | **0.79** | **26** |
| PID1 | phosphotyrosine interaction domain containing 1 | 0.79 | 30 |
| KIAA0355 | KIAA0355 | 0.79 | 27 |
| MLH3 | mutL homolog 3 (E. coli) | 0.79 | 25 |
| ISG20L2 | interferon stimulated exonuclease gene 20kDa-like 2 | 0.79 | 26 |
| HERC4 | hect domain and RLD 4 | 0.79 | 26 |
| AFG3L2 | AFG3 ATPase family gene 3-like 2 (S. cerevisiae) | 0.79 | 26 |
| RIC8B | resistance to inhibitors of cholinesterase 8 homolog B (C. elegans) | 0.79 | 26 |
| DBT | dihydrolipoamide branched chain transacylase E2 | 0.8 | 29 |
| GOLM1 | golgi membrane protein 1 | 0.8 | 34 |
| LRRC52 | leucine rich repeat containing 52 | 0.8 | 27 |
| **BPIFB4** | **BPI fold containing family B, member 4** | **0.8** | **32** |
| M6PR | mannose-6-phosphate receptor (cation dependent) | 0.8 | 26 |
| SSR4 | signal sequence receptor, delta | 0.8 | 26 |
| MEI1 | meiosis inhibitor 1 | 0.8 | 28 |
| CSF2RA | colony stimulating factor 2 receptor, alpha, low-affinity (granulocyte-macrophage) | 0.8 | 26 |
| RTN2 | reticulon 2 | 0.81 | 30 |
| C12orf66 | chromosome 12 open reading frame 66 | 0.81 | 30 |
| RAB3A | RAB3A, member RAS oncogene family | 0.81 | 27 |

| | | | |
|---|---|---|---|
| MPP7 | membrane protein, palmitoylated 7 (MAGUK p55 subfamily member 7) | 0.81 | 27 |
| TMEM143 | transmembrane protein 143 | 0.81 | 32 |
| ADAM20 | ADAM metallopeptidase domain 20 | 0.81 | 27 |
| SETDB2 | SET domain, bifurcated 2 | 0.81 | 25 |
| SLC5A6 | solute carrier family 5 (sodium-dependent vitamin transporter), member 6 | 0.81 | 25 |
| PALMD | palmdelphin | 0.81 | 26 |
| CASZ1 | castor zinc finger 1 | 0.82 | 26 |
| RANBP3 | RAN binding protein 3 | 0.82 | 27 |
| RFFL | ring finger and FYVE-like domain containing 1 | 0.82 | 29 |
| RNF5 | ring finger protein 5 | 0.82 | 26 |
| ADD1 | adducin 1 (alpha) | 0.82 | 27 |
| PPP4C | protein phosphatase 4, catalytic subunit | 0.82 | 26 |
| CAND1 | cullin-associated and neddylation-dissociated 1 | 0.82 | 25 |
| SLC38A10 | solute carrier family 38, member 10 | 0.82 | 26 |
| MIR22HG | MIR22 host gene (non-protein coding) | 0.82 | 26 |
| TMEM101 | transmembrane protein 101 | 0.83 | 25 |
| TEPP | testis, prostate and placenta expressed | 0.83 | 29 |
| FBXL17 | F-box and leucine-rich repeat protein 17 | 0.83 | 28 |
| EBAG9 | estrogen receptor binding site associated, antigen, 9 | 0.83 | 30 |
| PRAF2 | PRA1 domain family, member 2 | 0.83 | 30 |
| PTPN20B | protein tyrosine phosphatase, non-receptor type 20B | 0.83 | 27 |
| MARVELD3 | MARVEL domain containing 3 | 0.83 | 28 |
| STAG2 | stromal antigen 2 | 0.83 | 28 |
| CDC42EP3 | CDC42 effector protein (Rho GTPase binding) 3 | 0.83 | 26 |
| FAM200A | family with sequence similarity 200, member A | 0.83 | 27 |
| SURF6 | surfeit 6 | 0.83 | 25 |
| C9orf170 | chromosome 9 open reading frame 170 | 0.83 | 25 |
| LRRN4CL | LRRN4 C-terminal like | 0.84 | 29 |
| UBE2D4 | ubiquitin-conjugating enzyme E2D 4 (putative) | 0.84 | 27 |
| ZNF468 | zinc finger protein 468 | 0.84 | 28 |
| CIB3 | calcium and integrin binding family member 3 | 0.84 | 26 |
| PDZD8 | PDZ domain containing 8 | 0.84 | 27 |
| **IGFBP1** | **insulin-like growth factor binding protein 1** | **0.84** | **25** |
| TRAM2 | translocation associated membrane protein 2 | 0.14 | 58 |
| CHRM5 | cholinergic receptor, muscarinic 5 | 0.45 | 33 |

| | | | |
|---|---|---|---|
| KCNG2 | potassium voltage-gated channel, subfamily G, member 2 | 0.49 | 27 |
| UROC1 | urocanase domain containing 1 | 0.52 | 34 |
| C9orf123 | chromosome 9 open reading frame 123 | 0.53 | 30 |
| ART5 | ADP-ribosyltransferase 5 | 0.55 | 26 |
| ZNF350 | zinc finger protein 350 | 0.55 | 32 |
| **BRCA2** | **breast cancer 2, early onset** | **0.57** | **31** |
| ZNF512 | zinc finger protein 512 | 0.57 | 32 |
| ZNF79 | zinc finger protein 79 | 0.58 | 26 |
| TRIM11 | tripartite motif containing 11 | 0.59 | 31 |
| NPFFR1 | neuropeptide FF receptor 1 | 0.6 | 34 |
| IQCA1 | IQ motif containing with AAA domain 1 | 0.6 | 27 |
| DMRT1 | doublesex and mab-3 related transcription factor 1 | 0.61 | 30 |
| FBXO31 | F-box protein 31 | 0.61 | 32 |
| DGCR2 | DiGeorge syndrome critical region gene 2 | 0.62 | 29 |
| GABRD | gamma-aminobutyric acid (GABA) A receptor, delta | 0.62 | 28 |
| C3orf54 | chromosome 3 open reading frame 54 | 0.62 | 29 |
| PARP10 | poly (ADP-ribose) polymerase family, member 10 | 0.63 | 37 |
| SUV39H2 | suppressor of variegation 3-9 homolog 2 (Drosophila) | 0.63 | 34 |
| ANKRD39 | ankyrin repeat domain 39 | 0.63 | 27 |
| SLC16A11 | solute carrier family 16, member 11 (monocarboxylic acid transporter 11) | 0.64 | 28 |
| C16orf85 | chromosome 16 open reading frame 85 | 0.64 | 26 |
| HAND2 | heart and neural crest derivatives expressed 2 | 0.64 | 27 |
| GFPT1 | glutamine--fructose-6-phosphate transaminase 1 | 0.65 | 30 |
| ACTN4 | actinin, alpha 4 | 0.65 | 25 |
| HMCN1 | hemicentin 1 | 0.65 | 25 |
| HIPK1 | homeodomain interacting protein kinase 1 | 0.66 | 29 |
| CDK20 | cyclin-dependent kinase 20 | 0.66 | 28 |
| S1PR5 | sphingosine-1-phosphate receptor 5 | 0.67 | 30 |
| ZNF425 | zinc finger protein 425 | 0.67 | 27 |
| AAK1 | AP2 associated kinase 1 | 0.67 | 27 |
| KLHDC9 | kelch domain containing 9 | 0.68 | 28 |
| RASL11B | RAS-like, family 11, member B | 0.68 | 25 |
| FGFR1OP2 | FGFR1 oncogene partner 2 | 0.69 | 26 |
| SHROOM2 | shroom family member 2 | 0.7 | 26 |
| IFI6 | interferon, alpha-inducible protein 6 | 0.7 | 25 |

| | | | |
|---|---|---|---|
| TRH | thyrotropin-releasing hormone | 0.7 | 25 |
| HIST3H3 | histone cluster 3, H3 | 0.71 | 26 |
| PPID | peptidylprolyl isomerase D | 0.71 | 29 |
| TCEAL1 | transcription elongation factor A (SII)-like 1 | 0.72 | 26 |
| RDH8 | retinol dehydrogenase 8 (all-trans) | 0.74 | 25 |
| NOP10 | NOP10 ribonucleoprotein homolog (yeast) | 0.74 | 25 |
| UBE3C | ubiquitin protein ligase E3C | 0.85 | 31 |
| C1orf51 | chromosome 1 open reading frame 51 | 0.85 | 27 |
| ZNF675 | zinc finger protein 675 | 0.85 | 30 |
| UBE2R2 | ubiquitin-conjugating enzyme E2R 2 | 0.85 | 26 |
| CUL4A | cullin 4A | 0.87 | 29 |
| APBA2 | amyloid beta (A4) precursor protein-binding, family A, member 2 | 0.87 | 32 |
| ERAP2 | endoplasmic reticulum aminopeptidase 2 | 0.87 | 26 |
| OR2A1 | olfactory receptor, family 2, subfamily A, member 1 | 0.87 | 27 |
| TCTEX1D2 | Tctex1 domain containing 2 | 0.89 | 25 |

# Appendix II Publisher's/author's permissions for figure reprints

License agreement with Springer Nature

**SPRINGER NATURE LICENSE**
**TERMS AND CONDITIONS**

May 30, 2019

This Agreement between Mr. Shunfei Yan ("You") and Springer Nature ("Springer Nature") consists of your license details and the terms and conditions provided by Springer Nature and Copyright Clearance Center.

| | |
|---|---|
| License Number | 4599070555764 |
| License date | May 30, 2019 |
| Licensed Content Publisher | Springer Nature |
| Licensed Content Publication | Nature Reviews Cancer |
| Licensed Content Title | DNA repair dysregulation from cancer driver to therapeutic target |
| Licensed Content Author | Nicola J. Curtin |
| Licensed Content Date | Nov 23, 2012 |
| Licensed Content Volume | 12 |
| Licensed Content Issue | 12 |
| Type of Use | Thesis/Dissertation |
| Requestor type | academic/university or research institute |
| Format | electronic |
| Portion | figures/tables/illustrations |
| Number of figures/tables/illustrations | 5 |
| High-res required | no |
| Will you be translating? | no |
| Circulation/distribution | <501 |
| Author of this Springer Nature content | no |
| Title | A Genome-wide RNAi Screen Identifies Combinatorial Efficacy of CX-5461 with Homologous Recombination Deficiency and Topoisomerase I inhibition in Ovarian Cancer |
| Institution name | Peter MacCallum Cancer Centre |
| Expected presentation date | Jul 2019 |
| Portions | Figure 2-6 |
| Requestor Location | Mr. Shunfei Yan<br>Level 12, 305 Grattan Street<br><br>Melbourne, Victoria 3000<br>Australia<br>Attn: Mr. Shunfei Yan |
| Total | 0.00 AUD |
| Terms and Conditions | |

**Springer Nature Terms and Conditions for RightsLink Permissions**

**Springer Nature Customer Service Centre GmbH (the Licensor)** hereby grants you a non-exclusive, world-wide licence to reproduce the material and for the purpose and requirements specified in the attached copy of your order form, and for no other use, subject to the conditions below:

1. The Licensor warrants that it has, to the best of its knowledge, the rights to license reuse of this material. However, you should ensure that the material you are requesting is original to the Licensor and does not carry the copyright of another entity (as credited in the published version).

   If the credit line on any part of the material you have requested indicates that it was reprinted or adapted with permission from another source, then you should also seek permission from that source to reuse the material.

2. Where **print only** permission has been granted for a fee, separate permission must be obtained for any additional electronic re-use.

3. Permission granted **free of charge** for material in print is also usually granted for any electronic version of that work, provided that the material is incidental to your work as a whole and that the electronic version is essentially equivalent to, or substitutes for, the print version.

4. A licence for 'post on a website' is valid for 12 months from the licence date. This licence does not cover use of full text articles on websites.

5. Where **'reuse in a dissertation/thesis'** has been selected the following terms apply: Print rights of the final author's accepted manuscript (for clarity, NOT the published version) for up to 100 copies, electronic rights for use only on a personal website or institutional repository as defined by the Sherpa guideline (www.sherpa.ac.uk/romeo/).

6. Permission granted for books and journals is granted for the lifetime of the first edition and does not apply to second and subsequent editions (except where the first edition permission was granted free of charge or for signatories to the STM Permissions Guidelines http://www.stm-assoc.org/copyright-legal-affairs/permissions/permissions-guidelines/), and does not apply for editions in other languages unless additional translation rights have been granted separately in the licence.

7. Rights for additional components such as custom editions and derivatives require additional permission and may be subject to an additional fee. Please apply to Journalpermissions@springernature.com/bookpermissions@springernature.com for these rights.

8. The Licensor's permission must be acknowledged next to the licensed material in print. In electronic form, this acknowledgement must be visible at the same time as the figures/tables/illustrations or abstract, and must be hyperlinked to the journal/book's homepage. Our required acknowledgement format is in the Appendix below.

9. Use of the material for incidental promotional use, minor editing privileges (this does not include cropping, adapting, omitting material or any other changes that affect the meaning, intention or moral rights of the author) and copies for the disabled are permitted under this licence.

10. Minor adaptations of single figures (changes of format, colour and style) do not require the Licensor's approval. However, the adaptation should be credited as shown in Appendix below.

**Appendix — Acknowledgements:**

**For Journal Content:**
Reprinted by permission from [**the Licensor**]: [**Journal Publisher** (e.g. Nature/Springer/Palgrave)] [**JOURNAL NAME**] [**REFERENCE CITATION** (Article name, Author(s) Name), [**COPYRIGHT**] (year of publication)

For **Advance Online Publication papers:**
Reprinted by permission from [**the Licensor**]: [**Journal Publisher** (e.g. Nature/Springer/Palgrave)] [**JOURNAL NAME**] [**REFERENCE CITATION** (Article name, Author(s) Name), [**COPYRIGHT**] (year of publication), advance online publication, day month year (doi: 10.1038/sj.[JOURNAL ACRONYM].)

**For Adaptations/Translations:**
Adapted/Translated by permission from [**the Licensor**]: [**Journal Publisher** (e.g. Nature/Springer/Palgrave)] [**JOURNAL NAME**] [**REFERENCE CITATION** (Article name, Author(s) Name), [**COPYRIGHT**] (year of publication)

**Note: For any republication from the British Journal of Cancer, the following credit line style applies:**

Reprinted/adapted/translated by permission from [**the Licensor**]: on behalf of Cancer Research UK: : [**Journal Publisher** (e.g. Nature/Springer/Palgrave)] [**JOURNAL NAME**] [**REFERENCE CITATION** (Article name, Author(s) Name), [**COPYRIGHT**] (year of publication)

For **Advance Online Publication** papers:
Reprinted by permission from The [**the Licensor**]: on behalf of Cancer Research UK: [**Journal Publisher** (e.g. Nature/Springer/Palgrave)] [**JOURNAL NAME**] [**REFERENCE CITATION** (Article name, Author(s) Name), [**COPYRIGHT**] (year of publication), advance online publication, day month year (doi: 10.1038/sj. [JOURNAL ACRONYM])

**For Book content:**
Reprinted/adapted by permission from [**the Licensor**]: [**Book Publisher** (e.g. Palgrave Macmillan, Springer etc) [**Book Title**] by [**Book author**(s)] [**COPYRIGHT**] (year of publication)

**Other Conditions**:

Version 1.1

**Questions? customercare@copyright.com or +1-855-239-3415 (toll free in the US) or +1-978-646-2777.**

Permission from Prof Joaquim Roca Bosch

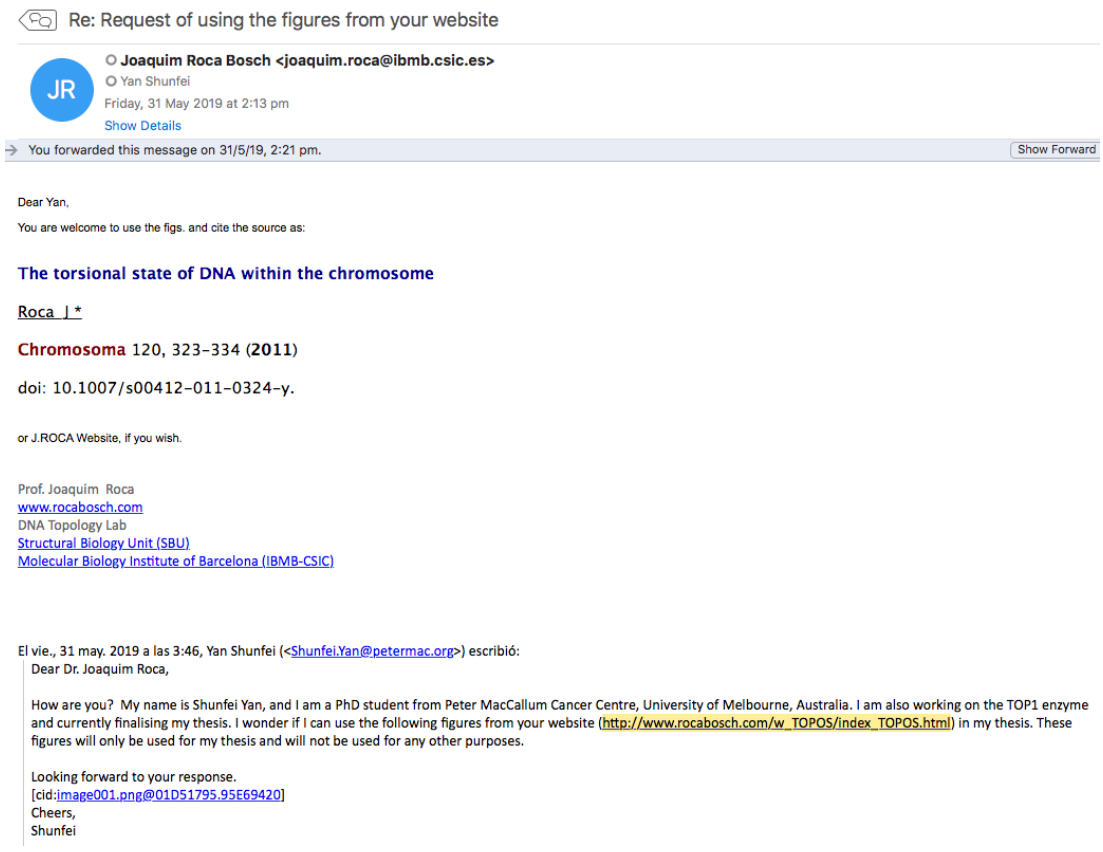

Re: Request of using the figures from your website

JR

Joaquim Roca Bosch <joaquim.roca@ibmb.csic.es>
Yan Shunfei
Friday, 31 May 2019 at 2:13 pm
Show Details

You forwarded this message on 31/5/19, 2:21 pm. Show Forward

Dear Yan,

You are welcome to use the figs. and cite the source as:

**The torsional state of DNA within the chromosome**

Roca J *

**Chromosoma** 120, 323-334 (**2011**)

doi: 10.1007/s00412-011-0324-y.

or J.ROCA Website, if you wish.

Prof. Joaquim Roca
www.rocabosch.com
DNA Topology Lab
Structural Biology Unit (SBU)
Molecular Biology Institute of Barcelona (IBMB-CSIC)

El vie., 31 may. 2019 a las 3:46, Yan Shunfei (<Shunfei.Yan@petermac.org>) escribió:

> Dear Dr. Joaquim Roca,
>
> How are you? My name is Shunfei Yan, and I am a PhD student from Peter MacCallum Cancer Centre, University of Melbourne, Australia. I am also working on the TOP1 enzyme and currently finalising my thesis. I wonder if I can use the following figures from your website (http://www.rocabosch.com/w_TOPOS/index_TOPOS.html) in my thesis. These figures will only be used for my thesis and will not be used for any other purposes.
>
> Looking forward to your response.
> [cid:image001.png@01D51795.95E69420]
> Cheers,
> Shunfei